



THE HONG KONG  
POLYTECHNIC UNIVERSITY

香港理工大學

Pao Yue-kong Library

包玉剛圖書館

---

## Copyright Undertaking

This thesis is protected by copyright, with all rights reserved.

**By reading and using the thesis, the reader understands and agrees to the following terms:**

1. The reader will abide by the rules and legal ordinances governing copyright regarding the use of the thesis.
2. The reader will use the thesis for the purpose of research or private study only and not for distribution or further reproduction or any other purpose.
3. The reader agrees to indemnify and hold the University harmless from and against any loss, damage, cost, liability or expenses arising from copyright infringement or unauthorized usage.

If you have reasons to believe that any materials in this thesis are deemed not suitable to be distributed in this form, or a copyright owner having difficulty with the material being included in our database, please contact [lbsys@polyu.edu.hk](mailto:lbsys@polyu.edu.hk) providing details. The Library will look into your claim and consider taking remedial action upon receipt of the written requests.



**STRUCTURAL HEALTH MONITORING  
AND CONDITION ASSESSMENT OF  
BRIDGE STRUCTURES**

by

**Xu-Gang HUA**

B. Eng., M. Sc.

A Thesis Submitted for Partial Fulfillment for the Degree of  
**Doctor of Philosophy**

Department of Civil and Structural Engineering  
The Hong Kong Polytechnic University, Hong Kong

September 2006

**To my parents and sisters**

## DECLARATION

I hereby declare that this thesis entitled “*Structural Health Monitoring and Condition Assessment of Bridge Structures*” has not been, either in whole or in part, previously submitted for a degree in this or any other institution, and the work presented in this thesis is original unless otherwise acknowledged in the text.

SIGNED

---

Xu-Gang HUA

20 August 2006

## **ACKNOWLEDGEMENTS**

I am greatly indebted to my chief supervisor, Dr. Y. Q. Ni, for his valuable guidance and advice, high sense of responsibility, and dedication of his time throughout my study and preparation of the thesis. I deeply appreciate his critical guidance to keep me on track while giving me sufficient freedom to pursue research. His conscientious and meticulous work attitude benefits me inexhaustibly in my future career. I also wish to express sincere gratitude to my co-supervisor, Prof. J. M. Ko, for his constant encouragement throughout the course of my PhD project.

Sincere appreciation goes to Prof. Z. Q. Chen at Hunan University, China for his continuous support, encouragement and constructive advice during the course of my study. Special thanks are also due to Dr. K. Y. Wong at the Highways Department of Hong Kong SAR Government for providing field measurement data. I am also grateful to Drs. X. Q. Zhu, X. Y. Wang, J. Y. Wang, Y. F. Duan, H. F. Zhou, Y. J. Wang, Mr. X. W. Ye, and Mr. T. K. Chan for their helpful discussions.

The financial supports from the university by means of student fellowship and attendance of international conferences are gratefully acknowledged. The kind help of staff in the university library, research office, and general office of Department of Civil and Structural Engineering is also appreciated during my stay at the university.

Last but not least, I wish to thank all my family members for their understanding and strong support during these years. The dissertation could not have been completed without their support and understanding.

## ABSTRACT

Engineering structures continuously accumulate damage during their service life due to material degradation, human error, and unexpected catastrophic events. Such damage adversely affects the safety and performance of structures. The work described in this thesis is concerned with condition assessment of bridge structures using long-term monitoring data, including vibration-based damage detection and structural reliability evaluation, modelling of the temperature-frequency correlation, and condition assessment of bridge expansion joints.

A crucial issue in vibration-based damage detection is the treatment of the ill-conditioned and noisy system of equations, and it is pursued in this study by two numerical regularization methods, namely Tikhonov regularization and truncated singular value decomposition. Three approaches, including the L-curve method, generalized cross validation and minimum product criterion, to selecting the regularization parameters are presented. The performances of the two regularization methods with three regularization-parameter-selection approaches are rigorously examined and assessed through numerical studies of a truss bridge using both noise-free and noisy ‘measurement’ data. Minimum product criterion is shown effective and robust in the selection of appropriate regularization parameters for these two regularization methods.

In order to take into account the uncertainty in the measured modal parameters, a novel method for stochastic FE model updating is proposed. The proposed method follows a two-stage model updating scheme. The first stage refers to the

identification of probability density functions (PDFs) of updating parameters based on measured random modal parameters and the second stage deals with the determination of posterior PDFs of structural parameters from the identified PDFs and the prior PDFs of structural parameters. An improved perturbation method and the Monte Carlo simulation (MCS) method are used to perform the first-stage updating. At the second stage updating, the first-stage updating results are combined with the prior distribution of updating parameters (if available) by means of Bayesian theory to achieve the posterior distribution. Two numerical examples are provided to demonstrate and verify the proposed method. Three types of uncertainty in modal parameters are considered, and the updating parameter statistics is obtained using the improved perturbation method and verified by the MCS method for each type of uncertainties. The numerical studies show that the perturbation method generates satisfactory model updating results in the case of low uncertainty however the results may be less accurate in the case of high uncertainty.

Using the stochastically updated FE model, structural reliability theory is applied to determine the failure probability and reliability index for the predefined limit state. With the obtained failure probability and reliability index, rational inspection and maintenance strategies can be laid down according to the correspondence between reliability index and required maintenance action established by other researchers. Such a systematic procedure bridges the gap currently existing between structural health monitoring technologies and bridge maintenance and management exercises, and the procedure is also capable of taking into account the uncertainty to make a decision on inspection/maintenance strategies. Following this approach, structural health monitoring is able to provide quantitative information regarding bridge inspection and maintenance. The proposed approach is demonstrated through

numerical studies with respect to the nominal, updated, and actual models of two truss bridges.

A combined method of principal component analysis (PCA) for feature extraction and support vector regression (SVR) for data-based statistical learning is proposed to characterize the correlation between modal frequency and temperatures using one-year monitoring data from the cable-stayed Ting Kau Bridge. The well-defined nature of temperature effects on modal parameters makes it possible to discriminate abnormal modal change caused by structural damage from normal modal change due to temperature variation. Research is focused on the optimal selection of predominant features and SVR hyper-parameters to achieve correlation models with good generalization capability. The performance of the formulated SVR models with the hyper-parameters determined by a grid search method with cross validation and a heuristic method, respectively, is examined. Both the ‘dynamic’ regression model taking into account thermal inertia effect and the ‘static’ regression model without considering thermal inertia effect are formulated and compared. Additionally, the proposed method is compared with the method directly using measurement data to train SVR models and the multivariate linear regression (MLR) method.

A procedure for the assessment of bridge expansion joints making use of long-term monitoring data is developed. Based on the measurement data of expansion joint displacement and bridge temperature, the normal correlation pattern between the effective temperature and thermal movement is first established. Alarms will be raised when a future pattern deviates from this normal pattern. The extreme temperatures for a certain return period are derived using the measurement data for design verification. The annual or daily-average accumulative movements

experienced by expansion joints are then estimated from the monitoring data for comparison with the expected values in design. The proposed procedure is applied to the assessment of expansion joints in the Ting Kau Bridge with the use of one-year monitoring data.

In summary, the research described in this dissertation involves the development of a systematic approach from statistical identification of structural parameters to assessment of component reliability and condition based on long-term monitoring data. This approach enables structural damage identification and monitoring-based reliability assessment to be explored both in a probabilistic framework taking into account uncertainty and randomness inherent in measurement data and structures. Following this approach, structural health monitoring technology can provide quantitative information for bridge managers to enable decision making on the optimization and prioritization of bridge inspection and maintenance.

## LIST OF PUBLICATIONS

### *Journal Articles*

- Y. Q. Ni, X. G. Hua, K. Q. Fan, and J. M. Ko** (2005), “Correlating modal properties with temperature using long-term monitoring data and support vector machine technique”, *Engineering Structures*, Vol. 27, No. 12, 1762-1773.
- Y. Q. Ni, X. G. Hua, and J. M. Ko** (2006), “Reliability-based assessment of bridges using long-term monitoring data”, *Key Engineering Materials*, Vol. 321-323, 217-222.
- X. G. Hua, Y. Q. Ni, J. M. Ko, and K. Y. Wong** (2006), “Modeling of temperature-frequency correlation using combined principal component analysis and support vector regression technique”, accepted to *Journal of Computing in Civil Engineering*, ASCE, in press.
- Y. Q. Ni, X. G. Hua, K. Y. Wong, and J. M. Ko** (2006), “Assessment of bridge expansion joints using long-term displacement and temperature measurement”, accepted to *Journal of Performance of Constructed Facilities*, ASCE, in press.
- X. G. Hua, Z. Q. Chen, Y. Q. Ni, and J. M. Ko** (2006), “Flutter analysis of long-span bridges using ANSYS”, tentatively accepted to *Wind and Structures*, in re-review.
- X. G. Hua, Y. Q. Ni, and J. M. Ko** (2006), “Tikhonov regularization for output-error-based finite element model updating”, submitted to *Computers and Structures*, in review.

**X. G. Hua, Y. Q. Ni, and J. M. Ko** (2006), “Improved perturbation method for statistical identification of structures”, submitted to *Journal of Vibration and Control*, in review.

**Y. Q. Ni, J. M. Ko, X. G. Hua, T. K. Chan, and H. F. Zhou** (2006), “Variability of measured modal frequencies of a cable-stayed bridge under different wind conditions”, invited to *Smart Structures and Systems*, in review.

### ***Conference Papers***

**Y. Q. Ni, X. G. Hua, K. Q. Fan, and J. M. Ko** (2004), “Correlating modal frequency with temperature using long-term monitoring data and support vector machine technique”, *Progress in Structural Engineering, Mechanics and Computation*, A. Zingoni (editor), A.A. Balkema, Rotterdam, Netherlands, 627-633.

**Y. Q. Ni, X. G. Hua, H. F. Zhou, and J. M. Ko** (2004), “Structural health monitoring system for cable-stayed Sutong Bridge”, *Proceedings of the 3rd International Conference on Advances in Structural Engineering and Mechanics*, C. K. Choi, S. H. Kim, and H. G. Kwak (editors), Techno-Press, Daejeon, Korea, 1769-1777.

**Y. Q. Ni, J. M. Ko, H. F. Zhou, and X. G. Hua** (2004), “Challenges in developing structural health monitoring system for a long-span cable-stayed bridge”, *Proceedings of the US-Korea Joint Seminar/Workshop on Smart Structures Technologies*, Techno-Press, Daejeon, Korea, 373-386.

**X. G. Hua, Y. Q. Ni, H. F. Zhou, and J. M. Ko** (2005), “Instrumentation for durability monitoring of a long-span cable-stayed bridge”, *Smart Structures and Materials 2005: Sensors and Smart Structures Technologies for Civil*,

*Mechanical, and Aerospace Systems*, M. Tomizuka (editor), SPIE, Bellingham, WA, Vol. 5765, 982-991.

**X. G. Hua, Y. Q. Ni, and J. M. Ko** (2005), “Characterization of modal variability in Ting Kau Bridge using support vector machine and principal component analysis”, *Structural Health Monitoring 2005: Advancements and Challenges for Implementation*, F. K. Chang (editor), DEStech Publications, Lancaster, PA, 349-357.

**X. G. Hua, J. Kolackova, Y. Q. Ni, and J. M. Ko** (2005), “Condition assessment of expansion joints via long-term displacement measurement”, *Proceedings of the 2nd International Workshop on Advanced Smart Materials and Smart Structures Technology*, C. B. Yun, and B. F. Spencer Jr. (editors), Techno-Press, Daejeon, Korea, 703-713.

**Y. Q. Ni, J. M. Ko, T. K. Chan, and X. G. Hua** (2005), “Variability of measured modal frequencies of a cable-stayed bridge under different wind conditions”, *Proceedings of the 2nd International Workshop on Advanced Smart Materials and Structures Technology*, C. B. Yun, and B. F. Spencer Jr. (editors), Techno-Press, Daejeon, Korea, 613-623.

**X. G. Hua, Y. Q. Ni, and J. M. Ko** (2005), “Probabilistic identification of structural parameters using an integrated perturbation and Bayesian method”, *Structural Health Monitoring and Intelligent Infrastructure*, J. P. Ou, H. Li, and Z. D. Duan (editors), Taylor & Francis, London, Vol. 2, 1021-1027.

**J. M. Ko, X. G. Hua, and Y. Q. Ni** (2006), “Structural damage detection of cable-stayed bridges using change in cable force”, *Proceedings of the 3rd International Workshop on Advanced Smart Materials and Smart Structures Technology*, 29-30 July 2006, Lake Tahoe, CA, USA.

**X. G. Hua, Y. Q. Ni, and J. M. Ko** (2006), “Estimation of probability density function of long-term strain measurement for reliability assessment”, *Proceedings of the 1st Asia-Pacific Workshop on Structural Health Monitoring*, 4-6 December 2006, Yokoham, Japan.

**Y. Q. Ni, K. F. Wat, J. M. Ko, and X. G. Hua** (2006), “Damage evaluation of truss bridges using a reliability-based assessment technique”, *Proceedings of the Asia-Pacific Workshop on Structural Health Monitoring*, 4-6 December 2006, Yokohama, Japan.

## LIST OF FIGURES

<b>Figure</b>	<b>Description</b>	<b>Page</b>
Figure 2.1	Procedure for damage detection and condition assessment .....	2-3
Figure 3.1	Flowchart of sensitivity-based FE model updating .....	3-5
Figure 3.2	A typical L-curve .....	3-20
Figure 3.3	Geometry configuration of truss bridge.....	3-27
Figure 3.4	Finite element model and simulated reduction factors of Young's modulus for truss bridge.....	3-28
Figure 3.5	Condition number versus number of measured modes.....	3-30
Figure 3.6	Plot of discrete SV, and Fourier coefficient (left ordinate) and Picard condition number (right ordinate) when using 4 modes.....	3-31
Figure 3.7	Plot of discrete SV, and Fourier coefficient (left ordinate) and Picard condition number (right ordinate) when using 5 modes.....	3-31
Figure 3.8	Plot of discrete SV, and Fourier coefficient (left ordinate) and Picard condition number (right ordinate) when using 6 modes.....	3-32
Figure 3.9	Plot of discrete regularized SV, and Fourier coefficient (left ordinate) and Picard condition number (right ordinate): (a) using 4 modes; (b) using 5 modes.....	3-33
Figure 3.10	Iteration results of model updating using fixed regularization parameter scheme.....	3-34
Figure 3.11	Iteration results of model updating using adaptive regularization parameter scheme.....	3-34
Figure 3.12	L-curve and its curvature at different iteration steps.....	3-35
Figure 3.13	GCV function at different iteration steps.....	3-37
Figure 3.14	Product function at different iteration steps.....	3-38
Figure 3.15	Four L-curves superimposed with optimal regularization parameters.....	3-39

Figure 3.16	Plot of discrete regularized SV, and Fourier coefficient (left ordinate) and Picard condition number (right ordinate) obtained by GCV method when using 5 modes .....	3-41
Figure 3.17	Relative difference in eigenvalues after model updating by LCM and MPC when using 5 modes .....	3-41
Figure 3.18	L-curve for truncated SVD.....	3-43
Figure 3.19	GCV and product functions for truncated SVD at 1st iteration when using 4 modes.....	3-44
Figure 3.20	GCV function for truncated SVD at different iteration steps when using 4 modes .....	3-45
Figure 3.21	Plot of discrete SV, and Fourier coefficient (left ordinate) and Picard condition number (right ordinate) for noisy data: (a) using 5 modes; (b) using 5 modes; (c) using 6 modes.....	3-48
Figure 3.22	Model updating results with 2% measurement noise for Tikhonov regularization: (a) reduction factor; (b) relative difference in eigenvalues.....	3-52
Figure 3.23	Model updating results with 2% measurement noise for truncated SVD: (a) reduction factor; (b) relative difference in eigenvalues.....	3-53
Figure 3.24	Ratio of consecutive SVs at different iteration steps.....	3-55
Figure 3.25	Comparison of MRE obtained by different methods: (a) using 4 modes; (b) using 5 modes; (c) using 6 modes.....	3-57
Figure 3.26	Comparison of number of divergences for different methods: (a) using 4 modes; (b) using 5 modes; (c) using 6 modes.....	3-58
Figure 4.1	Flowchart of proposed stochastic FE model updating.....	4-6
Figure 4.2	Geometry configuration of statically determinate truss bridge.....	4-19
Figure 4.3	Finite element model and simulated reduction factors of Young's modulus for statically determinate truss bridge.....	4-20
Figure 4.4	Comparison of model updating results using perturbation method for 10% natural randomness: (a) mean of reduction factor; (b) COV.....	4-24
Figure 4.5	Comparison of model updating results using fully-populated covariance matrix and diagonal covariance matrix.....	4-25
Figure 4.6	Variation in mean and COV with respect to trail number of MCS for 10% natural randomness (a) mean of reduction factor; (b) COV.....	4-26
Figure 4.7	Sample sequences of reduction factors in MCS method for 10% natural randomness.....	4-30
Figure 4.8	Probability density functions of reduction factors in MCS method for 10% natural randomness.....	4-33

Figure 4.9	Cumulative density functions of reduction factors in MCS method for 10% natural randomness.....	4-36
Figure 4.10	Comparison of perturbation method and MCS method for 10% natural randomness: (a) mean of reduction factor; (b) COV.....	4-39
Figure 4.11	Comparison of model updating results using perturbation method for 1% measurement noise: (a) mean of reduction factor; (b) COV.....	4-41
Figure 4.12	Modal sensitivities of the first six eigenvalues.....	4-42
Figure 4.13	Variation in mean and COV with respect to trail number of MCS for 1% measurement noise.....	4-43
Figure 4.14	Probability density functions of reduction factors in MCS method for 1% measurement noise.....	4-44
Figure 4.15	Comparison of perturbation method with MCS method for 1% measurement noise.....	4-47
Figure 4.16	Map of probability density function between input and output.....	4-50
Figure 4.17	Relationship between the first six modal frequencies and the first updating parameter.....	4-50
Figure 4.18	Sample sequences, PDFs, and CDFs of elements 1 and 8 for 0.1% measurement noise.....	4-52
Figure 4.19	Variation in mean of reduction factors with respect to noise level: (a) elements 1-10; (b) elements 11-21 .....	4-53
Figure 4.20	Variation in COVs of updating parameters with respect to noise level: (a) elements 1-10; (b) elements 11-21.....	4-54
Figure 4.21	Probability distribution functions of reduction factors at different noise levels: (a) element 1; (b) element 5; (c) element 8.....	4-55
Figure 4.22	Comparison of COVs between perturbation method and MCS method under different noise levels.....	4-56
Figure 4.23	Average relative errors between perturbation method and MCS method.....	4-59
Figure 4.24	Illustration of NSI of eigenvalues and eigenvectors.....	4-62
Figure 4.25	Illustration of NSI of eigenvectors.....	4-62
Figure 4.26	Illustration of ANSI of modal properties: (a) eigenvalues; (b) eigenvectors.....	4-63
Figure 4.27	Illustration of damage sensitivity of modal properties: (a) eigenvalues; (b) eigenvectors.....	4-63
Figure 4.28	Comparison of perturbation method with MCS method for 10% randomness and 1% measurement noise (case study 1): (a) mean of reduction factor; (b) COV.....	4-67
Figure 4.29	Prior, identified, and posterior PDFs of structural parameters: (a) element 1; (b) element 5; (c) element 3; (d) element 21.....	4-71

Figure 4.30	Geometry configuration of statically indeterminate truss bridge.....	4-72
Figure 4.31	Finite element model and simulated reduction factor of Young's modulus for statically indeterminate truss bridge.....	4-73
Figure 4.32	Comparison of perturbation method with MCS method for 10% natural randomness and 1% measurement noise (case study 2): (a) mean of reduction factor; (b) COV.....	4-74
Figure 4.33	Prior, identified and posterior PDF of structural parameters: (a) element 4; (b) element 8; (c) element 16; (d) element 28.....	4-75
Figure 5.1	Safe and failure sets separated by limit-state surface.....	5-5
Figure 5.2	Transformation to standard normal space for a single random variable.....	5-9
Figure 5.3	One-to-one mapping from $\mathbf{x}$ -space to $\mathbf{u}$ -space.....	5-10
Figure 5.4	HL-RF algorithm for finding design point in $\mathbf{u}$ -space.....	5-12
Figure 5.5	Flowchart of FE reliability method.....	5-22
Figure 5.6	Illustration of a planar truss element.....	5-24
Figure 5.7	Illustration of a planar frame element.....	5-24
Figure 5.8	Example of statically determinate truss bridge.....	5-32
Figure 5.9	Variation of reliability index with displacement threshold for statically determinate truss bridge.....	5-32
Figure 5.10	Deformed shape at design point for statically determinate truss bridge.....	5-34
Figure 5.11	Example of statically indeterminate truss bridge.....	5-35
Figure 5.12	Variation of reliability index with displacement threshold for statically indeterminate truss bridge.....	5-36
Figure 5.13	Deformed shape at design point for statically indeterminate truss bridge.....	5-37
Figure 5.14	Dimensionless reliability index sensitivity with respect to distribution parameters for displacement limit state function: (a) mean; (b) standard deviation.....	5-37
Figure 5.15	Dimensionless reliability index sensitivity with respect to means of variables for stress limit state function.....	5-39
Figure 6.1	Probabilistic approach for health monitoring and condition assessment.....	6-5
Figure 6.2	Bridge reliability profile without maintenance and management (after Frangopol <i>et al.</i> 2001).....	6-11
Figure 6.3	Configuration of statically determinate truss bridge.....	6-13

Figure 6.4	Nominal model for statically determinate truss bridge.....	6-13
Figure 6.5	Actual model for statically determinate truss bridge .....	6-14
Figure 6.6	Reliability index profile versus damage level.....	6-17
Figure 6.7	Configuration of statically indeterminate truss bridge.....	6-23
Figure 6.8	Actual model for statically indeterminate truss bridge .....	6-23
Figure 7.1	Flowchart of the combined PCA-SVR method.....	7-5
Figure 7.2	$\varepsilon$ -insensitive loss function for linear SVR.....	7-11
Figure 7.3	Deployment of temperature sensors and accelerometers on Ting Kau Bridge.....	7-19
Figure 7.4	Variation of hourly-average temperatures from 20 temperature sensors.....	7-20
Figure 7.5	Variation of measured modal frequencies: (a) from vertically oriented accelerometers; (b) from laterally oriented accelerometers.....	7-20
Figure 7.6	Modal frequency versus hourly-average temperature: (a) 1st mode; (b) 5th mode.....	7-22
Figure 7.7	MSE versus $C$ and $\gamma$ : (a) $\varepsilon = 0$ ; (b) $\varepsilon = 0.0001$ ; (c) $\varepsilon = 0.0005$ ; (d) $\varepsilon = 0.001$ .....	7-25
Figure 7.8	Minimal MSE versus $\varepsilon$ .....	7-25
Figure 7.9	MSE versus $C$ and $\gamma$ for SVR1: (a) $\varepsilon = 0$ ; (b) $\varepsilon = 0.0001$ ; (c) $\varepsilon = 0.0005$ ; (d) $\varepsilon = 0.001$ .....	7-28
Figure 7.10	MSE versus $C$ and $\gamma$ for SVR2: (a) $\varepsilon = 0$ ; (b) $\varepsilon = 0.0001$ ; (c) $\varepsilon = 0.0005$ (d) $\varepsilon = 0.001$ .....	7-29
Figure 7.11	Minimal MSE versus $\varepsilon$ for SVR1 and SVR2.....	7-29
Figure 7.12	Residual of SVR1 and SVR2.....	7-30
Figure 7.13	Graph of eigenvalues of covariance matrix for temperature data....	7-32
Figure 7.14	Modal frequency versus the first PC: (a) 1st mode; (b) 5th mode...	7-32
Figure 7.15	MSE versus $C$ and $\gamma$ when using 20 PCs: (a) $\varepsilon = 0$ ; (b) $\varepsilon = 0.0001$ ; (c) $\varepsilon = 0.0005$ ; (d) $\varepsilon = 0.001$ .....	7-33
Figure 7.16	Dependency between optimal $C$ and $\gamma$ for $\varepsilon = 0$ .....	7-34
Figure 7.17	Minimal MSE versus $\varepsilon$ when using 20 PCs.....	7-35
Figure 7.18	Residual of SVR model and MLR model: (a) optimal SVR model; (b) linear SVR model with extremely large $C$ and zero $\varepsilon$ .....	7-37
Figure 7.19	Comparison between predicted and observed modal frequencies...	7-38
Figure 7.20	Probability distribution of residual: (a) PDF; (b) CDF.....	7-40

Figure 8.1	Ting Kau Bridge: (a) elevation; (b) cross-section.....	8-11
Figure 8.2	Layout of sensors on Ting Kau Bridge: (a) displacement transducer at Tsing Yi abutment; (b) temperature sensors on deck cross-section.....	8-12
Figure 8.3	Hourly-average temperatures on deck cross-section: (a) in structural steel; (b) in structural concrete; (c) in atmosphere; (d) in asphalt.....	8-13
Figure 8.4	Hourly-average displacements of expansion joints.....	8-14
Figure 8.5	Time histories of displacement and effective temperature.....	8-15
Figure 8.6	Measured and fitted relations between displacement and effective temperature: (a) at the Ting Kau abutment; (b) at the Tsing Yi abutment.....	8-17
Figure 8.7	Sequence of measured effective temperatures.....	8-18
Figure 8.8	Sequences of measured maximum and minimum effective temperatures: (a) maximum temperature; (b) minimum temperature.....	8-19
Figure 8.9	Measured and fitted relations between extreme temperature and reduced variate $R$ : (a) maximum temperature; (b) minimum temperature.....	8-19
Figure 8.10	Instantaneous displacements of expansion joints.....	8-20
Figure 8.11	Accumulative displacements of expansion joints .....	8-21

## LIST OF TABLES

<b>Table</b>	<b>Description</b>	<b>Page</b>
Table 3.1	Comparison of ‘experimental’ and analytical eigenvalues.....	3-29
Table 3.2	Comparison of model updating results using noise-free data.....	3-42
Table 3.3	Summary of truncation parameter at different iteration steps.....	3-44
Table 3.4	Model updating results using truncated SVD.....	3-46
Table 3.5	Model updating results when using 4 modes with 1% measurement noise for Tikhonov regularization.....	3-49
Table 3.6	Model updating results when using 5 modes with 1% measurement noise for Tikhonov regularization.....	3-50
Table 3.7	Model updating results when using 6 modes with 1% measurement noise for Tikhonov regularization.....	3-51
Table 3.8	Model updating results using modal properties with 1% measurement noise for truncated SVD.....	3-54
Table 4.1	ARE of mean and standard deviation of updating parameters.....	4-22
Table 4.2	Comparison of MCS results with the simulated exact values.....	4-28
Table 4.3	Summary of normalized sensitivity index and average normalized sensitivity index.....	4-64
Table 4.4	Comparison of MCS method with perturbation method for three cases.....	4-68
Table 4.5	Summary of prior, identified, and posterior distribution parameters.....	4-70
Table 5.1	Failure probability and reliability index for example 1 ( $p_f \times 10^{-3}$ )....	5-28
Table 5.2	Sensitivities of failure probability and reliability index with respect to distribution parameters.....	5-29
Table 5.3	Failure probability and reliability index when following type I EVD for the largest value ( $p_f \times 10^{-3}$ ).....	5-29

Table 5.4	Distribution type and its parameters .....	5-30
Table 5.5	Failure probability and reliability index results ( $p_f \times 10^{-1}$ ).....	5-30
Table 5.6	Comparison of mean-value point and design point.....	5-33
Table 5.7	Sensitivities of failure probability and reliability index with respect to distribution parameters.....	5-34
Table 5.8	Comparison of mean-value point with design point for displacement and stress limit states.....	5-38
Table 6.1	Relation between reliability index and maintenance action.....	6-11
Table 6.2	Failure probability for displacement limit state (case 1).....	6-16
Table 6.3	Failure probability for displacement limit state (case 2).....	6-18
Table 6.4	Failure probability for displacement limit state.....	6-22
Table 6.5	Failure probability for stress limit state.....	6-22
Table 7.1	Statistics of identified modal frequencies.....	7-22
Table 7.2	Heuristic optimal values of SVR hyper-parameters.....	7-26
Table 7.3	Eigenvalues of covariance matrix for temperature data.....	7-31
Table 7.4	Comparison of MSE values for different PCs.....	7-36
Table 7.5	Residual statistics and hypothesis test results.....	7-40
Table 8.1	Statistical parameters in regression analysis.....	8-16
Table 8.2	Identified Gumbel parameters for extreme temperature prediction...	8-19

## LIST OF ABBREVIATIONS

<b>Abbreviation</b>	<b>Description</b>
AMI	Analytical model improvement
ANN	Artificial neural network
ANSI	Average normalized sensitivity index
ARE	Average relative error
ARMA	Auto-regressive and moving average
BMMS	Bridge maintenance and management system
BRV(s)	Basic random variable(s)
CDF	Cumulative density function
CIS	Civil infrastructure system
CMIF	Complex modal indication function
COMAC	Coordinate modal assurance criterion
COV(s)	Coefficient of variation(s)
CSP	Change in structural parameters
DDM	Direct differentiation method
DLAC	Damage location assurance criterion
DLV	Damage localization vector
DOF(s)	Degree of freedom(s)
DPC	Discrete Picard condition
EEQ	Element energy quotient
ERM	Empirical risk minimization
EVA	Extreme value analysis
EVD	Extreme value distribution
FDM	Finite difference method

FE	Finite element
FERM	Finite element reliability method
FORM	First order reliability method
FOSM	First order second moment
GCV	Generalized cross validation
HL-RF	Hasofer-Lind and Rackwitz-Fiessler
KKT	Karush-Kuhn-Tucker
KMA	Stiffness $K$ matrix adjustment
LCM	L-curve method
MAC	Modal assurance criterion
MCS	Monte Carlo simulation
MLR	Multivariate linear regression
MRPT	Minimum rank perturbation theory
MSECR	Modal strain energy change ratio
MRE	Mean of relative error
MSE	Mean squared error
NDE	Non-destructive evaluation
NSI	Normalized sensitivity index
PC(s)	Principal component(s)
PCA	Principal component analysis
PDF(s)	Probability density function(s)
PM	Projector matrix
PSFEM	Perturbation-based stochastic finite element method
QP	Quadratic programming
SC	Stiffness coefficient
SHM	Structural health monitoring
SMO	Sequential minimal optimization
SORM	Second order reliability method
SOSM	Second order second moment
SRF	Stiffness reduction factor
SRM	Structural risk minimization

STREC	Structural translational and rotational error checking
SV(s)	Singular value(s)
SVD	Singular value decomposition
SVM	Support vector machine
SVR	Support vector regression
ULS	Uniform load surface

# CONTENTS

DECLARATION	Page i
ACKNOWLEDGEMENTS	ii
ABSTRACT	iii
LIST OF PUBLICATIONS	vii
LIST OF FIGURES	xi
LIST OF TABLES	xvii
LIST OF ABBREVIATIONS	xix

## **CHAPTER 1 INTRODUCTION.....1-1**

1.1	Research Motivation.....	1-1
1.2	Research Objectives.....	1-5
1.3	Outline of the Thesis.....	1-7

## **CHAPTER 2 LITERATURE REVIEW.....2-1**

2.1	General Concepts and Overview.....	2-1
2.1.1	Classification of structural damage detection.....	2-3
2.1.2	Static- versus vibration-based methods.....	2-4
2.2	Damage Index Methods.....	2-6
2.2.1	Methods using modal frequencies.....	2-7
2.2.2	Methods using modal shapes.....	2-11
2.2.3	Methods using curvature/strain modes.....	2-14
2.2.4	Methods using modal strain energy.....	2-16
2.2.5	Methods using modal flexibility.....	2-18
2.3	Model Updating Methods.....	2-23
2.3.1	Optimal matrix updating methods.....	2-26
2.3.2	Eigenstructure assignment methods.....	2-35
2.3.3	Sensitivity-based updating methods.....	2-38
2.3.4	Stochastic model updating methods.....	2-46
2.3.5	Regularization methods.....	2-51
2.4	Critical Issues and Shortcomings in Existing Methods.....	2-57

**CHAPTER 3 REGULARIZATION METHODS FOR FE  
MODEL UPDATING AND DAMAGE  
DETECTION..... 3-1**

3.1	Introduction.....	3-1
3.2	Output-Error-Based Model Updating Method.....	3-4
3.2.1	Objective function.....	3-4
3.2.2	Mode shape paring.....	3-7
3.3.3	Sensitivity analysis of modal properties.....	3-8
3.3.4	Solution of nonlinear least squares problem.....	3-9
3.3	Regularization Techniques.....	3-10
3.3.1	Ill-conditioning of least squares problem.....	3-11
3.3.2	Tikhonov regularization.....	3-14
3.3.3	Truncated singular value decomposition.....	3-16
3.4	Determination of Regularization Parameter.....	3-17
3.4.1	L-curve method.....	3-19
3.4.1.1	Curvature computation by FDM.....	3-21
3.4.1.2	Curvature computation by DDM.....	3-22
3.4.2	Generalized cross validation.....	3-23
3.4.3	Minimum product criterion.....	3-26
3.5	Numerical Examples.....	3-27
3.5.1	Illustration of ill-conditioning.....	3-29
3.5.2	Model updating using noise-free data.....	3-32
3.5.2.1	Tikhonov regularization.....	3-33
3.5.2.2	Truncated SVD.....	3-43
3.5.3	Model updating using noise-corrupted data.....	3-47
3.5.3.1	Tikhonov regularization.....	3-47
3.5.3.2	Truncated SVD.....	3-51
3.5.3.3	Comparison of different method combinations.....	3-55
3.6	Summary.....	3-59

**CHAPTER 4 A NOVEL APPROACH FOR STOCHASTIC  
FE MODEL UPDATING..... 4-1**

4.1	Introduction.....	4-1
4.2	First-Stage Stochastic FE Model Updating.....	4-5

4.2.1	Basis of FE model updating.....	4-5
4.2.2	First-order perturbation method.....	4-8
4.2.3	Computational issues.....	4-14
4.3	Bayesian Updating for Determination of Posterior Distribution.....	4-15
4.4	Case Study 1: A Statically Determinate Truss Bridge.....	4-18
4.4.1	Uncertainty due to natural randomness.....	4-20
4.4.1.1	Stochastic model updating using perturbation method.....	4-21
4.4.1.2	Stochastic model updating using MCS method.....	4-27
4.4.2	Uncertainty due to measurement noise.....	4-39
4.4.2.1	Stochastic model updating using perturbation method.....	4-40
4.4.2.2	Stochastic model updating using MCS method.....	4-42
4.4.2.3	Effect of uncertainty level.....	4-51
4.4.2.4	Effect of random modal properties.....	4-59
4.4.3	Uncertainty due to measurement noise and natural randomness.....	4-66
4.4.3.1	Stochastic model updating using perturbation and MCS methods.....	4-66
4.4.3.2	Second-stage Bayesian updating.....	4-69
4.4	Case Study 2: A Statically Indeterminate Truss Bridge.....	4-71
4.5	Summary.....	4-75

**CHAPTER 5 DEVELOPMENT OF COMPUTER CODE FOR LINEAR FE RELIABILITY ANALYSIS..... 5-1**

5.1	Introduction.....	5-1
5.2	First- and Second-Order Reliability Methods.....	5-3
5.2.1	Fundamentals of structural reliability.....	5-3
5.2.2	Transformation to standard normal space.....	5-6
5.2.3	Determination of design point.....	5-10
5.2.4	First-order reliability method.....	5-13
5.2.5	Second-order reliability method.....	5-14
5.2.6	Parameter sensitivity measures.....	5-19
5.3	Linear FE Reliability Analysis Method.....	5-21

5.3.1	Computation of response.....	5-22
5.4.2	Computation of response gradient.....	5-25
5.4	Numerical Examples.....	5-26
5.4.1	Example 1: reliability for a linear limit-state function.....	5-27
5.4.2	Example 2: reliability for a nonlinear limit-state function...	5-30
5.4.3	Example 3: reliability for a statically determinate truss.....	5-31
5.4.4	Example 4: reliability for a statically indeterminate truss.....	5-35
5.5	Summary.....	5-40

**CHAPTER 6 RELIABILITY-BASED CONDITION ASSESSMENT OF BRIDGES USING STOCHASTIC FE MODEL UPDATING RESULTS..... 6-1**

6.1	Introduction.....	6-1
6.2	Probabilistic Approach for Health Monitoring and Condition Assessment.....	6-4
6.2.1	Stochastic FE model updating.....	6-5
6.2.2	Structural reliability evaluation.....	6-7
6.2.3	Decision making on maintenance.....	6-10
6.3	Applications.....	6-12
6.3.1	Example 1: a statically determinate truss bridge.....	6-12
6.3.2	Example 2: a statically indeterminate truss bridge.....	6-18
6.4	Summary.....	6-23

**CHAPTER 7 MODELLING OF TEMPERATURE-FREQUENCY CORRELATION USING COMBINED PCA AND SVR TECHNIQUE..... 7-1**

7.1	Introduction.....	7-1
7.2	Presentation of Method.....	7-4
7.2.1	Overview of combined PCA and SVR method.....	7-4
7.2.2	PCA for extracting feature vectors.....	7-6
7.2.3	SVR for data-based statistical learning.....	7-9
7.2.4	Determination of SVR hyper-parameters.....	7-16
7.3	Experimental Data.....	7-18
7.3.1	Measurement data of temperature.....	7-19

7.3.2	Measurement data of modal frequency.....	7-21
7.4	Model Development.....	7-23
7.4.1	Training and validation using original data.....	7-23
7.4.2	SVR model considering thermal inertia effect.....	7-27
7.4.3	PCA-based compression of temperature data.....	7-30
7.4.4	Training and validation using PCA-compressed data.....	7-32
7.4.5	Comparison between SVR and MLR models.....	7-36
7.4.5	Assessment of model performance.....	7-38
7.5	Summary.....	7-41

**CHAPTER 8 ASSESSMENT OF BRIDGE EXPANSION JOINTS USING LONG-TERM DISPLACEMENT AND TEMPERATURE MEASUREMENT..... 8-1**

8.1	Introduction.....	8-1
8.2	Presentation of Procedure.....	8-3
8.2.1	Establishment of normal correlation pattern.....	8-3
8.2.2	Prediction of extreme temperatures.....	8-7
8.2.3	Estimation of accumulative displacements.....	8-9
8.3	Application to Ting Kau Bridge.....	8-10
8.3.1	Measurement data.....	8-10
8.3.2	Analysis and assessment.....	8-14
8.4	Summary.....	8-21

**CHAPTER 9 CONCLUSIONS AND RECOMMENDATIONS 9-1**

9.1	Conclusions.....	9-1
9.2	Recommendations.....	9-7

**REFERENCES..... Ref.-1**

**APPENDIX I..... A-1**

# Chapter 1

## INTRODUCTION

### 1.1 Research Motivation

Civil infrastructure systems (CIS) deteriorate with time and continuously accumulate damage throughout their service life due to material deterioration, human error, and natural hazards such as earthquakes, storms, fires, long-term fatigue and corrosion. Such damage left undetected and uncorrected could potentially cause more damage and eventually lead to catastrophic structural failure with loss of human life. In order to ensure the serviceability and safety of structures, structural damage detection is necessary at the earliest possible stage. Collected data would not only indicate potential damage arising from the detected damage, it would also be of essential value to the bridge authorities enabling faster and safe decisions on whether or not repair, partial replacement or demolition is necessary. Such information on structural damage is particularly crucial in cases of both severe natural hazards and long-term usage.

Bridges are vital components of transportation infrastructure systems. They are important not only because of their representation of large capital investment, but also because of the cost implications if their capacity is impaired or if they fail to function. However, bridges cannot last forever. Whatever form of construction is

used and whatever materials adopted, sooner or later the effects of degradation appear. The contributory factors which affect the nature and degree of degradation and damage include inadequate maintenance, excessive loading, and adverse environmental conditions. The material deterioration and structural damage could make bridge components unserviceable and finally even might lead to collapse of bridge if damage develops to a significant level. Failures of important bridge components and even collapse of bridge arising from such as improper design and consideration, lack of inspection and maintenance, natural and man-made disasters have been widely addressed and acknowledged in the literature by the bridge engineering community (Shepherd and Frost 1995; Wang *et al.* 2002). A notable example is the failure of Ashtabula Bridge in 1876 attributed to the passage of a high-speed train during severe storm, approximate eighty deaths were caused. Investigation showed that this failure resulted from buckling and fracture of critical members due to lack of inspection and maintenance.

The increasing demand for and interest in the ability to monitor a bridge structure and detect the onset of structural damage at the earliest possible stage, as a result of such catastrophic structural failure, has led to the development of a variety of damage detection methods. The approaches to detection, localization, and quantification of damage in structural systems are, in general, divided into two categories: local nondestructive evaluation (NDE) and global structural health monitoring (SHM). The former uses either visual inspection or nondestructive testing to examine the local properties of a structure, such as fatigue cracks in steel, corrosion of steel, and deterioration of concrete; while SHM explores the concept of system identification in which an analytical structural model and the measured response are combined via a parameter estimation procedure (Liu and Yao 1978;

Aktan *et al.* 1997). First category methods prevalent in the current bridge management and maintenance system (BMMS) have been proven inefficient for large-scale bridges, as they require the vicinity of damage to be known *a priori* and the portion of structures inspected to be readily accessible. Furthermore, execution of these methods in such situations is expensive, time consuming, and labour intensive. The most significant challenge for any local NDE technologies is the difficulty in directly relating the testing results to the global condition of the bridge in question for the purpose of maintenance and management.

The need for global and cost-effective damage detection methods suitable to large-scale bridges has led to the development of structural health monitoring technologies and research into damage detection methods that examine changes in the global characteristics of structures due to damage. Among various damage detection methods, the vibration-based ones are the most widely studied. Vibration-based damage detection methods for detecting, localizing, and characterizing the structural damage work based on the fact that changes in physical properties, such as mass, stiffness and boundary conditions, give rise to changes in dynamic properties. Therefore the monitoring and examination of changes in these dynamic properties allows the assessment of structural damage. SHM, in short, monitors and measures these changes either periodically or continuously throughout the lifecycle of a structure for the subsequent tracking and assessment of damage, condition, and health of the structure by integrating recent advances in sensing, data acquisition, computing, communication, and data and information management technology.

Because of the great promise shown by SHM in damage detection and condition assessment of structures, on-structure instrumentation systems have been

implemented on bridges worldwide (Andersen and Pedersen 1994; Cheung *et al.* 1997; Barrish *et al.* 2000; Sumitro *et al.* 2001; Mufti 2002; Koh *et al.* 2003; Wang *et al.* 2003; Wong 2004; Ko and Ni 2005; Ou and Li 2005; Wang 2005). So far over 40 long-span bridges (more than 100 m main span) have been instrumented with SHM systems (Ni and Hua 2004). These systems continuously collect the measurement data regarding the health and condition of bridges and attempt to detect significant changes in structural properties. Although the underlying philosophy of vibration-based damage detection appears intuitive and considerable research efforts have been devoted to it in recent years, assessing structural damage in large-scale bridges remains still a challenging task. The main pitfalls limiting the practical applicability of vibration-based damage detection methods include the insensitivity of modal properties to local damage of bridge structures, uncertainty and incompleteness in measurement data, modal variability arising from varying operational and environmental conditions, and modelling errors in the analytical model. The insensitivity of modal properties and the incompleteness of measurement data generally lead to the ill-conditioning of model updating and damage detection problems, where small measurement noises could be magnified. Furthermore, the uncertainty in the measured modal properties could give rise to damage identification results that are affected by both structural damage and measurement noise, and therefore requires probabilistic approaches for model updating and damage detection. Most importantly, as model updating or damage detection in itself is not an end, a gap between health monitoring technologies and bridge inspection, management and maintenance exercises currently exists which impedes bridge managers benefiting from the monitoring systems.

Stimulated by the deficiencies stated above, the aim of the present study is to develop a unified probabilistic approach for health monitoring and condition assessment of bridge structures. This approach starts with the statistical identification of structural parameters from the measured uncertain modal properties, and is capable of dealing with the ill-conditioning arising from parameter identification and model updating. Based on the statistical identification results, structural reliability analysis is then performed to obtain the reliability index and failure probability of the damaged structure. Next, the proposed approach utilizes the established correspondence between reliability index and required maintenance action to make a rational decision on maintenance and management exercise. Following this approach, health monitoring technology can provide the evidence for maintenance exercise and bridge managers can eventually benefit from monitoring systems. Besides the proposed probabilistic approach, methodologies for interpreting real measurement data from monitoring systems, which are imperative for bridge condition assessment, are also addressed.

## **1.2 Research Objectives**

The aim of this research is to study vibration-based damage detection and structural reliability evaluation, modelling of temperature-frequency correlations, and condition assessment of expansion joints of bridge structures by using the monitoring data. The specific objectives of this research are:

- (1) To investigate the regularization methods for treatment of the ill-conditioning in output-error-based FE model updating from the measured modal properties. Two

regularization methods will be addressed with the research emphasis on optimization of their regularization parameters.

- (2) To develop a method, consistent with structural reliability analysis, for statistical identification of structural parameters (and therefore for probabilistic damage detection) using measured uncertain modal parameters. The method should also be capable of accounting for both the knowledge and confidence about the measurement data from experimentalists and about the FE model from structural analysts.
- (3) To propose a systematic approach for linking health monitoring technologies with bridge inspection/maintenance exercises. The envisaged approach will begin with stochastic finite element (FE) model updating. Then it is intended to combine the stochastically updated model with structural reliability analysis to determine reliability indices. Finally this approach will proceed to decision making on maintenance strategies according to the established correspondence between reliability index and required maintenance action.
- (4) To develop a program for linear FE reliability analysis which is able to compute the failure probability for both explicitly and implicitly given limit state functions. The developed program should also be capable of dealing with various distributions of random variables and incorporating most commonly used methods for structural reliability analysis.
- (5) To experimentally formulate a nonlinear regression model characterizing the temperature-frequency correlation for damage detection using long-term monitoring data. A method of combining principal component analysis (PCA)

and support vector regression (SVR) technique will be developed for modelling the temperature-frequency correlation.

- (6) To propose a procedure for condition assessment of bridge expansion joints based on long-term monitoring data. The procedure is intended to pursue the establishment and checking of the temperature-displacement pattern and the prediction and verification of the maximum displacement range, extreme temperature and accumulative movement.

### **1.3 Outline of the Thesis**

This dissertation comprises nine chapters, and is organized as follows.

Chapter 1 introduces the motivation for the present research and expounds the objective to be pursued in this PhD project.

Chapter 2 contains a review of the literature on four topics: damage index methods for damage localization, FE model updating methods, stochastic FE model updating methods, and regularization methods for FE model updating. After an introduction to the general concept and overview of structural damage detection, damage index methods that utilize modal properties before and after structural damage to synthesize damage indices for damage localization are surveyed. Subsequently various FE model updating methods for both model refinement and damage detection applications are reviewed. These methods include optimal matrix updating methods, eigenstructure assignment methods, sensitivity-based updating methods, statistical methods for model updating, and regularization methods used in model updating

algorithms. In the end, a discussion on critical issues and shortcomings related to the existing methods is provided.

Chapter 3 focuses on regularization methods for the solution of the ill-conditioned and noisy system of equations in the context of output-error-based model updating. First, the theoretical framework for model updating is presented on the basis of minimization of the discrepancies between analytical modal properties and experimental ones. Tikhonov regularization and truncated singular value decomposition (SVD) are implemented at each linearized step of the nonlinear optimization problem to alleviate the ill-conditioning. Three approaches to the optimal choice of regularization parameters in Tikhonov regularization and truncated SVD are presented. Intensive numerical studies in regard to a truss bridge are performed to assess the effectiveness and robustness of two regularization methods in combination with the optimization procedure of regularization parameters.

In Chapter 4, a method for statistical identification of structural parameters is proposed. The approach pursues a two-stage model updating scheme. The first stage model updating refers to the identification of the probability density functions (PDFs) of updating parameters from measured uncertain modal properties; the second stage updating deals with the determination of the posterior PDFs from the identified PDFs and the prior PDFs of structural parameters. The first-stage stochastic model updating is accomplished by integrating uncertainty-propagation approaches with conventional FE model updating algorithms, in which an improved perturbation method and the Monte Carlo simulation (MCS) method are used to obtain the PDFs of updating parameters. At the second-stage updating, the statistically identified structural parameters incorporate the prior distribution of updating structural

parameters, if available, by means of the Bayesian theory to achieve the posterior distribution. Two numerical examples are provided to demonstrate and verify the proposed method. The stochastically updated structural parameters are further used for subsequent probabilistic structural analysis and reliability evaluation in order to assess the impact of damage on structural performance and safety as described in Chapter 6.

In Chapter 5, a computer program for linear FE reliability analysis is developed. The developed program is able to compute the failure probability for explicitly and implicitly given limit-state functions. It is capable of dealing with various distributions of random variables and incorporating most commonly used methods for structural reliability analysis. Numerical examples are provided to demonstrate the reliability analysis and to verify the developed code. The achievement in this chapter indeed paves the way for reliability-based condition assessment of existing structures by using the stochastic model updating results given in Chapter 4.

In Chapter 6, a systematic approach is explored, which bridges the gap currently existing between health monitoring technologies and bridge maintenance and management exercises. As consistent with structural reliability analysis, this unified approach begins with the statistical identification of structural parameters using monitoring data as addressed in Chapter 4, and proceeds to the determination of reliability index on the basis of the statistical identification results and FE reliability analysis. This approach finally makes use of the established correspondence between reliability index value and required maintenance action to decide maintenance/repair strategy. Following the proposed approach, the structural health monitoring system is capable of providing quantitative information for bridge inspection and maintenance.

Two examples are provided to demonstrate this approach, and for each example the reliability indices and failure probabilities computed from the nominal, updated, and actual models are compared.

In Chapter 7, a combined method of principal component analysis (PCA) and support vector regression (SVR) is proposed to characterize the temperature-frequency correlation using long-term monitoring data. The philosophies of principal component analysis for predominant feature extraction and support vector regression for data-based statistical learning are presented. Research effort has been made on selecting appropriate temperature feature vectors and determining the optimal SVR hyper-parameters to achieve correlation models with good generalization capability. A grid search method with cross validation and a heuristic method are applied to determine the optimal values of SVR hyper-parameters. Making use of one-year monitoring data from the cable-stayed Ting Kau Bridge, the proposed method is compared with the method directly using measurement data to train SVR models and the multivariate linear regression (MLR) method. In addition, both the ‘dynamic’ regression model taking into account thermal inertia effect and the ‘static’ regression model without considering thermal inertia effect are examined in terms of their generalization performance.

In Chapter 8, a procedure is presented for design verification and condition assessment of bridge expansion joints making use of long-term monitoring data. The normal correlation pattern between the effective temperature and thermal movement is first established with the use of expansion joint displacement and bridge temperature monitoring data. Alarms will be raised if a future pattern deviates from this normal pattern. With the established correlation pattern, the expansion joint

displacements under the design maximum and minimum temperatures are predicted and compared with the design allowable values for validation. The extreme temperatures for a certain return period are also derived for design verification. Then the annual or daily-average accumulative movements experienced by expansion joints are estimated using the monitoring data, which provide a basis for decision making on inspection or replacement of expansion joints. The proposed procedure is applied to the assessment of expansion joints in the cable-stayed Ting Kau Bridge with the use of one-year monitoring data.

Chapter 9 summarizes the contributions, findings and conclusions achieved from both the theoretical and experimental studies in this PhD project. Recommendations for future work are also presented.

## Chapter 2

### LITERATURE REVIEW

#### 2.1 General Concepts and Overview

The interest in the ability to monitor a structure and detect damage at the earliest possible stage is pervasive, and damage detection has firmly established itself as a prominent concern in civil, mechanical, and aerospace engineering communities. The traditional damage detection methods include visual inspection and localized nondestructive evaluation (NDE) such as radiographic, X-ray, acoustic emission, eddy current, and ultrasonic techniques. All these techniques require that the damage locations are known *a priori* and the vicinity of damage regions or the portions of structures to be inspected are readily accessible. Subject to these deficiencies, the above methods can only detect damage on or near the surface of structures. In addition, these methods are inefficient when applied to large and complex structures. The need for global damage detection methods that can be applied to large and complex structures, such as cable-supported bridges, high-rise buildings, and offshore platforms, has led to the development and continued research of methods that examine changes in the global characteristics of structures (Doebbling *et al.* 1998).

The underlying premise of the damage detection methods based on changes in global dynamic characteristics is that modal parameters of a structure are functions of the physical parameters (mass, damping and stiffness) of the structure. As a result, changes in these physical parameters, such as reduction in stiffness resulting from the onset of cracks or loosening of a connection, will cause changes in vibration characteristics of the structure such as modal properties. Therefore, measuring and monitoring these changes allows the evaluation of occurrence, localization, and severity of structural damage.

A typical procedure for damage detection and condition assessment of an existing structure based on vibration measurement is outlined in **Figure 2.1**. First, the responses of structure under ambient excitations are measured, and modal properties are extracted through experimental modal analysis. Then the extracted modal properties are combined with an initial FE model of the structure to achieve an updated FE model by means of model updating; a comparison of the updated model with the *baseline* FE model indicates the information on structural damage. The accomplishment of this step requires the integration of experimental techniques and analytical arts and has been widely addressed in literature (Aktan *et al.* 1997). Next, the updated FE model is further utilized to determine the safety and reliability of the structure (possibly damaged) for the predefined limit states under the expected future loadings. Finally, the resulting failure probability, reliability index, or the remaining load-carrying capacity is combined with the economical considerations to make decision on inspection and maintenance strategies. When combined with long-term

structural health monitoring, the procedure is able to continuously track the health, condition, as well as reliability of structures through the effective utilization of the continuously and reliably measured monitoring data.

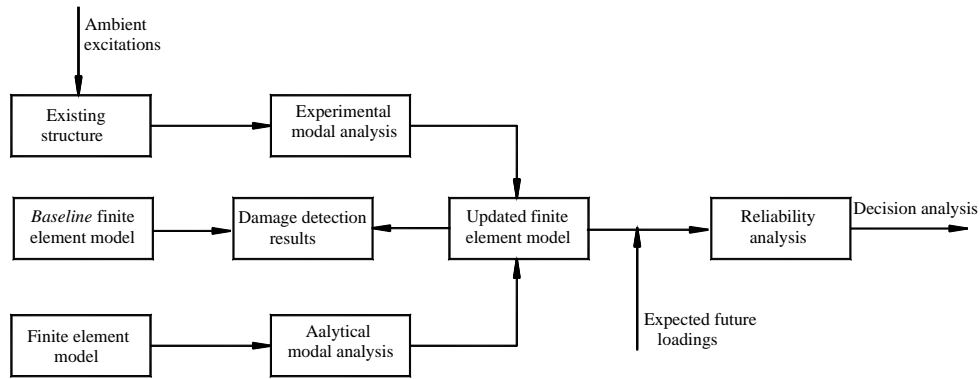


**Figure 2.1 Procedure for damage detection and condition assessment**

### 2.1.1 Classification of Structural Damage Detection

Depending on the classification criteria used, the existing damage detection approaches can be categorized into various types. According to the amount of information provided regarding the damage state, the damage detection approaches can be classified into four levels, namely (Rytter 1993):

- Level 1: Determination of the occurrence of structural damage
- Level 2: Localization of structural damage if damage has occurred
- Level 3: Quantification of the severity of damage
- Level 4: Evaluation of the impact of damage on structure performance

Most of the damage detection methods developed to date limit themselves to Level 1 to Level 3. Level 4 methods require the knowledge associated with the disciplines

such as structural design, fracture mechanics and structural reliability, and are still very limited (Yao and Natke 1994; Park *et al.* 1997; Stubbs *et al.* 2000; Xia and Brownjohn 2003).

### **2.1.2 Static- versus Vibration-Based Methods**

According to the type of measurement data used, damage detection methods can also be classified as the static-based methods and the vibration-based methods. The commonly used vibration-based methods assess structural damage based on the measured changes in modal properties before and after damage occurrence. As the modal properties can be identified through vibration testing, the vibration-based methods are therefore showing great promise for on-line SHM and have been extensively studied.

Similarly, the static-based methods for damage detection are based on the premise that changes in stiffness of a structure will give rise to changes in displacements or strains of the structure. Likewise, monitoring and measuring these changes under designated loading cases allow the evaluation of changes in structural stiffness. However, as it requires simultaneous measurement of the applied loads and the resulting static responses being either displacements (Sanayei and Onipede 1991; Banan *et al.* 1994a, b; Hjelmstad and Shin 1997; Yeo *et al.* 2000) or strains (Sanayei and Saletnik 1996a, b; Liu and Chian 1997; Mehrabi *et al.* 1998), the traditional static-based methods might not be suitable for on-line SHM. Recently, Ko *et al.* (2006) proposed a static-based method that is particularly suited for the damage

detection of cable-stayed bridges. In recognition that the redistribution of dead load effects will take place when damage occurs for a statically indeterminate structure (there would be no redistribution of internal forces for statically determinate structures), the method uses the measured changes in cable forces to implement the damage detection in bridge girders. Shenton and his co-workers (Hu and Shenton 2003; Zhao and Shenton 2005) have also developed a similar approach independently.

The research area of damage detection is very broad and encompasses a variety of techniques ranging from the simple and straightforward comparison of damage index to the complicated statistical pattern recognition algorithms such as artificial neural networks (ANNs) and support vector machines (SVMs). Doebling *et al.* (1998) and Sohn *et al.* (2004) presented a comprehensive review of the existing global damage detection methods. Other review papers include those of Mottershead and Friswell (1993) who extensively surveyed the model updating methods and the accessory techniques, Carden and Fanning (2004) who summarized the state-of-the-art in vibration-based condition monitoring with the emphasis on structural engineering applications. The scope of literature review in this chapter will limit itself to the damage index methods and the model updating methods using modal data. The signal-based methods such as wavelet methods and recently developed empirical mode decomposition, which show promise for damage alarming but usually lack the capability in relating to damage magnitudes, are excluded from this review. ANN-

and SVM-based methods, which generally require a large amount of data regarding various damage states of a structure and have proven satisfactory for fault detection of rotating machinery but may become incompetent for civil applications, are also precluded from this review.

In what follows, a survey of the damage index methods for damage localization directly using modal parameters from pre-damage and post-damage structures, respectively, is first presented. Then a review of the model updating methods both for damage detection and model refinement applications and the algorithms for treating the ill-conditioning problem in model updating is provided. Finally, some critical issues and shortcomings in the existing methods are discussed from the writer's perspective.

## **2.2 Damage Index Methods**

Making use of the measured modal properties of a structure at both intact and damage stages, the damage index methods seek to synthesize an appropriate damage indicator for damage localization. Modal properties of the intact structure can be either extracted from testing data or simulated from the analytical FE model that has been correlated to testing results of the intact structure; the measured modal properties can be acquired by testing the structure at different stages throughout its service life. The damage index methods are relatively simple and straightforward, and do not require complex computations. However, these methods generally do not provide the information regarding damage severity. Nevertheless, damage

localization is an important step in damage detection; after doing so, other techniques, such as local NDE techniques and model updating methods, can be subsequently applied for damage quantification.

According to the type of modal properties used to synthesize damage indicators, the existing damage index methods may be roughly classified into the following five categories: (i) methods using modal frequencies; (ii) methods using mode shapes; (iii) methods using curvature or strain modes; (iv) methods using modal strain energy; and (v) methods using modal flexibility.

### ***2.2.1 Methods Using Modal Frequencies***

The vibration-based damage detection methods were initiated from the observation that changes in structural properties give rise to changes in modal frequencies. Modal frequencies can be more cheaply and reliably obtained from dynamic testing than other modal quantities, and the most direct damage detection methods are those using changes in modal frequencies. Furthermore, it is widely recognized that modal frequencies are least contaminated by measurement noise and can be generally measured with good accuracy. The amount of literature addressing damage detection using changes in modal frequencies is quite large (Salawu 1997). There are two types of methods. In the first type of methods, the damage detection problem is treated as a forward problem, where the patterns of measured frequency changes are compared with those of analytical frequency changes for all possible damage cases and then the damage case which produces the best match to the measured frequency changes is

regarded as the suspect one. This type of methods takes the advantage that some patterns of measured frequency changes are the function of damage location only. The second type of methods, which essentially is the model updating methods, deals with damage detection as an inverse problem and is able to calculate both damage location and damage magnitude.

Cawley and Adams (1979) treated damage detection as a forward problem and proposed a formula for the localization of structural damage using changes in modal frequencies. In their method, the change in the natural frequency of mode  $i$  of a structure due to local damage,  $\delta\omega_i$ , is expressed as a function of the position vector of the damage,  $\mathbf{r}$ , and the reduction in stiffness caused by the damage,  $\delta k$ , as

$$\delta\omega_i = f(\delta k, \mathbf{r}) \quad (2.1)$$

For single-damage case with small damage magnitude, they linearized Equation (2.1) at the undamaged state ( $\delta k = 0$ ), as

$$\delta\omega_i = f(0, \mathbf{r}) + \delta k \frac{\partial f(0, \mathbf{r})}{\partial(\delta k)} \quad (2.2)$$

Since there is no frequency change prior to damage,  $f(0, \mathbf{r}) = 0$  for all  $\mathbf{r}$ . Thus the ratio of frequency changes between two modes is shown to be a function of damage location only, as

$$\frac{\delta\omega_i}{\delta\omega_j} = \frac{g_i(\mathbf{r})}{g_j(\mathbf{r})} = h(\mathbf{r}) \quad (2.3)$$

Location where theoretically determined ratio  $\delta\omega_i/\delta\omega_j$  equals the experimentally measured value is the possible damage location. When more than one pair of modes are used, the total error  $e_r$ , corresponding to the damage at position  $\mathbf{r}$ , is the sum of the errors in all the mode pairs,  $\sum_{\text{all pairs } i,j} e_{rij}$ . The damage location,  $\mathbf{r}$ , corresponding to the minimal  $e_r$  is the most likely damage position. According to the underlying assumption made in the theoretical development, this method is only applicable to single-damage cases with small level of damage. Penny *et al.* (1993) and Friswell *et al.* (1994) attempted to improve this method by using a least squares fitting technique, and further used two criteria to assess the similarity of the two sets of ratios, namely the correlation coefficient and the closeness of exponent and coefficient to unity.

Another improvement to Cawley and Adams's method was presented by Messina *et al.* (1996). They adopted the straightforward concept of correlation factor between analytical frequency changes and measured frequency changes for detecting a single-damage site. If  $\Delta\mathbf{f}$  is the vector of measured frequency change and  $\delta\mathbf{f}_j$  represents the vector of analytical frequency change for a particular damage location  $j$ , Damage Location Assurance Criterion (DLAC) for location  $j$  is defined as

$$\text{DLAC}(j) = \frac{(\Delta\mathbf{f}^T \delta\mathbf{f}_j)^2}{(\Delta\mathbf{f}^T \Delta\mathbf{f})^2 (\delta\mathbf{f}_j^T \delta\mathbf{f}_j)^2} \quad (2.4)$$

where the subscript  $T$  denotes the vector/matrix transpose. DLAC value ranges between 0 and 1. The localization  $j$  giving the largest DLAC value indicates the best match to the measured frequency change pattern and therefore is determined as the

location most susceptible to damage. Later they extended the approach to multiple-damage cases (Messina *et al.* 1998).

The above forward methods require the computation of modal frequency changes for all possible damage cases. They would have become impractical for detection of single-damage scenarios in large-scale structures with hundreds and thousands of structural members; even worse are the multiple-damage cases where the combinations of possible damage locations could grow explosively for large-scale structures.

Lifshitz and Rotem (1969) were among the first to treat the damage detection using modal frequencies as an inverse problem. Systematic research work on this topic was due to Stubbs and his-coworkers (Stubbs *et al.* 1990; Stubbs and Osegueda 1990a, b). Making use of sensitivity analysis, they developed a method for identifying damage that relates changes in modal frequencies to changes in member stiffness. This method is essentially a sensitivity-based FE model updating method, and its accuracy, as most damage detection methods based on model updating, is dependent on the quality of the FE model used to compute the modal sensitivities.

There are several merits associated with the frequency-based damage detection approaches, which include that: 1) the measurement of modal frequency can be performed only using very few sensors; and 2) the modal frequency has least statistical variation from random error sources than other modal properties. However,

the disadvantages seem to overwhelm their merits. Modal frequency is a global parameter and is insensitive to local damage. Furthermore, it generally does not provide spatial information regarding damage location in particular for symmetric structures. Multiple frequency changes can provide spatial information about structural damage because stiffness changes at different locations of a structure will cause different combinations of changes in the modal frequencies. However, as pointed out by many researchers there are often an insufficient number of modal frequencies with enough changes to determine damage locations uniquely.

### ***2.2.2 Methods Using Mode Shapes***

As the largest change in mode shapes is expected to occur in the vicinity of damage, it is intuitive to incorporate them for damage localization. Two most commonly used methods to compare two sets of measured mode shapes are the modal assurance criterion (MAC) and the coordinate modal assurance criterion (COMAC) where one set of data is measured from the intact structure and the other is measured after the structure is damaged. MAC indicates the correlation between two sets of mode shapes and COMAC indicates the correlation between the mode shapes at a selected measurement point on the structure.

The MAC between mode  $i$  of the first data set  $A$  and mode  $j$  of the second data set  $B$  is defined as follows (Allemang and Brown 1982)

$$\text{MAC}(i, j) = \frac{(\Phi_{Ai}^T \Phi_{Bj})^2}{(\Phi_{Ai}^T \Phi_{Ai}) \times (\Phi_{Bj}^T \Phi_{Bj})} \quad (2.5)$$

where  $\phi_{Ai}$  is the mode shape vector for mode  $i$  of data set  $A$ ; and  $\phi_{Bj}$  is the mode shape vector for mode  $j$  of data set  $B$ . A MAC value close to unity indicates that two modes are well correlated and a value close to zero is indicative of uncorrelated modes. The MAC technique was originally developed for mode correlation and matching between experimental and analytical mode shapes. West (1984) first adapted this technique for damage localization by directly comparing the mode shapes before and after damage in structure. To do this, he partitioned the structure into several segments using various partitioning techniques, and then MAC value for each segment was calculated to localize the damage. Small MAC values close to zero indicate possible damage locations. Fox (1992) showed that the single-member measures of mode shape changes such as MAC were relatively insensitive to damage in a beam with saw cut, and the node-line MAC, a MAC based on measurement point close to a node point for a particular mode, was a more sensitive indicator of mode shape changes due to damage. He also suggested scaling the relative changes in mode shapes to better identify the damage location. Mayes (1992) developed a method known as structural translational and rotational error checking (STREC) based on the changes in mode shapes. By using the ratios of relative modal displacements, STREC assessed the difference of structural stiffness between two different sets of degrees of freedom (DOFs).

As the MAC technique only uses one pair of modes for damage localization, one potential problem is how to select an appropriate mode for MAC calculation. To

circumvent this problem, Lieven and Ewins (1988) proposed COMAC for damage localization, which is defined as

$$\text{COMAC}(i) = \frac{\left( \sum_{r=1}^m \phi_{Ar}^i \phi_{Br}^i \right)^2}{\left( \sum_{r=1}^m \phi_{Ar}^i \phi_{Ar}^i \right) \left( \sum_{r=1}^m \phi_{Br}^i \phi_{Br}^i \right)} \quad (2.6)$$

where  $\phi_{Ar}^i$  and  $\phi_{Br}^i$  are modal component of the  $r$ th mode shape at measurement location  $i$  for the two paired mode shapes, respectively; and  $m$  is the number of measured modes. The location where a COMAC value is close to zero is the possible damage location.

Ko *et al.* (1994) presented a method that uses a combination of MAC, COMAC, and sensitivity analysis to detect damage in steel-framed structures. The sensitivities of the analytically derived mode shapes to particular damage locations were first computed to determine which DOFs are the most relevant. The authors then analyzed the MAC between the measured modes from the pre-damage structure and those from the post-damage structure to select the modes to be used in the analysis. Using the modes and DOFs selected with the above criteria, the COMAC was computed and used as a damage indicator. The results demonstrated that particular mode pairs could indicate damage; but when all mode pairs were used, the indication of damage might be masked by modes that were not sensitive to the damage. Salawu and Williams (1995) conducted modal tests of a full-scale bridge before and after rehabilitation. They concluded that natural frequencies of the bridge did not change significantly as a result of structural repairs, and both MAC and COMAC were able

to give good indications of the presence and location of the repairs. It was also concluded that the performance of MAC and COMAC depends on the modes and measurement locations used for damage localization.

Thus, one of key issues in implementing damage indicators using changes in mode shapes is the selection of the modes and the optimum placement of sensors in the case of limited sensors. Such an issue has been addressed by Cobb and Liebst (1997) and Shi *et al.* (2000a) via eigenvector sensitivity analysis.

### ***2.2.3 Methods Using Curvature/Strain Modes***

An alternative to using mode shapes to obtain spatial information regarding the damage location is to utilize the mode shape derivatives, such as curvatures. For beam, plate, and shell structures, there is a direct relationship between curvature and bending strain. Pandey *et al.* (1991) have demonstrated that absolute changes in mode shape curvature can be a good indicator of damage for beam structures. The curvature values are computed from the analytical modal displacements using a finite difference method, as

$$\kappa_i = (\phi_{i+1} - 2\phi_i + \phi_{i-1})/h^2 \quad (2.7)$$

where  $\phi_i$  is the modal displacement at measurement point  $i$ ; and  $h$  is the length of the elements.

Chance *et al.* (1994) found that the numerical calculation of curvature by

differentiation of mode shapes could result in unacceptable errors. Instead, they utilized the measured strain mode shape which has shown a significant improvement for damage localization. Nwosu *et al.* (1995) evaluated changes in strain resulting from the appearance of a crack in a T-joint. They found these changes to be much greater than any shifts in frequency and to be measurable even at a relatively large distance from the crack. Ratcliffe (1997) developed an approach for damage localization that used the finite difference approximation of a Laplacian differential operator to mode shape. The approach was shown to be best suited for the mode shape of the fundamental natural frequency. The mode shapes from higher natural frequencies can be used to verify the identified location of damage, but they are not as sensitive as the lower modes.

Wang *et al.* (2000) presented a numerical study of damage detection in the suspension Tsing Ma Bridge using the normalized changes in mode shape curvatures, namely

$$Index_j(i) = \frac{|\kappa_j^d(i) - \kappa_j^u(i)|}{\sum_i |\kappa_j^d(i) - \kappa_j^u(i)|} \quad (2.8)$$

where  $i$  represents the segment number along the longitudinal direction of bridge. The superscripts  $u$  and  $d$  denote the undamaged and damaged structures, respectively; and  $\kappa_j(i)$  is the  $j$ th mode shape curvature as defined in Equation (2.7). The above index has been combined with statistical methods to localize damage.

Despite the advantage of providing spatial information regarding the location of structural damage, methods of damage localization based on mode shapes and their derivatives suffer from several limitations in application: 1) dense array of measurement points is required for an accurate configuration of mode shapes and curvature mode shapes; 2) the mode shape has larger statistical variation than does modal frequency; 3) the mode shape based methods, especially the curvature mode shape based methods, are not readily applicable for structures with complex configuration; and 4) it is required to select a mode shape, yet it is a *priori* unknown which mode suffers from significant change due to particular structural damage.

#### ***2.2.4 Methods Using Modal Strain Energy***

To achieve more effective approaches for damage localization, some researchers make use of the measured mode shapes and the information from a FE model to construct new damage indicators. Some studies indicated that modal strain energy is useful in localizing structural damage. The general definition of modal strain energy of a structure with respect to the  $r$ th mode can be expressed as

$$\text{MSE}_r = \frac{1}{2} \boldsymbol{\phi}_r^T \mathbf{K} \boldsymbol{\phi}_r \quad (2.9)$$

where  $\mathbf{K}$  is the stiffness matrix of a structure.

Stubbs *et al.* (1992) presented the pioneer work on using modal strain energy for damage localization. They proposed a damage localization method based on the decrease in modal strain energy between two structural DOFs defined by the

curvature. Topole and Stubbs (1995) examined the feasibility of using a limited set of modal properties for structural damage detection. Later, Stubbs and Kim (1996) improved the method by using modal strain energy to localize the damage and estimate the damage size without baseline modal properties. In their approach, the contribution of element  $j$  to the  $r$ th modal strain energy is given by

$$C_{rj} = \frac{\tilde{\Phi}_r^T k_j \tilde{\Phi}_r}{\Phi_r^T \mathbf{K} \Phi_r} \quad (2.10)$$

where  $\tilde{\Phi}_r$  is the displacement vector of the  $r$ th mode associated with the  $j$ th element; and  $k_j$  is the stiffness matrix of element  $j$ . They assumed that modal strain energy kept same before and after damage. This approximation gives the ratio of the undamaged and damaged flexural rigidities of potential damage location, which is then used as a damage indicator on a statistical base. Law *et al.* (1998) presented another damage indicator on the use of modal strain energy, called element energy quotient (EEQ). The EEQ of element  $j$  for the  $r$ th mode is defined as

$$\text{EEQ}_{rj} = \frac{\tilde{\Phi}_r^T k_j \tilde{\Phi}_r}{\tilde{\Phi}_r^T m_j \tilde{\Phi}_r} \quad (2.11)$$

where  $m_j$  is the mass matrix of element  $j$ . Shi *et al.* (1998) utilized the concept of modal strain energy change ratio (MSECR) and found it to be a good damage indicator. The MSECR is defined as the absolute relative change of element modal strain energy before and after damage

$$\text{MSECR}_{rj} = \frac{|\text{MSE}_{rj}^u - \text{MSE}_{rj}^d|}{|\text{MSE}_{rj}^u|} \quad (2.12)$$

where  $MSE_{rj}^u$  and  $MSE_{rj}^d$  are modal strain energy of element  $j$  for the  $r$ th mode before and after damage, respectively. As the stiffness matrix of element  $j$  after damage is unknown, they approximated it with that of undamaged structure.

The original formulation by Stubbs *et al.* (1992) is inherently limited to beam-like structures that are characterized by one-dimensional curvature (i.e., curvature that is uniquely a function of one independent spatial variable). Cornwell *et al.* (1999a) generalized this method to plate-like structures that are characterized by two-dimensional curvature.

### ***2.2.5 Methods Using Modal Flexibility***

Based on the governing equation of structural dynamics, Berman and Flannelly (1971) showed that higher modes contribute more to stiffness matrix than lower modes. Therefore, to obtain a good estimate of stiffness matrix or its change as required for damage localization, one needs to measure all the modes of a structure, especially the higher modes. Due to practical limitations, it is extremely difficult to measure higher frequency response data, and this presents a severe constraint on the accuracy of stiffness difference methods. To avoid this difficulty, another class of damage identification methods arise which use dynamically measured flexibility matrix to estimate the change in structural stiffness.

With the mode shapes normalized to unity as  $\Phi^T \mathbf{M} \Phi = \mathbf{I}$ , the dynamically measured modal flexibility can be approximated using the first  $m$  mode shapes and modal frequencies (Berman and Flannelly 1971), as

$$\mathbf{F} = \Phi \Lambda^{-1} \Phi^T = \sum_{i=1}^m \frac{1}{\omega_i^2} \phi_i \phi_i^T \quad (2.13)$$

The formula of flexibility matrix is approximate due to the fact that in general only the first few modes of a structure (typically the several lowest frequency modes) are measured. Hugue *et al.* (1991) developed a methodology for identification of constructed facilities that permits synthesis of the localized flexibility coefficients. The static and dynamic testing results indicated that the flexibility coefficients could be synthesized very accurately using only the low-order modes even when several closely spaced modes existed and a simple modal identification algorithm was used. Raghavendrchar and Aktan (1992) proposed the use of measured flexibility as a ‘condition index’ to indicate the relative integrity of a bridge. Toksoy and Aktan (1994) computed the measured flexibility of a bridge and examined the cross-sectional deflection profile with and without a baseline data set, and showed that anomalies in the deflection profile could indicate damage even without a baseline data set.

Based on the formula of modal flexibility matrix, some researchers directly utilized the changes in modal flexibility matrices before and after structural damage for damage localization. Pandey and Biswas (1994; 1995) presented a damage localization algorithm based on changes in the measured flexibility, and showed that

the damage localization could be achieved using only the first several modes. Mayes (1995) used the measured flexibility to locate damage from the results of a modal test on a bridge. He also proposed a method using the measured flexibility as input for damage detection, which evaluated changes in the load-deflection behaviour of a spring-mass model of the structure. Wang *et al.* (2000) defined the normalized changes in modal flexibility for achieving more reliable damage localization. Rather than direct utilization of the changes in measured modal flexibility for damage localization, Bernal (2002) first performed the singular value decomposition of the changes in modal flexibility matrices to attain the so-called damage localization vectors (DLVs). The internal force of each element under the action of DLVs is then analyzed, and finally the structural elements whose internal forces are zero are determined as the damage ones. Gao and Spencer (2005) discussed the issues relating to the synthesis of modal flexibility matrix from ambient and forced vibration data and implemented DLV method for online damage localization.

Doebling and Peterson (1997) presented a method for computing the statically complete flexibility matrix from a dynamically measured flexibility matrix, which requires the solution of a system of linear equations only. The method was derived and applied to both numerically and experimentally measured flexibility matrices, and the improved accuracy of static flexibility over dynamically measured flexibility was demonstrated.

It is known that the coefficients of the  $i$ th column of flexibility matrix are the

deflection of the structure with a unit load applied at the  $i$ th DOF. The sum of all columns of the flexibility matrix represents the deformed shape if a unit load is applied at each DOF, and this shape is referred to as uniform load surface (ULS). Zhang and Aktan (1995) stated that the change in curvature of the ULS could be used to determine the location of damage. They suggested calculating curvature of the ULS by finite difference method. Wu and Law (2004) extended this method for damage localization for a two-dimension plate-like structure where the Chebyshev polynomial approximation to ULS curvature was adopted to avoid the errors caused by finite difference method.

The major advantage of the methods using dynamically measured flexibility for damage localization is that it can be constructed and synthesized with good accuracy from a few low-order modes without the need of a FE model. The underlying assumption made in the derivation of dynamically measured flexibility is that the mass-normalized mode shapes should be used which might become infeasible in ambient vibration tests. This kind of methods also need a fine mesh of measurement points for an enough accurate representation of mode shapes used for synthesis of modal flexibility.

The experimental comparison of various damage index methods has also been conducted by a number of researchers through field testing. Farrar and Jauregui (1998), and Jauragui and Farrar (1998) conducted experimental and numerical comparison of five damage index methods using the simulated and experimental data

from I-40 Bridge. Most of the methods identified damage location correctly for the most severe damage case. However, for some of these methods, if they were applied blindly, it would be difficult to tell whether damage had not also occurred at locations other than the actual one. In addition, the methods were inconsistent and did not clearly identify the damage location when they were applied to the less severe damage cases. Park *et al.* (2001) compared the results of damage index methods with visual inspection results by using the periodical measurement data from a concrete box-girder bridge. They first applied a mode updating procedure to correct the boundary conditions and macro-parameters in the FE model based on measured modal frequencies, and then proceeded to the implementation of damage indicators using the measured mode shapes and the analytical mode shapes from the correlated FE model. The result indicated there was a strong correlation between predicted damage locations and observed damage locations. They further pointed out that the environmental conditions might significantly affect the accuracy of damage index methods. Huth *et al.* (2005) measured the modal data before and after damage and used them for implementing damage indicators. The results showed that it was difficult to localize the damage at earlier stage even using the modal flexibility matrix. Their study emphasized the need for elimination of temperature effect on modal data for practical implementation of damage detection methods.

## 2.3 Model Updating Methods

With the use of system identification concepts, the measured modal properties can be used to construct or modify the structural analytical model as well as to diagnose structural damage. In contrast to modal system identification, which is used to identify the modal properties of structure, structural system identification basically falls into two categories. They either attempt to construct an analytical model, or seek to correct and modify a pre-established analytical model using the available experimental data. Due to the inconsistency in number of DOFs between analytical model and experimental test (sparseness of measurement data) as well as the incompleteness of measurement data, it is impossible to construct a unique analytical model directly from the testing data without resorting to a reference model. To eliminate the non-uniqueness in structural system identification, a reference model is required and structural system identification then reduces to modifying the system parameters to match as closely as possible the testing results, or more precisely, reduces to parameter estimation. Natke (1988a) named the first type of structural system identification as *direct* system identification while the second type, that essentially is model updating, as *indirect* one as it requires a reference model.

Making use of the concept of indirect system identification and measured modal data, another category of damage detection method is established through the modification of intact (reference) structural model matrices such as mass, stiffness and damping, or the macro-parameters so that the modified ones reproduces as closely as possible

the measured modal properties. These methods solve for the updating parameters by forming a constrained optimization problem that minimizes some kind of errors/residuals subject to various constraints. Comparisons of the updated parameters with the original ones associated with the intact structure provide an indication of damage location as well as damage magnitude. Three commonly used residuals for model updating are equation residuals, output residuals, or a combination of them according to Natke (1988b).

It should be noted that model updating algorithms used for model improvement and damage detection share the similar objectives, i.e. seeking an analytical model that is close to the real structure. The purpose of model improvement is to achieve an analytical model which is dynamically equivalent to the tested structure. The updated model is subsequently utilized for response prediction and structural modification. The model improvement is performed in face of numerous simplifications in FE model building. Often there are complex geometrical features that cannot be modelled accurately. In addition, boundary conditions and joint parameters between components are seldom fully understood. Mottershead and Friswell (1993) summarized three commonly encountered modelling errors, which could give rise to significant discrepancy between analytical predictions and testing values, as: 1) model structure errors, which are liable to occur when there is uncertainty concerning the governing equations of motion; 2) model order errors, which are often arising from discretizing the complex structures and can result in a model with insufficient order; and 3) model parameter errors, which typically include inappropriate boundary

conditions, inaccurate assumptions used in order to simplify the model, and inconsistent material properties. These modelling errors may exist only in a few locations or can be extensively distributed in the whole structure.

On the other hand, the damage detection aims to detect and identify the changes in stiffness, mass and damping matrices due to damage instead of modelling errors. The changes in the measured quantities caused by structural damage are often smaller than those observed between the healthy (i.e. undamaged) structure and its FE model. Consequently, it becomes almost impossible to discern between inadequate modelling and actual changes due to damage. To distinguish damage from modelling errors, an original FE model that accurately represents the intact structure is required. This is accomplished with a first-stage model improvement procedure which is performed in order to correlate this original model with testing data of the intact structure (Titurus *et al.* 2003a). The improved model is commonly used as the *baseline* model and can be then further correlated with testing data of possibly damaged structures for damage detection by using a similar updating procedure (Titurus *et al.* 2003b). Therefore a two-step scheme is generally required for damage detection application using model updating methods with the first step correcting the modelling errors and the second step detecting structural damage. For a large-scale structure, the modelling errors could spread over the whole structure while the damage generally tends to concentrate on several locations.

Considerable research efforts have been devoted to developing various model updating methods during the past several decades. Survey literature on model updating in structural dynamics began to appear in the early 1970s. Among them, Hart and Yao (1977), Liu and Yao (1978), Natke (1988b), Imregun and Visser (1991), Natke (1991), Zimmerman and Smith (1992), Mottershead and Friswell (1993), and Link (2001) are worthy of attention. The model updating methods, either for model improvement or for damage detection applications, can be classified into three categories: 1) optimal matrix updating methods; 2) eigenstructure assignment methods; and 3) sensitivity-based updating methods.

### ***2.3.1 Optimal Matrix Updating Methods***

Methods that use a direct and sometimes closed-form solution to compute the correction (perturbation) to analytical system property matrices using the measured modal data are commonly referred to as optimal matrix updating methods. The system property matrices include the stiffness, mass and damping matrices. In these methods, the elements of these property matrices are treated as variables, and are estimated by using the constrained optimization techniques. Depending on the type of objective functions used, the optimal matrix updating methods can be classified as the minimum norm perturbation method, which minimizes the Frobenius or weighted Frobenius norm of the perturbation matrix, and the minimum rank perturbation method which minimizes the rank of the perturbation matrix. In order to determine

the correction to original analytical stiffness and mass matrices, the optimal matrix updating method uses the following constrained optimization function

$$\text{Min}_{\Delta\mathbf{M}, \Delta\mathbf{K}} \{J(\Delta\mathbf{M}, \Delta\mathbf{K}) + \lambda R(\Delta\mathbf{M}, \Delta\mathbf{K})\} \quad (2.14)$$

where  $\Delta\mathbf{M} = \mathbf{M} - \mathbf{M}_A$ , is the correction to original mass matrix;  $\Delta\mathbf{K} = \mathbf{K} - \mathbf{K}_A$ , is the correction to original stiffness matrix;  $\mathbf{M}_A$  and  $\mathbf{K}_A$  are the original (reference) mass and stiffness matrices, respectively;  $J$  is the objective function;  $\lambda$  is the Lagrange multiplier; and  $R$  is the constraint function. The commonly used constraint function includes orthogonality, equation of motion, symmetry, sparseness, and positive definiteness, detailed as follows:

Equation of motion:  $\mathbf{K}\Phi = \mathbf{M}\Lambda\Phi^T$  (2.15)

Orthogonality condition:  $\Phi^T\mathbf{K}\Phi = \Lambda; \Phi^T\mathbf{M}\Phi = \mathbf{I}$  (2.16)

Symmetry:  $\mathbf{K} = \mathbf{K}^T; \mathbf{M} = \mathbf{M}^T$  (2.17)

Sparseness:  $\text{sparse}(\mathbf{M}) = \text{sparse}(\mathbf{M}_A); \text{sparse}(\mathbf{K}) = \text{sparse}(\mathbf{K}_A)$  (2.18)

Positive definiteness:  $\mathbf{x}^T\Delta\mathbf{M}\mathbf{x}; \mathbf{x}^T\Delta\mathbf{K}\mathbf{x}$  (2.19)

Early work in the area of optimal matrix updating for structure matrix identification using vibration tests dates from the late 1960's. Rodden (1967) used the results from ground vibration tests to derive the matrix of structural influence coefficients, which required the number of coordinates used in the model be equal to the number of measured normal modes. Ross (1967), and Berman and Flannelly (1971) discussed the problem that the number of coordinates is often larger than the number of

measured modes to cover the frequency range of interest. They presented methods for identifying the parameters in the discrete, linear model of a structure using the measured incomplete number of normal modes but measured at all coordinates to modify an analytical model.

Most recent optimal matrix updating methods follow a common idea from the work of Baruch and Bar Itzhack (1978), and Baruch (1978), in which the problem of model updating is formulated as a Lagrange-multiplier-based optimization problem with various constraints. This type of methods is also called *reference basis methods* because one of the quantities, namely the mass matrix, the stiffness matrix, or the measured modal data needs to be assumed to be exact or as the reference, and the other two are corrected. In their work on the orthogonalization of measured mode shapes, Baruch and Bar Itzhack developed a mass reference method for the weighted orthogonalization of measured mode shapes, in which the mass matrix is assumed to be known and the measured mode shapes are orthogonalized to the mass matrix. Making use of the orthogonalized modal data, they further calculated the updated stiffness matrix from the direct and closed-form solution to a constrained optimization problem, which is the closest matrix to a previously given stiffness matrix (generally estimated from its FE model) and complied with the required orthogonality conditions. In this method, the orthogonalized mode shapes and corrected stiffness matrix are expressed as  $\mathbf{X} = \mathbf{\Phi}(\mathbf{\Phi}^T\mathbf{M}\mathbf{\Phi})^{-1/2}$  and  $\mathbf{K} = \mathbf{M}\mathbf{X}\mathbf{\Lambda}\mathbf{X}^T\mathbf{M}$ , respectively, where  $\mathbf{\Phi}$  is the matrix of measured mode shapes,  $\mathbf{\Lambda}$  is the diagonal matrix of measured eigenvalues, and  $\mathbf{M}$  is the exact mass matrix. The analytical

model with the mass matrix and the updated stiffness matrix is able to exactly reproduce the measured modal data. Noting that both mass and stiffness matrices may be incorrect (Berman 1979), Baruch (1982) improved his previous work by sequentially updating the stiffness and mass matrices. Later, he suggested another approach for sequentially adjusting the mass and stiffness matrices (Baruch 1984), in which the stiffness matrix is first corrected using the incomplete set of static loads and deflections from static tests and the mass matrix is then modified to fulfill the eigenvalue equation based on the corrected stiffness matrix and the modal data. Berman and Nagy (1983) developed an analytical model improvement (AMI) procedure for model refinement which combined the stiffness matrix adjustment procedure of Baruch and Bar Itzhack (1978) with the mass matrix adjustment procedure of Berman (1979). In AMI procedure, static modal expansion method is first applied to expand the DOFs of measured mode shapes to the complete set of DOFs corresponding to analytical model. After doing that, AMI procedure then seeks a corrected mass matrix that is the closest to an analytical mass matrix and satisfies the mass orthogonality conditions by solving a constrained optimization problem as follows:

$$J_{\mathbf{M}} = \left\| \mathbf{M}_{\mathbf{A}}^{-1/2} (\mathbf{M} - \mathbf{M}_{\mathbf{A}}) \mathbf{M}_{\mathbf{A}}^{-1/2} \right\| + \sum_{i=1}^m \sum_{j=1}^m \lambda_{ij} (\mathbf{\Phi}^T \mathbf{M} \mathbf{\Phi} - \mathbf{I})_{ij} \quad (2.20)$$

where  $\mathbf{M}$  is the  $n \times n$  the stiffness matrix to be determined;  $\mathbf{M}_{\mathbf{A}}$  is the  $n \times n$  analytical stiffness matrix which is generally estimated from a FE model;  $\lambda_{ij}$  is a Lagrange multiplier used to enforce mass orthogonality conditions;  $\mathbf{\Phi}$  is the  $n \times m$  expanded

modal shapes;  $\mathbf{I}$  is the identity matrix; and  $n$  and  $m$  are the number of DOFs in analytical model and the number of measured modes, respectively. The minimization procedure results in the expression for the corrected mass matrix, as

$$\mathbf{M} = \mathbf{M}_A + \mathbf{M}_A \Phi \mathbf{m}_A^{-1} (\mathbf{I} - \mathbf{m}_A) \mathbf{m}_A^{-1} \Phi^T \mathbf{M}_A \quad (2.21)$$

where  $\mathbf{m}_A = \Phi^T \mathbf{M}_A \Phi$ . Following the computation of the corrected mass matrix  $\mathbf{M}$ , a similar procedure for the correction of stiffness matrix can be applied by minimizing another constrained optimization function, as

$$\begin{aligned} J_{\mathbf{K}} = & \left\| \mathbf{M}^{-1/2} (\mathbf{K} - \mathbf{K}_A) \mathbf{M}^{-1/2} \right\| + \sum_{i=1}^n \sum_{j=1}^m \lambda_{Kij} (\mathbf{K} \Phi - \mathbf{M} \Phi \Lambda)_{ij} \\ & + \sum_{i=1}^m \sum_{j=1}^m \lambda_{Oij} (\Phi^T \mathbf{K} \Phi - \Lambda)_{ij} + \sum_{i=1}^n \sum_{j=1}^i \lambda_{Sij} (\mathbf{K} - \mathbf{K}^T)_{ij} \end{aligned} \quad (2.22)$$

where various Lagrange multipliers are used to enforce the equations of motion, the orthogonality conditions, and the symmetry of stiffness matrix; and  $\mathbf{K}_A$  is the analytical stiffness matrix which again is generally estimated from the FE model. The stiffness correcting equation can be finally written as

$$\mathbf{K} = \mathbf{K}_A + (\Delta + \Delta^T) \quad (2.23)$$

where  $\Delta = \frac{1}{2} \mathbf{M} \Phi (\Phi^T \mathbf{K}_A \Phi + \Lambda) \Phi^T \mathbf{M} - \mathbf{K}_A \Phi \Phi^T \mathbf{M}$ . It is seen that both Baruch and Berman's method corrected the mass matrix and stiffness matrix in a sequential manner. Wei (1990a) noticed the effect of interaction between correction of stiffness and mass matrices and presented a generalized weighted method for simultaneous correction of these matrices, whose solution requires the inverse of a very large matrix. Wei (1990b) later found that the inverse of this large matrix could be avoided

at some specific weighting. Fiswell *et al.* (1997) extended this method to the simultaneous correction of stiffness and damping matrices. They further introduced an additional parameter to enable the norm of stiffness term and the norm of damping term to be weighted differently. However the inclusion of this parameter made the closed-form solution impossible. In addition, the measured modal data may not be reproduced exactly using the corrected matrices because a pseudo-inverse was required to calculate the Lagrange multiplier matrix.

The previous approaches will generally produce a model whose analytical modes exactly replicate those used in the correction. However, the corrected mass and stiffness matrices could be drastically altered and become fully populated. Particularly the adjustment of the stiffness and mass coefficients from values of zero to large nonzero values violates the structural connectivity and introduces extra load paths which do not exist in the actual structures. As a result, the updated system matrices may not have any physical meanings and are hard to interpret. To avoid this problem, Kabe (1985) developed a procedure called stiffness  $K$  matrix adjustment (KMA) method where the structural connectivity conditions are enforced as an additional constraint through correcting only nonzero coefficients in the stiffness matrix. The addition of model connectivity information to the constrained minimization formulation enables the KMA method to identify the stiffness matrix exactly in certain cases even when some of the test modes are not known, while for Baruch's method this is achieved only if all the test modes are used in the identification process. However, prior to correcting the stiffness matrix, KMA

requires the solution of an auxiliary system of linear equations to determine the involved Lagrange multiplier matrix, whose solution is quite computationally expensive because of large size and asymmetry of its coefficient matrix. KMA procedure is theoretically elegant but becomes quite complicated and computationally intractable for large-scale structures. Kammer (1988) developed a projector matrix (PM) method that was mathematically simple, computationally efficient and turned out to be equivalent to Kabe's method in most cases. Chen and Garba (1988), and Lim (1990) developed a procedure similar to the Kabe's method and presented numerical studies on damage detection of a relatively large structure. Smith and Beattie (1991) demonstrated the linkage between matrix updating methods and various constrained optimization algorithms. They further overcame the inconsistent problem existent in Kabe's formulation by solving the simultaneous minimization of perturbation matrix norm and the norm of modal force residuals subject to matrix symmetry and structural connectivity, in which modal force residual of the  $i$ th mode is expressed as  $\mathbf{f}_i = \mathbf{K}_d \boldsymbol{\phi}_i - \mathbf{M} \omega_i^2 \boldsymbol{\phi}_i$ . This improvement makes the coefficient matrix of the auxiliary problem symmetric and positive semi-definite which could be solved efficiently using direct or iterative methods. Making use of the merits of FE method to preserve the global connectivity and to reduce the number of unknown updating parameters, Liu (1995) presented a straightforward method for identifying the element properties in truss structures using measured modal data. In this method, the model updating problem is formulated as minimization of the norm of modal force residuals. A perturbation

technique is further adapted for error propagation. Other studies that address the minimum norm perturbation methods include Abdalla *et al.* (1998) who examined the use of alternating projection method to iteratively enforce the constraints of the symmetry, sparseness, positive definiteness, and equation of motion for damage detection, Kenigsbuch and Halevi (1998) who incorporated the prior knowledge regarding the accuracy of the FE model using a general weighting scheme, and Cha and de Phillis (2001) who sequentially identified the mass and stiffness matrices using the modal data before and after attaching the known mass to the structure.

The algorithms described above formulate the correction of property matrices as a constrained optimization problem in which the Frobenius norm of perturbation matrices is adopted as the objective function with a variety of constraints. Another type of the optimal matrix updating methods involves minimization of the rank of the perturbation matrices rather than the norm of the perturbation matrices. Zimmerman and Kaouk (1994) observed that modelling errors in model refinement and damage detection applications will generally tend to concentrate in a few structural members rather than distributing throughout a large number of structural members. Thus, the perturbation matrices will tend to be of small rank. They proposed an algorithm based on the minimum rank perturbation theory (MRPT) for adjusting the mass, stiffness, and damping matrices so that the ranks of the perturbation to these system matrices are minimal. In this approach, modal force residuals are computed and utilized to solve for the perturbation to the system matrices by means of MRPT. Further investigations were subsequently conducted by them and their colleagues to

correct any two of the three property matrices (Kaouk and Zimmerman 1994), to implement MRPT for damage detection using the combined multiple static and modal data (Zimmerman and Simmermacher 1995), to simultaneously identify these three property matrices (Kaouk *et al.* 2000), and to adjust the stiffness, mass and damping matrices using the measured frequency response function (FRF) data (Zimmerman *et al.* 2005). Doebling (1996) presented a method to compute a minimum rank update for elemental parameter vector rather than for global or elemental stiffness matrices. This approach adopted the same basic formulation as MRPT but constrained the global stiffness matrix perturbation to be an explicit function of the diagonal elemental stiffness parameter. A limitation of this method, as with all minimum rank procedures, is that the rank of perturbation matrix is always equal to the number of modes used in the computation of modal force residuals. In addition, as pointed out by Friswell and Penny (1997), MRPT does not necessarily ensure that the change in stiffness will be local, as the stiffness change could be global but of low rank.

One of important features of many optimal matrix updating methods is that they reproduce the measured modes exactly; therefore the corrected model are said to be *representational*. This is strength in that the updated model is able to reproduce data. On the other hand, the measured data and the analytical data are unlikely to be equal due to model inadequacy as well as measurement noise. Model updating should be executed in an attempt to correct the parameters in the model but not with the intention of exactly producing the measurement noise. If the updated model exactly

reproduces inaccurate measurement, the analysis results based on this model may become unreliable. Furthermore, the updated model could produce additional, spurious modes in the frequency range of interest. One prominent problem in these methods is the necessities to expand the measured mode shapes to the full DOFs of the FE model, or to reduce DOFs of the FE model to the measured DOFs. Both of modal expansion and model reduction will introduce additional errors which could make error localization and damage detection impossible. A major drawback of these methods is that the corrected mass and stiffness cannot be related to physical parameters in the structure, such as Young's modulus and mass density.

### ***2.3.2 Eigenstructure Assignment Methods***

Another group of matrix updating methods, known as eigenstructure assignment methods, is developed based on the design of a fictitious controller that would minimize the modal force residuals. The controller gains are then interpreted as the perturbation to the system matrices. The eigenstructure assignment methods were originally developed for structural control to force a structure to respond in a predetermined way, and were adapted to model updating by Minas and Inman (1988). In the eigenstructure assignment approach, state feedback is used to describe the right-hand side of the dynamic equation of motion in terms of the displacement and velocity states. The problem for model updating then reduces to determining the terms in the feedback gains matrix such that the eigenvalues and eigenvectors of the closed loop system are identical to the measured modal data. The result of this

procedure is that modifications are made to the stiffness and damping matrices but the analytical mass matrix remains unchanged. The corrected stiffness and damping matrices are given by

$$\mathbf{K} = \mathbf{K}_A + \mathbf{B}_0 \mathbf{G} \mathbf{C}_0 \quad \mathbf{C} = \mathbf{C}_A + \mathbf{B}_0 \mathbf{G} \mathbf{C}_1 \quad (2.24)$$

where  $\mathbf{B}_0$  is an input distribution matrix;  $\mathbf{C}_0$  and  $\mathbf{C}_1$  are the matrices relating the outputs and states; and  $\mathbf{G}$  is the feedback gain matrix. The matrices  $\mathbf{B}_0$ ,  $\mathbf{C}_0$  and  $\mathbf{C}_1$  are derived from the excitation positions and the location and type of measurement. The matrix  $\mathbf{B}_0$  may be chosen arbitrarily, and  $\mathbf{C}_0$  and  $\mathbf{C}_1$  must be chosen such that  $\mathbf{C}_1 \mathbf{\Phi} \mathbf{\Lambda} + \mathbf{C}_0 \mathbf{\Phi}$  is non-singular in which the matrices  $\mathbf{\Phi}$  and  $\mathbf{\Lambda}$  contain the incomplete measured mode shapes and eigenvalues. In general the correction matrices  $\mathbf{B}_0 \mathbf{G} \mathbf{C}_0$  and  $\mathbf{B}_0 \mathbf{G} \mathbf{C}_1$  will not be symmetric. Therefore an iterative procedure for the determination of symmetric corrections is generally required. Minas and Inman (1990) proposed a two-step, iterative scheme where  $\mathbf{C}_0$  and  $\mathbf{C}_1$  matrices are fixed, then the original stiffness and damping matrices are replaced by the symmetric updated matrices, and the eigenstructure assignment process is repeated. This forces the corrected matrices to be symmetric and to reproduce the measured modes. Zimmerman and Widengren (1990) developed another method to enforce the symmetry of stiffness and damping matrices that used a generalized algebraic Riccati equation to calculate symmetric corrections to the stiffness and damping matrices directly. An additional step is further introduced to enforce the structural connectivity.

Studies which addressed the correction to the global stiffness matrix or damage detection using eigenstructure assignment methods were reported by Zimmerman and Kaouk (1992). They used a subspace rotation algorithm to improve the assignability of the mode shapes and to preserve the structural connectivity in the updated model. A major difficulty associated with the approach is that the method identifies the matrix coefficient changes and thus requires an additional step to correlate these changes with structural damage. Lim and Kashangaki (1994) and Lim (1995) proposed a damage detection approach using eigenstructure assignment that directly identifies change of element-level stiffness. In this approach, the *best achievable eigenvector* is first expressed in terms of measured eigenvectors by selection of control gains such that the modal force residuals between the nominal structural model for intact structure and the modal parameters measured from the damaged structure is minimal. The relationship between the measured mode shapes and the best achievable eigenvectors is then used as a measure of damage location. For detection of multiple damage locations, they used a sequential damage detection scheme in which the most probable damage member was identified at a time in the sequential fashion. However, it is questionable that this procedure will correctly identify the damage members and damage magnitudes due to interaction effects between multiple damage locations. Other studies regarding the use of eigenstructure assignment methods include the work of Cobb and Liebst (1997) who developed an optimization strategy to minimize the deviations between measured and analytical modal data for determining the diagonal control gain matrix which directly related to

the damage coefficients, and the work of Kiddy and Pines (2000) who adapted the eigenstructure assignment approach to account for the centrifugal forces for damage detection in rotating structures.

As indicated by Lim (1995), one special merit of eigenstructure assignment methods is that they can be not only used for damage detection and health monitoring of structures, but also for monitoring the sensor and actuator performance in a unified manner. However, the eigenstructure structure assignment methods for damage detection and model refinement suffer from the same drawbacks as the optimal matrix updating methods. Furthermore they may require a large amount of computation in particular for nonlinear optimization. In addition, there are no physical meanings of the assigned matrices.

### ***2.3.3 Sensitivity-Based Updating Methods***

The sensitivity-based updating methods are another class of model updating methods. In this approach, model updating problem reduces to the solution of an optimization problem which minimizes a penalty function of either the equation errors or the output errors. In the equation-error-based model updating methods, the errors in eigenvalue equations expressed in terms of measured modes are minimized (Fritzen 1986; Fritzen and Zhu 1991; Friswell and Mottershead 1995). Minimization of the equation errors leads to a linear system of equations if the elements of stiffness are linear functions of updating parameters such as flexural rigidity, Young's modulus. The disadvantage of the equation error approach is that it requires the measurement

data at all modelled DOFs; otherwise either a modal expansion or a model reduction procedure is necessary. In addition the estimated parameters are biased because of both sides of system of equations are contaminated with measurement errors (Fritzen 1986). The instrumental variable method (Fritzen 1986) and total least squares method (Ziaei-Rad and Imregun 1999) have been applied to mitigate the biasness of parameter estimator.

In contrast to model updating on the basis of equation error, the output error approaches for model updating minimize the output errors between analytical modal data and experimental ones. The virtues of the approaches encompass the unbiased estimation as well as the fact that the match between analytical and measurement DOFs is not required. As modal parameters are nonlinear functions of updating parameters, the output error approaches generally give rise to nonlinear optimization problems in which the problems of convergence and computation time could appear. Furthermore, the iterative scheme requires the evaluation of eigenvalue problem and eigensensitivity at each of iteration. Nevertheless the sensitivity-based methods have been widely accepted and have been proven very promising due to the fact that they can be readily applied to practical cases where measured coordinates are incomplete.

When solving the nonlinear optimization problem with a gradient-based approach, the calculation of sensitivity is indispensable. Of concern is the eigensensitivity analysis, i.e. the calculation of changes in modal properties with respect to physical parameter variation, which is also very useful in other disciplines such as structural

modification, structural design optimization, and analysis of random system. The determination of eigenvalue derivatives is shown to be simple and straightforward (e.g. Fox and Kapoor 1968). Taking the derivative of the eigenvector equation for the  $i$ th eigenvalue, with respect to the  $j$ th design variable, one obtains

$$\left( \frac{\partial \mathbf{K}}{\partial \theta_j} - \lambda_i \frac{\partial \mathbf{M}}{\partial \theta_j} \right) \boldsymbol{\phi}_i - \frac{\partial \lambda_i}{\partial \theta_j} \mathbf{M} \boldsymbol{\phi}_i + (\mathbf{K} - \lambda_i \mathbf{M}) \frac{\partial \boldsymbol{\phi}_i}{\partial \theta_j} = 0 \quad (2.25)$$

Premultiplying by the transpose of the eigenvector,  $\boldsymbol{\phi}_i^T$ , and then applying mass orthogonality, Equation (2.25) reads as

$$\frac{\partial \lambda_i}{\partial \theta_j} = \boldsymbol{\phi}_i^T \left( \frac{\partial \mathbf{K}}{\partial \theta_j} - \lambda_i \frac{\partial \mathbf{M}}{\partial \theta_j} \right) \boldsymbol{\phi}_i \quad (2.26)$$

This expression in Equation (2.26) is simple to calculate and requires only the  $i$ th eigenvalue and eigenvector. However, the calculation of eigenvector derivatives is found much more complicated. Fox and Kapoor (1968) presented two approaches for the determination of eigenvector derivatives. In the first approach, the eigenvector derivative is expressed as a linear function of all the eigenvectors. Although analytically simple and mathematically elegant, this approach becomes prohibitively expensive for large-scale structures as it requires the calculation of all eigenvectors. The second approach involves the use of eigenvalue equations together with an equation derived from the mass orthogonality equation to generate  $n+1$  equations with the  $n$  unknown element of eigenvector derivatives. The solution of this set of equations by a pseudo-inverse technique is also computationally expensive due to loss of symmetry and banded form of the equations. Nelson (1976) developed an

efficient method for the calculation of derivatives of the  $i$ th eigenvector by just using the modal data of that mode. However, a matrix inverse of system dimension (in fact, of dimension of  $n-1$  where  $n$  is the dimension of the system), which is not readily available from the byproducts of generalized eigenvalue problem, is required for each mode in order to solve the linear algebraic equations involved. In order to improve the computational efficiency, an improved approach that utilized the calculated lower modes and the known flexibility matrix to approximate the required eigenvector derivatives was proposed by Lim *et al.* (1987). Ojalvo (1987), Sutter *et al.* (1988), Tan (1989), and Alvin (1997) used iterative methods for the calculation of eigenvector derivatives. Close or repeated eigenvalues can cause ill-conditioning or slow convergence in these methods, and in these systems the simple algorithms of Fox and Kapoor (1968) and Nelson (1976) cannot be implemented satisfactorily. Works that addressed the eigenvalue and eigenvector sensitivities of the systems with repeated eigenvalues were reported by Millscurran (1988) and Dailey (1988).

Collins *et al.* (1974) were among the first to propose the sensitivity-based method of FE model updating. The solution is obtained by successively linearizing modal data as a function of structural parameters

$$\begin{Bmatrix} \Delta \mathbf{f} \\ \Delta \Phi \end{Bmatrix} \approx \begin{Bmatrix} \frac{\partial \mathbf{f}(\boldsymbol{\theta})}{\partial \boldsymbol{\theta}} \\ \frac{\partial \Phi(\boldsymbol{\theta})}{\partial \boldsymbol{\theta}} \end{Bmatrix} \Delta \boldsymbol{\theta} \quad (2.27)$$

where  $\Delta \boldsymbol{\theta}$  is the perturbation in the parameters;  $\Delta \mathbf{f}$  and  $\Delta \Phi$  are the discrepancies in eigenvalues and eigenvectors between analytical predictions and testing results,

respectively; and  $\partial \mathbf{f} / \partial \boldsymbol{\theta}$  and  $\partial \boldsymbol{\phi} / \partial \boldsymbol{\theta}$  are the sensitivities of eigenvalues and eigenvectors with respect to updating parameters evaluated at the linearization point, respectively. Furthermore they incorporated the Bayesian theorem for parameter estimation in which confidence levels in the analytical models and the measurement data are considered. Both the measurements and the current parameter estimates are assumed to have uncertainties given in terms of their estimated variances, namely  $\mathbf{V}_{\boldsymbol{\varepsilon}}$  and  $\mathbf{V}_{\boldsymbol{\theta}}$ . The updated parameters with the minimum variance are then calculated as

$$\Delta \boldsymbol{\theta} = \mathbf{V}_{\boldsymbol{\theta}} \mathbf{S}^T [\mathbf{S}^T \mathbf{V}_{\boldsymbol{\theta}} \mathbf{S} + \mathbf{V}_{\boldsymbol{\varepsilon}}]^{-1} \boldsymbol{\varepsilon} \quad (2.28)$$

and the variance of this updated parameter is estimated as

$$\mathbf{V}_{\boldsymbol{\theta}}^* = \mathbf{V}_{\boldsymbol{\theta}} - \mathbf{V}_{\boldsymbol{\theta}} \mathbf{S}^T [\mathbf{S}^T \mathbf{V}_{\boldsymbol{\theta}} \mathbf{S} + \mathbf{V}_{\boldsymbol{\varepsilon}}]^{-1} \mathbf{S} \mathbf{V}_{\boldsymbol{\theta}} \quad (2.29)$$

where  $\boldsymbol{\varepsilon}$  is the combined vector of discrepancies in eigenvalues and eigenvectors,  $\boldsymbol{\varepsilon} = \{\Delta \mathbf{f}^T \Delta \boldsymbol{\phi}^T\}^T$ ; and similarly  $\mathbf{S}$  is the combined vector of eigenvalue and eigenvector derivatives. However, this derivation is based on the assumption that the measured data and the analytical data are statistically independent. In general, this will be true only for the first iteration. After the first iteration, the measured data have been used to update the parameters, and therefore the assumption of statistical independence is a gross simplification. Friswell (1989) calculated the correlation between the measurements and the updated parameter estimates at each of iteration and the correlation matrix was used to calculate the next parameter vector estimate. This improvement seems to converge more quickly. Torkamani and Ahmadi (1988) argued that the method of Collins *et al.* (1974) is not realistic because it forces the

updating parameters at each iteration to converge to the initial parameters, and presented an improved method which is rapidly convergent to the desired solution. Ricles and Kosmatka (1992) combined the modal force residual method of Chen and Garba (1988) for damage localization and the statistical identification method of Collins *et al.* (1974) for damage quantification.

Chen and Garba (1980) argued that it is difficult to determine the confidence levels associated with the updating parameters and the measurement data, and that only those data considered to be 100% accurate should be taken into consideration in order to avoid leading to totally erroneous updated model. Zhang *et al.* (1987) extended the sensitivity-based method first to localize the dominant modelling errors/damage and then to update the analytical model by iteratively correcting the selected parameters. Noticing that difficulties could be encountered in matching modes and convergence when the analyzed structure has quasi-multiple eigenvalues, Zhang and Lallement (1989) introduced the selective structural modifications to allow the separation of neighboring eigenvalues. Lin *et al.* (1995) proposed an improvement in which the computation of sensitivity matrix was accomplished using the combined analytical and experimental modal data, and the advantage of the improved method over the traditional method in terms of fast convergence and convergence region was demonstrated. Teughels *et al.* (2002) formulated damage functions as approximation to stiffness distribution within the damage area with the purpose of reducing the number of updating parameters. The application of sensitivity-based model updating methods for model refinement and damage

detection of bridge structures was reported by Brownjohn and Xia (2000), Zhang *et al.* (2000), Zapico *et al.* (2003), Unger *et al.* (2005), and Huth *et al.* (2005).

Similar to damage index methods for damage localization, one of the distinctions between various sensitivity-based methods is the type of measurement data used for model updating. The selection of the residuals to be minimized is a crucial step as the residuals should be sensitive to local and small modelling errors or slight structural damage. Basically, in addition to commonly used modal data, FRF data, time series of response data, or the combination of these, can be used. For the modal domain data, besides the modal frequencies and mode shapes, the modal strain energy (Stubbs and Kim 1996; Shi *et al.* 2000b), modal flexibility (Wu and Law 2004), and curvature mode shape (Ruotolo and Surace 1997; Maeck and De Roeck 1999) also have been used for model refinement and damage detection. However, a study by Abdel Wahab (2001) indicated that the inclusion of curvature mode shapes does not improve the convergence of sensitivity-based model updating algorithms. In addition, one recent paper by Worden *et al.* (2005a) argued that the quantities that are sensitive to local structural damage will also be sensitive to environmental conditions and measurement noises. As modal data are indirect measurement data, they could be contaminated by measurement errors as well as modal extraction errors. To avoid the modal extraction errors, the FRF data in frequency domain may be used directly to update the FE model without extracting the natural frequencies and mode shapes (Fritzen and Zhu 1991; Friswell and Penny 1992; Fritzen *et al.* 1998; Zimmerman *et al.* 2005). One problem associated with model updating using FRF data is that the

damping must be considered in the analytical FE model to achieve good updating results. The system identification and model updating can also be accomplished with the direct use of time domain data (e.g., Choi and Stubbs 2005; Kang *et al.* 2005).

Parameterization is a key issue in FE model updating (Friswell *et al.* 2001). It is important that the chosen updating parameters should be able to clarify the ambiguity of the model, and it is necessary for the model output to be sensitive to the parameters. Usually selection of elements in the mass and stiffness matrices as candidate parameters performs very poorly, and this is one reason why the direct methods of model updating such as optimal matrix updating methods and eigenstructure assignment methods are not favored (Friswell and Mottershead 1995). The strategy of selecting physical parameters such as the flexural rigidity of a beam element, Young's modulus, and geometrical dimension, is commonly used in model refinement and damage detection applications. Despite the clear physical meanings, these methods are difficult to model the joint stiffness and cannot correct both the model structure and model order errors. The generic element theory proposed by Gladwell and Ahmadian (1995) shows a good balance between the matrix-element updating scheme and physical-parameter updating strategy. The updated model is correlated to the experimental data by automatically introducing relevant effects which original FE model does not possess, while keeping the structural connectivity defined by the original FE model. The main obstacle is that one cannot give physical explanation of updated generic parameters, which hinders the wide application of

generic element theory to damage detection and model refinement (Ahmadian *et al.* 1997).

#### **2.3.4 Stochastic Model Updating Methods**

Although Chen and Garba (1980) argued only those data considered to be 100% accurate should be taken into consideration in order to avoid leading to totally erroneous updated model, such an argument is not justified in practice as the measurement data from the sensor always contains some, albeit small, amounts of noises superimposed in the desired signal. One important drawback existent in most of the previous model updating methods is that they do not account for the statistical variation both in the material properties and in the measured modal properties. The uncertainties in measured modal properties may arise from the following two obvious sources.

**Source A.** The measured modal properties are inevitably corrupted with measurement noises no matter how precise the instrumentations are, whereby the measurement noises are generally characterized to have a zero mean and their magnitude depend on the experimental equipment, the test environment and data processing (Sanayei *et al.* 2001). Furthermore, the errors can also be introduced when identifying the modal properties from the time-domain signals such as accelerations.

**Source B.** It is widely known that many structural parameters such as Young's modulus and material strength are inherently random variables that can only be

characterized from the standpoint of statistics. However, for a specific structure, each of the above parameter value in this structure is given as the deterministic quantity rather than a random quantity, and this value represents a realization (sample) of random variable which is not exactly known. The determination of these quantities could resorts to the deterministic system identification/model updating approaches. Nevertheless, when the structure operates in varying operational and environmental conditions, some of parameters and therefore the whole structure exhibits a certain degree of randomness. One witness is *natural modal variability* mainly caused by the varying temperature which would alter the Young's modulus of structures (Sohn *et al.* 1999; Peeters and De Roeck 2000; Ko *et al.* 2003). As it is well known that the Young's modulus varies with environmental temperature  $T$ , the Model Code 90 issued by the CEB in 1991 suggested the correlation between temperature and Young's modulus as:  $E(T) = E_{20^{\circ}\text{C}} \times (1.06 - 0.003 \times T)$  in which  $E_{20^{\circ}\text{C}}$  is Young's modulus at the temperature of 20 Celsius degree (Breccolotti *et al.* 2004). Accordingly the modal parameters measured from a SHM system will show their statistical variations.

In practice both uncertainties contribute to the variability of measured modal data. In the presence of uncertain modal properties, it is important to study and quantify their effect on the model updating results, as well as to estimate the resulting statistics of updating parameters. For simplicity, the stochastic model updating or statistical system identification can be described as follows: given the statistics of measured modal data, determine the statistics of structural parameters in the updated FE model

by an uncertainty-propagation approach. This review will be concerned exclusively with probabilistic methods for the modelling of uncertainty in measured modal data. In other words, the measured modal properties are characterized with continuous random variables with known distributions. Other uncertainty models, such as fuzzy logic (Cherki *et al.* 1999) and interval method (Nakagiri and Suzuki 1999; Worden *et al.* 2005b), are equally valid, and model updating based on uncertain measured modal data may also be formulated for these uncertainty models.

The commonly used method for uncertainty propagation is the Monte Carlo simulation (MCS) method. The basic concept behind the MCS method is simple and straightforward: the MCS method first generates large amounts of samples following the predefined probability density functions (PDFs) or the joint PDFs of modal properties; the model updating algorithm is then repeatedly executed for these samples to obtain the corresponding solution samples of updating parameters; and the PDFs of updating parameters are finally obtained from the solution samples. Agbabian *et al.* (1988) employed the MCS method to identify the statistical properties of stiffness coefficients in a linear system. In their simulation study, they computed the time histories of the applied excitation as well as the accelerations, velocities, and displacements of a system. The calculated data were then corrupted with a set of Gaussian noise. By separately applying the model updating procedure to different time segments, ensembles of stiffness coefficients were identified. Subsequent statistical analysis yielded statistical measures such as mean, variance, and PDF. This work has been later extended to statistical identification of a nonlinear

system approximated by an equivalent linear one (Smyth *et al.* 2000). Banan *et al.* (1994a, b), Sanayei and Saletnik (1996a, b), Yeo *et al.* (2000), and Zhou *et al.* (2003) adopted similar approaches for studying the effect of measurement noise on identification results. However, the MCS method is by itself computationally intensive as it requires a large number of simulations to obtain an accurate and valid statistics, and the further need for iterative scheme in each run of model updating algorithm would be prohibitive for most problems.

Perturbation method is another very popular technique for uncertainty propagation. It has been applied very successfully in the discipline of stochastic structural analysis where the perturbation technique in conjunction with the FE analysis is applied to evaluate the response variability and failure probabilities associated with prescribed limit states (Kleiber and Hien 1992). Perturbation method expands the nonlinear function in terms of random variables either by a linear function or by a quadratic one at a particular point. Second moment technique is then applied to evaluate the mean and standard deviation of the response, or to evaluate the failure probabilities. Liu (1995) might be the first to adapt this technique to model updating. In her work, the identification of structural parameters is formulated in a linear least squares problem to minimize the modal force residuals. To investigate the influence of measurement errors, the author expanded each term in a system of linear equations (identification equations) in terms of random variables (random modal properties). Making use of the expanded sets of linear equations, the mean and covariance of updating parameters are finally derived. Papadopoulos and Garcia (1998) presented a

two-step probabilistic method for damage assessment to determine the statistics of stiffness coefficients (SC) of the damaged structure. They first used the measured statistical changes in modal frequencies and mode shapes to obtain the statistics of stiffness reduction factor (SFR). These statistics of SFR along with the statistics of SC corresponding to healthy structure are then combined to determine the statistics of SC of the damaged structure. A set of graphical and statistical probability damage quotients was then used to assess the existence of damage by the comparison of statistics of SC before and after damage. Xia *et al.* (2002), and Xia and Hao (2003) updated the statistics of stiffness of the damaged structure in a single step and used the statistics of stiffness before and after structural damage to implement probabilistic damage detection. Other researches addressing the statistical parameter estimation using uncertain modal data include the work of Li and Roberts (2001a, b) who incorporated the uncertainty-propagation approach with extended Kalman filter method for recursive identification of random structural parameters, Araki and Hjelmstad (2001) who used the higher-order perturbation method based on the concept of optimum sensitivity, Fonseca *et al.* (2005) who combined the maximum likelihood method with perturbation technique for estimating the statistics of random location of a mass.

The method of statistical identification of structures which is capable of dealing with uncertainties both in FE model and measured modal properties was first developed by Collins *et al.* (1974), and later improved by Friswell (1989) to accelerate the convergence rate. They presented a minimum variance method for statistical

estimation of flexural and torsional stiffness based on Bayesian theorem. In their method, both structural parameters and measured modal properties are assumed to have errors given in terms of their variances. The estimation of mean and variance of the updating parameters is iteratively obtained and the iteration will cease if the difference of parameter estimation in two consecutive iterations is small. A more rigorous and comprehensive Bayesian updating has been developed by Beck and his co-workers (Beck and Katafygiotis 1998; Katafygiotis and Beck 1998; Yuen and Katafygiotis 2005).

### ***2.3.5 Regularization Methods***

Most of sensitivity-based model updating methods require the inversion of a matrix, which could lead to numerical difficulties as well as the general problem of conditioning and uniqueness in model updating due to incomplete measurement data (Hjelmstad 1996). It is usually not feasible to measure the response of physical system at all DOFs of the analytical model, and to collect the data from all natural modes that the analytical model possesses. Generally the measurement data only contain fewer modes than the order of the analytical model and are said to be incomplete. Thus the observed dynamic behaviour lies in a narrow knowledge space of the investigated structure (Mottershead and Friswell 1993). The problem introduced by the incompleteness can become significant in large structures where it is expensive to take measurements at a large number of locations and to process large volumes of data. It is well known that the incompleteness could lead to

under-determined system of equations as well as give rise to problems of ill-conditioning and non-uniqueness in model updating, resulting in an infinite number of least squares solution. The ill-conditioning associated with the under-determined system of equations is generally named as physical ill-conditioning. One approach to overcome the physical ill-conditioning is to take the missing information from a prior model instead of from the measurement records. Other techniques to overcome the physical ill-conditioning include the methods by reducing the number of updating parameters such as substructure technique (Koh *et al.* 1991; Yun and Lee 1997; Pothisiri and Hjelmstad 2003), damage function (Teughels *et al.* 2002), selective sensitivity technique (Ben-Haim and Prells 1993; Prells and Ben-Haim 1993; Pham and Bucher 2005), modelling errors/damage localization technique (Natke 1991), as well as the methods by enriching the observed knowledge space of the investigated structure such as attaching fictitious mass or stiffness to the structure (Nalitolela *et al.* 1993; Cha and de Phillis 2001), boundary perturbation technique (Rade and Lallement 1998), and combination of static and dynamic testing data (Hajela and Soeiro 1990; Wang *et al.* 2001).

In contrast to the physical ill-conditioning associated with under-determined system of equations, the numerical ill-conditioning could take place for both of determined and over-determined systems of linear equations with a general form of  $\mathbf{Ax} = \mathbf{b}$  when one or more columns of matrix  $\mathbf{A}$  can be expressed as a linear or nearly linear combination of the other columns. The linear or almost linear dependency occurs when two neighbouring elements of a FE model have nearly the same effects on the

dynamics of the structure. This can be manifested through the singular value decomposition (SVD) of matrix  $\mathbf{A}$  whose singular values (SVs) can either decay gradually to zero or be separately clustered. Hansen (1998) defined two types of the ill-conditioned problems. The first type is a rank-deficient problem where there is a well-determined gap between large and small SVs of matrix  $\mathbf{A}$ . The second type is the discrete ill-posed problem where all SVs decay gradually to zero. Both of them could lead to erroneous results as well as convergence issues in nonlinear optimization problems. This effect is exacerbated when the measurement data are contaminated by measurement noises. Therefore the treatment of ill-conditioned and noisy systems of equations is a problem central to FE model updating and has been addressed by Mottershead and Foster (1991), Natke (1993; 1998), Maia and Silva (1997), Fritzen *et al.* (1998), Ahmadian *et al.* (1998), and Friswell *et al.* (2001). Interested in this study is the numerical treatment of ill-conditioning of system of  $n$  equations with  $m$  unknown updating parameters ( $n \geq m$ ) in model updating by using the numerical regularization methods.

The extended weighted least squares procedure is a form of regularization adopted by a number of researchers. In this method, the model updating problem reduces to minimization of the following quadratic objection function

$$J(\boldsymbol{\theta}) = \boldsymbol{\varepsilon}(\boldsymbol{\theta})^T \mathbf{W}_{\varepsilon\varepsilon} \boldsymbol{\varepsilon}(\boldsymbol{\theta}) + (\boldsymbol{\theta} - \boldsymbol{\theta}_0)^T \mathbf{W}_{\theta\theta} (\boldsymbol{\theta} - \boldsymbol{\theta}_0) \quad (2.30)$$

where  $\boldsymbol{\varepsilon}(\boldsymbol{\theta})$  is the residual vector between analytical predictions and measurement results of modal parameters; the vector  $\boldsymbol{\theta}_0$  designates the prior knowledge with

respect to  $\boldsymbol{\theta}$ ; and  $\mathbf{W}_{\boldsymbol{\varepsilon\varepsilon}}$  and  $\mathbf{W}_{\boldsymbol{\theta\theta}}$  are the weighting matrices for the residual norm and the solution norm, respectively. When  $\mathbf{W}_{\boldsymbol{\varepsilon\varepsilon}}$  and  $\mathbf{W}_{\boldsymbol{\theta\theta}}$  are the diagonal matrices of inverse covariance matrices  $\mathbf{C}_{\boldsymbol{\varepsilon\varepsilon}}^{-1}$  and  $\mathbf{C}_{\boldsymbol{\theta\theta}}^{-1}$ , Equation (2.30) leads to the well-known Bayesian approach (Collins *at al.* 1974; Torkamani and Ahmadi 1988). The determination of weighting matrices is a key issue. Link (1993; 2001) related the weighting matrix for the solution norm in Equation (2.30) to the inverse of squared sensitivity matrix, as

$$\mathbf{W}_{\boldsymbol{\theta\theta}} = w\mathbf{B} \quad (2.31)$$

where  $\mathbf{B} = \text{mean}(\mathbf{g}) \times \mathbf{g}^{-1} / \text{mean}(\mathbf{g}^{-1})$ ;  $\mathbf{g} = \text{diag}(\mathbf{S}^T \mathbf{W}_{\boldsymbol{\varepsilon\varepsilon}} \mathbf{S})$ ; and  $\mathbf{S}$  is the modal sensitivity with respect to parameter vector  $\boldsymbol{\theta}$ . This definition allows to constraining the parameter modification according to the sensitivity of the parameters. The  $k$ th parameter  $\theta_k$  will remain unchanged if its sensitivity approaches zero. Otherwise, it could change significantly if its sensitivity is large. However, the method for choosing the parameter  $w$  was not discussed in his papers. Prells (1996) formulated a weighting matrix based on data sensitivities calculated from an approach similar to the MCS method.

Another type of regularization is the well-known Tikhonov regularization, also called Tikhonov-Phillips method as Tikhonov and Phillips independently developed the method. In Tikhonov regularization, instead of minimization of the residual norm of  $\|\mathbf{Ax} - \mathbf{b}\|_2^2$ , the regularized optimization problem is reformulated as the minimization of a quadratic objective function, as

$$\tilde{J}_{\mathbf{x}} = \|\mathbf{Ax} - \mathbf{b}\|_2^2 + \lambda^2 \|\mathbf{x}\|_2^2 \quad (2.32)$$

in which  $\lambda$ , called Tikhonov parameter, controls the weight given to the solution norm  $\|\mathbf{x}\|_2^2$ , which is a smoothness measure of solution, relative to the residual norm  $\|\mathbf{Ax} - \mathbf{b}\|_2^2$ , which is a goodness-of-fit measure of solution. The difficulty in this class of regularization method is to choose the Tikhonov parameter  $\lambda$  such that it gives a suitable balance between the residual norm and the solution norm. Naturally, if  $\lambda$  is too small the regularized problem will be too close to the original ill-posed one and the solution process will still be highly oscillatory due to noise amplification; if  $\lambda$  is too large then the solution will be too smooth and have little connection with the original problem.

Early work on the application of Tikhonov method to system identification and model updating includes those of Rothwell and Drachman (1989), Ojalvo and Ting (1990), Mottershead and Foster (1991), and Fregolent *et al.* (1996). In these studies the Tikhonov parameter was determined through trial-and-error. Problems will occur when Tikhonov method is blindly applied to the practical problems. Busby and Trujillo (1997) studied the effect of Tikhonov regularization in the reconstruction of dynamic loadings from the strain measurement. They applied both the L-curve method (LCM) and generalized cross validation (GCV) to choice of optimal regularization parameter. Ahmadian *et al.* (1998) numerically and experimentally investigated Tikhonov regularization for the equation-error-based FE model updating. They used GCV for determination of the truncation level in the truncated SVD and

LCM for choice of the optimal Tikhonov parameter. Ziaei-Rad and Imregun (1999) summarized the existing regularization methods applied to model updating. They further examined the performance of Tikhonov regularization, truncated SVD, total least squared method, and the maximum entropy method for FRF-based model updating technique. Mares *et al.* (2002) explored the robust estimation technique and Tikhonov regularization method for the output-error-based model updating using measured modal frequencies, and applied an uncertainty bound model and LCM to determine the regularization parameters, respectively.

Truncated SVD is another form of regularization by truncating the last several smallest SVs to improve the conditioning of matrix. Likewise, the difficulty existing in this type of regularization is the determination of the truncation parameter. A trial-and-error procedure is used by Mottershead and Foster (1991) to determine the truncation parameter. D'Ambrogio and Fregolent (1998) determined the truncation parameter by simultaneous minimization of the natural frequency error and the response residual error. Ren (2005) presented a method for determination of the truncation level. In his method, those SVs, the ratios of which to residual norm are smaller than a prescribed value, are disregarded. However, the success of the method depends on the choice of the prescribed value which was not discussed in the study. The small value could cause the iteration divergent, while the large value gives rise to a low convergence rate.

## 2.4 Critical Issues and Shortcomings in Existing Methods

Although the idea of vibration-based damage detection appears intuitive and considerable research effort has been devoted to it during the past decades, assessing structural damage in large-scale bridges still remains a challenging task for civil engineers. The primary sources of difficulty for reliable damage detection includes the insensitivity of modal properties to local damage, the uncertainty and incompleteness of measurement data, the natural modal variability arising from varying operational and environmental conditions, and the modelling errors in the analytical models.

The first obstacle to reliable implementation of vibration-based damage detection methods is the insensitivity of modal properties (in particular modal frequencies and mode shapes) to local structural damage and the incompleteness of measurement data. Some derivatives (indices) which might be more sensitive to local structural damage have been constructed from the basic modal properties; however the statistical uncertainties associated with these derivatives have not yet been quantified, to the best of the writer's knowledge. It is commonly acknowledged that modal frequencies are measured more accurately than mode shapes. Typical resolution for the modal frequencies of a lightly damped structure is 0.1%; whereas typical mode shape error is 10% or more (Friswell and Penny 1997). It is presumable that these synthesized derivatives could have more uncertainty than those associated with mode shapes. A study by Worden *et al.* (2005a) indicated that those indices sensitive to local damage

are also sensitive to environmental conditions and measurement noise. Thus, in the writer's opinion, utilizing the derivatives for damage detection may be not very fruitful. The incompleteness of measurement data further complicates the reliable damage detection. Both the insensitivity and incompleteness of modal properties could lead to the ill-conditioned system of equations in both model refinement and damage detection. Recently, although there have been attempts to deal with the ill-conditioned and noisy system of equations, these attempts are largely restricted to the linear least squares problem formulated by minimization of the equation error (Ahmadian *et al.* 1998; Ziaei-Rad and Imregun 1999; Friswell *et al.* 2001). However many model updating algorithms, especially those used in civil engineering community, leads to the nonlinear optimization problems in terms of updating parameters. The investigation of regularization methods in this type of model updating algorithms, in particular the methods to optimize regularization parameters, is still limited and requires further exploration.

The second obstacle is the uncertainty associated with measured modal parameters which also impedes reliable implementation of FE model updating algorithms. As uncertainty is inevitable in measurement data, it seems more natural to pursue the model updating in a framework of probability and statistics. However, most current investigations on system identification and model updating aim at developing methods for deterministic estimation of structural parameters on the assumption that all information about the structures (material properties, modal frequencies, and mode shapes, and so forth) is considered to be fixed quantities. These methods are

incapable of accommodating the stochastic nature of measured modal properties and lack robustness in dealing with uncertainties in the measured modal properties. In contrast to the myriad of literature addressing deterministic FE model updating, there is a paucity of publications on the statistical identification of structural systems. The application of statistical methods in model updating has been advocated by Collins *et al.* (1974) although their study was originally intended to overcome the ill-conditioning. The necessity to incorporate statistical methods into model updating algorithms has been recognized by several researchers (Liu 1995; Papadopoulos and Garcia 1998; Araki and Hjelmstad 2001; Xia *et al.* 2002; Fonseca *et al.* 2005; Zimmerman 2006). The current application of probabilistic methods in model refinement and damage detection is immature. More development and exploration are needed in the direction of stochastic model updating and probabilistic damage detection.

One issue arising from the stochastic FE model updating is how to use the model updating results. On the basis of model updating results, the conclusion can be reached that one or more members are damaged. However, further to this conclusion is the question what action should the bridge authorities take? Hence, it is apparent that one more step is called for through which the model refinement and damage detection results can eventually be channeled to the managers for decision making. In recognizing structural reliability to be a major decision factor throughout the life cycle of a civil infrastructure system, Yao, Natke and their colleagues defined health monitoring and structural reliability as a value chain (Yao and Natke 1994; Wong

and Yao 2001). Based on this concept, Stubbs *et al.* (2000) presented a methodology to continuously assess the safety of civil engineering structures. In their method, structural damage is first identified using the measurement data of modal parameters, and structural reliability methods are then applied to the possibly damaged structure to determine the failure probability of structural systems. However, that study is based on the deterministic system identification/damage detection approach that lacks the capability to take into account uncertainties in measurement data. To the best of the writer's knowledge, no work has been yet devoted to the use of stochastic model updating results for reliability evaluation and decision making. Additionally, a gap between health monitoring technology and bridge inspection, management and maintenance exercises currently exists which impedes bridge managers to benefit from the monitoring system.

It has been recognized recently that the performance of vibration-based damage detection algorithms is seriously attenuated due to the natural modal variability. Such natural modal variability is caused by varying environmental/operational conditions. In reality, civil engineering structures are subject to varying environmental and operational conditions such as temperature, traffic, wind, humidity, and solar-radiation. These environmental effects cause changes in physical parameters such as Young's module, structural mass, boundary conditions, and thermal-induced internal forces in redundant structures, and hence induce changes in modal parameters. For obtaining a reliable and accurate damage detection result, it is of paramount importance to characterize the normal modal variability and discriminate

such modal variability from the abnormal changes in modal parameters caused by structural damage. When the effects of normal environmental changes are well understood or quantified, it is possible to achieve reliable and accurate damage identification through incorporating the environmental effect models into the damage detection algorithms in either a statistical or deterministic way (Worden *et al.* 2002; Kim *et al.* 2004). Considerable research effort has been made on investigating the influence of environmental conditions on modal frequencies of bridges via field measurements and dynamic tests (Askegaard and Mousing 1988; Robert and Pearson 1996; Abdel Wahab and De Roeck 1997; Farrar *et al.* 1997; Cornwell *et al.* 1999b; Sohn *et al.* 1999; Alampalli 2000; Lloyd *et al.* 2000; Rohrmann *et al.* 2000; Bolton *et al.* 2001; Peeters and De Roeck 2001; Ko *et al.* 2003). Most of these investigations indicated that temperature was the critical source causing the variability of modal parameters, and the changes in modal frequencies caused by temperature might reach up to 4% or more in highway bridges. Although many field measurements and observations have been made, very few studies have addressed the modelling of environmental effects on modal frequencies.

Because of very few studies available in the literature, the following aspects deserve further exploration: 1) the treatment of ill-conditioning in output-error-based model updating; 2) the quantification of influence of uncertainty in measurement data on the quality of model updating/damage detection results; 3) the use of stochastically updated model for reliability analysis, condition assessment, and decision making; and 4) the interpretation of monitoring data in terms of structural health and

condition. The above issues will be addressed in this PhD study.

## **Chapter 3**

### **REGULARIZATION METHODS FOR FE MODEL UPDATING AND DAMAGE DETECTION**

#### **3.1 Introduction**

A FE model which can accurately represent the physical behaviour of a structure is very important in the disciplines of structural design and analysis, damage detection, structural health monitoring, and structural control. For example, in order to make a reliable prediction on load-carrying capacity of a structure, an adequate FE model of the structure is necessary. Despite the high sophistication of FE modelling, practical applications often reveal considerable discrepancies between analytical predictions and experimental results, which may originate from the uncertainties in simplified assumptions of geometry configuration, inappropriate values of material properties, and inaccurate boundary conditions. Thus the analytical model should be adjusted to coincide with the testing results. In practice, the verification and updating of analytical model is mainly based on comparing experimental modal properties with the analytical ones by means of FE model updating procedures.

Because of significant roles in model refinement and damage detection applications, FE model updating using experimental modal data has received wide attention from academic circles for several decades and has been increasingly acknowledged and used by engineering practitioners. Although many advanced and alternative

techniques, such as ANNs, genetic algorithms, and simulated annealing, have been developed and applied to model updating problems, sensitivity-based model updating algorithm still remains as a widely-accepted technique and is preferred in many applications due to its physical meanings.

Despite a lot of research efforts made, one of critical issues that remain in the sensitivity-based methods is how to deal with the resulting ill-conditioned equations (Friswell *et al.* 2001). It is generally recognized that model updating based on experimental modal properties often leads to ill-posed system of equations, where the existence, uniqueness and stability of solution are not assured and numerical instability is likely to take place in the course of solution process (Kravaris and Seinfeld 1985). The situation is further complicated by measurement noises as small measurement noises could be amplified, leading to totally erroneous solutions and convergence problems. There have been attempts to deal with the ill-conditioning in mode updating by using the numerical regularization methods (Rothwell and Drachman 1989; Ojalvo and Ting 1990; Mottershead and Forster 1991; Fregolent *et al.* 1996; Ren 2005). Although these studies indicated that accuracy of model updating could be greatly improved using regularization methods, the determination of regularization parameters in these studies was performed by trial-and-error. Anonymous and automatic selection of these parameters is a critical issue for the implementation of regularization methods. Ahmadian *et al.* (1998) advocated the use of L-curve method (LCM) and generalized cross validation (GCV) for automatic selection of regularization parameters. They implemented GCV for the determination of truncation level in the truncated SVD and LCM for the choice of the Tikhonov parameter. D'Ambrogio and Fregolent (1998) applied the truncated SVD to alleviate the ill-conditioning of model updating from FRF data. In their method, the choice of

truncation level requires a trade-off between the different needs and necessitates some manual intervention. Ziaei-Rad and Imregun (1999) further studied a number of regularization methods and concluded that the determination of optimal regularization parameter seems straightforward using LCM. The previous studies are limited to the equation-error-based FE model updating method. Mares *et al.* (2002) explored a robust estimation method and Tikhonov regularization method for output-error-based model updating by using only the measured modal frequencies, and applied an uncertainty bound model and LCM, respectively, to determine the regularization parameters for the two methods. In most applications of model updating for model refinement and damage detection, it is generally necessary to incorporate simultaneously both the measured modal frequencies and the measured mode shapes. It is presumable that the incorporation of mode shapes in model updating algorithms makes the system of equations more ill-conditioned as the magnitudes of eigenvalues and mode shapes often deviate in several orders.

This chapter addresses the implementation of regularization methods for output-error-based model updating using measured modal frequencies and mode shapes, with research focus on optimization of the regularization parameters. The outline of this chapter is as follows: First, the output-error-based model updating is procedure presented. The procedure consists of solving a nonlinear optimization problem in which an objective function measuring the discrepancies between analytical and experimental modal data is minimized. Two regularization techniques are then applied at each linearization step of the nonlinear optimization problem in order to alleviate the ill-conditioning, where regularization is accomplished either by adding an additional term or truncating the small singular values (SVs) of sensitivity matrix. Subsequently, three methods for optimal choices of the regularization parameters are

presented. The performances of the two regularization techniques accompanied with the three regularization-parameter-choice methods are rigorously examined and assessed through numerical studies on model updating of a truss bridge using both noise-free and noisy measurement data.

## 3.2 Output-Error-Based Model Updating Method

As outlined in **Figure 3.1**, sensitivity-based model updating using an output error approach is quite straightforward. The numerical modal data are first computed from the FE model with the initially estimated values of the unknown physical parameters; and the experimental modal data are obtained from ambient vibration tests on the structure. A process is devised for updating the parameter estimates to minimize the discrepancies between these two sets of modal properties, and it is repeatedly executed until the parameter variation between two consecutive iterations and the discrepancies between analytical and experimental modal data are small enough.

### 3.2.1 Objective Function

In FE model updating using the measured modal data, the identification of structural parameters is formulated in an optimization problem where structural parameters are sought so that the updated FE model can reproduce as closely as possible the measured modal properties. To this end, the objective function in the optimization problem, measuring the output error between analytical and experimental modal properties, is defined as

$$\tilde{J}(\boldsymbol{\theta}) = \tilde{\boldsymbol{\varepsilon}}^T \tilde{\boldsymbol{\varepsilon}} = \|\tilde{\mathbf{z}} - \mathbf{z}(\boldsymbol{\theta})\|_2^2 \quad \text{with } \tilde{\boldsymbol{\varepsilon}} = \tilde{\mathbf{z}} - \mathbf{z}(\boldsymbol{\theta}) \quad (3.1)$$

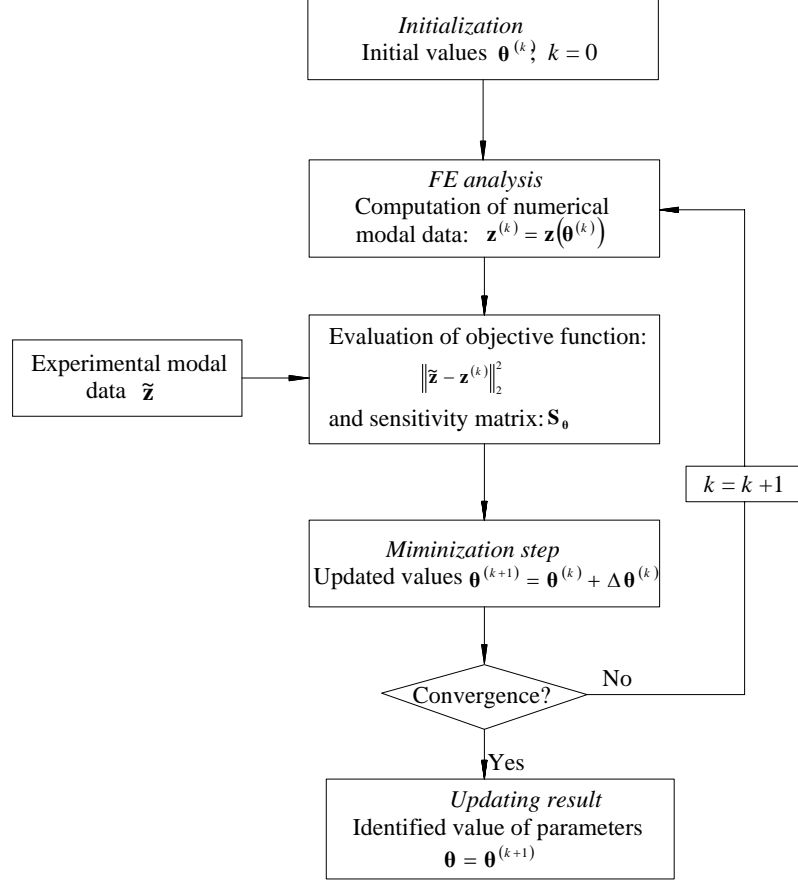


**Figure 3.1 Flowchart of sensitivity-based FE model updating**

where  $\tilde{\boldsymbol{\varepsilon}}$  is the output error of modal properties;  $\tilde{\mathbf{z}}$  and  $\mathbf{z}(\boldsymbol{\theta}) \in R^n$  are vectors of the experimental and analytical modal properties with  $n = n_f \times (n_m + 1)$ ;  $n_f$  and  $n_m$  are the numbers of measured natural frequencies and measured coordinates of each mode shape, respectively;  $\boldsymbol{\theta} \in R^m$  is a vector of  $m$  updating parameters; and the subscript  $T$  denotes vector/matrix transpose. In order to obtain a unique solution, the number of known modal data  $n$  should be not less than the number of unknown updating parameters  $m$ . The experimental modal data  $\tilde{\mathbf{z}}$  consists of the eigenvalues and mode shapes, with the form of

$$\tilde{\mathbf{z}}^T = \left( \tilde{\lambda}_1 \quad \tilde{\Phi}_1^T \quad \tilde{\lambda}_2 \quad \tilde{\Phi}_2^T \quad \cdots \quad \tilde{\lambda}_{n_f} \quad \tilde{\Phi}_{n_f}^T \right) \quad (3.2)$$

where  $\tilde{\lambda}_i$  is the  $i$ th experimental eigenvalues; and  $\tilde{\Phi}_i$  is the corresponding mode shapes. The analytical modal vector which is computed from initial FE model takes a similar form as

$$\mathbf{z}^T = (\lambda_1 \quad \Phi_1^T \quad \lambda_2 \quad \Phi_2^T \quad \dots \quad \lambda_{n_f} \quad \Phi_{n_f}^T) \quad (3.3)$$

where  $\lambda_i$  is the  $i$ th analytical eigenvalue; and  $\Phi_i$  is the corresponding mode shape.

Equation (3.1) represents the basic least squares formulation of model updating problem. A more general formulation is the weighted least squares expression by multiplying each error with a weighting in order to take the relative importance of different types of modal data and their accuracy into account, that is,

$$\boldsymbol{\varepsilon} = \mathbf{W}_\varepsilon (\tilde{\mathbf{z}} - \mathbf{z}(\boldsymbol{\theta})) \quad (3.4)$$

in which  $\mathbf{W}_\varepsilon$  is a diagonal matrix whose element represents the relative importance of each error. The weighted squared sum of the error vector is then formulated as

$$J(\boldsymbol{\theta}) = \tilde{\boldsymbol{\varepsilon}}^T \mathbf{W}_\varepsilon \tilde{\boldsymbol{\varepsilon}} = \|\mathbf{W}_\varepsilon (\tilde{\mathbf{z}} - \mathbf{z}(\boldsymbol{\theta}))\|_2^2 \quad (3.5)$$

whose minimization is essentially a nonlinear least squares problem as the modal vector  $\mathbf{z}$  generally is a nonlinear function in terms of the unknown updating parameter  $\boldsymbol{\theta}$ ; and  $\mathbf{W}_\varepsilon = \mathbf{W}^{1/2}$ . It is worth noting that in the alternative model updating approach based on equation error, the resulting least squares problem can be linear or nonlinear depending on the choice of updating parameters.

It has been shown that proper selection of the weighting matrix in Equation (3.4) is important to improve the updating results (Friswell and Mottershead 1995). Therefore the relative weights for eigenvalues and eigenvectors should be chosen

carefully. As the eigenvalues are measured more accurately than eigenvectors, more weights should be placed on the eigenvalues than on the eigenvectors. Throughout the simulation study in this chapter, the weights for eigenvalues are taken as unit and the weights for eigenvectors are taken as 0.1 (Friswell and Motteshhead 1995; Xia *et al.* 2002).

### 3.2.2 Mode Shape Paring

Before analytical and experimental modal data in Equations (3.2) and (3.3) can be compared, they must be paired correctly, i.e., the data must relate the same modes. Arranging the eigenvalues in ascending order of magnitude is not sufficient since the order of the modes in the analytical FE model will differ from the testing one due to the poor initialization values of updating parameters. Furthermore, the structure may have closely-spaced eigenvalues. Another problem in model paring is that some of experimental modes may be measured inaccurately, usually because the force excitation or the accelerometer is closed to a node of a particular mode shape. If a mode is not excited in the experiment, it should be also eliminated from the analytical modal vector.

Modal assurance criterion (MAC) is the most commonly used method for paring the experimental and analytical modes. MAC defines the correlation between two mode shapes as

$$\text{MAC}(i, j) = \frac{(\Phi_i^T \tilde{\Phi}_j)^2}{(\Phi_i^T \Phi_i) \times (\tilde{\Phi}_j^T \tilde{\Phi}_j)} \quad (3.6)$$

with  $\phi_i$  and  $\tilde{\Phi}_j$  are analytical mode shape and experimental mode shape, respectively. MAC value always lies in between 0 and 1. A MAC value close to 0 indicates bad correlation while a MAC value close to 1 is indicative of good correlation and therefore paired modes. In practice it is commonly accepted that a MAC value larger than 0.9 means the same mode pair.

### 3.2.3 Sensitivity Analysis of Modal Properties

The nonlinear least squares problem formulated in Equation (3.5) can be solved with a number of numerical optimization techniques among which the gradient-based optimization approach is commonly used. In the gradient-based optimization method, the Jacobian matrix (or the sensitivity matrix) needs to be calculated in each of iteration to ensure a correct search direction. The first-order partial derivatives of eigenvalues and eigenvectors with respect to structural parameters are of concern in this study (Fox and Kapoor 1968). The sensitivities of modal properties include those of eigenvalues and the mode shapes, namely

$$\frac{\partial \mathbf{z}}{\partial \boldsymbol{\theta}} = \begin{bmatrix} \frac{\partial \lambda_1}{\partial \theta_1} & \frac{\partial \lambda_1}{\partial \theta_2} & \dots & \frac{\partial \lambda_1}{\partial \theta_m} \\ \frac{\partial \Phi_1}{\partial \theta_1} & \frac{\partial \Phi_1}{\partial \theta_2} & \dots & \frac{\partial \Phi_1}{\partial \theta_m} \\ \vdots & \vdots & \ddots & \vdots \\ \frac{\partial \lambda_{n_f}}{\partial \theta_1} & \frac{\partial \lambda_{n_f}}{\partial \theta_2} & \dots & \frac{\partial \lambda_{n_f}}{\partial \theta_m} \\ \frac{\partial \Phi_{n_f}}{\partial \theta_1} & \frac{\partial \Phi_{n_f}}{\partial \theta_2} & \dots & \frac{\partial \Phi_{n_f}}{\partial \theta_m} \\ \frac{\partial \Phi_{n_f}}{\partial \theta_1} & \frac{\partial \Phi_{n_f}}{\partial \theta_2} & \dots & \frac{\partial \Phi_{n_f}}{\partial \theta_m} \end{bmatrix}_{\boldsymbol{\theta}=\boldsymbol{\theta}^{(k)}} \quad (3.7)$$

where  $\frac{\partial \lambda_i}{\partial \theta_j}$  and  $\frac{\partial \Phi_i}{\partial \theta_j}$  are the sensitivities of the  $i$ th eigenvalue and mode shape with respect to the  $j$ th updating parameter, and their derivations are given in Appendix I.

When only stiffness-related structural parameters are required for correction, the sensitivities of eigenvalues and mode shapes are simplified as

$$\frac{\partial \lambda_i}{\partial \theta_j} = \boldsymbol{\phi}_i^T \frac{\partial \mathbf{K}}{\partial \theta_j} \boldsymbol{\phi}_i \quad (3.8)$$

$$\frac{\partial \boldsymbol{\phi}_i}{\partial \theta_j} = \sum_{k=1, k \neq i}^N \frac{\boldsymbol{\phi}_k}{(\lambda_i - \lambda_k)} \left( \boldsymbol{\phi}_k^T \frac{\partial \mathbf{K}}{\partial \theta_j} \boldsymbol{\phi}_i \right) \quad (3.9)$$

where  $\boldsymbol{\phi}_i$  is the  $i$ th mass-normalized mode shape, i.e.  $\boldsymbol{\phi}_i^T \mathbf{M} \boldsymbol{\phi}_i = 1$ ;  $\frac{\partial \mathbf{K}}{\partial \theta_j}$  is the partial derivative of global stiffness matrix with respect to the  $j$ th updating parameters  $\theta_j$ ; and  $N$  is the total number of DOFs in the analytical model.

#### 3.2.4 Solution of Nonlinear Least Squares Problem

The solution of nonlinear optimization problem (3.5) is obtained using the gradient-based optimization method. It begins with an initial guess of values of the updating parameter  $\boldsymbol{\theta}^{(0)}$  and then generates a sequence of improved estimates  $\boldsymbol{\theta}^{(k)}$  until they reach the solution. Making use of the first-order Taylor expansion series in each iteration  $k$ , one obtains a linearized estimation of the analytical modal data as

$$\mathbf{z}(\boldsymbol{\theta}^{(k+1)}) \approx \mathbf{z}(\boldsymbol{\theta}^{(k)}) + \left. \frac{\partial \mathbf{z}}{\partial \boldsymbol{\theta}} \right|_{\boldsymbol{\theta}=\boldsymbol{\theta}^{(k)}} (\boldsymbol{\theta}^{(k+1)} - \boldsymbol{\theta}^{(k)}) \quad (3.10)$$

in which  $\left. \frac{\partial \mathbf{z}}{\partial \boldsymbol{\theta}} \right|_{\boldsymbol{\theta}=\boldsymbol{\theta}^{(k)}}$  represents the modal sensitivities with respect to updating parameters, evaluated at current parameter estimate  $\boldsymbol{\theta}^{(k)}$ . Substituting Equation (3.10) into Equation (3.5), and then forcing the first-order derivative of the objective function with respect to updating parameters  $\boldsymbol{\theta}$  to zero lead to a set of equations

$$\nabla J(\boldsymbol{\theta}) = -\left(\mathbf{W}_\varepsilon \frac{\partial \mathbf{z}}{\partial \boldsymbol{\theta}}\right)^T \mathbf{W}_\varepsilon \left[ \tilde{\mathbf{z}} - \mathbf{z}(\boldsymbol{\theta}^{(k)}) - \frac{\partial \mathbf{z}}{\partial \boldsymbol{\theta}} (\boldsymbol{\theta}^{(k+1)} - \boldsymbol{\theta}^{(k)}) \right] = 0 \quad (3.11)$$

The solution for updating parameters at the  $k$ th iteration is finally obtained as

$$\boldsymbol{\theta}^{(k+1)} = \boldsymbol{\theta}^{(k)} + \Delta \boldsymbol{\theta}^{(k)} \quad (3.12)$$

$$\Delta \boldsymbol{\theta}^{(k)} = \left[ \left( \frac{\partial \mathbf{z}}{\partial \boldsymbol{\theta}} \right)^T \mathbf{W} \frac{\partial \mathbf{z}}{\partial \boldsymbol{\theta}} \right]^{-1} \left( \frac{\partial \mathbf{z}}{\partial \boldsymbol{\theta}} \right)^T \mathbf{W} [\tilde{\mathbf{z}} - \mathbf{z}(\boldsymbol{\theta}^{(k)})] \quad (3.13)$$

where  $\Delta \boldsymbol{\theta}^{(k)}$  is the parameter variation at the  $k$ th iteration; and  $\tilde{\boldsymbol{\varepsilon}}^{(k)} = \tilde{\mathbf{z}} - \mathbf{z}(\boldsymbol{\theta}^{(k)})$  is discrepancies between the experimental and analytical modal properties at the  $k$ th iteration. By defining the weighted sensitivity matrix as  $\mathbf{S} = \mathbf{W}^{1/2} \frac{\partial \mathbf{z}}{\partial \boldsymbol{\theta}}$ , Equation

(3.13) becomes

$$\Delta \boldsymbol{\theta}^{(k)} = [\mathbf{S}^T \mathbf{S}]^{-1} \mathbf{S}^T \mathbf{W}^{1/2} [\tilde{\mathbf{z}} - \mathbf{z}(\boldsymbol{\theta}^{(k)})] \quad (3.14)$$

As discussed early, an iterative procedure is required to obtain the solution to nonlinear least squares problem (3.5). With the new estimates of updating parameters  $\boldsymbol{\theta}^{(k+1)} = \boldsymbol{\theta}^{(k)} + \Delta \boldsymbol{\theta}^{(k)}$  at the next iteration, the analytical modal properties  $\mathbf{z}(\boldsymbol{\theta}^{(k+1)})$  and the sensitivity matrix  $\mathbf{S}$  are re-calculated. The solution process is repeated until the parameter difference between two consecutive iterations is smaller than a predefined tolerance level.

### 3.3 Regularization Techniques

In FE model updating, the modal sensitivity matrix is often ill-conditioned, and the direct least squares solution, as given by (3.14), yields very poor estimates if the data

are polluted by round-off error and measurement noise. It is therefore important to use proper techniques to solve the system of equations. Such techniques include Tikhonov regularization, truncated SVD, truncated generalized SVD, and others (Hansen 1998).

### 3.3.1 *Ill-Conditioning of Least Squares Problem*

Least squares solution in Equation (3.14) is essentially equal to that of a determined or over-determined system of equations with the form of

$$\mathbf{S}\Delta\boldsymbol{\theta} = \mathbf{e} \quad (3.15)$$

with  $\mathbf{e} = \mathbf{W}^{1/2}(\tilde{\mathbf{z}} - \mathbf{z}(\boldsymbol{\theta}^{(k)}))$  is the weighted error vector at each iteration, in which  $\Delta\boldsymbol{\theta}$  is used instead of  $\Delta\boldsymbol{\theta}^{(k)}$  for simplification. SVD is one of the most convenient tools to solve the system of linear equations as given in Equation (3.15). The SVD of the weighted sensitivity matrix  $\mathbf{S}$  is applied as

$$\mathbf{S} = \mathbf{U}\boldsymbol{\Sigma}\mathbf{V}^T \quad (3.16)$$

where  $\mathbf{U} \in R^{n \times n}$  and  $\mathbf{V} \in R^{m \times m}$  are orthogonal matrices, i.e.  $\mathbf{U}^T\mathbf{U} = \mathbf{I}_n$  and  $\mathbf{V}^T\mathbf{V} = \mathbf{I}_m$ ; and  $\boldsymbol{\Sigma} = \text{diag}(\sigma_1, \sigma_2, \dots, \sigma_m)$  where SVs are arranged in a non-increasing order such that  $\sigma_1 \geq \sigma_2 \geq \dots \geq \sigma_m \geq 0$ . The condition number of  $\mathbf{S}$  is defined as the ratio of the largest SV to the smallest one, as  $\rho = \sigma_1/\sigma_m$ . It should be noted here that none of SVs will be numerically zero due to round-off error. A system of equations with a large condition number of coefficient matrix could be ill-conditioned. In the problem of ill-conditioning caused by round-off error on digital computers, the SVs tend to separate a group of large SVs and a second group of many orders of magnitude smaller; in the case of noisy vibration test data, this well-behaved

separation will not occur for equation-error-based model updating and, instead, the SVs spread evenly over a wide range (Mottershead and Foster 1991).

Making use of the SVD, the left-hand side of Equation (3.15) is rewritten as

$$\mathbf{S}\Delta\boldsymbol{\theta} = \sum_{i=1}^m \sigma_i \mathbf{u}_i (\mathbf{v}_i^T \Delta\boldsymbol{\theta}) \quad (3.17)$$

where  $\mathbf{u}_i$ ,  $\sigma_i$ , and  $\mathbf{v}_i$  are the  $i$ th left singular vector, singular value, and right singular vector of the weighted sensitivity matrix. Equation (3.17) shows that the high-order components related to small SVs have only a small contribution while they must have opposite effect on the inverse problem. After some manipulation of the SVD, the solution to Equation (3.17) and the solution norm are obtained as

$$\Delta\boldsymbol{\theta}_{\text{LS}} = \sum_{i=1}^m \frac{\mathbf{u}_i^T \mathbf{e}}{\sigma_i} \mathbf{v}_i \quad (3.18)$$

$$\|\Delta\boldsymbol{\theta}_{\text{LS}}\|_2^2 = \sum_{i=1}^m \left( \frac{\mathbf{u}_i^T \mathbf{e}}{\sigma_i} \right)^2 \quad (3.19)$$

which clearly indicates that the noise effect will be amplified if the Fourier coefficients  $|\mathbf{u}_i^T \mathbf{e}|$  corresponding to the small SVs  $\sigma_i$  do not decay as fast as the singular values. A necessary condition for obtaining a good and stable solution is that the Fourier coefficients must decay to zero faster than the SVs (Hansen 1990). This condition has been commonly referred to as the Discrete Picard Condition (DPC) in the ill-posed problems. When DPC is not satisfied, the least squares solution  $\Delta\boldsymbol{\theta}_{\text{LS}}$  will be dominated by the high-order components, and large oscillation in solution  $\Delta\boldsymbol{\theta}_{\text{LS}}$  could occur for small perturbation in vector  $\mathbf{e}$  either due to round-off error or

measurement noise. This is further illustrated by the following formula of bounds on estimation errors (Friswell and Mottershead 1995), namely

$$\frac{\|\Delta\boldsymbol{\theta}_{LS}(\delta) - \Delta\boldsymbol{\theta}_{LS}\|_2}{\|\Delta\boldsymbol{\theta}_{LS}\|_2} \leq \rho\delta \quad (3.20)$$

where  $\delta = \frac{\|\mathbf{e}(\delta) - \mathbf{e}\|_2}{\|\mathbf{e}\|_2}$  is the noise level in the weighted error vector  $\mathbf{e}$ ; and  $\rho$  is

condition number of the weighted sensitivity matrix. Equation (3.20) indicates a small disturbance in measurement data cannot produce large relative change in parameter variation  $\Delta\boldsymbol{\theta}_{LS}$  when the condition number  $\rho$  is small; while a large condition number may lead to quite large disturbance in parameter variation even for a small error in measurement data as the relative error in parameter variation could be amplified  $\rho$  times. This observation actually lays the theoretical foundation on many attempts to reduce the condition number by means of reduction of number of updating parameters and enrichment of measurement data.

For the ill-posed nonlinear least squares problem, the fact that the least squares solution at each iteration could become considerable oscillation may lead to problem of instability and divergence during the iteration process. In order to obtain a stable solution at each iteration, methods for dampening or filtering out the effect of the small SVs are required to enforce the parameter variation not too large to give rise to divergence results or physically meaningless solutions. The numerical regularization methods for treatment of the ill-posed problems seek to overcome the problem associated with the large condition number by replacing the problem with a ‘nearby’ well-conditioned one whose solution approximates, albeit is different from, the required solution (Hansen 1992). The well-known regularization methods are

Tikhonov regularization and truncated SVD. The former uses a Tikhonov parameter to dampen the effect of the small SVs, and the latter truncates the small SVs and removes them from the summation of Equation (3.18). A common feature of the two regularization methods is that they depend on a regularization parameter that controls how much filtering is introduced by the regularization. A key issue associated with these methods is to find a regularization parameter that gives a good balance between filtering out enough noise without losing too much information in the obtained solution.

### 3.3.2 Tikhonov Regularization

The most common and well-known form of regularization is Tikhonov regularization, which is also referred to as Tikhonov-Phillips regularization because Tikhonov and Phillips have independently developed the method. In Tikhonov regularization, instead of minimization of residual norm of  $\|\mathbf{S}\Delta\boldsymbol{\theta} - \mathbf{e}\|_2^2$ , the regularized optimization problem is redefined as the minimization of a quadratic cost function as

$$\tilde{J}_{\Delta\boldsymbol{\theta}_\lambda} = \|\mathbf{S}\Delta\boldsymbol{\theta}_\lambda - \mathbf{e}\|_2^2 + \lambda^2 \|\mathbf{L}\Delta\boldsymbol{\theta}_\lambda - \mathbf{d}\|_2^2 \quad (3.21)$$

in which  $\lambda$ , called Tikhonov parameter, controls the weight given to minimization of some kind of the solution norm  $\|\mathbf{L}\Delta\boldsymbol{\theta}_\lambda - \mathbf{d}\|_2^2$ , which is a smoothness measure of solution, relative to minimization of the residual norm  $\|\mathbf{S}\Delta\boldsymbol{\theta}_\lambda - \mathbf{e}\|_2^2$ , which is a goodness of fit measure of solution. The second term in right-hand side of Equation (3.21) is called side constraint which enforces the solution of least squares problem to behave in a predefined manner by appropriate choice of matrix  $\mathbf{L}$  and vector  $\mathbf{d}$ . The matrix  $\mathbf{L}$  is typically either the  $n \times n$  identity matrix  $\mathbf{I}$ , or a  $p \times n$  discrete

approximation of the  $(n-p)$ th derivative operator (Liu and Han 2003). One constraint could be that the parameter variation  $\Delta\boldsymbol{\theta}^{(k)}$  in each iteration  $k$  is minimized, whereby matrix  $\mathbf{L}$  will become an identity matrix; another constraint is to minimize the difference between two neighboring parameters at each iteration; and so forth. Throughout this study, the matrix  $\mathbf{L}$  is assumed to be an identity matrix and the vector  $\mathbf{d}$  is zero for the minimization of the norm of parameter variation.

By letting  $\mathbf{L} = \mathbf{I}$  and  $\mathbf{d} = \mathbf{0}$ , the minimization of Equation (3.21) is equivalent to the following regularized least squares problem

$$(\mathbf{S}^T \mathbf{S} + \lambda^2 \mathbf{I}) \Delta \boldsymbol{\theta}_\lambda = \mathbf{S}^T \mathbf{e} \quad (3.22)$$

Likewise, the solution to Equation (3.22), as a function of Tikhonov parameter  $\lambda$ , is obtained as

$$\Delta \boldsymbol{\theta}_\lambda = \sum_{i=1}^m f_i \frac{\mathbf{u}_i^T \mathbf{e}}{\sigma_i} \mathbf{v}_i \quad (3.23)$$

in which the quantities  $f_i = \sigma_i^2 / (\sigma_i^2 + \lambda^2)$  ( $i = 1, 2, \dots, m$ ), are called filter factors.

It is clear that Tikhonov regularization uses the filter factors to dampen the effects associated with the small SVs  $\sigma_i$ . Making use of the orthogonality of singular vectors, the solution norm  $\|\Delta \boldsymbol{\theta}_\lambda\|_2$  and residual norm  $\|\mathbf{S} \Delta \boldsymbol{\theta}_\lambda - \mathbf{e}\|_2$  can be similarly expressed as

$$\|\Delta \boldsymbol{\theta}_\lambda\|_2^2 = \sum_{i=1}^m \left( \frac{\sigma_i^2}{\sigma_i^2 + \lambda^2} \frac{\mathbf{u}_i^T \mathbf{e}}{\sigma_i} \right)^2 \quad (3.24)$$

$$\|\mathbf{S} \Delta \boldsymbol{\theta}_\lambda - \mathbf{e}\|_2^2 = \sum_{i=1}^m \left( \frac{\lambda^2}{\sigma_i^2 + \lambda^2} \mathbf{u}_i^T \mathbf{e} \right)^2 + \|(\mathbf{I} - \mathbf{U} \mathbf{U}^T) \mathbf{e}\|_2^2 \quad (3.25)$$

These two quantities represent the smoothness and fitness of the solution, and they should be balanced appropriately to have a good selection of the regularization parameter. The methods for selection of the Tikhonov parameter will be discussed in Section 3.4.

### 3.3.3 *Truncated Singular Value Decomposition*

A fundamental observation regarding Tikhonov regularization is the use of filter factors to dampen the effects associated with small SVs. An alternative way is to discard the items associated with small SVs from the summation in Equation (3.18) as they contribute very little to the vector  $\mathbf{e}$ . This is accomplished with the use of truncated SVD. This method amounts to truncating the SVD of the coefficient matrix  $\mathbf{S}$  in such a way that the last several smallest SVs of  $\mathbf{S}$  are discarded, and then solving the modified least squares problem

$$\mathbf{S}_{m_t} \Delta \boldsymbol{\theta}_{m_t} = \sum_{i=1}^{m_t} \sigma_i \mathbf{u}_i (\mathbf{v}_i^T \Delta \boldsymbol{\theta}_{m_t}) = \mathbf{e} \quad (3.26)$$

where  $S_{m_t}$  is the truncated sensitivity matrix; and  $m_t \leq m$  is the truncation parameter that controls the number of SVs set to zero. The truncated SVD yields the regularized solution

$$\Delta \boldsymbol{\theta}_{m_t} = \sum_{i=1}^{m_t} \frac{\mathbf{u}_i^T \mathbf{e}}{\sigma_i} \mathbf{v}_i \quad (3.27)$$

Hansen (1987) investigated the truncated SVD as a means of regularization and compared it with Tikhonov regularization. He proved that, under suitable conditions, for any valid truncation parameter  $m_t$  there always exists a regularization parameter  $\lambda$  for Tikhonov method such that the truncated SVD solution is close to the Tikhonov

solution.

Actually, both Tikhonov regularization and truncated SVD are developed for the solution of linear ill-posed problems. It is reasonably expected that a natural extension in the case of nonlinear least squares problems is to apply them at each of linearized iteration. However the connection between the stability and ill-posedness of a nonlinear problem and its linearization is not as strong as one might think (Engl *et al.* 1996). It is possible to construct a nonlinear operator such that the corresponding nonlinear problem is everywhere ill-posed, whereas the linearized operator is well-posed everywhere; on the other hand, well-posed nonlinear problems may have ill-posed linearization, which often occurs due to poorly assigned initial linearization point.

### **3.4 Determination of Regularization Parameter**

Central to Tikhonov regularization and truncated SVD is the choice of the regularization parameters, namely the Tikhonov parameter  $\lambda$  for Tikhonov regularization and the truncation parameter  $m_t$  for truncated SVD. For a variety of regularization methods, it is well known that the optimal value of the regularization parameter is a function of some unknown parameters and the unknown noise level as it relates to the smoothness of solution. When the noise level in the measurement data is available, the discrepancy principle developed by Morozov (1984) can be applied to determine an appropriate regularization parameter. Following the discrepancy principle, the regularization parameter is chosen such that the residual norm for the regularized solution satisfies

$$\|\mathbf{S}\Delta\boldsymbol{\theta}_{\text{reg}} - \mathbf{e}\|_2 = \|\mathbf{r}\|_2 \quad (3.28)$$

in which  $\|\mathbf{r}\|_2 = \delta\|\tilde{\mathbf{z}}\|_2$  is the norm of measurement noise with noise level of  $\delta$ . This criterion could produce very good regularization parameter for linear ill-posed problem, while sometimes it gives conservative choice of the regularization parameter and therefore yields over-smoothed solutions (Hansen 1998). In many practical applications, a further limitation of this method is that the information regarding the noise level and therefore the noise norm is not always available or reliable.

It is therefore necessary to consider alternative regularization-parameter-choice methods that do not require the knowledge of the noise level. In this study, three commonly used methods for choice of regularization parameters have been studied in the context of output-error-based model updating. The first method examined is LCM in which the curvatures of the L-curve, a log-log plot of residual norm versus solution norm for a wide range of the regularization parameter, are first computed at discrete points of the curve and the regularization parameter corresponding to the maximum-curvature point in the L-curve is selected as the optimal one. GCV is another very popular method. The idea of GCV is to maximize the predictability of the model through a proper setting of the regularization parameter. In comparison with LCM and GCV, minimum product criterion (MPC) seems less well known. This method selects the optimal regularization parameter on the basis of minimization of product of residual norm and solution norm.

The capability of the first two methods has been studied by a number of authors, and is shown to be satisfactory in most cases (Ahmadian *et al.* 1998; Ziaei-Rad and

Imregun 1999; Friswell *et al.* 2001). However the model updating algorithms used in their studies are based on the equation error approach which often leads to a linear least squares formulation for model updating. Contrarily, the output-error-based model updating algorithms used in the present study lead to a nonlinear least squares problem of which the solution requires an iterative scheme. To the best of the writer's knowledge, the performance of the first two methods has not been examined when both modal frequencies and mode shapes are used for output-error-based model updating. In addition, the last method, MPC, has not been used for determining the regularization parameter in model updating problem. Therefore there is a need to examine the performance of these methods in the output-error-based FE model updating.

### 3.4.1 *L-Curve Method*

The first criterion examined in this study is the L-curve method. This method, as advocated by Hansen (1992) works by plotting the residual norm  $\|\mathbf{S}\Delta\boldsymbol{\theta}_{\text{reg}} - \mathbf{e}\|_2$  versus the solution norm  $\|\Delta\boldsymbol{\theta}_{\text{reg}}\|_2$  in a log-log scale for a wide spectrum of regularization parameter, either the Tikhonov parameter  $\lambda$  or the truncation parameter  $m_t$ . An example of the L-curve is shown in **Figure 3.2** for the case of the Tikhonov parameter  $\lambda$ ; each point in the curve corresponds to a certain value of  $\lambda$ . The typical shape of the curve, giving the curve its name, is consisting of a steep part above a corner and a flat part to its right. The value of  $\lambda$  and hence the smoothness of solution increase from left to right. The flat portion (large value of  $\lambda$ ) represents over-smoothed solutions, which have had the measurement noise filter out, but also to some extent have lost genius information inherent in the data; conversely, the

steep portion (small value of  $\lambda$ ) corresponds under-smoothed solutions which may exhibit large oscillations due to only small measurement errors. The ‘corner’ of the curve therefore represents the point at which two types of error norm are balanced appropriately, and the corresponding regularization parameter is a good one. For an idealized L-curve, this point would be exactly at the ‘corner’. For most real cases, the ‘corner’ of L-curve becomes a region. Hansen and O’Leary (1993) specified the ‘corner’ of L-curve as the point at which the curvature of L-curve is maximal.

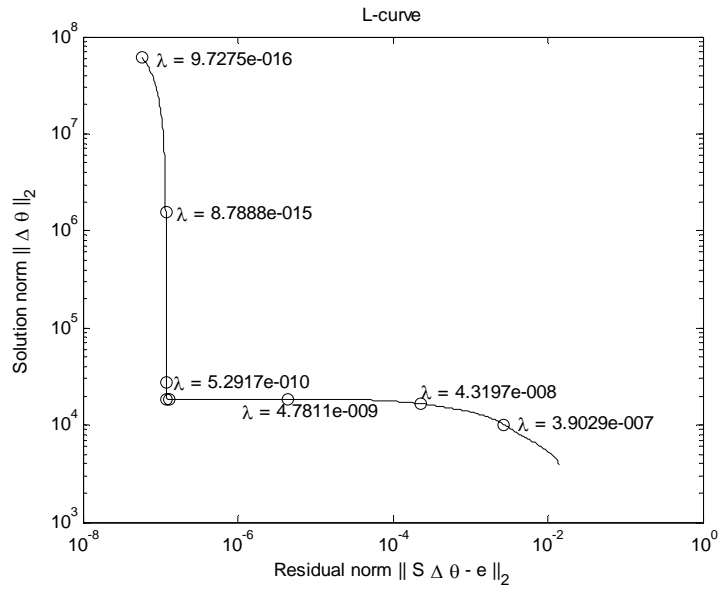


**Figure 3.2** A typical L-curve

For simplification of notation, we define

$$\hat{\eta} \equiv \log\left(\|\Delta \theta_{\text{reg}}\|_2\right) \quad \hat{\rho} \equiv \log\left(\|S \Delta \theta_{\text{reg}} - e\|_2\right) \quad (3.29)$$

As a result, the L-curve becomes a plot of which abscissa and ordinate are  $\hat{\rho}$  and  $\hat{\eta}$  respectively. For Tikhonov regularization, both the residual norm and solution norm can be expressed as a continuous function of the Tikhonov parameter  $\lambda$ , and

therefore the curvature of L-curve could be either determined analytically using direct differential method (DDM) or approximated numerically by means of finite difference method (FDM). However, as the regularized solution norm and residual norm of truncated SVD are discrete functions in terms of the truncation parameter  $m_t$ , the curvature of L-curve can only be determined numerically using FDM.

Given the log-log plot of residual norm and solution norm in L-curve, the curvature  $\kappa$  of L-curve, as a function of the regularization parameter, can be expressed as (Hansen and O'Leary 1993)

$$\kappa_{\text{reg}} \equiv \frac{\hat{\rho}' \hat{\eta}'' - \hat{\rho}'' \hat{\eta}'}{\left( (\hat{\rho}')^2 + (\hat{\eta}')^2 \right)^{3/2}} \quad (3.30)$$

where  $\hat{\eta}'$ ,  $\hat{\rho}'$ ,  $\hat{\eta}''$ , and  $\hat{\rho}''$  denote the first- and second-order derivatives of  $\hat{\eta}$  and  $\hat{\rho}$  with respect to the regularization parameter, respectively.

#### 3.4.1.1 Curvature computation by FDM

Probably the simplest procedure to compute the curvature of L-curve is FDM. Suppose that the L-curve is defined by a series of discrete points  $(\lambda_j, \hat{\eta}_j, \hat{\rho}_j)$ ,  $j = 1, 2, \dots, l$ , the first- and second-order derivatives of  $\hat{\eta}$  and  $\hat{\rho}$  are approximated as

$$\hat{\eta}'_j = \frac{\hat{\eta}_{j+1} - \hat{\eta}_j}{\lambda_{j+1} - \lambda_j} \quad \hat{\eta}''_j = \frac{\hat{\eta}'_{j+1} - \hat{\eta}'_j}{\lambda_{j+1} - \lambda_j} \quad (3.31)$$

$$\hat{\rho}'_j = \frac{\hat{\rho}_{j+1} - \hat{\rho}_j}{\lambda_{j+1} - \lambda_j} \quad \hat{\rho}''_j = \frac{\hat{\rho}'_{j+1} - \hat{\rho}'_j}{\lambda_{j+1} - \lambda_j} \quad (3.32)$$

The merit of FDM is its capability of computing the curvature of both continuous and discrete functions, thus it is suitable to both Tikhonov regularization and truncated SVD. The main disadvantage of FDM lies in the fluctuations which may appear because of the changes in local curvatures of L-curve, especially at the region of small value of the regularization parameter. Although the L-curve is nearly smooth, the local curvature can fluctuate because of computational error.

### 3.4.1.2 Curvature computation by DDM

As shown in Equations (3.24) and (3.25), both the solution norm and residual norm in the case of Tikhonov regularization can be explicitly expressed in terms of the regularization parameter, and therefore DDM can be applied to compute these derivatives. For simplicity, by defining

$$\eta(\lambda) = \|\Delta\theta_\lambda\|_2^2 \quad \rho(\lambda) = \|\mathbf{S}\Delta\theta_\lambda - \mathbf{e}\|_2^2 \quad (3.33)$$

and recalling

$$f_i = \frac{\sigma_i^2}{\sigma_i^2 + \lambda^2} \quad (3.34)$$

the first- and second-order derivatives of  $f_i$  with respect to  $\lambda$ ,  $f_i'$  and  $f_i''$ , are derived, respectively, as

$$f_i' = -\frac{2}{\lambda} f_i(1-f_i) \quad f_i'' = \frac{2}{\lambda^2} f_i(1-f_i)(3-4f_i) \quad (3.35)$$

Combining Equations (3.24) and (3.25) with Equations (3.33) to (3.35), the first- and second-order derivatives of  $\eta$  and  $\rho$  are obtained as

$$\eta' = 2 \sum_{i=1}^m f_i f_i' \left( \frac{\mathbf{u}_i^T \mathbf{e}}{\sigma_i} \right)^2 \quad \eta'' = 2 \sum_{i=1}^m \left( (f_i')^2 + f_i f_i'' \right) \left( \frac{\mathbf{u}_i^T \mathbf{e}}{\sigma_i} \right)^2 \quad (3.36)$$

$$\rho' = -2 \sum_{i=1}^m (1-f_i) f_i' (\mathbf{u}_i^T \mathbf{e})^2 \quad \rho'' = -2 \sum_{i=1}^m \left( -(f_i')^2 + (1-f_i) f_i'' \right) (\mathbf{u}_i^T \mathbf{e})^2 \quad (3.37)$$

Making use of Equations (3.29) and (3.33), the first- and second-order derivatives of  $\hat{\eta}$  and  $\hat{\rho}$  with respect to  $\lambda$  are then expressed as

$$\hat{\eta}' = \frac{\eta'}{2\eta} \quad \hat{\eta}'' = \frac{\eta'' \eta - (\eta')^2}{2\eta^2} \quad (3.38)$$

$$\hat{\eta}' = \frac{\eta'}{2\eta} \quad \hat{\eta}'' = \frac{\eta'' \eta - (\eta')^2}{2\eta^2} \quad (3.39)$$

Substitution of Equations (3.36) to (3.39) into Equation (3.32) allows evaluation of the curvature  $\kappa(\lambda)$ . The maximal curvature is found by evaluating  $\kappa(\lambda)$  over a wide spectrum of  $\lambda$ .

### 3.4.2 Generalized Cross Validation

Another very popular and successful method for choosing the regularization parameter is GCV. The GCV method is developed based on statistical considerations that a good regularized solution corresponding to one particular regularization parameter should predict the missing/unknown data well. In the GCV method, the regularized solution  $\Delta \mathbf{\theta}_{\text{reg}}^{[k]}$  corresponding to a particular regularization parameter is obtained by leaving out one data  $\tilde{z}_k, k = 1, 2, \dots, n$ , at a time, and the prediction error of this omitted data point is then determined using the regularized solution; this procedure is repeated for  $n$  times until the prediction error of each omitted data has

been determined, and the mean prediction error is finally calculated over these prediction errors. GCV determines the optimal regularization parameter as the one that minimizes the mean prediction error. This procedure is explained in the following steps for Tikhonov regularization.

(1) Find the estimate  $\Delta\boldsymbol{\theta}_\lambda^{[k]}$  which minimizes

$$\sum_{i=1, i \neq k}^n \left( e_i - \sum_{j=1}^m s_{ij} \Delta\theta_j \right)^2 + \lambda^2 \|\Delta\boldsymbol{\theta}\|_2^2 \quad (3.40)$$

(2) Predict the missing data point using the estimate

$$\hat{e}_k(\lambda) = \sum_{j=1}^m s_{kj} \Delta\theta_{\lambda, j}^{[k]} \quad (3.41)$$

in which  $\Delta\theta_{\lambda, j}^{[k]}$  represents the  $j$ th element of solution vector  $\Delta\boldsymbol{\theta}_\lambda^{[k]}$ .

(3) Choose the value of  $\lambda$  which minimizes the mean prediction error or the cross-validation (CV) function, as

$$V_0(\lambda) = \frac{1}{n} \sum_{k=1}^n (e_k - \hat{e}_k(\lambda))^2 \quad (3.42)$$

It has been proved that Equation (3.42) can be rewritten in the form of (Craven and Wahba 1979)

$$V_0(\lambda) = \frac{1}{n} \|\mathbf{Q}(\lambda)(\mathbf{S}\Delta\boldsymbol{\theta}_\lambda - \mathbf{e})\|_2^2 \quad (3.43)$$

where

$$\mathbf{Q}(\lambda) = \text{diag} \left( \frac{1}{1 - r_{ii}(\lambda)} \right), i = 1, 2, \dots, n \quad (3.44)$$

and  $r_{ii}$  is the  $i$ th diagonal element of the influence matrix  $\mathbf{R}(\lambda) = \mathbf{S}(\mathbf{S}^T \mathbf{S} + \lambda^2 \mathbf{I})^{-1} \mathbf{S}^T$ .

Golub *et al.* (1979) showed that the ordinary cross-validation method led to the solution of  $\lambda$  that was rotationally dependent. They replaced  $r_{ii}(\lambda)$  in Equation (3.44) with  $\text{trace}(\mathbf{R}(\lambda))/n$  to give the GCV function

$$G(\lambda) = \frac{\frac{1}{n} \|(\mathbf{S}\Delta\boldsymbol{\theta}_\lambda - \mathbf{e})\|_2^2}{\left(\frac{1}{n} \text{trace}(\mathbf{I} - \mathbf{R}(\lambda))\right)^2} \quad (3.45)$$

in which  $\text{trace}(\bullet)$  represents the matrix trace whose value is equal to the summation of all the diagonal elements. Taking the advantage of the property of matrix trace, Equation (3.45) is then simplified as

$$G(\lambda) = \frac{n \|(\mathbf{S}\Delta\boldsymbol{\theta}_\lambda - \mathbf{e})\|_2^2}{\left(n - \sum_{j=1}^m f_j\right)^2} \quad (3.46)$$

where  $f_j$  is the filter factor defined in Equation (3.23)

Similarly, the GCV function for truncated SVD is defined as

$$G(m_t) = \frac{n \|\mathbf{S}\Delta\boldsymbol{\theta}_{m_t} - \mathbf{e}\|_2^2}{(n - m_t)^2} \quad (3.47)$$

In summary, the GCV minimizes the GCV function in Equation (3.46) and Equation (3.47) for determination of the Tikhonov parameter  $\lambda$  and the truncation parameter  $m_t$ , respectively.

### 3.4.3 Minimum Product Criterion

Another less known technique to determine the optimal regularization parameter is MPC, which was initiated by Reginska (1996). Based on the observation that the ‘corner’ of L-curve is visible in the log-log plot of residual norm and solution norm, and could disappear in some scales, as also found in our studies, Reginska suggested the minimization of product of residual norm and solution norm as an alternative approach to the determination of regularization parameters. On the basis of the notations in Equation (3.29), the product function in MPC is defined as

$$\text{Tikhonov regularization: } P(\lambda) = \|\mathbf{S}\Delta\boldsymbol{\theta}_\lambda - \mathbf{e}\|_2^2 \times \|\Delta\boldsymbol{\theta}_\lambda\|_2^2 = \eta(\lambda) \times \rho(\lambda) \quad (3.48)$$

$$\text{Truncated SVD: } P(m_t) = \|\mathbf{S}_{m_t}\Delta\boldsymbol{\theta}_{m_t} - \mathbf{e}\|_2^2 \times \|\Delta\boldsymbol{\theta}_{m_t}\|_2^2 = \eta(m_t) \times \rho(m_t) \quad (3.49)$$

Letting the first-order derivative of Equation (3.48) with respect to the Tikhonov parameter  $\lambda$  equal to zero leads to the following expression,

$$\lambda^2 \sum_{i=1}^m \frac{\sigma_i^2 - \lambda^2}{(\sigma_i^2 + \lambda^2)^2} (u_i^T \mathbf{e})^2 - \|(\mathbf{I} - \mathbf{U}\mathbf{U}^T)\mathbf{e}\|_2^2 = 0 \quad (3.50)$$

which is indeed the same as another approach referred to as zero crossing criterion used in the inverse problem of Electrocardiography (Johnston and Gulrajani 1997).

The previous methods, in particular the first two methods, have been extensively studied and have received wide applications in various linear ill-posed problems. However, many model updating algorithms have been formulated in terms of nonlinear least squares problems, whose linearization around some approximate solution often leads to a series of ill-conditioned systems of linearized equations.

This requires applying regularization methods in combination with the regularization-parameter-choice methods at each of linearized iteration.

### 3.5 Numerical Examples

In this section, a steel truss bridge is used as an example to investigate the performance of two regularization methods with different regularization-parameter-selection methods in the context of the output-error-based model updating algorithm for damage detection application. The truss bridge, as shown in **Figure 3.3**, is a simply-supported pin-jointed steel bridge consisting of top members, bottom members, vertical members and diagonal members. An analytical model is established which has been correlated with the modal properties of as-built or undamaged state of the bridge, and therefore this *baseline* model is considered as a description of the bridge without damage. In this analytical model, a total of 21 planar truss elements, each with two DOFs at every node, are used. The material properties used in the baseline model are as follows: mass density  $\rho = 7800 \text{ kg/m}^3$ , area of cross section for each member  $A = 10^{-2} \text{ m}^2$ , and the Young's modulus  $E = 200 \text{ GPa}$ .

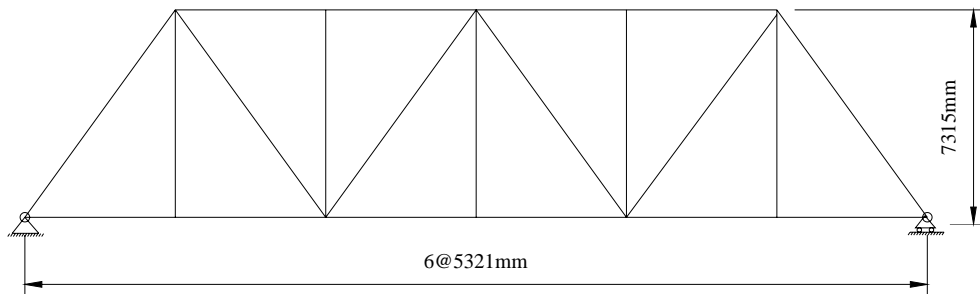


**Figure 3.3 Geometry configuration of truss bridge**

In order to accurately model real damage such as cracks and corrosion, a correct damage model should be used, which is out of the scope of this study. In the present study, the damage is simply modelled by a reduction of Young's modulus as adopted by a number of researchers (e.g. Fritzen and Zhu 1991; Xia and Hao 2003). Nevertheless, most model updating algorithms can be readily adapted to detect the change in other structural parameters than Young's modulus before and after damage, including the geometric dimensions of structural members, flexural and torsional stiffness, and generic parameters (Friswell *et al.* 2001).

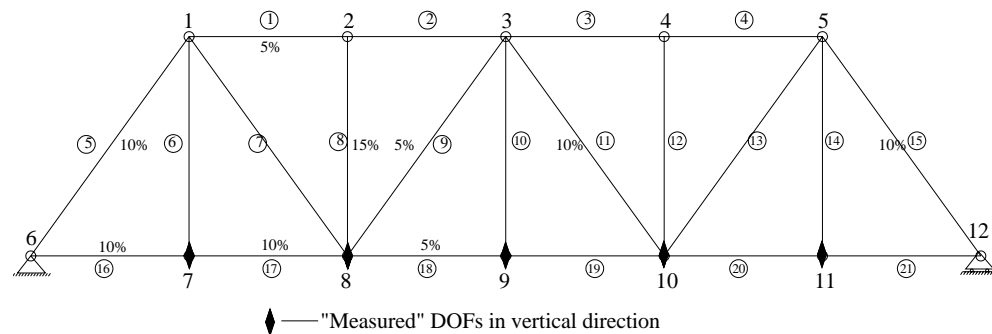


**Figure 3.4 Finite element model and simulated reduction factors of Young's modulus for truss bridge**

Another FE model with the same topology as the baseline model is constructed to generate the simulated experimental modal properties by artificial reduction of Young's modulus of each member to different levels, as shown in **Figure 3.4**. The modal properties computed from this FE model serve as the 'measured' modal properties from the damaged structure, thus the damage detection problem reduces to updating the 21 Young's modulus in an initial FE model to achieve a new FE model whose prediction results coincide with the 'measured' modal properties. The comparison in Young's modulus between the baseline model and the updated model

directly indicates the damage locations and damage magnitudes. In general, the baseline FE model is employed as the initial FE model for achievement of good convergence.

In reality, it is impractical to measure complete eigenvalues and eigenvectors, and it is also not economical to collect data at all DOFs corresponding to the analytical model for each eigenvector. For civil structures, only low-order eigenvalues and several components of the eigenvectors are available. To simulate incomplete measurement, only the first several eigenvalues and five vertical modal displacements for each of the eigenvectors, namely vertical modal displacements at nodes 7, 8, 9, 10, and 11 as illustrated in **Figure 3.4**, are assumed available throughout this numerical study. **Table 3.1** shows the analytical and simulated experimental eigenvalues, and the relative difference between them.

**Table 3.1 Comparison of ‘experimental’ and analytical eigenvalues**

<i>Mode No.</i>	<i>‘Experimental’</i>	<i>Analytical</i>	<i>Relative difference (%)</i>
1	5967.5	6261.7	4.93
2	17884.9	19211.0	7.41
3	45620.6	48837.3	7.05
4	98005.4	103285.0	5.39
5	131231.3	133520.3	1.74
6	141289.7	151629.9	7.32

### **3.5.1 Illustration of Ill-Conditioning**

As the total number of updating parameters is 21, the minimum number of measured modes, each consisting of one eigenvalue and five components of the eigenvector, is four in order to obtain the over-determined system of equations. **Figure 3.5** shows

the condition number versus the number of modes measured. It is obvious that the condition number decreases with the increase of the number of measured modes. Therefore the enrichment of available measurement data will make the model updating problem towards the direction of well-conditioning, although they are subject to the limitations from practical and economical considerations.

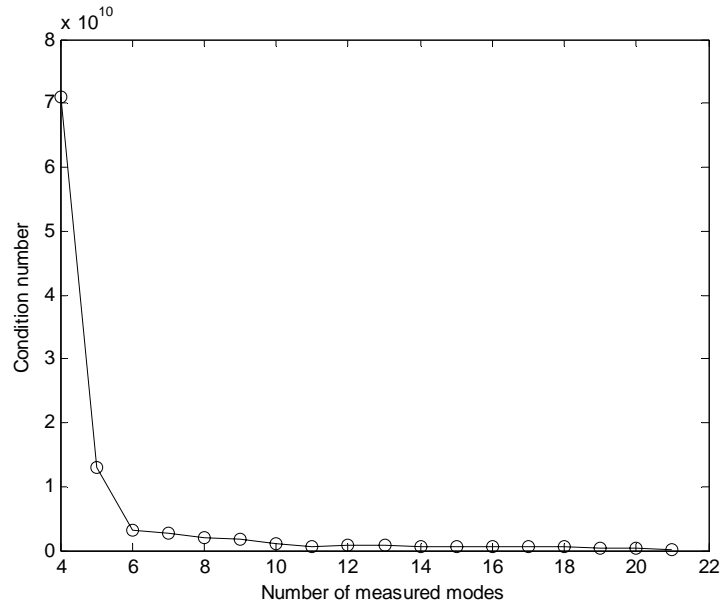


**Figure 3.5 Condition number versus number of measured modes**

For illustration of the ill-conditioning in model updating, **Figure 3.6** shows the discrete SV  $\sigma_i$ , Fourier coefficient  $|\mathbf{u}_i^T \mathbf{e}|$ , and Picard condition number  $|\mathbf{u}_i^T \mathbf{e} / \sigma_i|$  at the first iteration when the first four modes are used for updating. It is seen that the Fourier coefficients for small SVs stagnate around at the order of  $10^{-6}$  while their SVs still decay gradually. Therefore DPC is not satisfied and regularization methods must be applied to obtain a regularized and stable solution. Similarly, **Figure 3.7** and **Figure 3.8** illustrate the Picard plot at the first iteration when 5 modes and 6 modes are used, respectively. The discrete Picard conditions for these two cases are also

violated. Further numerical studies indicate that the iterations don't converge because the equations are too ill-conditioned for direct least-squares solution due to rounding-off error even when the noise-free measured modal properties are used.

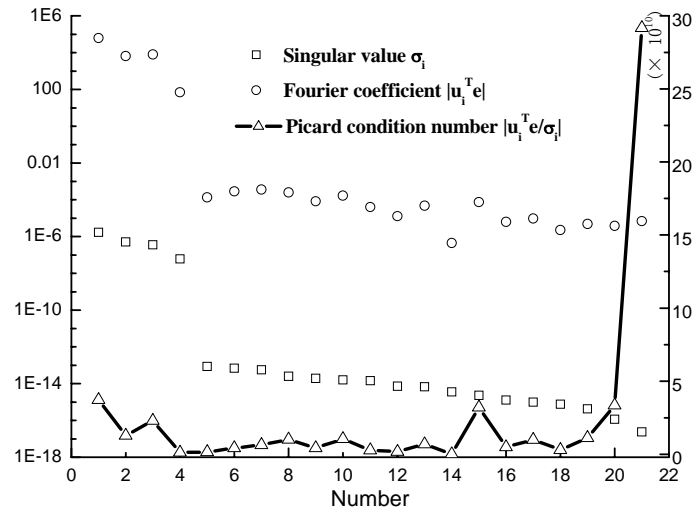


**Figure 3.6** Plot of discrete SV, and Fourier coefficient plotted (left ordinate) and Picard condition number (right ordinate) when using 4 modes

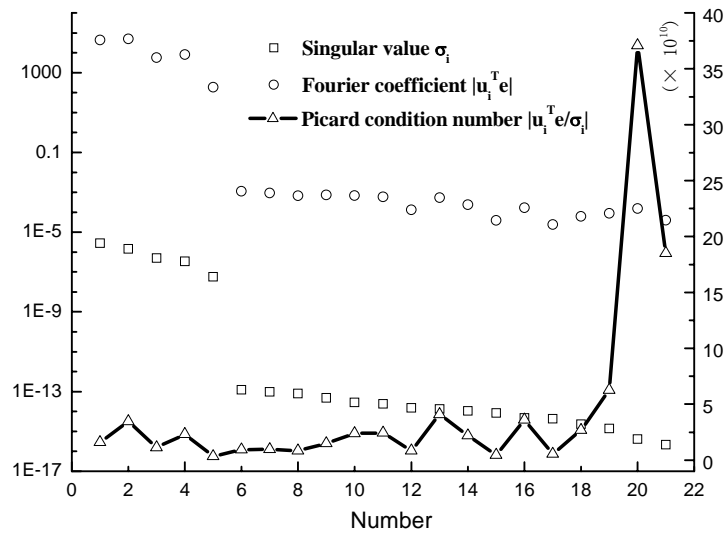


**Figure 3.7** Plot of discrete SV, and Fourier coefficient plotted (left ordinate) and Picard condition number (right ordinate) when using 5 modes

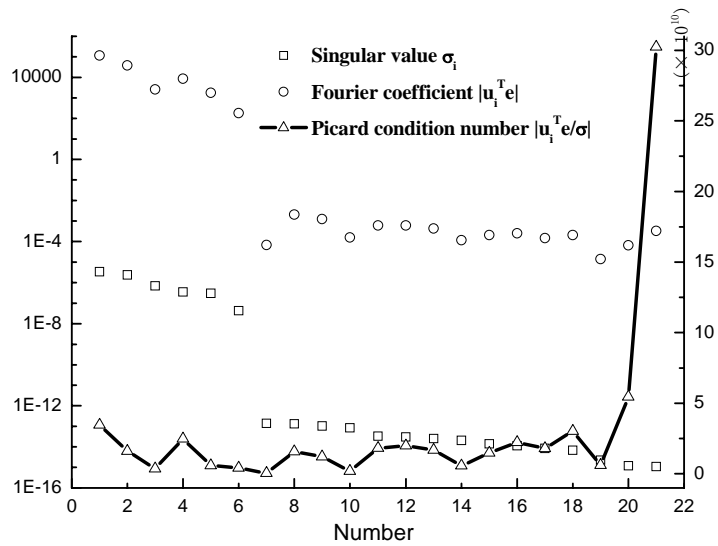


**Figure 3.8 Plot of discrete SV, and Fourier coefficient plotted (left ordinate) and Picard condition number (right ordinate) when using 6 modes**

### 3.5.2 Model Updating Using Noise-Free Data

First, the regularization methods are applied for model updating using noise-free simulated experimental modal data to mitigate the effect of rounding error. To assess the effectiveness and robustness of various regularization-parameter-choice methods for Tikhonov regularization and truncated SVD, three cases with different numbers of measured modes, namely 4 modes, 5 modes, and 6 modes, are considered for updating 21 unknown Young's modulus, respectively. Illustrated in **Figure 3.9** is the Picard plot of regularized system of equations at the first iteration when using 4 modes and 5 modes, respectively, in which LCM is used to determine the regularization parameter for Tikhonov regularization (other two methods can also be used). It is seen that DPC is satisfied due to the effect of filter factor  $f_i$  for both cases.

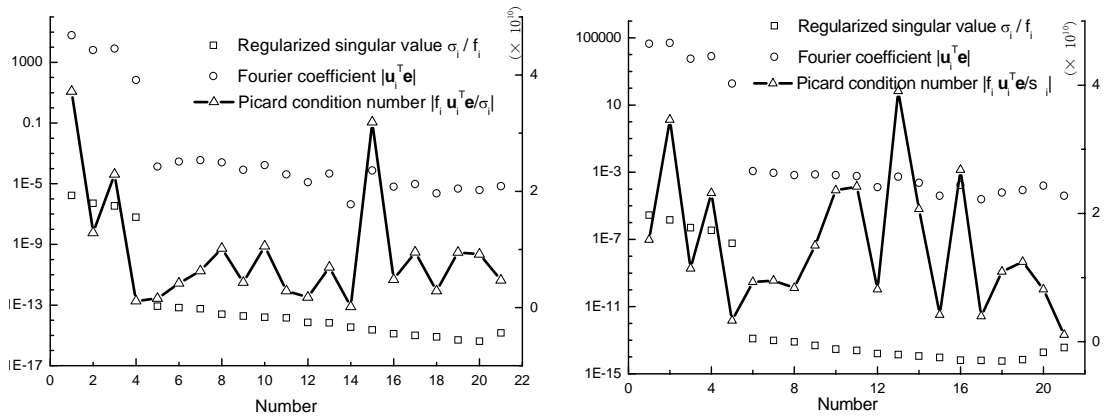


**Figure 3.9 Plot of discrete regularized SV, and Fourier coefficient plotted (left ordinate) and Picard condition number (right ordinate): (a) using 4 modes; (b) using 5 modes**

### 3.5.2.1 Tikhonov Regularization

#### *Adaptive regularization parameter versus fixed regularization parameter*

When applying Tikhonov method at each iteration, the Tikhonov parameter  $\lambda$  can either be fixed at the value determined at the first iteration or be adaptable at each iteration. **Figure 3.10** and **Figure 3.11** compare the model updating results with fixed regularization parameter and adaptive regularization parameter, respectively, when using 4 modes. In the fixed regularization parameter scheme, the regularization parameter throughout the iteration is fixed to the value determined at the first iteration by means of LCM; whereas LCM is sequentially applied at each iteration to determine the regularization parameter for the adaptive regularization parameter scheme. It is clear from **Figure 3.10** and **Figure 3.11** that the former scheme causes excessive iterations to attain required convergence due to the inappropriate regularization parameters and may cause the convergence problem if the regularization parameter at the first iteration is too small. A detailed inspection of the

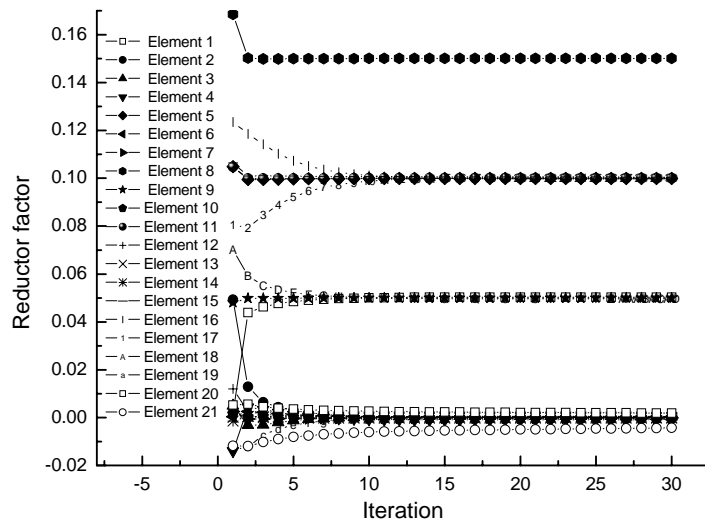


**Figure 3.10 Iteration results of model updating using fixed regularization parameter scheme**

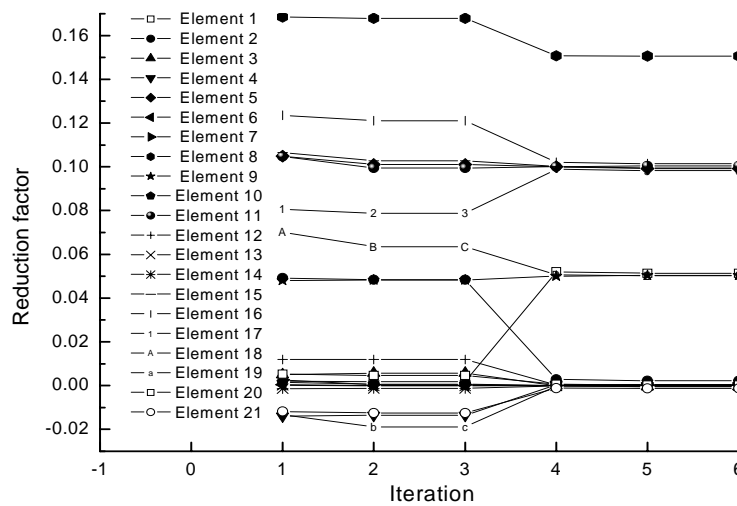


**Figure 3.11 Iteration results of model updating using adaptive regularization parameter scheme**

convergence curves for all updating parameters reveals that the fixed regularization parameter scheme does not produce consistently converged results and instead, they oscillate around their exact simulated values despite of the fluctuation level being small. In the case of adaptive regularization parameter scheme, the iteration

converges rapidly. Therefore the adaptive regularization parameter scheme is used for the subsequent analysis.

### *Comparison of three parameter-choice methods*

**Figures 3.12 to 3.14** show the evolution of the regularization parameters for the three methods at different iteration steps when using 4 modes. **Figure 3.12** clearly indicates that the so-called L-curve is not always to exhibit a well-behaved L-shape even plotted in the log-log scale and therefore the resulting large curvature could spread over the SV spectrum instead of concentrating on a local region. While for GCV and MPC methods, a specific region which is insensible to the Tikhonov parameter exists, which indicates a wide nearly optimal value of the regularization parameter. Furthermore, the regularization parameter varies significantly between two successive iterations, substantiating that adaptive regularization parameter algorithm is more efficient in terms of convergence rate of iteration.

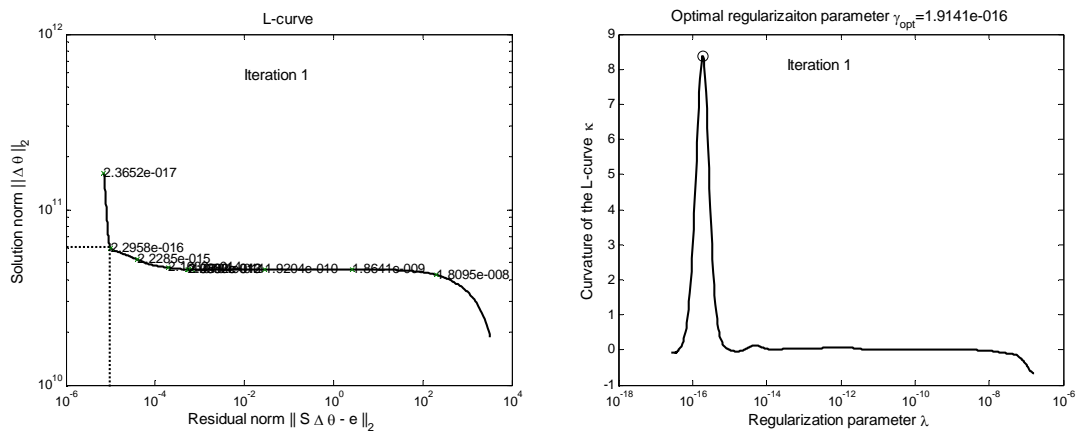


**Figure 3.12** L-curve and its curvature at different iteration steps

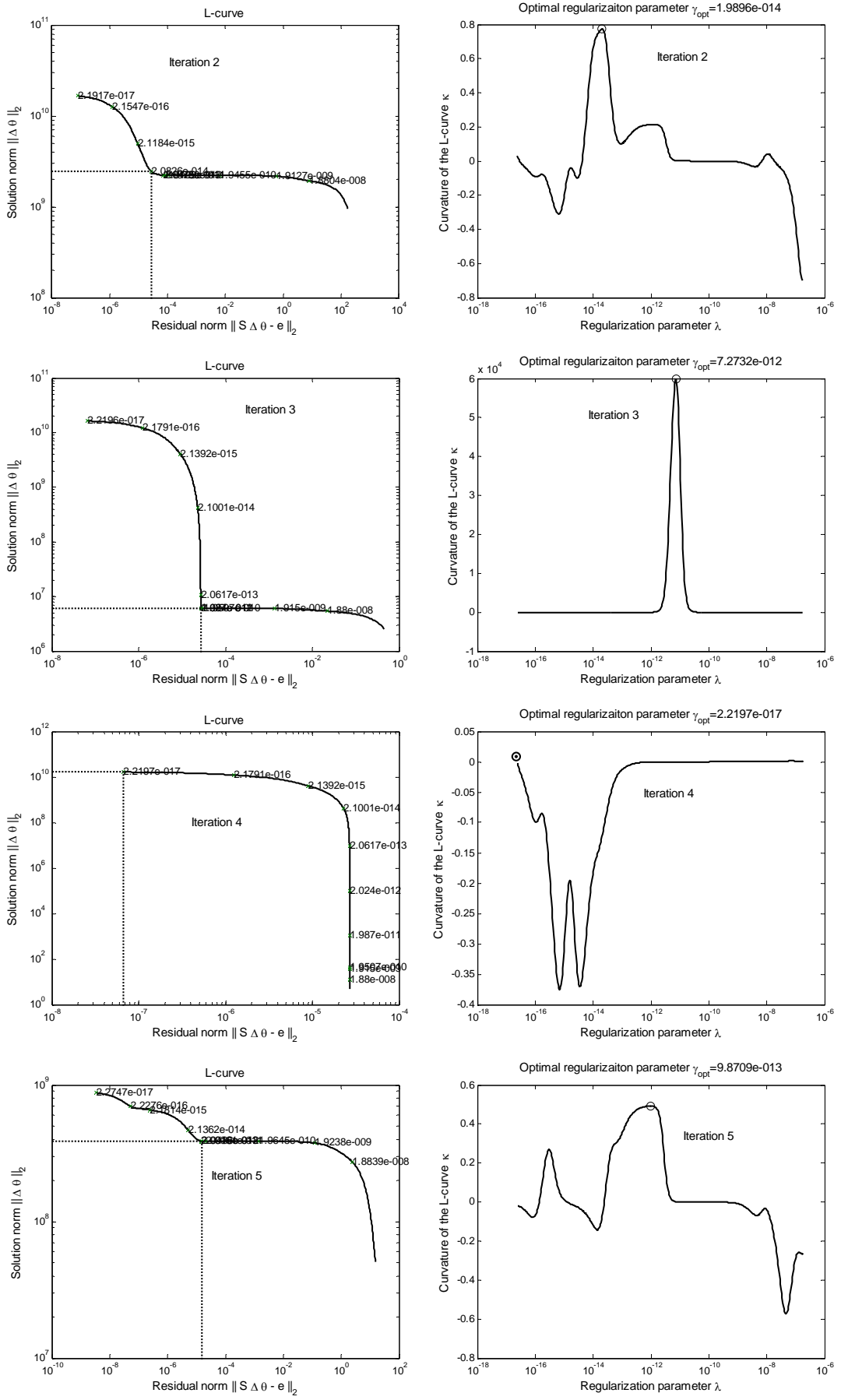
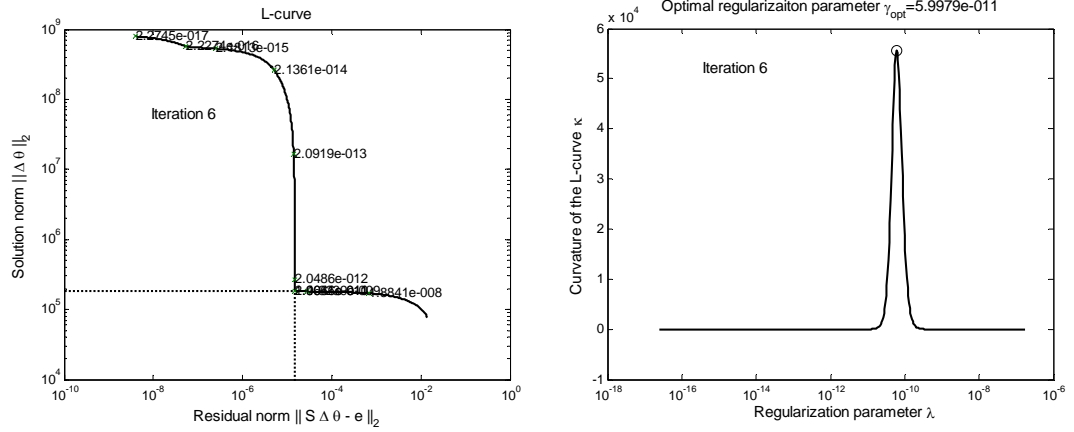
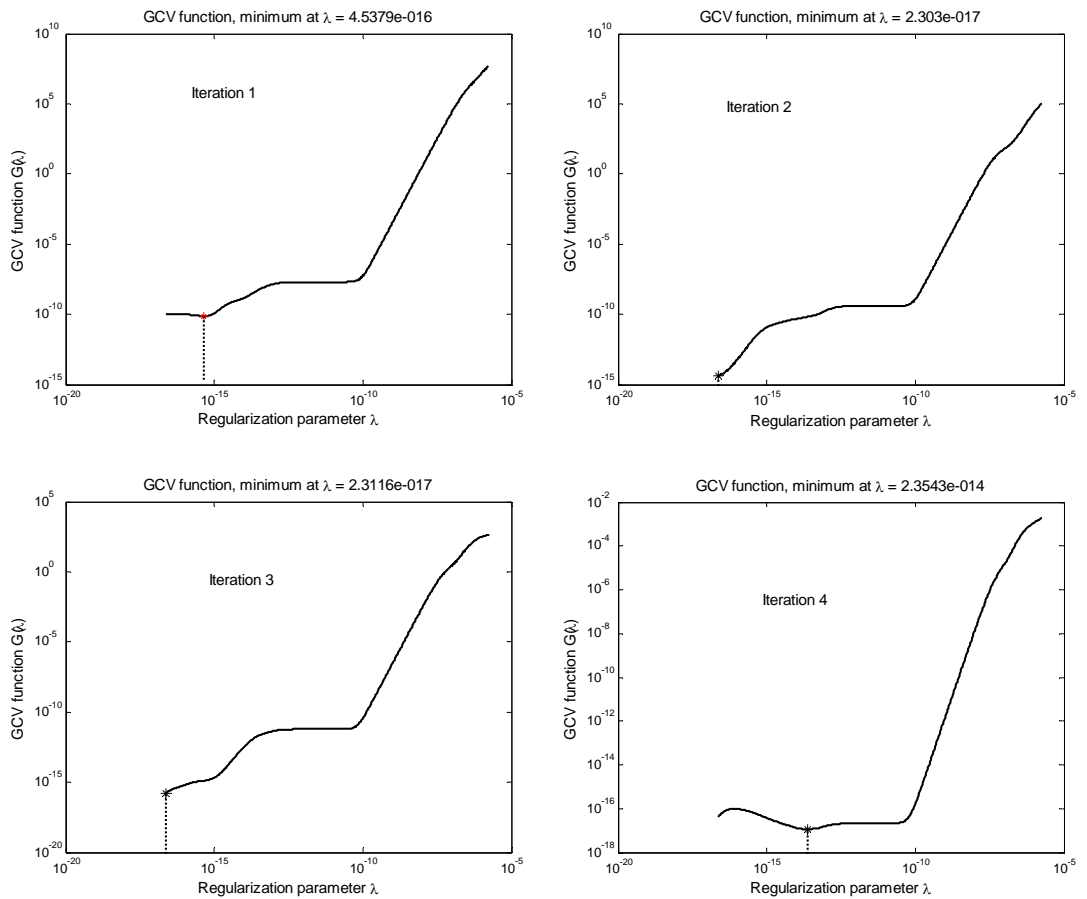


Figure 3.12 L-curve and its curvature at different iteration steps (Cont'd)



**Figure 3.12 L-curve and its curvature at different iteration steps (Cont'd)**



**Figure 3.13 GCV function at different iteration steps**

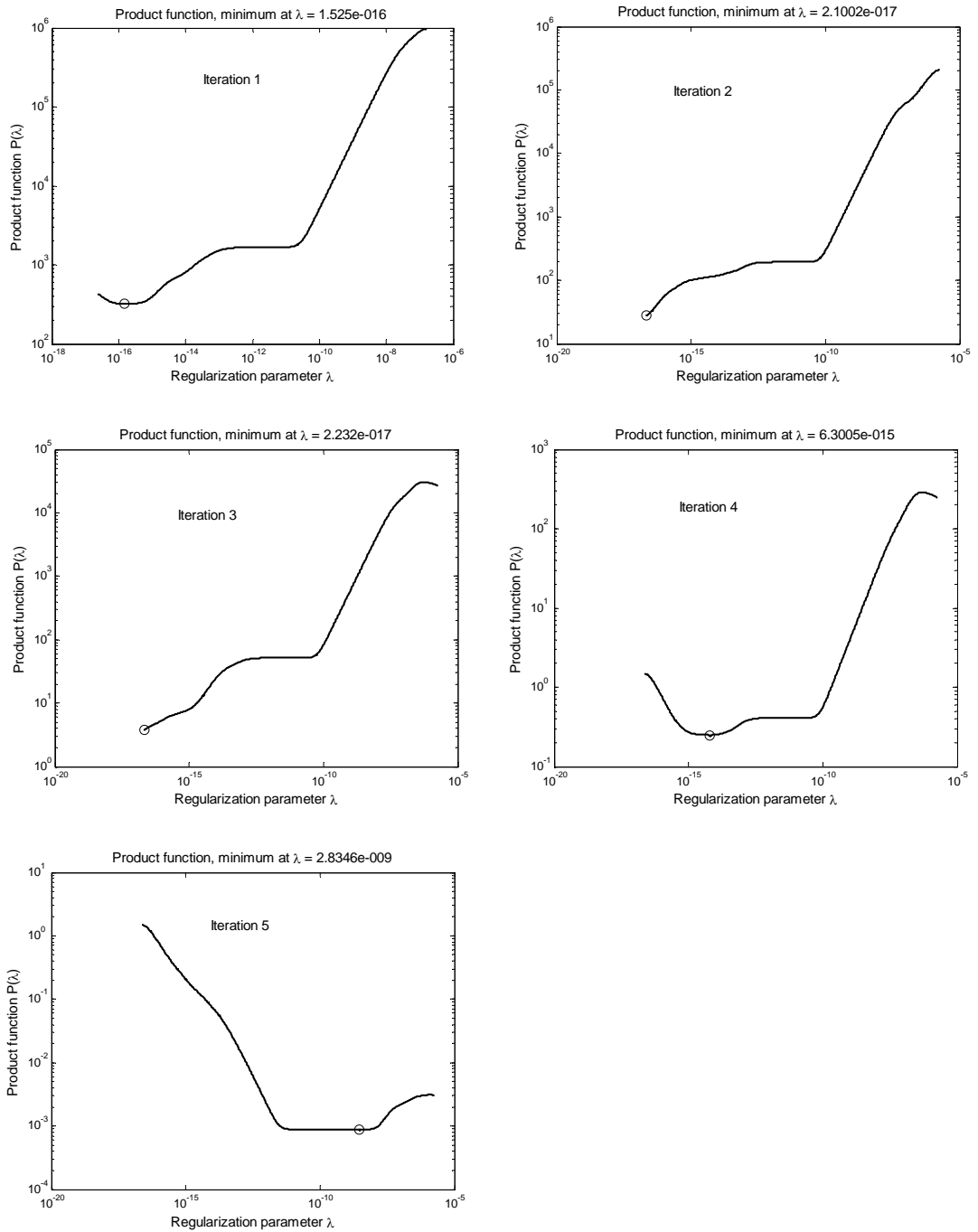


**Figure 3.14 Product function at different iteration steps**

**Figure 3.15** plots four L-curves superimposed with the optimal regularization parameters chosen by LCM, GCV, and MPC, respectively. The two L-curves in the first row has a distinct L-shape; the left L-curve in the second row has an ambiguous

L-shape; to this right the L-curve possesses moderate L-shape. It shows that the regularization parameters chosen by LCM and GCV can be close each other and may also differ significantly, whether the L-shape is well behaved or poorly posed. A surprising observation, which also occurs for the other two cases (model updating using 5 modes and 6 modes), is that the regularization parameter chosen by MPC tends to be adjacent to that chosen by LCM when the curve has a well-behaved L-shape while it will be close to that selected by GCV in the case of a poorly-posed L-curve. This observation is worthy of further exploration.

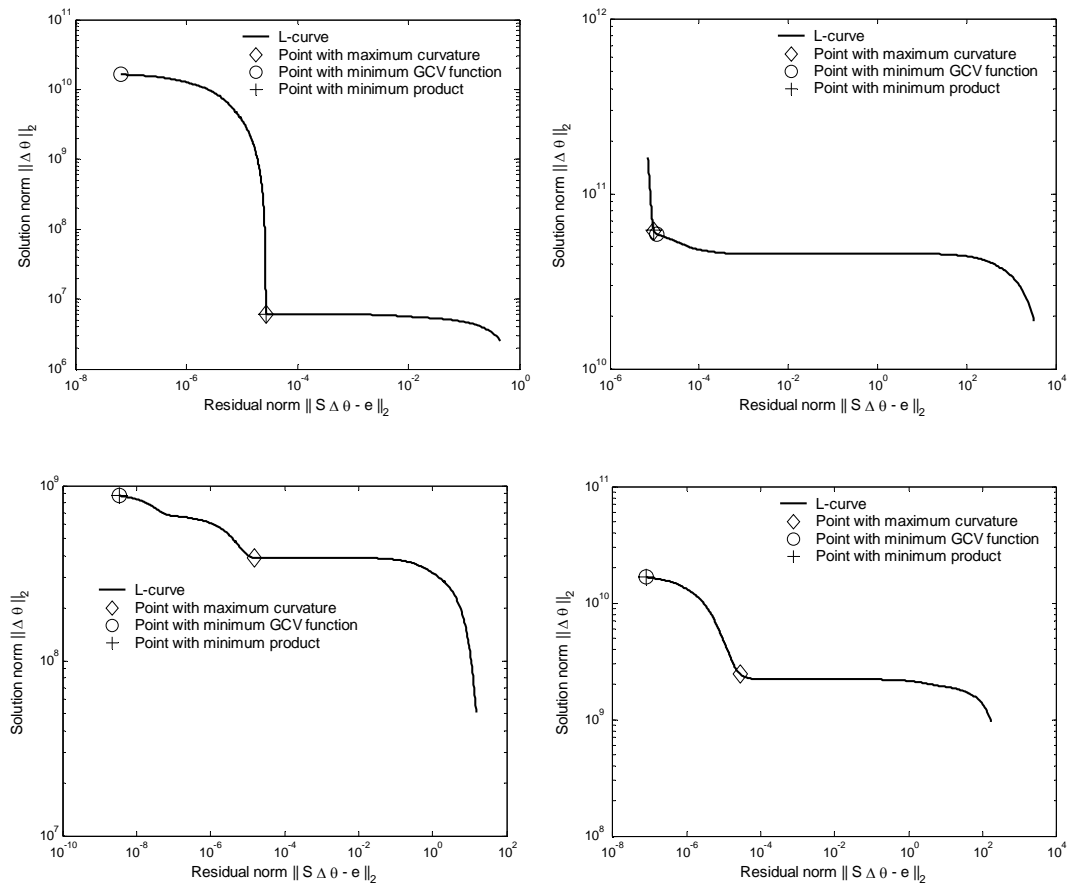


**Figure 3.15 Four L-curves superimposed with optimal regularization parameters**

**Table 3.2** summarizes the model updating results using Tikhonov regularization with different methods for selection of the regularization parameter. When using 4 modes, the model updating results from three methods, namely LCM, GCV, and MPC, are very close to the exact simulated reduction factors, indicating that both damage location and damage extent are well identified. GCV method uses the least number of iterations to achieve the convergence while seven iterations are required for LCM. In addition the evaluation of curvature for LCM is more computationally expensive than function values for GCV and MPC. When 5 modes are used for model updating, both LCM and MPC yield convergent model updating results; whereas GCV fails to give converged results as it chooses an extremely small regularization parameter at the first iteration and therefore gives rise to essentially a similar ill-posed system of equations in which the DPC is violated as shown in **Figure 3.16**. Although both LCM and MPC can give convergent results as well as the resulting errors of modal properties are quite small, damage is not correctly identified for some members. The reason is that the fifth mode is a local mode dominated by longitudinal displacements that are not used in the present analysis. Illustrated in **Figure 3.17** is the difference between analytical and experimental modal properties before and after updating. The small difference after updating indicates that the quality of FE model has been greatly improved after updating although the damage extents of some members are not exactly identified. It is shown that the identification results by using 6 modes agree well with the simulated values. In particular, the results from GCV method are surprisingly good and almost exactly reproduce the simulated damage.

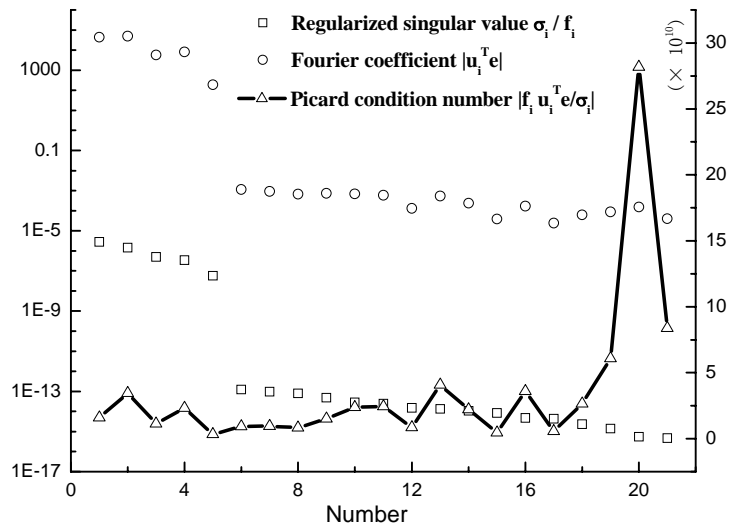


**Figure 3.16 Plot of discrete regularized SV, and Fourier coefficient plotted (left ordinate) and Picard condition number (right ordinate) obtained by GCV method when using 5 modes**

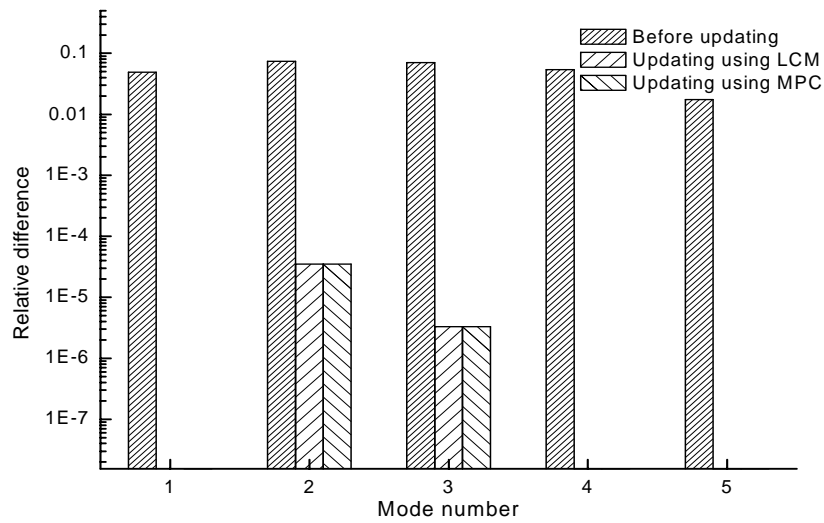


**Figure 3.17 Relative difference in eigenvalues after model updating by LCM and MPC when using 5 modes**

**Table 3.2 Comparison of model updating results using noise-free data**

<i>Element No.</i>	<i>Exact damage extent (%)</i>	<i>Identified reduction factor (%)</i>								
		<b>4 modes</b>			<b>5 modes</b>			<b>6 modes</b>		
		<b>LCM (6)*</b>	<b>MPC (5)</b>	<b>GCV (4)</b>	<b>LCM (6)</b>	<b>MPC (6)</b>	<b>GCV (N/A)</b>	<b>LCM (6)</b>	<b>MPC (6)</b>	<b>GCV (8)</b>
1	5	5.136	5.018	4.987	5.346	5.387		5.634	5.401	5.000
2	0	0.228	-0.009	0.010	-0.043	-0.038		0.071	-0.021	0
3	0	-0.050	0.031	-0.021	0.700	0.524		-2.088	-0.741	0
4	0	-0.009	-0.054	0.036	-1.354	-1.211		1.464	0.495	0
5	10	9.914	9.996	10.002	9.923	9.907		9.767	9.890	10.000
6	0	0.026	0.013	-0.007	0.284	0.333		0.736	0.417	0
7	0	0.023	-0.005	0.003	-0.159	-0.169		-0.181	-0.120	0
8	15	15.063	15.005	14.997	14.849	14.866		14.763	14.911	15.000
9	5	5.035	5.000	5.000	5.000	4.997		4.973	4.978	5.000
10	0	0.033	-0.001	0.001	-0.082	-0.068		0.238	0.128	0
11	10	10.035	10.001	10.000	10.022	10.02		9.879	9.939	10.000
12	0	0.021	0.020	-0.012	1.201	1.27		0.896	0.349	0
13	0	0.021	0.011	-0.006	0.170	0.176		0.152	0.081	0
14	0	0.011	-0.016	0.010	-0.214	-0.218		-0.436	-0.191	0
15	10	9.943	10.035	9.978	10.642	10.644		10.350	10.21	10.000
16	10	10.144	9.993	10.015	8.685	8.837		12.774	11.407	10.000
17	10	9.820	10.007	9.984	11.425	11.29		7.103	8.542	10.000
18	5	5.031	4.978	5.016	3.624	3.641		4.240	4.640	5.000
19	0	-0.041	0.025	-0.018	1.557	1.529		0.661	0.324	0
20	0	0.025	0.127	-0.079	1.653	1.637		0.430	0.368	0
21	0	-0.133	-0.289	0.178	-5.008	-5.018		-1.626	-1.204	-0.001

\* The figure in parentheses indicates the number of iterations used; N/A – no solution is found.

### 3.5.2.2 Truncated SVD

Likewise, truncated SVD is successively applied at each linearized step of the nonlinear least squares problem. For truncated SVD, the plot of L-curve is a discrete function in terms of the truncation parameter  $m_t$  and is considerably dispersed as illustrated in **Figure 3.18**; therefore the evaluation of curvature at the truncation parameter would be difficult and may not be accurate. As a result only GCV and MPC methods are used for choice of the truncation parameter in truncated SVD.

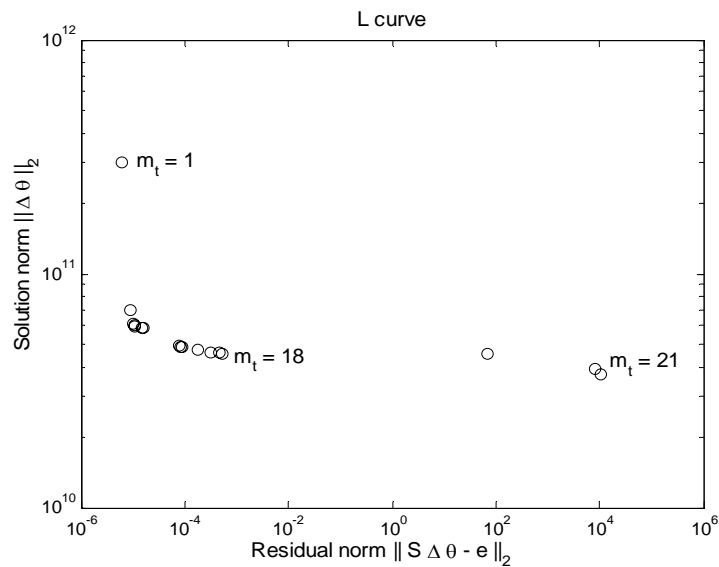


**Figure 3.18** L-curve for truncated SVD

**Figure 3.19** illustrates the GCV and product functions at the first iteration when using 4 modes. In this case, the GCV function is minimal when retaining the first seventeen SVs while the product function achieves its global minima after disregarding the last two smallest SVs. **Figure 3.20** shows the values of GCV function and the determined truncation parameter at different iteration steps when using 4 modes. Except for the first iteration, the remaining iterations tend to use all

the SVs to obtain the solution, indicating that no regularization is required for these remaining iterations. Should the solutions of the first iteration be used as the initial estimate of parameters, no regularization is needed when noise-free modal data are used for updating. With this observation, it is concluded that the ill-posedness associated with model updating may partially stem from the poorly-initialized estimate of updating parameters. **Table 3.3** lists the values of the truncation parameters at different iteration steps when using 4 modes, 5 modes, and 6 modes, respectively. For all the cases considered, GCV and MPC yield similar values of the truncation parameter.

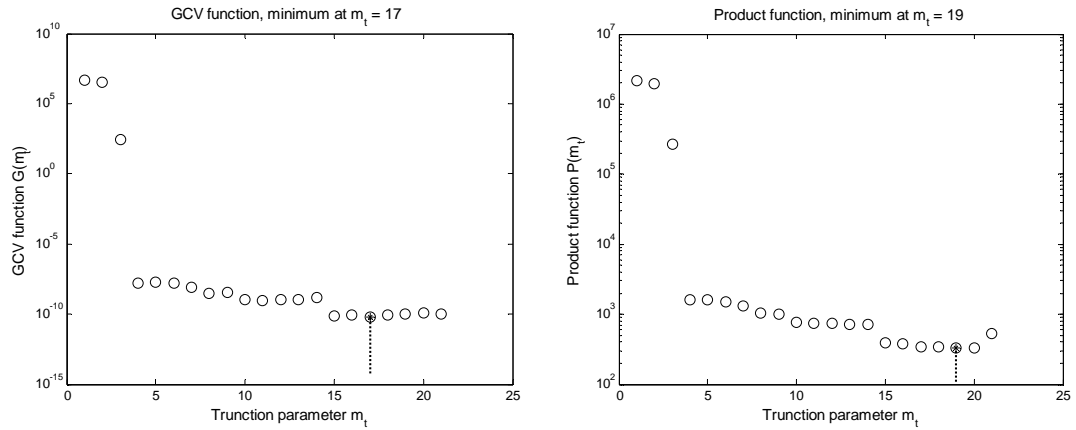


**Figure 3.19 GCV and product functions for truncated SVD at 1st iteration when using 4 modes**

**Table 3.3 Summary of truncation parameter at different iteration steps**

<i>Truncation parameter</i>		<i>Iteration number</i>						
		<b>1</b>	<b>2</b>	<b>3</b>	<b>4</b>	<b>5</b>	<b>6</b>	<b>7</b>
4 modes	GCV	17	21	21	21	21	--	--
	MPC	19	21	21	21	21	--	--
5 modes	GCV	18	19	20	21	21	21	20
	MPC	18	19	20	21	21	21	21
6 modes	GCV	16	19	19	21	21	21	--
	MPC	16	19	19	21	21	21	--

When using truncated SVD, it is observed that all model updating results for the three cases are almost the same although different regularization-parameter-choice-methods and different number of modes are used, and both damage locations and damage magnitudes are exactly identified as illustrated in **Table 3.4**. The results from truncated SVD are better than those obtained from Tikhonov regularization (**Tables 3.2**). It can be explained as follows: when noise-free data are used for model updating, the ill-conditioning is completely caused by round-off errors; truncated SVD effectively eliminates the ill-conditioning by ignoring the last several smallest SVs while Tikhonov regularization only mitigates the ill-conditioning by means of the filter factors which dampen the effects of both the small SVs and, to some extent, the large SVs.

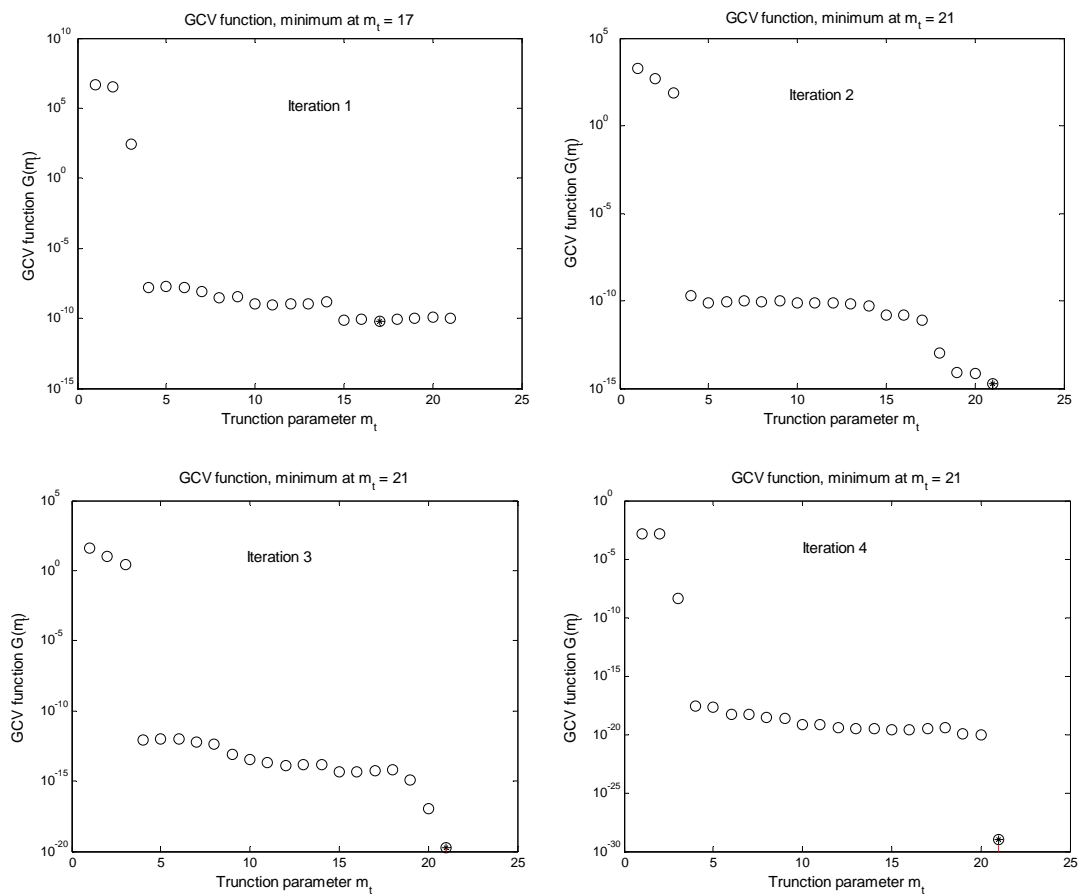


**Figure 3.20 GCV function for truncated SVD at different iteration steps when using 4 modes**

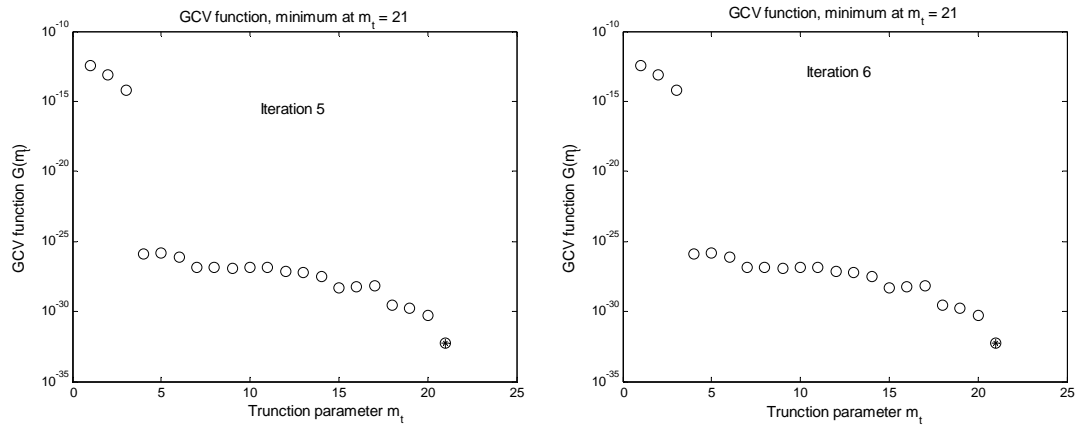


**Figure 3.20 GCV function for truncated SVD at different iteration steps when using 4 modes (Cont'd)**

**Table 3.4 Model updating results using truncated SVD**

<i>Element No.</i>	<i>Exact damage extent (%)</i>	<i>Identified reduction factor (%)</i>	
		<b>MPC</b>	<b>GCV</b>
1	5	5.000	5.000
2	0	0	0
3	0	0	0
4	0	0	0
5	10	10.000	10.000
6	0	0	0
7	0	0	0
8	15	15.000	15.000
9	5	5.000	5.000
10	0	0	0
11	10	10.000	10.000
12	0	0	0
13	0	0	0
14	0	0	0
15	10	10.000	10.000
16	10	10.000	10.000
17	10	10.000	10.000
18	5	5.000	5.000
19	0	0	0
20	0	0	0
21	0	0	0

### 3.5.3 Model Updating Using Noise-Corrupted Data

The performance of regularization methods accompanied with the parameter-choice methods is now investigated using the ‘measured’ noisy modal properties. The noisy modal properties are generated by adding simulated experimental modal properties with a random sequence following normal distribution with zero mean, as

$$\tilde{\mathbf{z}}_i = (1 + \alpha_i)\tilde{\mathbf{z}}_{d,i} \quad (3.51)$$

where  $\tilde{\mathbf{z}}$  is the noise-corrupted vector of modal properties;  $\tilde{\mathbf{z}}_d$  is the vector of simulated noise-free modal properties; and  $\alpha$  is Gaussian random variable with zero mean, whose standard deviation equals to the proportional noise level. For example, 1% measurement noise in a modal parameter implies that the standard deviation of this parameter is 0.01.

#### 3.5.3.1 Tikhonov Regularization

**Figure 3.21** shows the Picard plot obtained from noisy modal data when using 4 modes, 5 modes, and 6 modes, respectively. It is observed again that the Fourier coefficients stagnate around at certain levels while the SVs decay gradually to zero, indicating that DPC is violated. Tikhonov regularization is now applied to alleviate the effect of measurement noise in solving the ill-conditioned system of equations. **Table 3.5** summarizes the identified reduction factors in the case using 4 modes with 1% measurement noise. In this case, the L-curve method leads to divergence problem due to the poorly-posed L-shape during iterations and no solution is sought out; while both MPC and GCV give rise to convergent solutions. On the assumption that the value of the reduction factor larger than 5% is indicative of structural damage, the

correctly identified members are enclosed with solid lines in **Table 3.5**; and the members that are falsely identified are enveloped with dash lines. It is seen that most of the damaged members have been correctly identified. **Table 3.6** and **Table 3.7** present the model updating results when using 5 modes and 6 modes, respectively. As discussed earlier, the fifth mode is not informative, and the inclusion of this mode leads to worse results as given in **Table 3.6**.

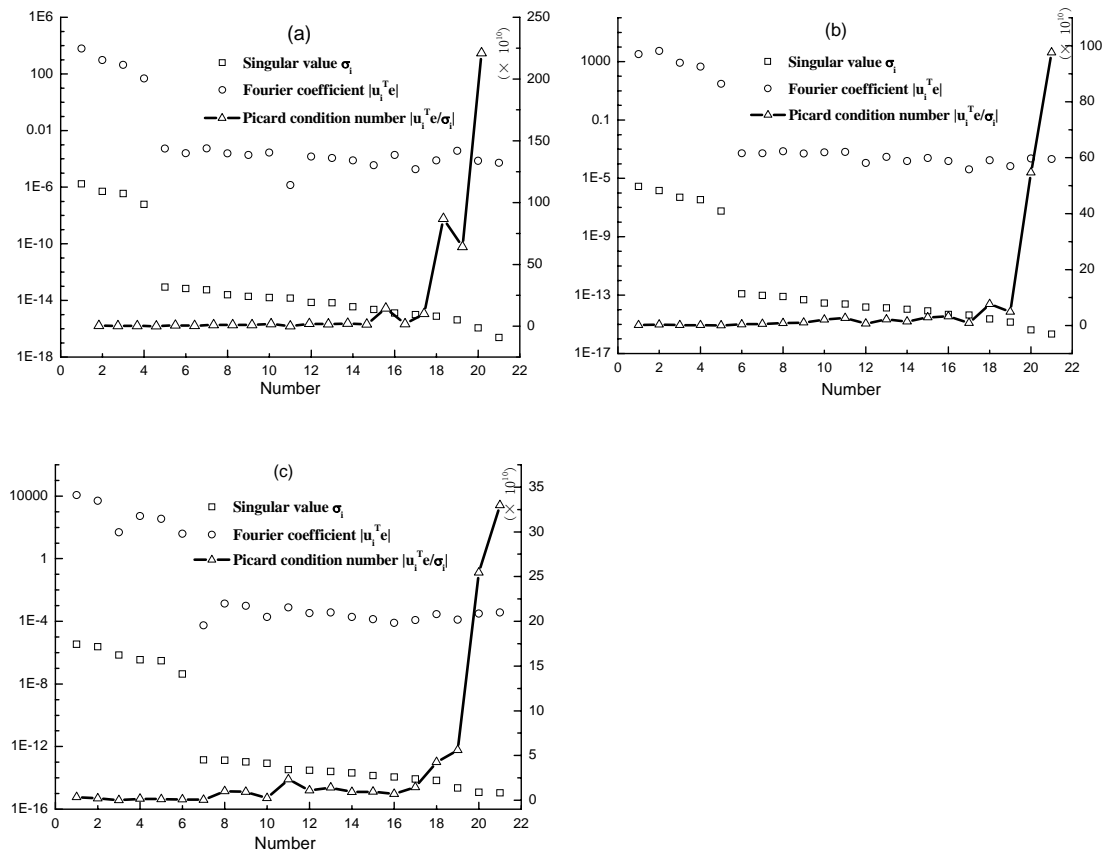


**Figure 3.21 Plot of discrete SV, and Fourier coefficient plotted (left ordinate) and Picard condition number (right ordinate) for noisy data: (a) using 4 modes; (b) using 5 modes; (c) using 6 modes**

**Figure 3.22** shows a comparison of real and identified reduction factors and the relative difference between the analytical modal properties of updated FE model and simulated noise-free modal properties in the case of 2% measurement noise. It is observed that the identification results of some elements, such as elements 5, 9, 11, and 15, are less insensitive to the number of modes and regularization-parameter-choice method used.

**Table 3.5 Model updating results when using 4 modes with 1% measurement noise for Tikhonov regularization**

<i>Element No.</i>	<i>Exact damage extent (%)</i>	<i>Identified reduction factor (%)</i>		
		<b>LCM (N/A)</b>	<b>MPC (4)*</b>	<b>GCV (4)*</b>
1	5		3.618	3.608
2	0		3.744	2.984
3	0		-3.406	-0.831
4	0		-1.597	-0.216
5	10		9.7007	10.356
6	0		3.135	1.494
7	0		0.365	1.570
8	15		0.407	0.664
9	5		6.0238	6.071
10	0		-1.444	-0.370
11	10		12.749	12.118
12	0		-0.631	0.260
13	0		-4.056	-3.319
14	0		1.315	1.075
15	10		9.275	9.257
16	10		6.459	6.260
17	10		7.242	6.157
18	5		0.247	-0.633
19	0		-1.533	-1.432
20	0		4.917	3.745
21	0		3.238	2.825

**Table 3.6 Model updating results when using 5 modes with 1% measurement noise for Tikhonov regularization**

<i>Element No.</i>	<i>Exact damage extent (%)</i>	<i>Identified reduction factor (%)</i>		
		<b>LCM (8)</b>	<b>MPC (4) *</b>	<b>GCV (4) *</b>
1	5	6.126	5.109	6.101
2	0	-9.920	-7.692	-9.629
3	0	-4.909	-2.626	-3.197
4	0	2.522	0.903	1.393
5	10	11.608	11.367	11.809
6	0	-1.300	-3.210	-3.088
7	0	1.258	3.623	2.709
8	15	-5.053	-1.778	-2.544
9	5	7.003	6.07	6.739
10	0	-2.454	2.584	0.978
11	10	10.836	9.628	9.799
12	0	9.522	4.154	6.33
13	0	-7.995	-6.673	-7.555
14	0	6.939	3.359	4.886
15	10	6.947	9.95	8.153
16	10	5.161	5.813	5.698
17	10	8.192	6.661	6.897
18	5	1.377	-1.366	-0.511
19	0	0.665	0.76	1.564
20	0	9.783	9.364	9.841
21	0	8.735	7.22	8.155

**Table 3.7 Model updating results when using 6 modes with 1% measurement noise for Tikhonov regularization**

<i>Element No.</i>	<i>Exact damage extent (%)</i>	<i>Identified reduction factor (%)</i>		
		<b>LCM (8)</b>	<b>MPC (4) *</b>	<b>GCV (4) *</b>
1	5	6.827	4.877	6.463
2	0	-6.848	-2.606	-5.491
3	0	-2.612	-1.341	-1.554
4	0	-2.181	-3.131	-2.993
5	10	10.255	9.091	10.154
6	0	-0.386	0.393	0.012032
7	0	1.978	2.976	2.144
8	15	5.165	3.325	4.851
9	5	7.695	7.031	7.554
10	0	-6.202	-3.773	-5.719
11	10	10.315	10.278	10.289
12	0	5.714	3.23	5.164
13	0	-4.173	-3.385	-3.955
14	0	3.858	2.512	3.566
15	10	9.307	11.624	9.606
16	10	8.934	7.956	8.514
17	10	6.88	6.968	7.186
18	5	-2.365	-2.958	-2.688
19	0	2.906	0.968	2.768
20	0	6.547	6.263	5.996
21	0	7.227	6.305	7.112

### 3.5.3.2 Truncated SVD

**Table 3.8** lists the model updating results by means of truncated SVD in the case of 1% measurement noise when using 4 modes, 5 modes and 6 modes, respectively. The results from GCV when using 6 modes is seem better than the others. Using truncated SVD, a similar analysis is also conducted in the case of 2% measurement noise and the corresponding model updating results are shown in **Figure 3.23**. A comprehensive comparison between Tikhonov regularization and truncated SVD will be made in the next section.

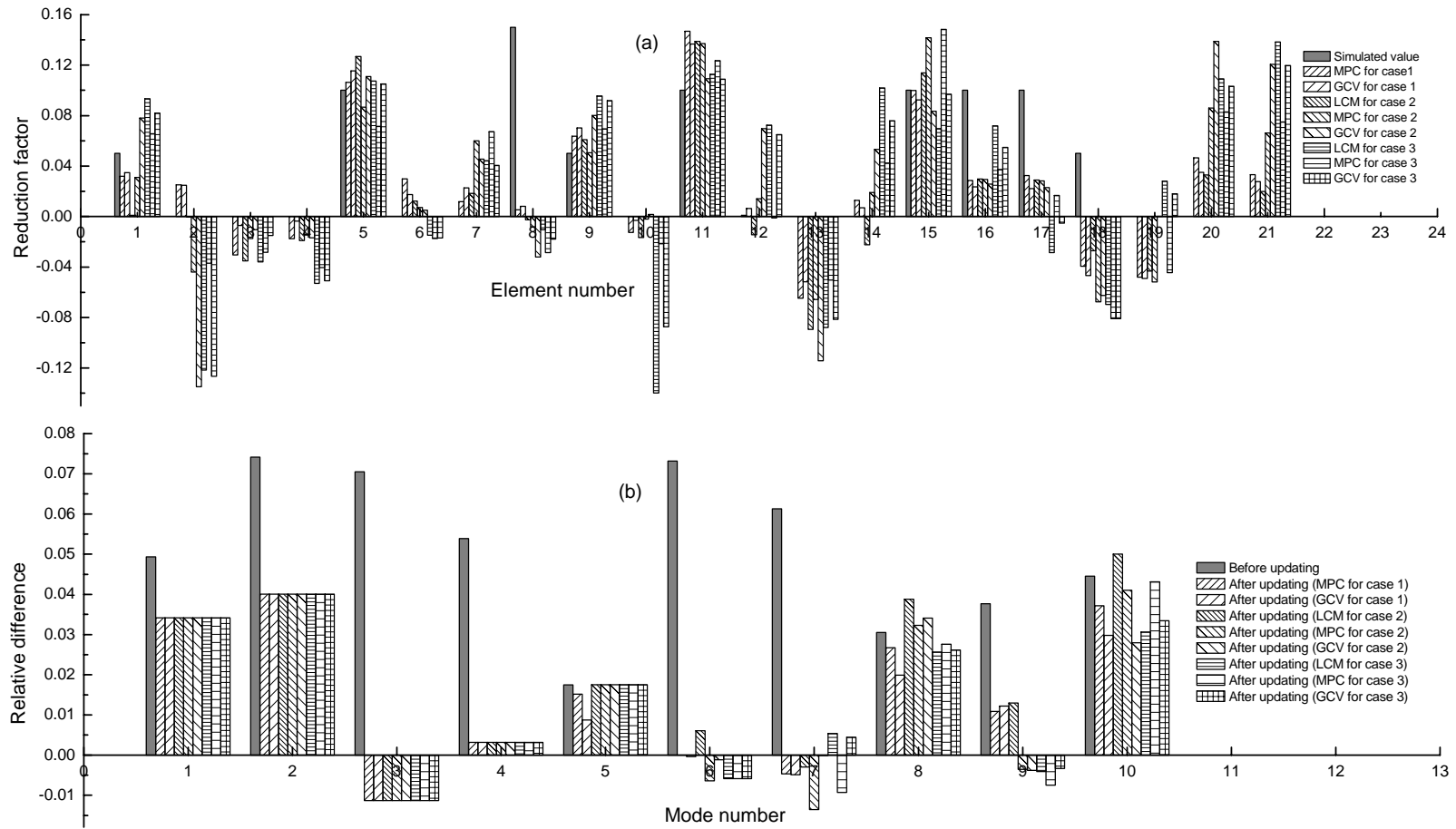


**Figure 3.22 Model updating results with 2% measurement noise for Tikhonov regularization:  
 (a) reduction factor; (b) relative difference in eigenvalues**

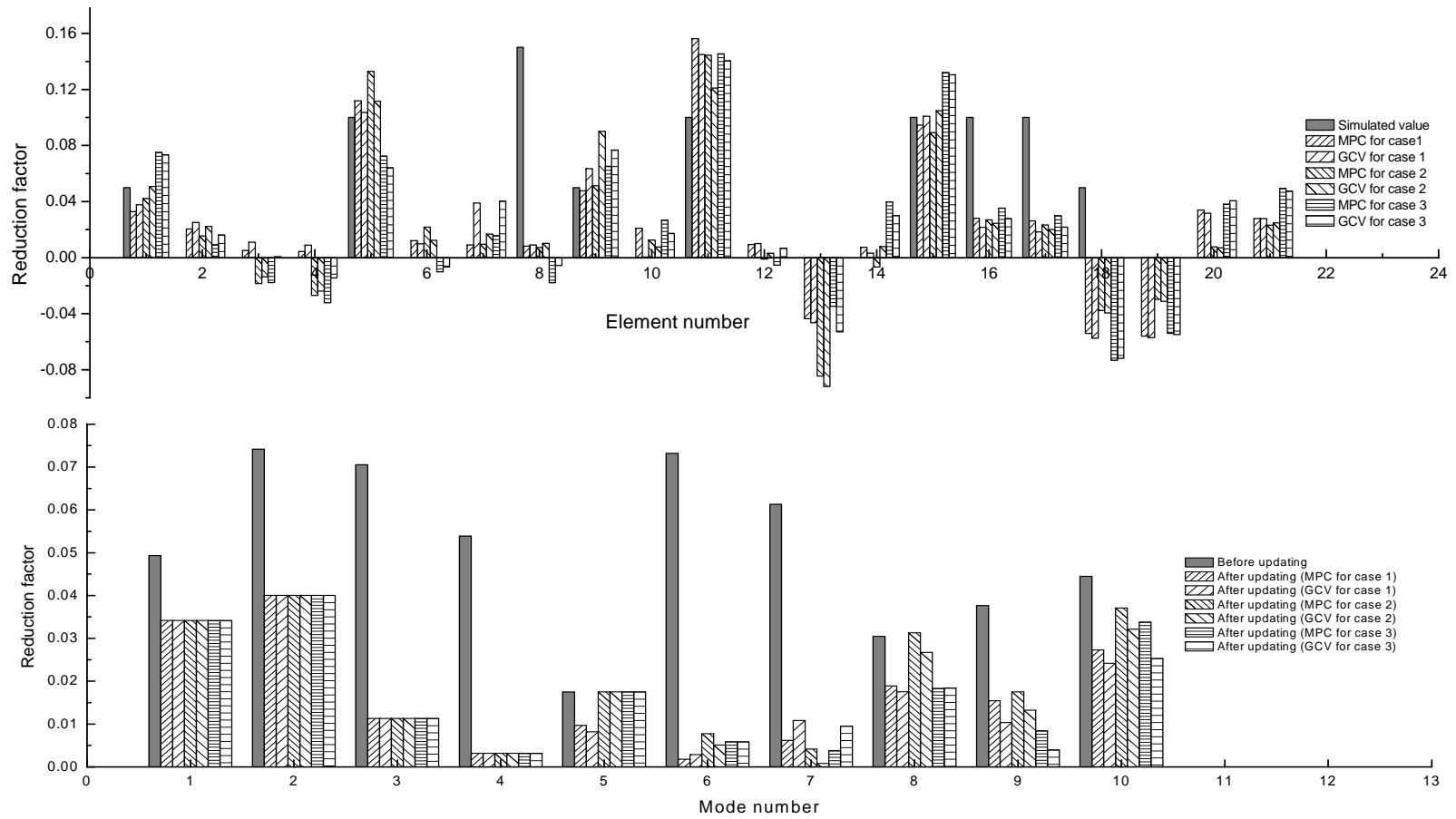


**Figure 3.23 Model updating results with 2% measurement noise for truncated SVD:  
(a) reduction factor; (b) relative difference in eigenvalues**

**Table 3.8 Model updating results using modal properties with 1% measurement noise for truncated SVD**

<i>Element No.</i>	<i>Simulated damage (%)</i>	<i>Using 4 modes</i>		<i>Using 5 modes</i>		<i>Using 6 modes</i>	
		<b>MPC</b>	<b>GCV</b>	<b>MPC</b>	<b>GCV</b>	<b>MPC</b>	<b>GCV</b>
1	5	2.686	2.686	-5.952	-5.952	-2.596	5.497
2	0	1.954	1.954	0.121	0.121	1.467	1.649
3	0	-3.870	-3.870	-3.019	-3.019	-3.805	-0.169
4	0	-3.148	-3.148	-0.329	-0.329	-3.271	-5.407
5	10	10.767	10.767	11.805	11.805	7.198	8.237
6	0	-0.319	-0.319	1.900	1.900	-5.612	5.898
7	0	0.096	0.096	-0.005	-0.005	1.982	0.593
8	15	0.910	0.910	-2.123	-2.123	-1.330	5.411
9	5	5.124	5.124	6.578	6.578	7.282	6.817
10	0	-2.148	-2.148	-3.915	-3.915	-5.877	-2.022
11	10	13.091	13.091	11.833	11.833	12.875	11.367
12	0	0.161	0.161	-6.173	-6.173	-4.721	1.827
13	0	-5.161	-5.161	-5.292	-5.292	-2.391	-2.250
14	0	2.332	2.332	-8.011	-8.011	-1.342	0.627
15	10	9.931	9.931	12.653	12.653	14.336	9.947
16	10	7.421	7.421	7.367	7.367	8.822	7.750
17	10	6.661	6.661	7.180	7.180	6.309	6.038
18	5	0.383	0.383	1.416	1.416	-1.046	-3.837
19	0	-0.322	-0.322	-2.54	-2.54	-2.614	1.387
20	0	3.645	3.645	5.983	5.983	9.338	5.994
21	0	2.883	2.883	1.446	1.446	3.373	7.651

**Figure 3.24** illustrates the ratio of consecutive SVs at different iteration steps when using 4 modes, in which a large ratio indicates a clear separation of the last two SVs from the others. It is shown that a well-behaved separation of SVs also occurs at all iteration steps even for noisy measurement data. In input-error-based FE model updating, however, the distinct separation disappears when using noisy measurement data (Mottershead and Foster 1991; Ahmadian *et al.* 1998; Ziaei-Rad and Imregun 1999).

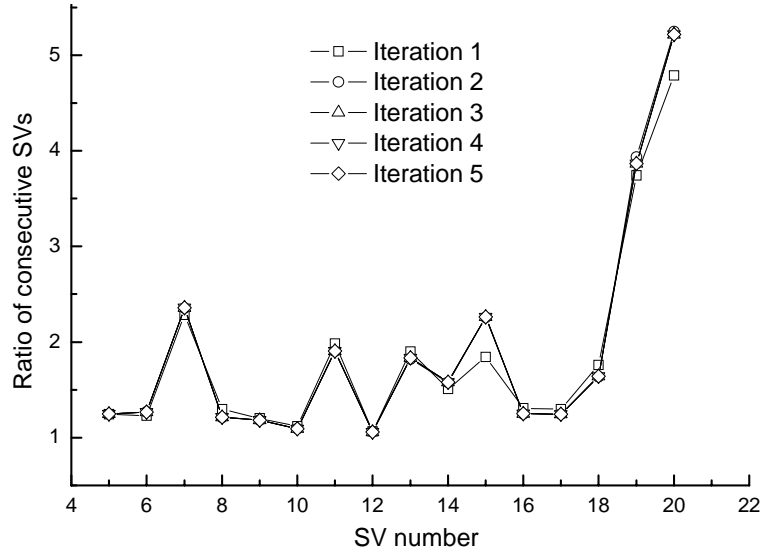


**Figure 3.24 Ratio of consecutive SVs at different iteration steps**

### 3.5.3.3 Comparison of different method combinations

The identification results discussed in the previous two sections are limited to a particular realization of random noise. In order to investigate the robustness of various combinations of the methods, random noise with zero mean and progressively increased variances is added to simulate the experimental modal properties. For each noise level, a total of 100 sets of ‘measured’ modal properties are generated by adding different realizations of random noise to the calculated modal properties. These noise-corrupted modal properties are then used for model updating; for each updating result, the relative error between the updating solutions and the exact simulated values is defined as

$$RE^{(i)} = \frac{\|\boldsymbol{\theta}^{(i)} - \boldsymbol{\theta}_d\|_2}{\|\boldsymbol{\theta}_d\|_2} \quad (3.52)$$

in which  $\boldsymbol{\theta}_d$  and  $\boldsymbol{\theta}^{(i)}$  denote the exact simulated value and the  $i$ th updating result. The

mean of relative error (MRE) is eventually obtained by averaging over the 100 sets of relative errors.

**Figure 3.25** presents a comparison of MRE obtained by Tikhonov regularization and truncated SVD with different regularization-parameter-choice methods. As expected, MRE increase steadily with increasing noise level. It is also found that the regularization methods are more effective even for high noise levels. Tikhonov regularization and truncated SVD in conjunction with MPC, on average, are consistently shown to give better results than the others. **Figure 3.26** illustrates the number of divergences for various combinations of the methods among the 100 trials. Tikhonov regularization and truncated SVD along with MPC always converge to a solution in the case of low noise level and they occasionally break down when the noise standard deviation exceeds 1.5%, regardless whether a local-minima solution or a global one is obtained. The Tikhonov method in combination with either LCM or GCV often gives rise to a large number of divergences. Obviously the number of divergences also increases with increasing noise level. It is noted that the results obtained from Tikhonov regularization along with GCV as shown in the second diagram of **Figure 3.26** are not convincing as such a method combination fails to obtain good results even for the noise-free data.

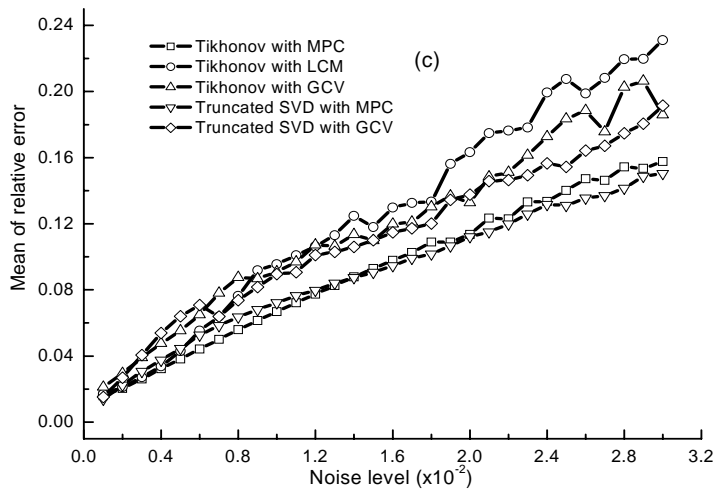
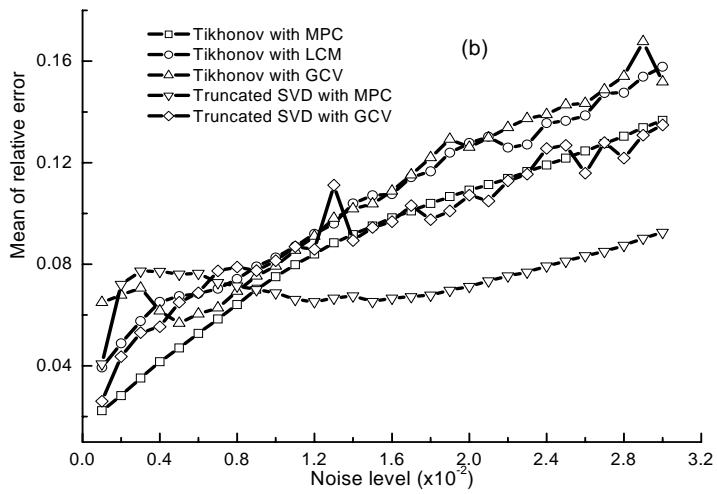
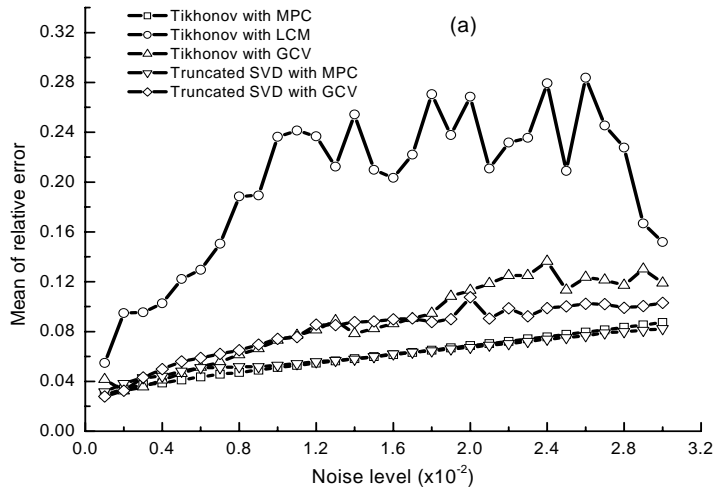


**Figure 3.25 Comparison of MRE obtained by different methods:  
 (a) using 4 modes; (b) using 5 modes; (c) using 6 modes**

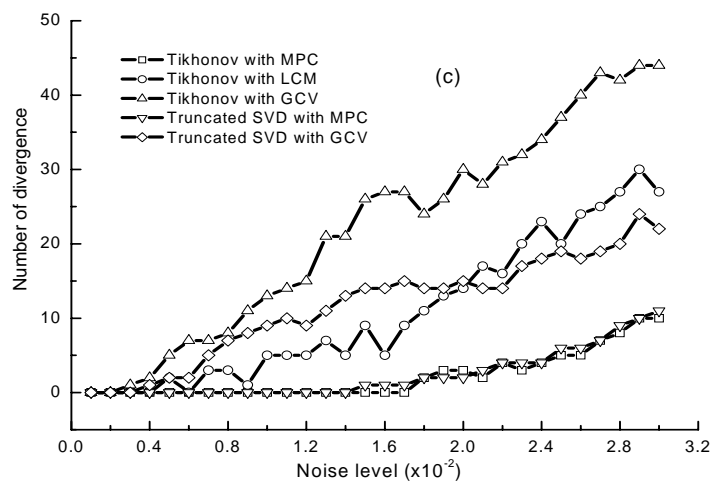
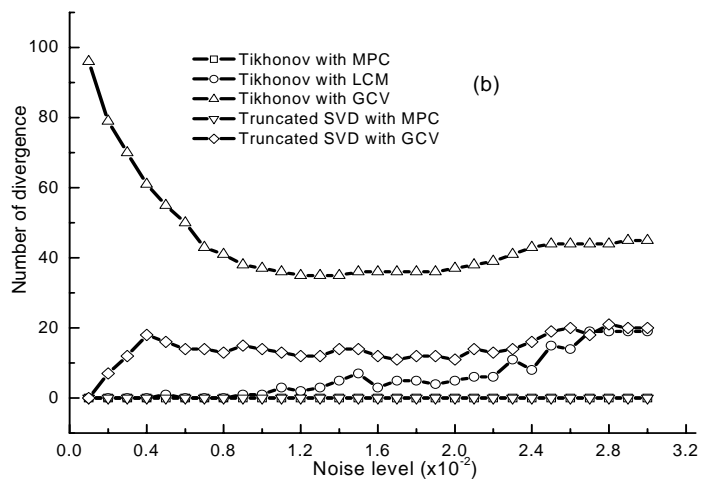
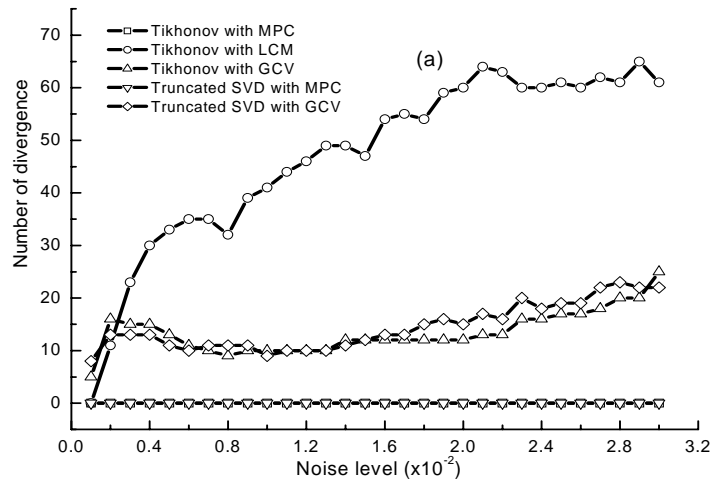


**Figure 3.26 Comparison of number of divergences for different methods: (a) using 4 modes; (b) using 5 modes; (c) using 6 modes**

### 3.6 Summary

The treatment of ill-conditioned and noisy system of equations is one of central problems in model updating. This problem was tackled with numerical regularization methods in this chapter. The performance of Tikhonov regularization and truncated SVD in combination with various regularization-parameter-choice methods for output-error-based model updating was rigorously investigated through numerical studies using both noise-free and noisy ‘measurement’ data. The procedures explored in this chapter lay the base for the study in the next chapter, which deals with the statistical model updating to take into account model uncertainty and measurement uncertainty.

The numerical results obtained from this chapter show that: (i) the well-behavedness of L-curve is not guaranteed in model updating, and a poorly-posed L-curve could make LCM fail to choose an appropriate regularization parameter; (ii) the regularization parameter obtained from MPC is close to that determined by LCM in the case of a well-behaved L-curve; otherwise it is close to that determined by GCV; (iii) truncated SVD and Tikhonov regularization when working with MPC are the most robust techniques for output-error-based model updating; (iv) in the output-error-based model updating approach, the SV spectrum has a distinct gap separating large SVs from small ones for both noise-free and noisy data. It is different from the equation-error-based in which the SVs spread evenly over the SV spectrum when noise-corrupted modal data are used for model updating.

## Chapter 4

### A NOVEL APPROACH FOR STOCHASTIC FE MODEL UPDATING

#### 4.1 Introduction

The need for incorporating the concept of probability and statistics in analysis and design of modern structures has led to the development of stochastic structural analysis techniques and structural reliability methods. The impetus to the research of structural reliability is originated from fluctuations of loadings, variability of material properties and uncertainties regarding analytical models (Madsen *et al.* 1986). Likewise, because of uncertainties in measured modal properties, there is also a necessity to integrate the methods of probability and statistics with the algorithms of FE model updating for uncertainty propagation, aiming at evaluating the effect of the uncertainties on model updating results.

The uncertainties in measured modal properties may arise from two sources, namely the measurement noise (source *A*) and the normal modal variability (source *B*), as discussed in section 2.3.4. Regarding the uncertainty associated with source *A*, it can be effectively diminished by averaging over large sets of the measured modal properties and taking the mean as true values. However the averaging technique does not resolve the problem of *irreducible* and *natural* uncertainties arising from source *B*. To consider the uncertainty due to the so-called natural modal variability, repeated

executions of model updating algorithms are necessary using all naturally-varying modal properties and the desired statistics of updating parameters are then estimated based on the model updating results. It is desired to eliminate the uncertainty associated with source *A* as thoroughly as possible to obtain nearly noise-free and ‘true’ modal properties. Unfortunately, in reality both reducible and irreducible uncertainties are often blended with each other, and it is difficult to separate them in the measurement data. In the case of uncertain modal properties, it is of considerable importance to estimate the statistical properties of updating parameters, and the model updating problem should be reasonably formulated in the statistical framework. With this in mind, the model updating from uncertain modal properties is stated as follows: given the distribution functions of input (measured modal properties), find certain statistical indices of output (updating parameters). Much research attention has recently been devoted to the application of statistical methods for model updating (Mares *et al.* 2006; Zimmerman 2006).

In general, the stochastic model updating works on the basis of integration of uncertainty-propagation approaches with conventional model updating algorithms. Two commonly-used numerical approaches to uncertainty propagation are Monte Carlo simulation (MCS) method and perturbation method. In MCS method, a large number of samples following the given probability distribution of modal properties are generated and then repeatedly used for model updating; the desired statistics are eventually estimated from these resulting updating results. An alternative approach to uncertainty propagation is the perturbation method. This approach expands a nonlinear function with a truncated Taylor series expansion at a known point and then proceeds to the approximation of the moments of solutions from the expansion. Intuitively, all model updating algorithms can be combined with MCS method and

perturbation method for uncertainty propagation. The combination of MCS method and model updating techniques has been used by a number of researchers (Agbabian *et al.* 1988; Banan *et al.* 1994b; Sanayei and Saletnik 1996b; Smyth *et al.* 2000; Yeo *et al.* 2000; Zhou *et al.* 2003). The minimum variance method making use of the concept of perturbation method was pioneered by Collins *et al.* (1974) to identify the statistical properties of updating parameters, and was later extended by Friswell *et al.* (1989). Beck and his-workers have reformulated this method in a more general framework of Bayesian theorem (Beck and Katafygiots 1998; Katafygiots and Beck 1998; Yuen and Katafygiots 2005). Similar approaches include those of perturbation method in combination with linear least squares method (Liu 1995; Papadopoulos and Garcia 1999), with extended Kalman filter method (Li and Roberts 1999a, b), with nonlinear least squares method (Araki and Hjelmstad 2001; Xia *et al.* 2002; Xia and Hao 2003), with maximum likelihood method (Fonseca *et al.* 2005), and with minimum rank perturbation method (Zimmerman 2006).

As discussed in the previous chapter, output-error-based model updating approach is effective in implementation as it does not require measuring all coordinates of a mode shape. However, this approach leads to a nonlinear least squares problem where it is very difficult, if not impossible, to obtain a closed-form solution of the distribution functions of output (updating parameters) in terms of those of input (measured modal properties). In the existing perturbation methods for approximating the distribution functions of updating parameters, it is assumed that the measured modal properties and updating parameters in the FE model are statistically independent. In general, however, this will be true only for the first iteration. After that, the measured data have been used to update the structural parameters and the

updated parameters are correlated with the measured modal properties for all of the remaining iterations (Hua *et al.* 2005).

This chapter develops a novel approach to stochastic model updating using uncertain modal properties. This approach pursues a two-stage updating scheme. The first stage refers to the identification of the probability distributions of updating parameters from measured uncertain modal properties, and the second stage deals with the determination of posterior distributions from the identified probability distributions and the prior probability distributions of updating parameters. The remaining of this chapter is organized as follows. The theoretical method of the first-stage stochastic model updating is first presented. Making use of an improved first-order perturbation method, the terms in the governing equation is expressed as Taylor series expansions at specific values of random variables. This leads to two recursive systems of deterministic equations of which the solutions are used to estimate the first-order approximation of the mean and covariance of updating parameters. Then Bayesian updating is applied to obtain the posterior distribution on the basis of the identified statistics and the prior distributions of structural parameters. The proposed method is finally applied for simulation study of stochastic model updating of two truss bridges. Both the improved perturbation method and MCS method are used to calculate the statistical properties of updating parameters based on simulated uncertain modal properties, and the results of the perturbation method for various types of uncertainty are discussed and compared with those of MCS method. The stochastically updated FE model enables structural damage detection, and condition assessment and evaluation in the framework of probability and statistics, which will be discussed in the following chapters.

## 4.2 First-Stage Stochastic FE Model Updating

The underlying philosophy of the present approach is quite straightforward. There are a variety of sources (data) which can be used to estimate the parameters of an unknown system, and each of the estimators is subject to a certain level of confidence and uncertainty due to the uncertainty in the sources. A combination of the estimators for different sources may lead to a better representation of the unknown system. **Figure 4.1** shows the flowchart of the proposed approach for stochastic FE model updating. Following this approach, stochastic FE model updating is first performed using the measured uncertain modal properties. Both MCS method and an improved perturbation method are employed to conduct the model updating. Next, the identified distributions of updating parameters are combined with the prior distributions of updating parameters (if available) via Bayesian updating to achieve the posterior distributions of the updating parameters. Thus the obtained posterior distributions rationally incorporate the knowledge and confidence in both experimentalist and structural analyst and could provide a better representation of the investigated structure. In this section, the first-stage stochastic model updating using an improved perturbation method is presented.

### 4.2.1 Basis of FE Model Updating

The basic formulation in Chapter 3 is briefly reviewed before proceeding to the presentation of the proposed method. In FE model updating using measured modal data, the identification of structural parameters is formulated as an optimization problem where structural parameters are sought so that the updated FE model can reproduce as closely as possible the measurement data. The objective function is

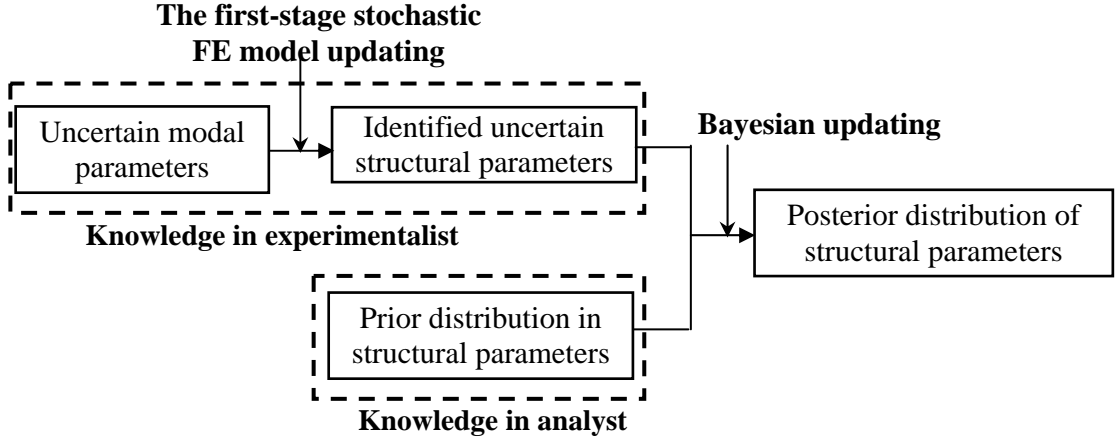


**Figure 4.1** Flowchart of proposed stochastic FE model updating

defined as a sum of weighted squared error

$$J(\boldsymbol{\theta}) = \tilde{\boldsymbol{\varepsilon}}^T \mathbf{W} \tilde{\boldsymbol{\varepsilon}} = \|\mathbf{W}_\varepsilon (\tilde{\mathbf{z}} - \mathbf{z}(\boldsymbol{\theta}))\|_2^2 \quad \text{with } \tilde{\boldsymbol{\varepsilon}} = \tilde{\mathbf{z}} - \mathbf{z}(\boldsymbol{\theta}) \quad (4.1)$$

where  $\tilde{\boldsymbol{\varepsilon}}$  is the output error of modal properties;  $\tilde{\mathbf{z}}$  and  $\mathbf{z}(\boldsymbol{\theta}) \in R^n$  are vectors of the experimental and analytical modal properties with  $n = n_f \times (n_m + 1)$ ;  $n_f$  and  $n_m$  are the numbers of measured natural frequencies and measured coordinates of each mode shape, respectively;  $\boldsymbol{\theta} \in R^m$  is a vector consisting of  $m$  updating parameters;  $\mathbf{W}_\varepsilon = \mathbf{W}^{1/2}$  is the diagonal weighting matrix; and the subscript  $T$  represents the transpose of matrix/vector. In order to obtain a unique solution, the number of known modal data  $n$  should be not less than the number of unknown updating parameters  $m$ .

The nonlinear least squares problem in Equation (4.1) can be solved with a gradient-based optimization approach. Beginning with an initial estimate of updating parameters, the solution for updating parameters in at the  $k$ th iteration is obtained as

$$\boldsymbol{\theta}^{(k+1)} = \boldsymbol{\theta}^{(k)} + \Delta\boldsymbol{\theta}^{(k)} \quad (4.2)$$

$$\mathbf{S}^{(k)}\Delta\boldsymbol{\theta}^{(k)} = \mathbf{e}^{(k)} \quad (4.3)$$

where  $\mathbf{e}^{(k)} = \mathbf{W}^{1/2}(\tilde{\mathbf{z}} - \mathbf{z}(\boldsymbol{\theta}^{(k)}))$  is the weighted error vector at the current iteration; and  $\mathbf{S} = \mathbf{W}^{1/2} \frac{\partial \mathbf{z}}{\partial \boldsymbol{\theta}}$  is the weighted sensitivity matrix of modal properties. The weights for eigenvalues are taken as unit, and the weights for eigenvectors are taken as 0.1 throughout this chapter (Friswell and Motteshhead 1995; Xia *et al.* 2002).

In deterministic model updating, the measured modal properties  $\tilde{\mathbf{z}}$  are known as fixed quantities which are obtained either from one test or by averaging the results from a series of tests. Due to the presence of irreducible randomness such as normal modal variability, the averaging technique does not make sense and a stochastic model updating procedure is necessary. A simple and straightforward yet brute-force approach to stochastic model updating is the MCS method. The problem with this approach is that a great many runs are required for a reliable estimate of updating parameter statistics, and the number of runs grows explosively with the number of modal properties used. The computational complexity is further exacerbated as the model updating algorithm itself is nonlinear and requires an iterative scheme. An alternative to MCS method is the perturbation method as will be elaborated later. Throughout this chapter, the uncertain modal properties are characterized by continuous random variables complying with normal distributions, and as a result the stochastic model updating reduces to finding the mean and covariance information of updating parameters when adopting the perturbation method.

#### 4.2.2 First-Order Perturbation Method

When the uncertainties in measured modal properties are taken into consideration, the model updating problem becomes much complicated in the sense that updated structural parameters at each iteration will be random and consequently the modal sensitivity matrix  $\mathbf{S}$  will also become stochastic. In order to take the uncertainty into account, the measured modal properties are expressed as the summation of a deterministic part and a random part

$$\tilde{z}_i = \bar{z}_i + X_i \quad (i = 1, 2, \dots, n) \quad (4.4)$$

where  $\bar{z}_i$  is the mean of the measured modal parameter  $\tilde{z}_i$ ;  $X_i$ , called basic random variable (BRV), represents the uncertainties in the measured modal parameters due to natural randomness and measurement noises.

Depending on the truncation order of Taylor series expansion used by the perturbation method, different accuracies of approximation to the solution statistics can be achieved. In practical applications, either the first-order second moment (FOSM) approach or the second-order second moment (SOSM) approach is employed to approximate the solution moments. FOSM approximates the nonlinear function with a linear expansion at a point of random variables, and the obtained mean and covariance are of first-order accuracy. A limitation of the first-order perturbation method is that uncertainties must not be too large as well as that the nonlinearity is not significant. Quadratic accuracy can be achieved by approaching the nonlinear function with a second-order Taylor series expansion. For overwhelming majority of applications in structural engineering, the simple first-

order theory fulfills all practical needs and its numerical accuracy is usually more than sufficient (Rackwitz 2001).

Making use of the first-order perturbation technique, the terms in Equation (4.3), namely the change in structural parameters (CSP)  $\Delta\boldsymbol{\theta}^{(k)}$ , modal sensitivity  $\mathbf{S}^{(k)}$ , and weighted error  $\mathbf{e}^{(k)}$  at the  $k$ th iteration can be approximately expanded as linear functions in terms of BRVs around the mean value point, as

$$\mathbf{S}^{(k)} = \bar{\mathbf{S}}^{(k)} + \sum_{i=1}^n \frac{\partial \mathbf{S}^{(k)}}{\partial X_i} X_i \quad (4.5)$$

$$\Delta\boldsymbol{\theta}^{(k)} = \Delta\bar{\boldsymbol{\theta}}^{(k)} + \sum_{i=1}^n \frac{\partial \Delta\boldsymbol{\theta}^{(k)}}{\partial X_i} X_i \quad (4.6)$$

$$\mathbf{e}^{(k)} = \bar{\mathbf{e}}^{(k)} + \sum_{i=1}^n \frac{\partial \mathbf{e}^{(k)}}{\partial X_i} X_i \quad (4.7)$$

where  $X_i$  ( $i = 1, 2, \dots, n$ ) represents the  $i$ th BRV; and the sensitivity coefficients above are often termed as experimental sensitivities which relate the change of the involved quantities with respect to the change in the measurement data.

Substituting Equations (4.5) to (4.7) into Equation (4.3) and comparing the zeroth-order and first-order terms of  $X_i$  lead to two recursive systems of deterministic equations (Hart and Collins 1970; Kleiber and Hien 1992), as

$$\bar{\mathbf{S}}^{(k)} \Delta\bar{\boldsymbol{\theta}}^{(k)} = \bar{\mathbf{e}}^{(k)} \quad (4.8)$$

$$\bar{\mathbf{S}}^{(k)} \frac{\partial \Delta\boldsymbol{\theta}^{(k)}}{\partial X_i} = \left( \frac{\partial \mathbf{e}^{(k)}}{\partial X_i} - \frac{\partial \mathbf{S}^{(k)}}{\partial X_i} \Delta\bar{\boldsymbol{\theta}}^{(k)} \right) \quad (4.9)$$

or

$$\bar{\mathbf{S}}^{(k)} \frac{\partial \Delta \boldsymbol{\theta}^{(k)}}{\partial X_i} = \left( \mathbf{W}^{1/2} \left( \frac{\partial \tilde{\mathbf{z}}}{\partial X_i} - \frac{\partial \mathbf{z}^{(k)}}{\partial X_i} \right) - \frac{\partial \mathbf{S}^{(k)}}{\partial X_i} \Delta \bar{\boldsymbol{\theta}}^{(k)} \right) \quad (4.10)$$

where the partial derivatives of  $\mathbf{z}^{(k)}$  and  $\mathbf{S}^{(k)}$  with respect to the BRV  $X_i$  at each iteration can be evaluated by means of the chain rule of differential calculus, as

$$\frac{\partial \mathbf{z}^{(k)}}{\partial X_i} = \frac{\partial \mathbf{z}^{(k)}}{\partial \boldsymbol{\theta}^{(k)}} \frac{\partial \boldsymbol{\theta}^{(k)}}{\partial X_i} \quad (4.11)$$

$$\frac{\partial \mathbf{S}^{(k)}}{\partial X_i} = \sum_{j=1}^m \frac{\partial \mathbf{S}^{(k)}}{\partial \theta_j^{(k)}} \frac{\partial \theta_j^{(k)}}{\partial X_i} \quad (4.12)$$

$$\frac{\partial \boldsymbol{\theta}^{(k)}}{\partial X_i} = \frac{\partial (\boldsymbol{\theta}^{(k-1)} + \Delta \boldsymbol{\theta}^{(k-1)})}{\partial X_i} \quad (4.13)$$

or

$$\frac{\partial \boldsymbol{\theta}^{(k)}}{\partial X_i} = \frac{\partial \boldsymbol{\theta}^{(0)}}{\partial X_i} + \sum_{j=1}^{k-1} \frac{\partial (\Delta \boldsymbol{\theta}^{(j)})}{\partial X_i} \quad (4.14)$$

in which  $\frac{\partial \mathbf{z}^{(k)}}{\partial \boldsymbol{\theta}^{(k)}}$  and  $\frac{\partial \mathbf{S}^{(k)}}{\partial \theta_j^{(k)}}$  are essentially the first-order and the weighted second-order modal sensitivities, respectively. The expressions of them are given in Appendix I.

From Equations (4.8) to (4.14), one can sequentially solve for the mean of CSP and the first-order derivatives of CSP. The mean of CSP can be readily obtained from Equation (4.8). Further substitution of the obtained mean of CSP along with Equations (4.11) to (4.14) into Equation (4.10) allows the computation of the first-order derivative of CSP with respect to BRV  $X_i$ . Repeating this operation over all BRVs one obtains the  $(m \times n)$ -dimension matrix of  $\partial \Delta \boldsymbol{\theta}^{(k)} / \partial \mathbf{X}$  needed to compute

the covariance matrix. It is noted that the derivative of CSP with respect to BRVs takes the form of

$$\frac{\partial \Delta \boldsymbol{\theta}^{(k)}}{\partial \mathbf{X}} = \begin{bmatrix} \frac{\partial \Delta \theta_1^{(k)}}{\partial X_1} & \frac{\partial \Delta \theta_1^{(k)}}{\partial X_2} & \dots & \frac{\partial \Delta \theta_1^{(k)}}{\partial X_n} \\ \frac{\partial \Delta \theta_2^{(k)}}{\partial X_1} & \frac{\partial \Delta \theta_2^{(k)}}{\partial X_2} & \dots & \frac{\partial \Delta \theta_2^{(k)}}{\partial X_n} \\ \vdots & \vdots & \ddots & \vdots \\ \frac{\partial \Delta \theta_m^{(k)}}{\partial X_1} & \frac{\partial \Delta \theta_m^{(k)}}{\partial X_2} & \dots & \frac{\partial \Delta \theta_m^{(k)}}{\partial X_n} \end{bmatrix} \quad (4.15)$$

In practice the first two moments, i.e. the expected value and variance of a random variable, are often of interests. Thus, taking the expected values of both sides of Equation (4.2) gives rise to the means of updating parameters at the  $k$ th iteration

$$\bar{\boldsymbol{\theta}}^{(k+1)} = \bar{\boldsymbol{\theta}}^{(k)} + \Delta \bar{\boldsymbol{\theta}}^{(k)} \quad (4.16)$$

The variance-covariance matrix of updating parameters at the  $k$ th iteration is then defined as

$$\text{Var}(\boldsymbol{\theta}^{(k+1)}, \boldsymbol{\theta}^{(k+1)}) = \text{E}[(\boldsymbol{\theta}^{(k+1)} - \bar{\boldsymbol{\theta}}^{(k+1)})(\boldsymbol{\theta}^{(k+1)} - \bar{\boldsymbol{\theta}}^{(k+1)})] \quad (4.17)$$

By substituting Equations (4.2) and (4.16) into Equation (4.17) and further using Equation (4.6), Equation (4.17) is rewritten as

$$\text{Var}(\boldsymbol{\theta}^{(k+1)}, \boldsymbol{\theta}^{(k+1)}) = \text{E} \left[ \sum_{i=1}^n \sum_{j=1}^n \left( \frac{\partial \boldsymbol{\theta}^{(k)}}{\partial X_i} + \frac{\partial \Delta \boldsymbol{\theta}^{(k)}}{\partial X_i} \right) \left( \frac{\partial \boldsymbol{\theta}^{(k)}}{\partial X_j} + \frac{\partial \Delta \boldsymbol{\theta}^{(k)}}{\partial X_j} \right) X_i X_j \right] \quad (4.18)$$

or in the matrix form

$$\begin{aligned} \text{Var}(\boldsymbol{\theta}^{(k+1)}, \boldsymbol{\theta}^{(k+1)}) &= \text{Var}(\boldsymbol{\theta}^{(k)}, \boldsymbol{\theta}^{(k)}) + \text{Var}(\boldsymbol{\theta}^{(k)}, \Delta \boldsymbol{\theta}^{(k)}) \\ &+ \text{Var}(\Delta \boldsymbol{\theta}^{(k)}, \boldsymbol{\theta}^{(k)}) + \text{Var}(\Delta \boldsymbol{\theta}^{(k)}, \Delta \boldsymbol{\theta}^{(k)}) \end{aligned} \quad (4.19)$$

$$\text{Var}(\boldsymbol{\theta}^{(k)}, \boldsymbol{\theta}^{(k)}) = \left[ \frac{\partial \boldsymbol{\theta}^{(k)}}{\partial \mathbf{X}} \right] \boldsymbol{\Sigma}_x \left[ \frac{\partial \boldsymbol{\theta}^{(k)}}{\partial \mathbf{X}} \right]^T \quad (4.20)$$

$$\text{Var}(\boldsymbol{\theta}^{(k)}, \Delta \boldsymbol{\theta}^{(k)}) = \left[ \frac{\partial \boldsymbol{\theta}^{(k)}}{\partial \mathbf{X}} \right] \boldsymbol{\Sigma}_x \left[ \frac{\partial \Delta \boldsymbol{\theta}^{(k)}}{\partial \mathbf{X}} \right]^T \quad (4.21)$$

$$\text{Var}(\Delta \boldsymbol{\theta}^{(k)}, \boldsymbol{\theta}^{(k)}) = \left[ \frac{\partial \Delta \boldsymbol{\theta}^{(k)}}{\partial \mathbf{X}} \right] \boldsymbol{\Sigma}_x \left[ \frac{\partial \boldsymbol{\theta}^{(k)}}{\partial \mathbf{X}} \right]^T \quad (4.22)$$

$$\text{Var}(\Delta \boldsymbol{\theta}^{(k)}, \Delta \boldsymbol{\theta}^{(k)}) = \left[ \frac{\partial \Delta \boldsymbol{\theta}^{(k)}}{\partial \mathbf{X}} \right] \boldsymbol{\Sigma}_x \left[ \frac{\partial \Delta \boldsymbol{\theta}^{(k)}}{\partial \mathbf{X}} \right]^T \quad (4.23)$$

where  $\boldsymbol{\Sigma}_x$  is the covariance matrix of BRVs, as

$$\boldsymbol{\Sigma}_x = \begin{bmatrix} \text{Var}(X_1) & \text{Cov}(X_1, X_2) & \cdots & \text{Cov}(X_1, X_n) \\ \text{Cov}(X_2, X_1) & \text{Var}(X_2) & \cdots & \text{Cov}(X_2, X_n) \\ \vdots & \vdots & \ddots & \vdots \\ \text{Cov}(X_n, X_1) & \text{Cov}(X_n, X_2) & \cdots & \text{Var}(X_n) \end{bmatrix} \quad (4.24)$$

It is shown that the mean and covariance of updating parameters at each iteration are explicitly expressed in terms of the statistics of the measured modal properties. The existing perturbation methods for model updating assume that the measured modal properties and updating parameters in the FE model are statistically independent. Under this assumption, the quantity in Equation (4.13) becomes zero and therefore the first three quantities in the right-hand side of Equation (4.18) will vanish (Xia and Hao 2003). In general, however, this assumption is true only for the first iteration. After that, the measured data have been used to update structural parameters, and the updated parameters will be correlated with the measured modal properties for all remaining iterations. As a substantial improvement to the existing methods, the present approach calculates the partial derivatives of updating parameters,  $\partial \boldsymbol{\theta}^{(k)} / \partial \mathbf{X}$ ,

and CSP,  $\partial\Delta\boldsymbol{\theta}^{(k)}/\partial\mathbf{X}$ , with respect to BRVs and therefore the correlation between them at each iteration. The covariance of updating parameters is then evaluated with the updated partial derivatives at each iteration. Therefore the present approach is accurate in the first-order sense for nonlinear least squares problems.

For the algorithm implementation of the proposed approach, the following remarks are made:

1) As the measured modal properties are uncorrelated random variables,

$$\frac{\partial\tilde{\mathbf{z}}}{\partial X_i} = \left\{ \begin{array}{ccc} \overbrace{0 \cdots}^{1 \sim (i-1)} & 1 & \overbrace{\cdots 0}^{(i+1) \sim n} \end{array} \right\}_{n \times 1}^T \text{ at all iteration steps;}$$

2) The vector  $\frac{\partial\boldsymbol{\theta}^{(k)}}{\partial X_i}$  is  $\mathbf{0}$  for the first iteration as there is no correlation between updating parameters and measurement data. It is then determined from Equation (4.14) along with the solution to Equation (4.10) for the remaining iterations.

In the present approach, the derived mean and covariance of updating parameters are of the first-order accuracy as a linear Taylor series expansion is employed to approximate the nonlinear function between the updating parameters and the modal data. Furthermore, the distribution functions of updating parameters generally will not comply with the normal ones even when each of the measured modal properties follows a normal distribution. It is therefore required to verify the accuracy and applicability of this approximation using the MCS method.

### 4.2.3 Computational Issues

Because the modal sensitivity matrix in FE model updating is often ill-conditioned, direct solution to Equations (4.8) and (4.10) may yield very poor estimates. The regularization methods elaborated in the previous chapter should be applied to obtain a stable and sound solution. For the convenience of presentation, Equations (4.8) and (4.9) are expressed as a general form of

$$\mathbf{Ax} = \mathbf{b} \quad (4.25)$$

Regularization methods combined with various regularization-parameter-choice procedures can be applied to Equation (4.25) to obtain a regularized solution. In the case of Tikhonov regularization, the regularized solution is

$$\mathbf{x}_\lambda = \sum_{i=1}^m \frac{\sigma_i^2}{\sigma_i^2 + \lambda^2} \frac{\mathbf{u}_i^T \mathbf{b}}{\sigma_i} \mathbf{v}_i \quad (4.26)$$

in which  $\lambda$  is the Tikhonov parameter; and the quantities  $\sigma_i^2$ ,  $\mathbf{u}_i$ , and  $\mathbf{v}_i$  are the  $i$ th SV, left singular vector, and right singular vector of the weighted sensitivity matrix, respectively. In the case of truncated SVD, the regularization solution becomes

$$\mathbf{x}_{m_t} = \sum_{i=1}^{m_t} \frac{\mathbf{u}_i^T \mathbf{b}}{\sigma_i} \mathbf{v}_i \quad (4.27)$$

in which  $m_t$  is the truncation parameter that controls the number of SVs set to zero.

The computer implementation of the stochastic FE model updating procedure is as follows:

- 1) Determine the mean and covariance from a series of measured modal properties  $\tilde{\mathbf{z}}$ , and set  $k = 0$ ;

- 2) Compute the analytical modal properties  $\mathbf{z}^{(k)}$  and the weighted modal sensitivity matrix with respect to updating parameter  $\mathbf{S}^{(k)}$  from the FE model;
- 3) Solve Equation (4.8) for the mean of CSP  $\Delta\bar{\boldsymbol{\theta}}^{(k)}$ ; solve Equation (4.10) to obtain the first-order derivatives of CSP with respect to BRV,  $\partial\Delta\boldsymbol{\theta}^{(k)} / \partial X_i$ , and repeat this procedure for all random variables. In the solution course, the regularized solutions are obtained;
- 4) Check whether the convergence criterion is satisfied. If yes, go to step (5), otherwise  $k = k + 1$ , return to step (2);
- 5) Derive the means and covariance matrix of updating structural parameters using Equations (4.18) to (4.24) and update FE model with structural parameters  $\boldsymbol{\theta}^{(k+1)}$ .

### **4.3 Bayesian Updating for Determination of Posterior Distribution**

The first-stage stochastic model updating involves the use of measured uncertain modal properties to determine the statistical properties of updating parameters. The updating results in this stage correspond to the experimentalist's knowledge and confidence on the estimates of structural parameters. In practice, structural parameters may be also estimated from other sources which are also subject to uncertainties. Such an estimate of structural parameters, termed as prior information, can be obtained, for example, by another group of experimentalist, local nondestructive evaluation technique, and engineering judgment. Interested here is the case that the prior information on the estimates of structural parameters is given by structural analyst. As a result, two (or more) sets of information on the estimates of

structural parameters with uncertainties exist and the second-stage updating reduces to a rational combination of them to yield a new estimate.

Bayesian updating approach is very useful when one faces with two sets of uncertain information and needs to know which to believe. It uses both the prior information and the newly obtained information to account for the relative uncertainty associated with each other. In the present study, the prior information is given by structural analyst prior to testing of a structure while the newly obtained information is from the first-stage stochastic model updating results, and Bayesian updating is applied to achieve a new (posterior) distribution from the above information.

Assume that before the new information is available, a random structural parameter  $\theta$  is believed to have a probability density function (PDF)  $f_1(\theta)$ . Through the first-stage stochastic model updating using measured uncertain modal properties, the identified PDF of updating parameter can be described by  $f_2(\theta)$ . Following the theory of Bayesian updating, the posterior PDF of structural parameter which uses both sets of information and provides the best use of both can be expressed as (Ang and Tang 1975)

$$f(\theta) = kL(\theta)f_2(\theta) \quad (4.28)$$

where  $L(\theta)$  represents the likelihood function; and  $k$  is the normalizing constant.

For the case where the PDFs of both  $f_1(\theta)$  and  $f_2(\theta)$  are normally distributed, the posterior PDF of structural parameter  $f(\theta)$  will also comply with a normal distribution whose mean and standard deviation are obtained, respectively, as

$$\mu = \frac{\mu_1(\sigma_2)^2 + \mu_2(\sigma_1)^2}{(\sigma_1)^2 + (\sigma_2)^2} \quad (4.29)$$

$$\sigma = \sqrt{\frac{(\sigma_1)^2(\sigma_2)^2}{(\sigma_1)^2 + (\sigma_2)^2}} \quad (4.30)$$

where  $\mu_1$  and  $\mu_2$  are the means of prior and identified distribution functions, respectively; and  $\sigma_1$  and  $\sigma_2$  are the corresponding standard deviations, respectively.

It is clear that both mean and standard deviation of the posterior distribution functions are weighted average of the prior and the identified distribution functions of structural parameters. As a result of increasing knowledge on the estimate of structural parameters, it is important to observe that the posterior variance of structural parameters  $\sigma$  is always less than the variance of the prior variance  $\sigma_1$  and the identified variance  $\sigma_2$ . By using the Bayesian theory, the knowledge in the analyst and experience in the experimentalist can be rationally incorporated.

With the stochastically updated FE model of a structure, probabilistic damage detection can be carried out to determine the probability of damage occurrence (Papadopoulos and Garcia 1999; Xia *et al.* 2002; Xia and Hao 2003; Beck *et al.* 2001; Ching and Beck 2004), and safety reliability analysis can be performed taking into account the random structural parameters (Natke and Yao 1988; Papadimitriou *et al.* 2001).

#### 4.4 Case Study 1: A Statically Determinate Truss Bridge

A statically determinate truss bridge, as shown in **Figure 4.2**, is used as the first example to illustrate and verify the proposed method. The truss bridge, which is the same as in **Figure 3.3**, is a simply supported pin-jointed steel bridge consisting of top members, bottom members, vertical members and diagonal members. An analytical FE model is established which has been correlated with the modal properties of as-built or undamaged state of the bridge, and therefore this *baseline* model is representative of the bridge without damage. In this analytical model as shown in **Figure 4.2**, a total of 21 planar truss elements, each with two DOFs at every node, are used. The material properties used in this analytical model are as follows: mass density  $\rho = 7800 \text{ kg/m}^3$ , area of cross section for each member  $A = 10^{-2} \text{ m}^2$ , and the Young's modulus  $E = 200 \text{ GPa}$ .

Another FE model with the same topology as the baseline model is constructed to provide the simulated experimental modal properties by artificial reduction of Young's modulus of each member to different levels, as shown in **Figure 4.3**. The modal properties computed from this FE model serve as the mean of 'measured' modal properties from the damaged structure (the covariance of 'measured' modal properties will be discussed in the following sections). For the purpose of simulating incomplete measurement, only the first six eigenvalues and five vertical modal displacements for each of the eigenvectors, namely vertical modal displacements at nodes 7, 8, 9, 10 and 11 as shown in **Figure 4.3**, are assumed available throughout this numerical study.

In this study, different sources of uncertainties in the measured modal properties are considered. The first case (case 1) investigates the stochastic model updating by using the uncertain modal properties arising from natural randomness of structure. For simplicity, the natural randomness is modelled as a result of variation in Young's modulus with the environmental temperature, which has been shown to be a major contribution to the measured natural modal variability (Xia *et al.* 2006). The covariance matrix of updating parameters obtained in this case indicates the natural randomness in the updating parameters. The next case (case 2) studies the stochastic model updating with uncertain modal properties associated with measurement noise. The obtained covariance matrix in this case indeed gives the evidence on how reliable the model updating results are in view of the measurement noise in the data. The last case (case 3) addresses the stochastic model updating by using the uncertainties in modal properties due to both natural randomness and measurement noise. For each case, the statistics of updating structural parameters are first obtained by the improved perturbation method and then verified by the MCS method.

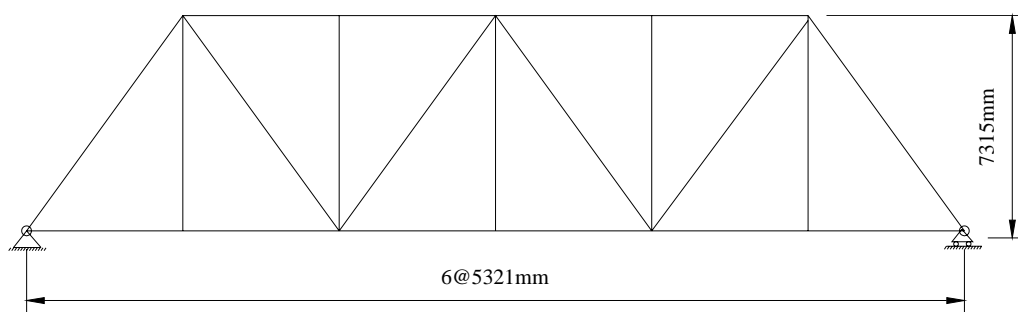


**Figure 4.2 Geometry configuration of statically determinate truss bridge**

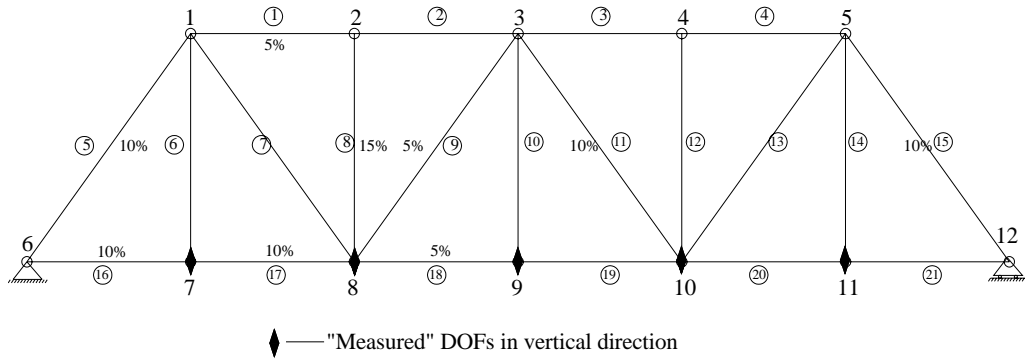


**Figure 4.3 Finite element model and simulated reduction factors of Young's modulus for statically determinate truss bridge**

#### *4.4.1 Uncertainty due to Natural Randomness*

In this section, the stochastic model updating method is applied to obtain the statistic properties of updating parameters using the measured uncertain modal properties caused by the natural randomness of structure. The natural randomness of a structure may be caused by the temperature-dependent Young's modulus. By modelling the temperature data in one year as random variables, one can obtain the distribution function of temperature. The distribution function of Young's modulus of a member can then be readily derived from the relation between temperature and Young's modulus. In this case, as both the mean and the covariance of updating parameters are known, the accuracy of both the perturbation method and the MCS method in identifying the statistics of updating parameters can be assessed.

For brevity, it is assumed that the coefficient of variation (COV) of Young's modulus of each member in the damaged structure, which is defined as the ratio of standard deviation to the mean, is 0.1, and the assumed variability in structural parameters are then used to obtain covariance of the modal properties. To do so, the

perturbation-based stochastic finite element method (PSFEM) is employed (Kleiber and Hien 1992). Following the first-order PSFEM, the means of modal properties are directly computed from the means of Young's modulus in the damaged structure, and the covariance matrix are approximated as

$$\text{Var}(\tilde{\mathbf{z}}, \tilde{\mathbf{z}}) = \mathbf{S}_d \boldsymbol{\Sigma}_E \mathbf{S}_d^T \quad (4.31)$$

where  $\mathbf{S}_d$  is the modal sensitivity matrix with respect to Young's modulus evaluated at their means for the damaged structure; and  $\boldsymbol{\Sigma}_E$  is the given covariance matrix of Young's modulus. Alternatively, the MCS method can be performed to obtain the statistics of modal properties by conducting the following steps: (1) generation of samples of Young's modulus in accordance with the given distribution functions; (2) repeat executions of modal analysis to obtain solutions; and (3) assembly of the mean and covariance from a series of modal solutions.

#### 4.4.1.1 Stochastic Model Updating Using Perturbation Method

Given the mean and the covariance of simulated experimental modal properties, the mean and the covariance of updating structural parameters can be estimated by the improved perturbation method. The means of updating parameters are computed on the basis on Equation (4.8) and the estimation of covariance matrix is accomplished with Equations (4.18) to (4.24) with the help of regularization methods at each iteration step.

**Figure 4.4** compares the mean and the coefficient of variance of updating results obtained under different combinations of regularization methods with regularization-parameter-choice procedures. For the convenience of comparison and presentation, the means of reduction factors, instead of the means of updating parameters, are

shown in **Figure 4.4(a)**. It seems that all methods produce favorable identification results of the means of updating parameters. However, they produce quite different estimates on COV as illustrated in **Figure 4.4(b)**. For the purpose of providing quantitative information regarding the performance of various methods, the average relative errors (ARE) of mean and standard deviation of the updating results using perturbation method are defined, respectively, as

$$\text{ARE}_{\text{mean}} = \sqrt{\frac{1}{m} \sum_{i=1}^m \left( \frac{\mu_{pi}}{\mu_i} - 1 \right)^2} \quad (4.32)$$

$$\text{ARE}_{\text{std}} = \sqrt{\frac{1}{m} \sum_{i=1}^m \left( \frac{\sigma_{pi}}{\sigma_i} - 1 \right)^2} \quad (4.33)$$

where  $\mu_p$ , and  $\mu$  are means of updating parameters obtained by the perturbation method and the simulated exact values, respectively;  $\sigma_p$  and  $\sigma$  are standard deviations of the updating parameters obtained by the perturbation method and the simulated exact values, respectively; and  $m$  is the number of updating parameters. **Table 4.1** lists a comparison of ARE values obtained from different method combinations. All the method combinations are satisfactory for the estimation of mean value but some of them perform poorly for the estimation of covariance matrix. It is shown that Tikhonov regularization along with MPC gives the closest results to the exact values.

**Table 4.1 ARE of mean and standard deviation of updating parameters**

<i>ARE</i>	<i>Tikhonov regularization</i>			<i>Truncated SVD</i>	
	<b>MPC</b>	<b>LCM</b>	<b>GCV</b>	<b>MPC</b>	<b>GCV</b>
Mean	0.006	0.013	0.000	0.000	0.000
STD	0.390	2.199	4.723	0.849	0.682

In practice the variance-covariance matrix of measured modal properties often reduces to a diagonal matrix rather than a fully-populated one because the covariance between two variables is not readily available or is often ignored (Doebbling and Farrar 1997; Arici and Mosalam 2005). Therefore it is worth further investigating the accuracy of the perturbation method in the absence of correlation between random variables. In comparison with the simulated exact values, **Figure 4.5** shows the updating results obtained from the fully-populated covariance matrix and the diagonal covariance matrix. It is found that neglecting the correlation between measured modal properties may give unreliable estimation on the standard deviation.

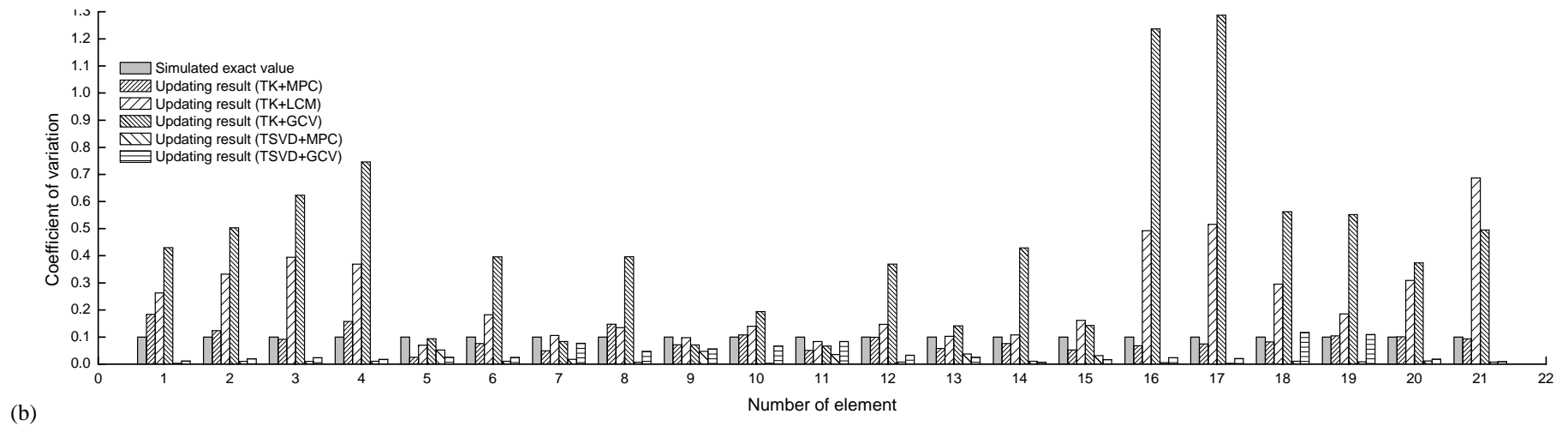
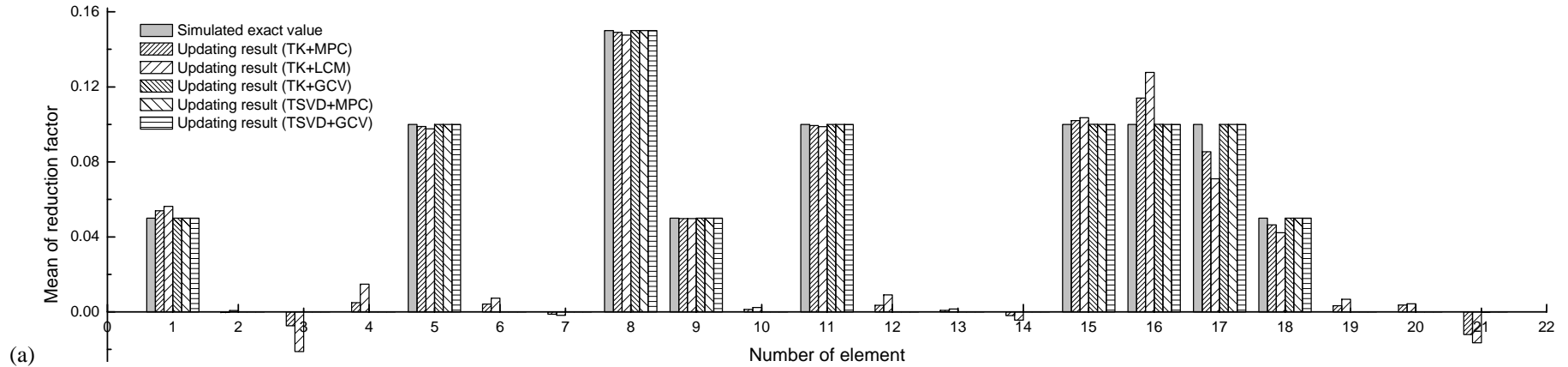


**Figure 4.4 Comparison of model updating results using perturbation method for 10% natural randomness:  
(a) mean of reduction factor; (b) COV**

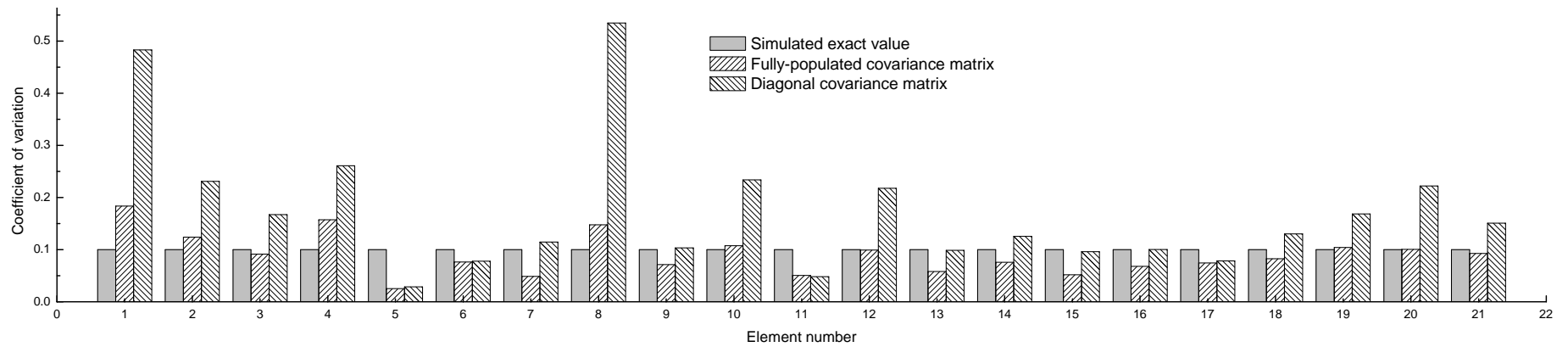


**Figure 4.5 Comparison of model updating results using fully-populated covariance matrix and diagonal covariance matrix**

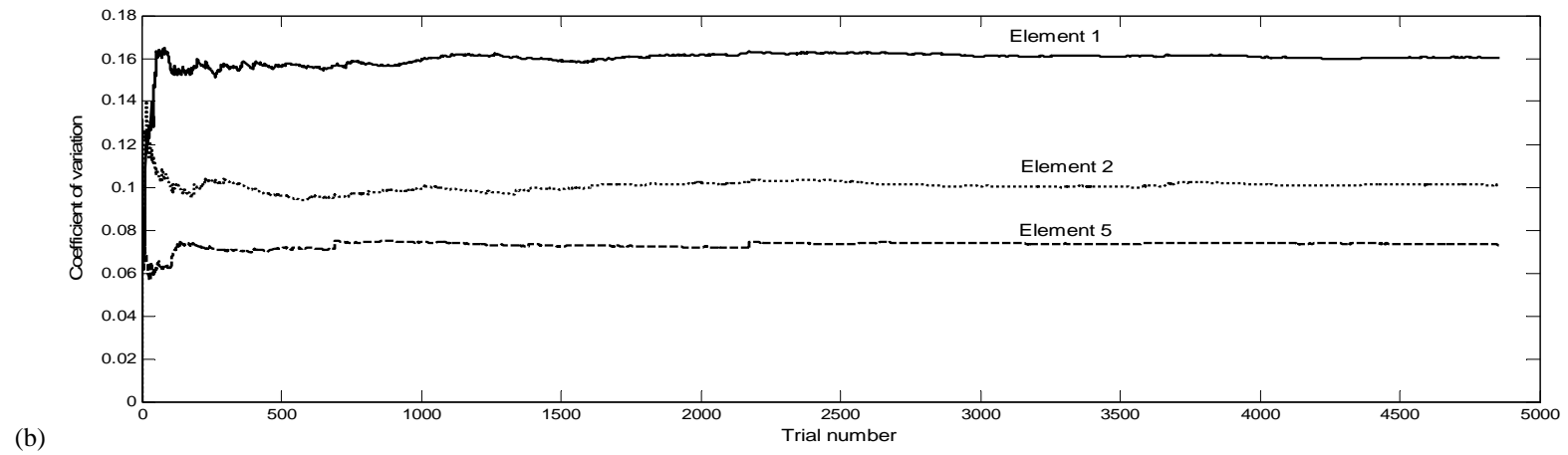
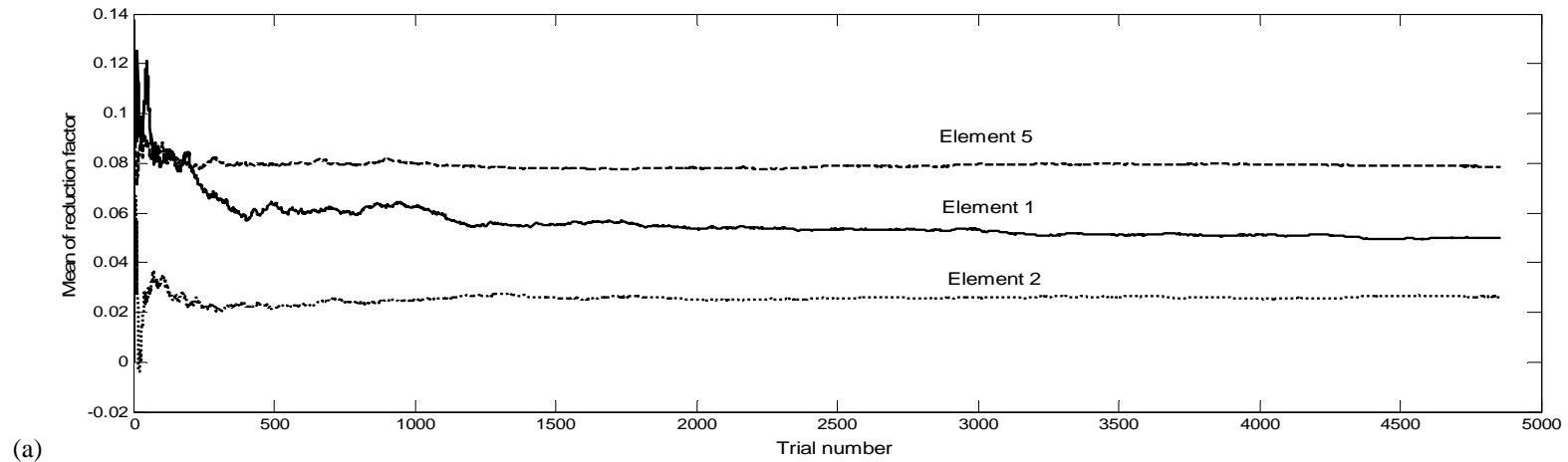


**Figure 4.6 Variation in mean and COV with respect to trail number of MCS for 10% natural randomness: (a) mean of reduction factor; (b) COV**

#### 4.4.1.2 Stochastic Model Updating Using MCS Method

The MCS method is now applied to obtain the statistics of updating parameters, and the updating results are compared with both the simulated exact values and those from the perturbation method. In the MCS method, we first compute a series of modal properties from a number of generated samples (5,000) of uncertain structural parameters; these modal properties are then used to identify the statistical properties of updating parameters through repeated runs of the deterministic model updating algorithm; and finally the statistic properties of updating parameters are estimated from the sequences of updating results. The combined Tikhonov-MPC method is used to obtain the regularized solution for the consistency in comparison.

**Figure 4.6** illustrates the variation in mean and COV of several updating parameters with respect to the trial number of MCS. These variations are observed to become stable when the trial number of MCS exceeds 2,000. Thus it is concluded that 5,000 trials of MCS are sufficient to approximate the mean and COV of updating parameters. **Figure 4.7** shows the MCS sample sequences of reduction factors for updating parameters. Among the 5,000 simulation runs, more than 4,800 runs converge, demonstrating a good performance of the combined Tikhonov-MPC method. It is shown that the sample sequences of some elements are rather scattered, indicating large COV; and vice versa. **Table 4.2** compares the mean and COV estimated from MCS sample sequences with the simulated exacted values. It is clear that the larger the COV is, the more dispersed the plot of sample sequences is. Furthermore, the estimated means do not coincide well with the exact values for some elements. The discrepancy between the MCS results and the exact values comes from two reasons. The first reason is that the finite number of MCS samples is

not distributed exactly as the target distribution of uncertain modal properties, introducing bias in the estimates. Apart from this, the existence of many local minima associated with the nonlinear least squares problem also contributes to the observed discrepancy. In a nonlinear least squares problem, many simulation runs may be entrapped to local minima due to improper initialization of starting values. One effective solution to this problem is to combine the gradient-based optimization approach with a global optimization method, such as genetic algorithm, to attain the global minima of objective functions. However the genetic algorithm is very slow in execution since the method employed is based on a stochastic search.

**Table 4.2 Comparison of MCS results with the simulated exact values**

<i>Element No.</i>	<i>Simulated exact values</i>		<i>MCS results</i>	
	$\mu$ (%)	$\sigma$	$\mu$ (%)	$\sigma$
1	5	0.1	6.122	0.116
2	0	0.1	1.745	0.089
3	0	0.1	0.143	0.091
4	0	0.1	0.599	0.088
5	10	0.1	9.579	0.077
6	0	0.1	-2.041	0.116
7	0	0.1	1.834	0.102
8	15	0.1	6.752	0.186
9	5	0.1	6.871	0.088
10	0	0.1	2.201	0.110
11	10	0.1	9.583	0.103
12	0	0.1	-1.493	0.116
13	0	0.1	-0.314	0.092
14	0	0.1	-2.112	0.101
15	10	0.1	9.0572	0.096
16	10	0.1	10.513	0.086
17	10	0.1	9.1005	0.086
18	5	0.1	3.4363	0.093
19	0	0.1	1.8863	0.093
20	0	0.1	3.4428	0.111
21	0	0.1	0.753	0.080

The PDFs of updating parameters constructed from the MCS sample sequences are plotted in **Figure 4.8**, and the corresponding CDFs are shown in **Figure 4.9**. For the purpose of comparison, the theoretical normal distribution with the mean and standard deviation of the updating sequences is also superimposed in the figures. The observed PDF of each updating parameter is well approximated with a normal distribution. **Figure 4.10** compares the results from the perturbation and MCS methods with the simulated exact values. The perturbation method gives acceptable estimation of COV though it is less accurate than the MCS method.

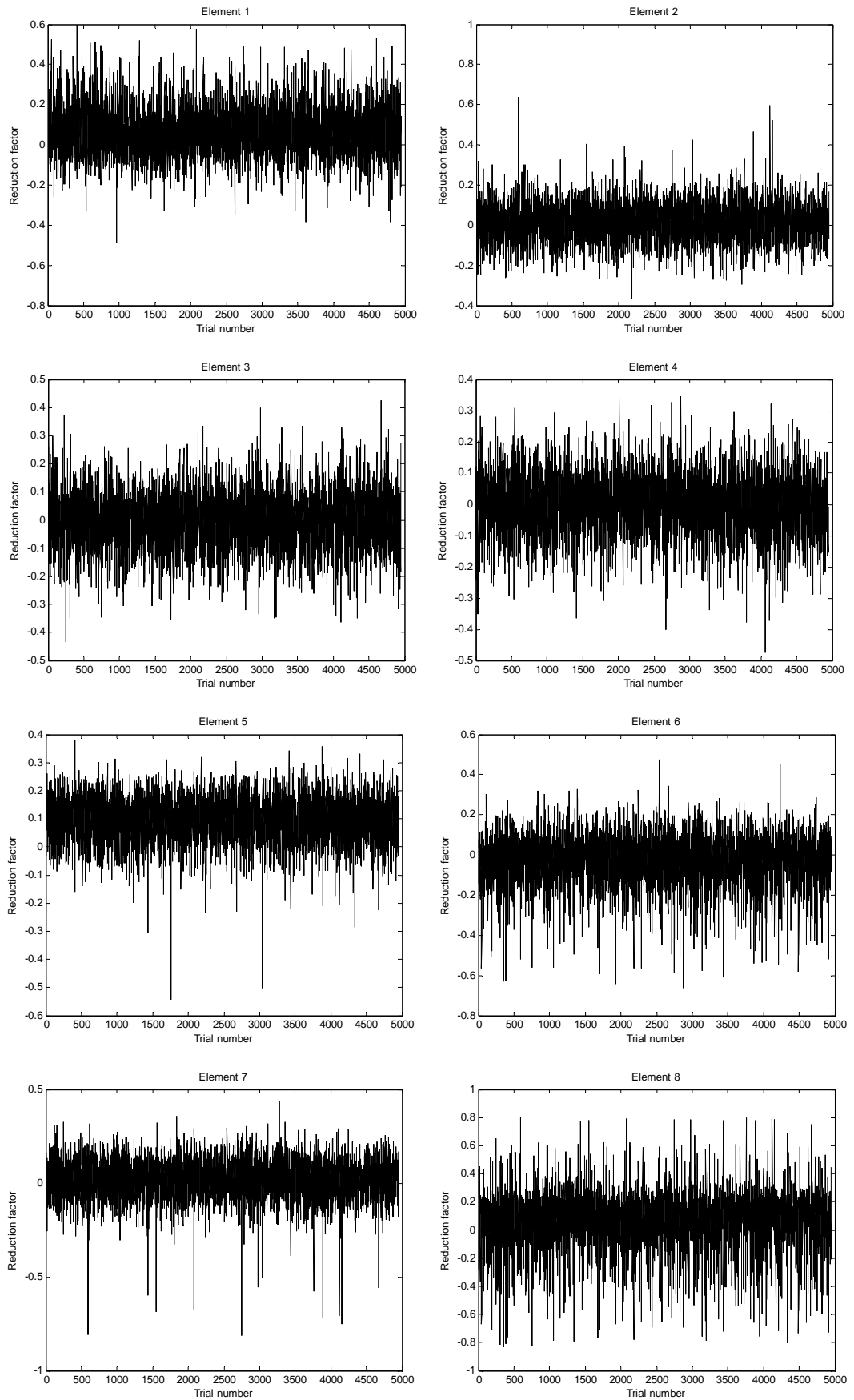


**Figure 4.7 Sample sequences of reduction factors in MCS method for 10% natural randomness**

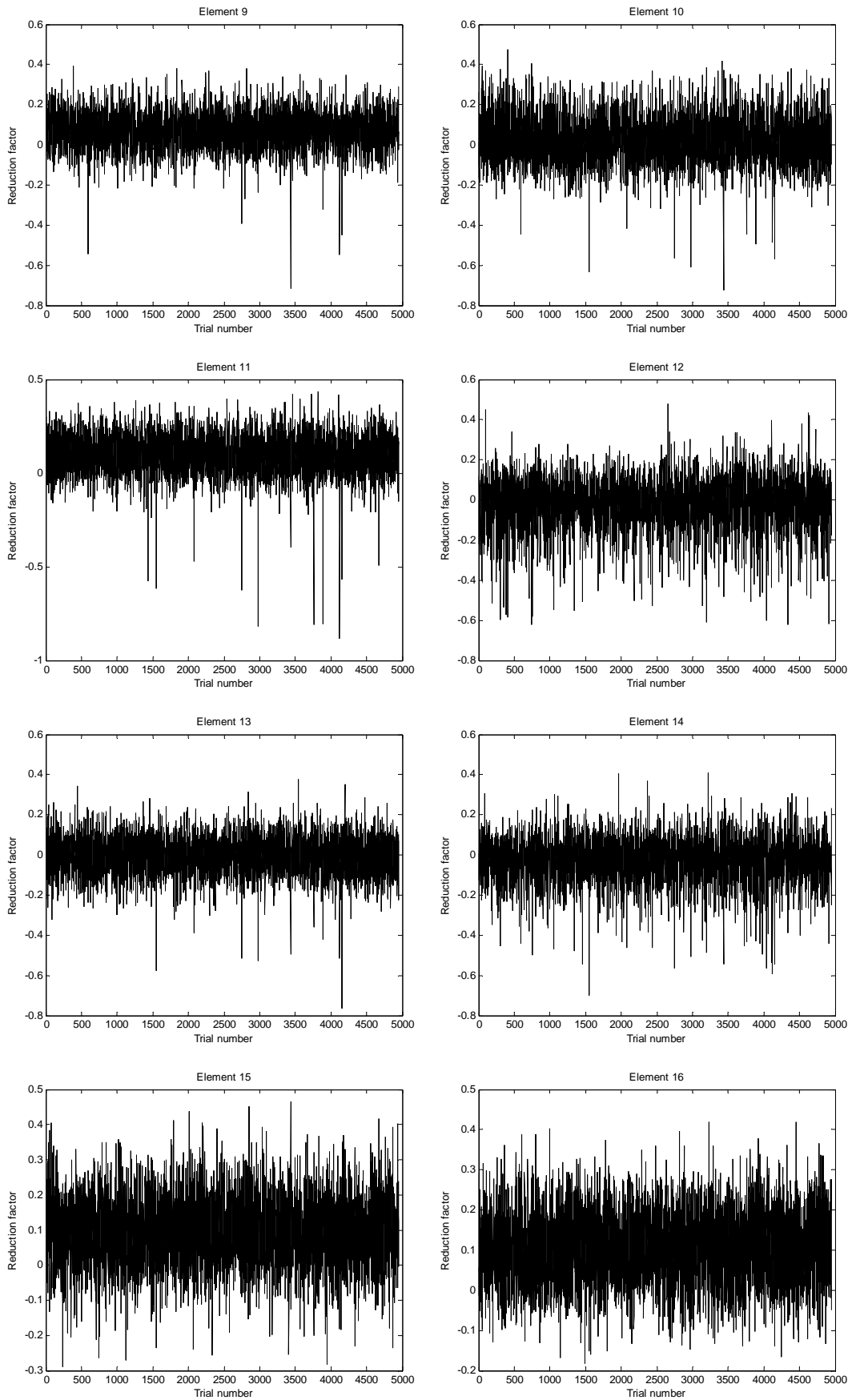


**Figure 4.7 Sample sequences of reduction factors in MCS method for 10% natural randomness (Cont'd)**

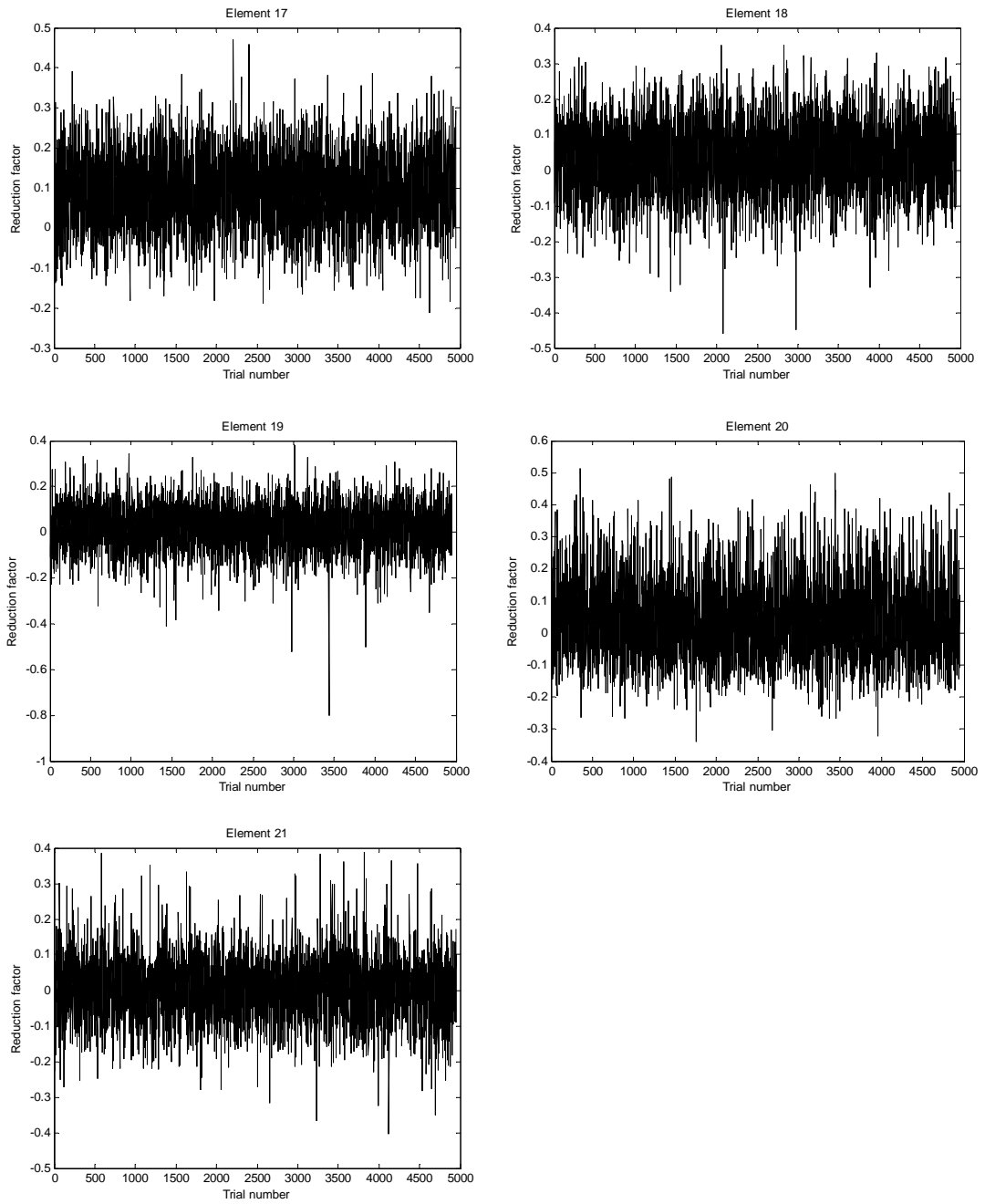


**Figure 4.7 Sample sequences of reduction factors in MCS method for 10% natural randomness (Cont'd)**

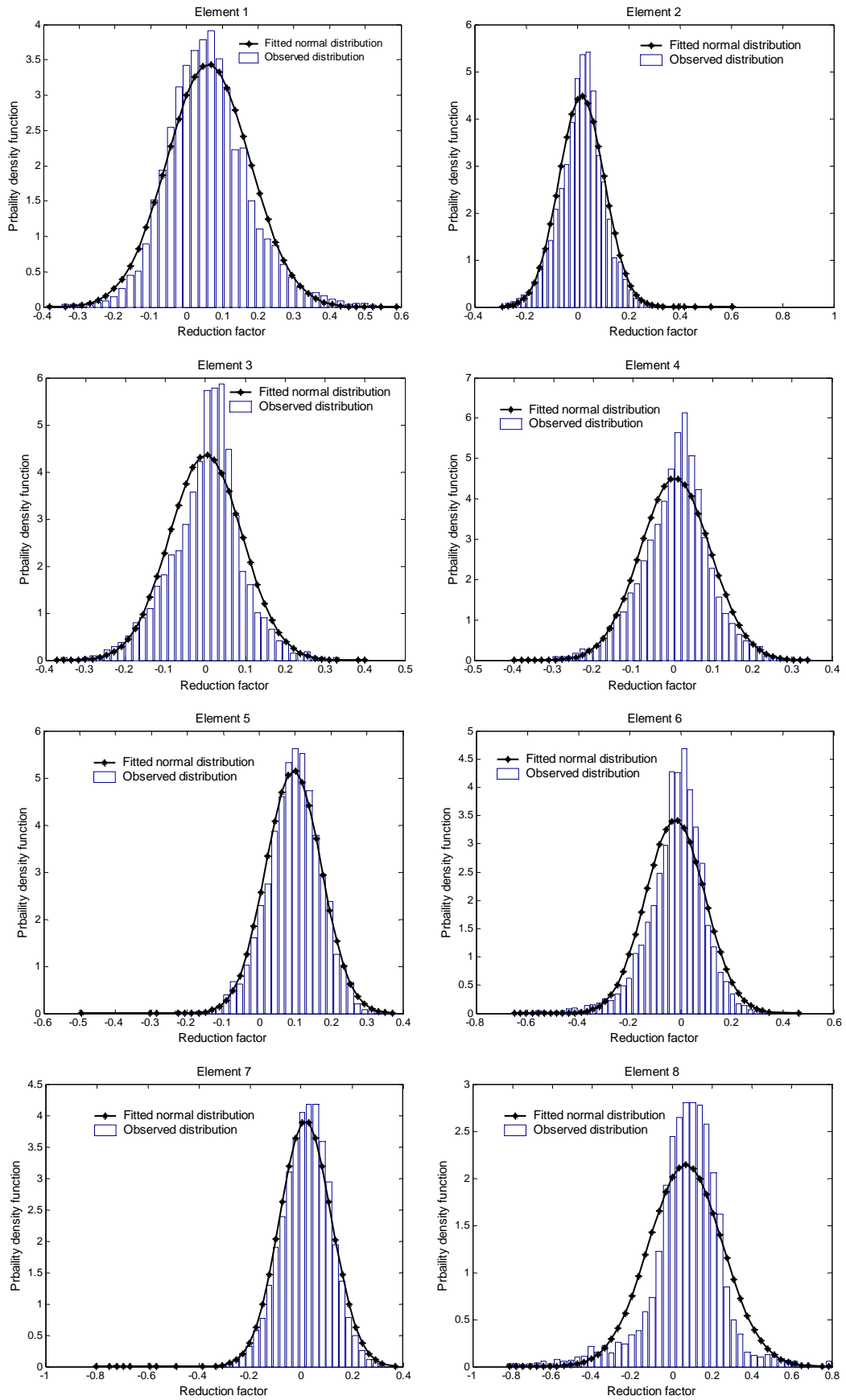


**Figure 4.8** Probability density functions of reduction factors in MCS method for 10% natural randomness

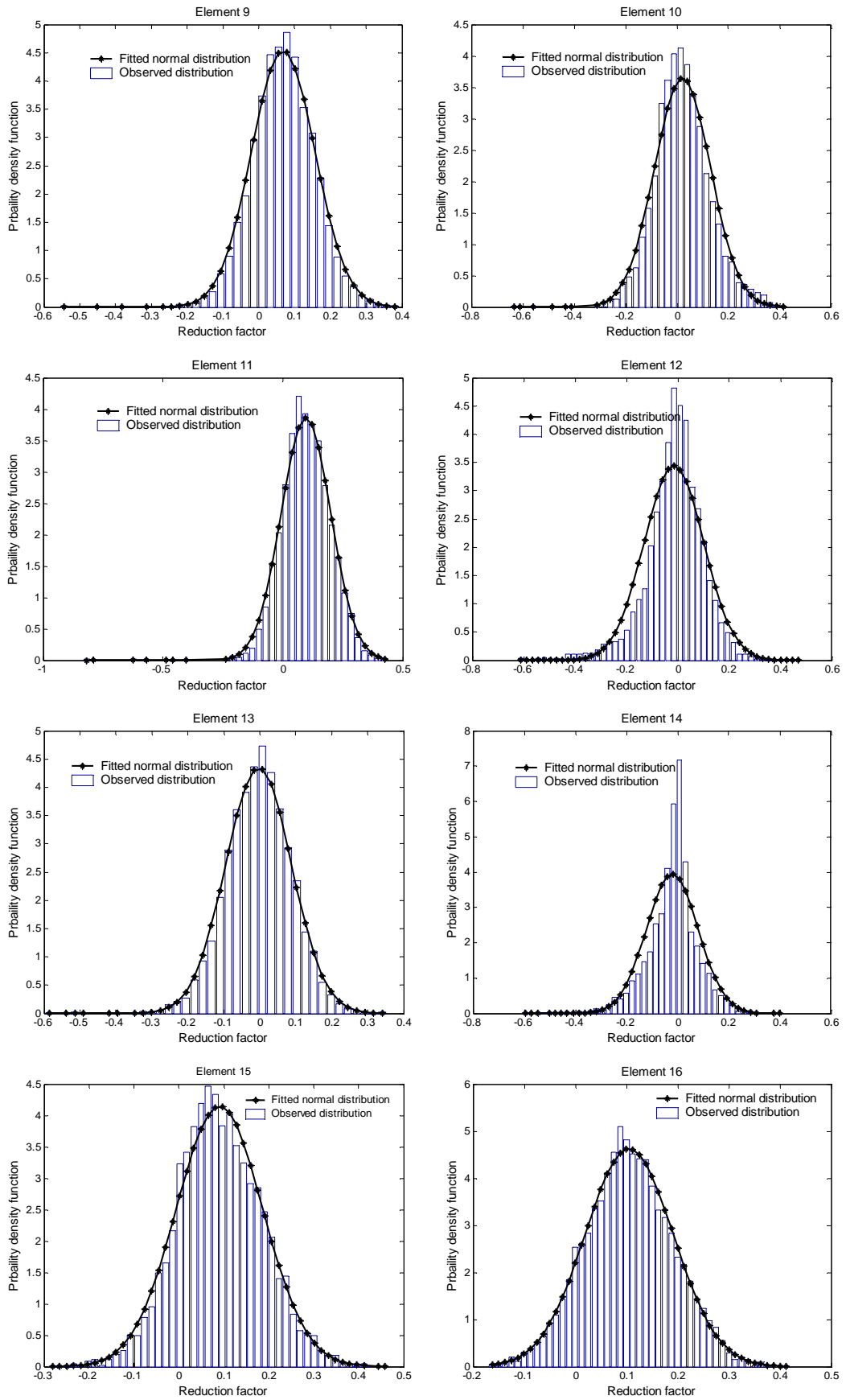


**Figure 4.8 Probability density functions of reduction factors in MCS method for 10% natural randomness (Cont'd)**

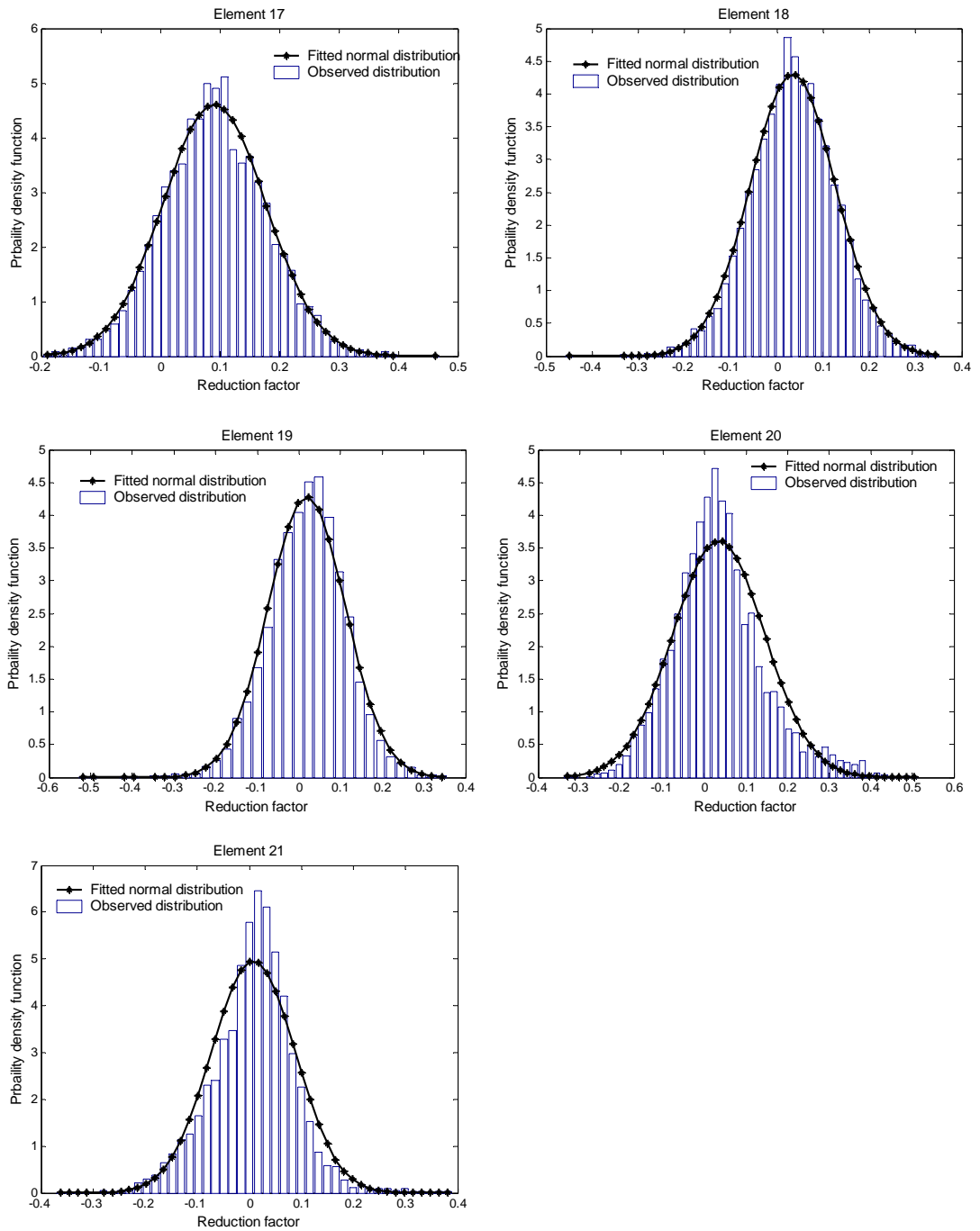


**Figure 4.8 Probability density functions of reduction factors in MCS method for 10% natural randomness (Cont'd)**

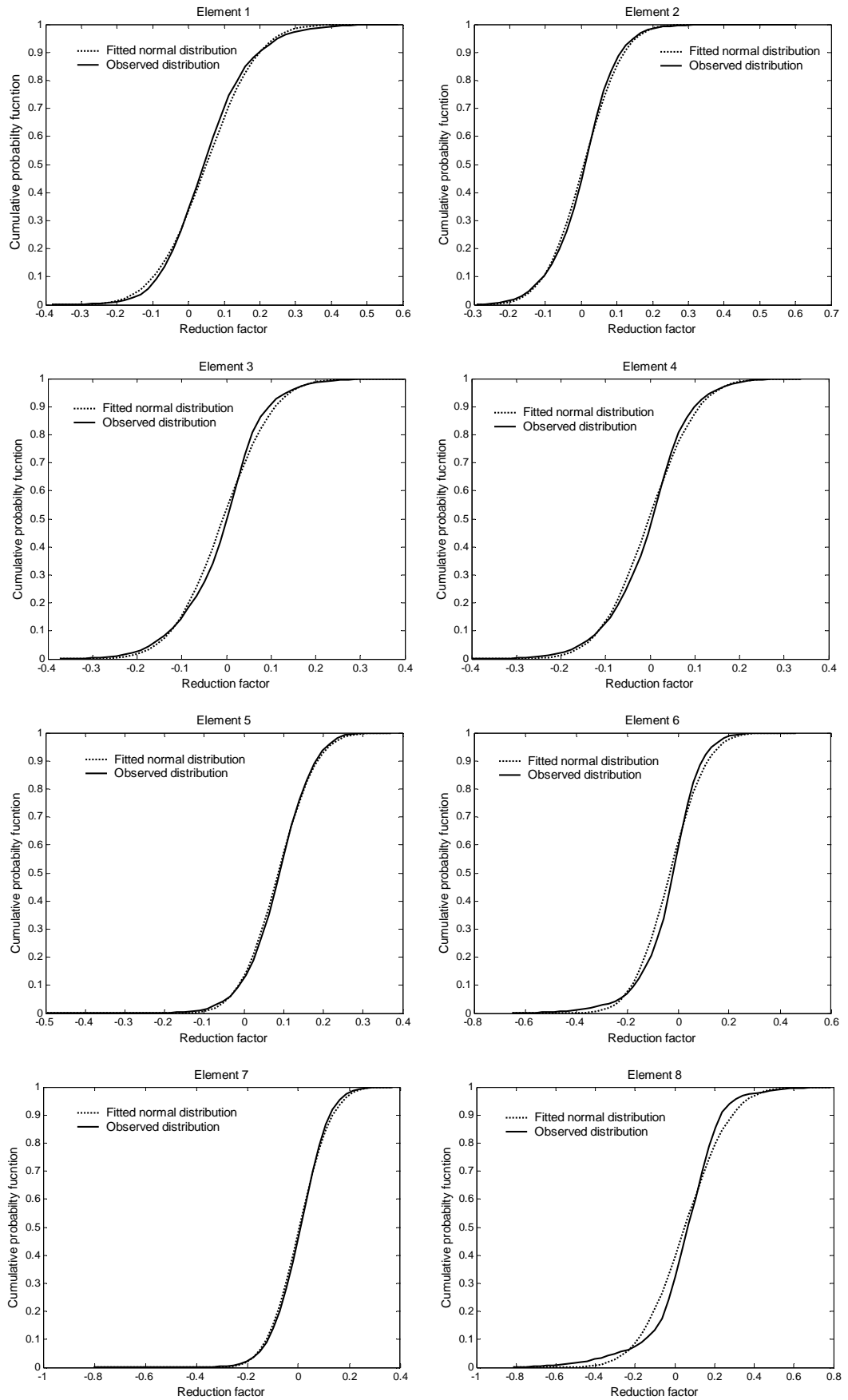


**Figure 4.9 Cumulative density function of reduction factors in MCS method for 10% natural randomness**

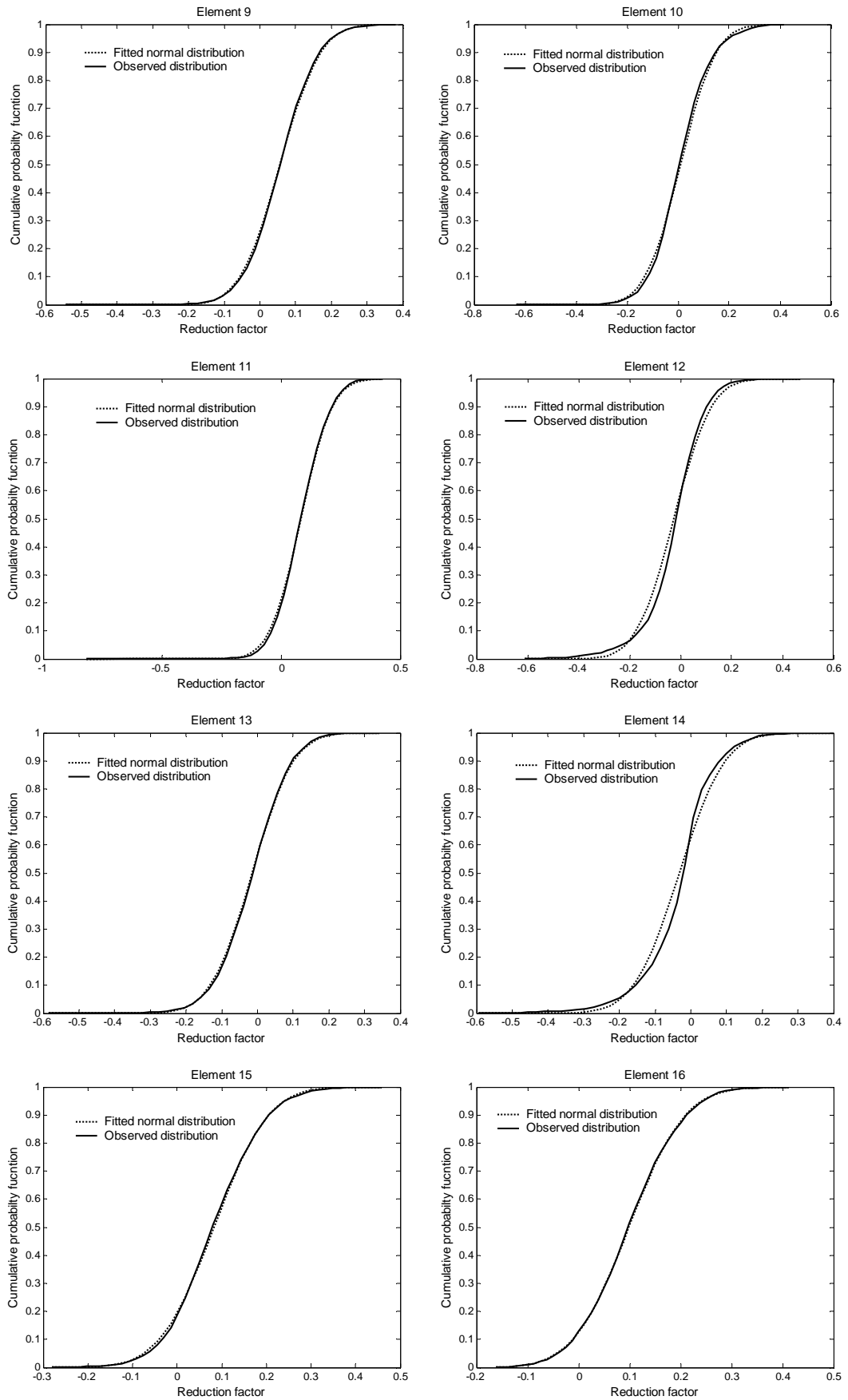


**Figure 4.9 Cumulative density function of reduction factors in MCS method for 10% natural randomness (Cont'd)**

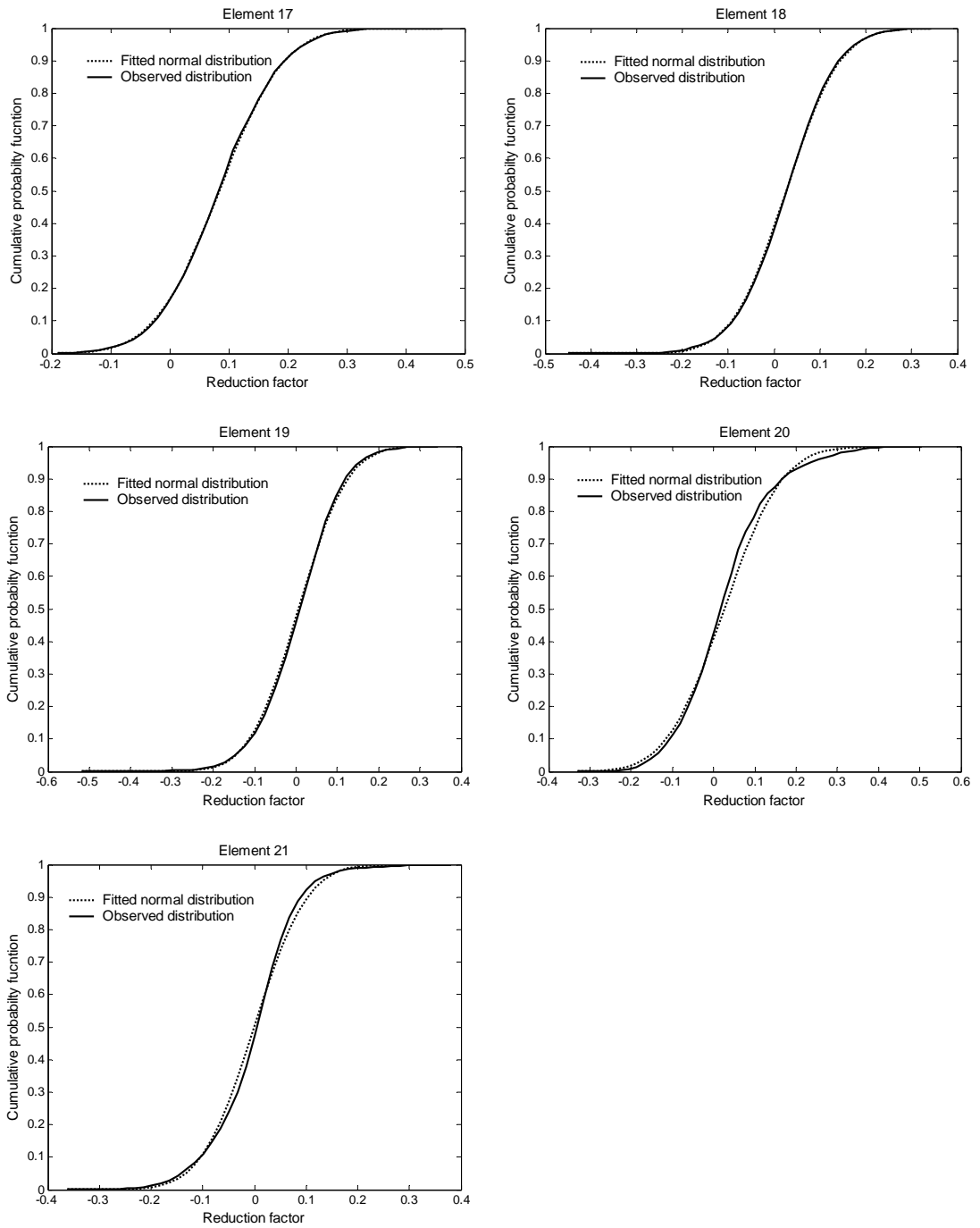


**Figure 4.9 Cumulative density function of reduction factors in MCS method for 10% natural randomness (Cont'd)**

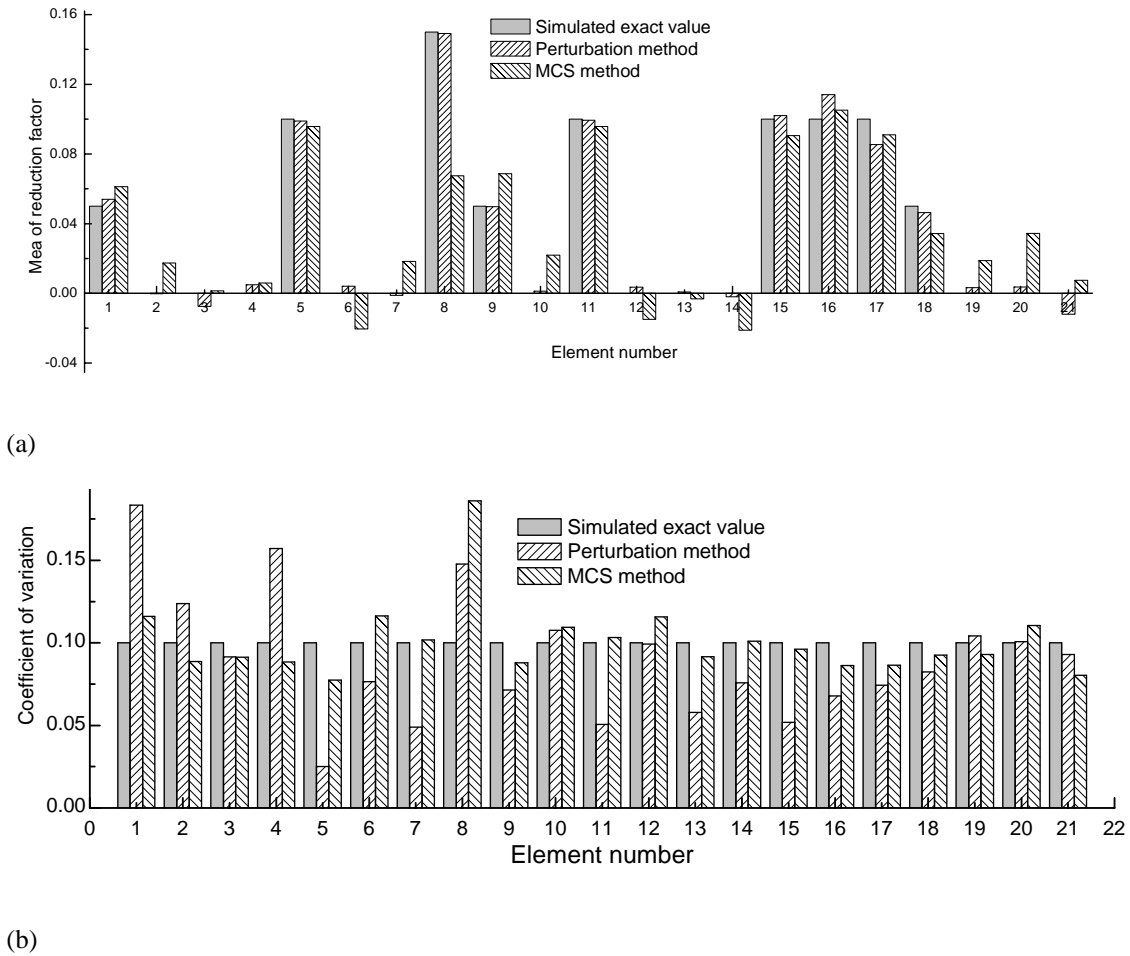


**Figure 4.10 Comparison of perturbation method and MCS method for 10% natural randomness: (a) mean of reduction factor; (b) COV**

#### 4.4.2 Uncertainty due to Measurement Noise

The stochastic FE model updating method is then applied to obtain the statistics of updating parameters using the uncertain modal properties due to measurement noise. In this case, the uncertainty in modal parameters is caused by the measurement noise and the modal parameter estimation error, and the obtained covariance matrix of updating parameters indeed tells us how reliable the model updating results are in view of the measurement noise in the data. Small values of the diagonal entries in covariance matrix imply that the estimates of updating parameters are robust to

measurement noise, while large values indicate that they are sensitive to measurement noise and therefore are unreliable. It is noted that, in contrast to the first case where both the means and standard deviations of updating parameters are known, the means of updating parameters are known while their standard deviations are unknown in this case.

Only normally distributed random noise with zero mean is considered in this study. In order to analyze the effect of measurement noise on model updating results, it is assumed that 1% Gaussian uncorrelated random noise exists in each of uncertain modal properties (the perturbation method is also applicable to the case with correlated random variables). Therefore the covariance matrix of basic random variables  $\mathbf{X}$  becomes a diagonal matrix as follows

$$\text{Var}(X_i, X_j) = \begin{cases} 0 & \text{for } i \neq j \\ (1\%)^2 \bar{z}_i^2 & \text{for } i = j \end{cases} \quad (4.34)$$

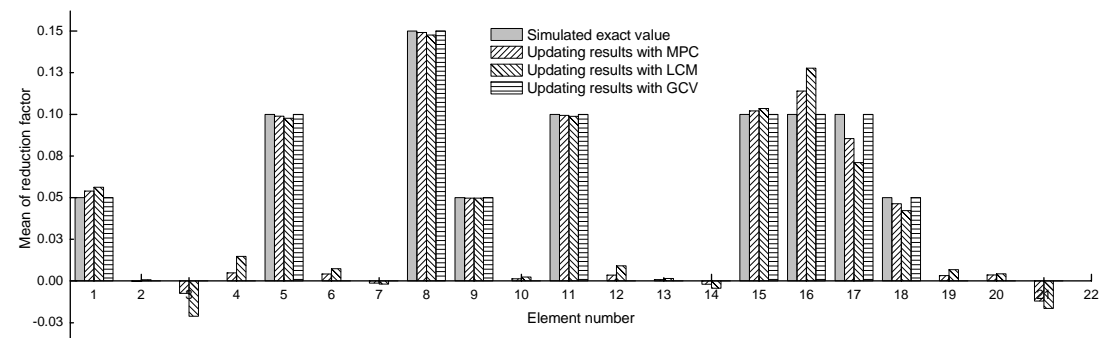
where  $\bar{z}_i$  is the mean of the  $i$ th measured modal parameter.

#### 4.4.2.1 Stochastic Model Updating Using Perturbation Method

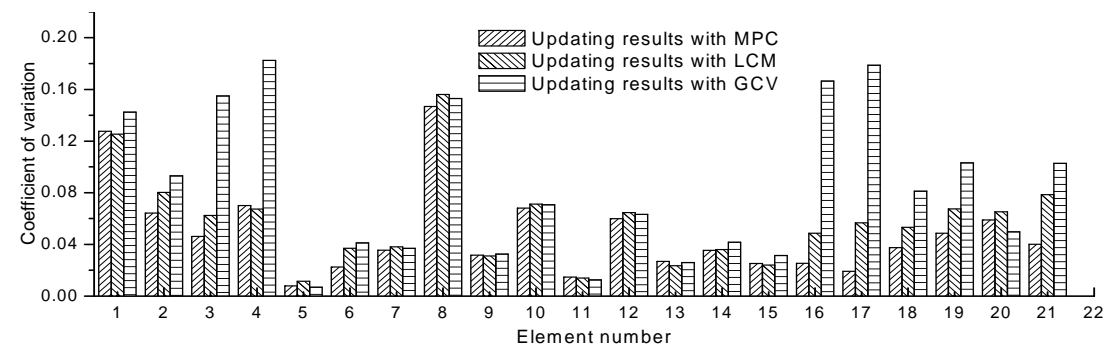
Similarly, the means and covariance of updating parameters can be estimated by the perturbation method from the statistic properties of measured uncertain modal properties. Likewise, the means are computed from Equation (4.8) and the estimation of covariance matrix is estimated from Equation (4.24) in conjunction with Equations (4.9) to (4.14) incorporating regularization methods.

**Figure 4.11** compares the mean and the coefficient of variance of updating results obtained under different combinations of regularization methods with regularization-

parameter-choice procedures. Again, it is observed that all the method combinations produce fairly agreeable identification results of the means of updating parameters, but, quite different estimates on COV are obtained for some elements as illustrated in **Figure 4.11(b)** for some elements. In addition, the identified COVs of updating parameters are significantly different in magnitude for different members, ranging from 1% to almost 20%. A small value of COV of updating parameter assures that the updating parameter can be identified with good accuracy in the presence of measurement noise, while a large one indicates the identification result could be totally annihilated by measurement noise.



(a)



(b)

**Figure 4.11 Comparison of model updating results using perturbation method for 1% measurement noise: (a) mean of reduction factor; (b) COV**

**Figure 4.12** shows the modal sensitivities with respect to each of updating parameters for the first six eigenvalues. It is found that the updating parameters with low coefficients of sensitivity are consistent with those with large values of COVs in **Figure 4.11(b)**. This explains why in most cases those updating parameters with large modal sensitivity should be included for model improvement and damage detection, otherwise erroneous results may be obtained.

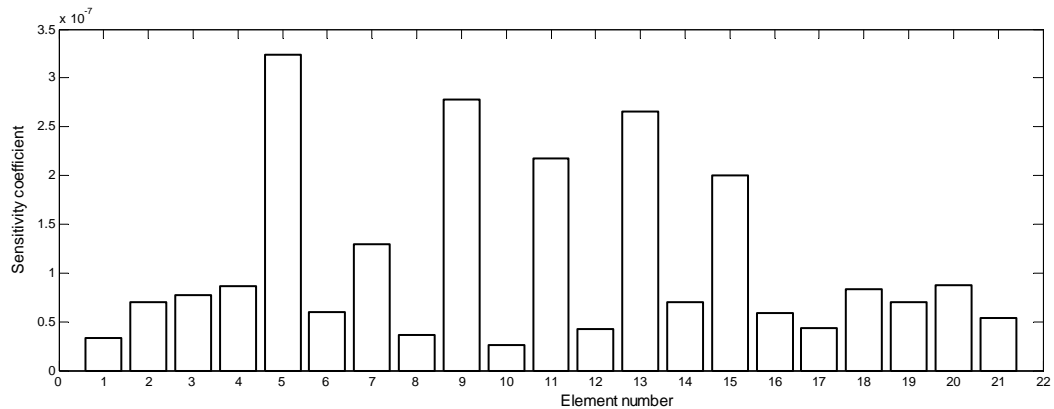


**Figure 4.12 Modal sensitivities of the first six eigenvalues**

#### 4.4.2.2 Stochastic Model Updating Using MCS Method

The MCS method is now applied to obtain the statistics of updating parameters for verifying updating results obtained by the perturbation method. The number of MCS trials is adjusted as 5,000 because little change was observed in the estimated statistics of updating parameters when more trials are used as shown in **Figure 4.13**. The updating solutions from 5,000 trials are used to construct the probability density function and cumulative density function, as well as to approximate the means and standard deviations of updating structures. **Figure 4.14** shows the probability density functions of reduction factors constructed using the simulation results along with the

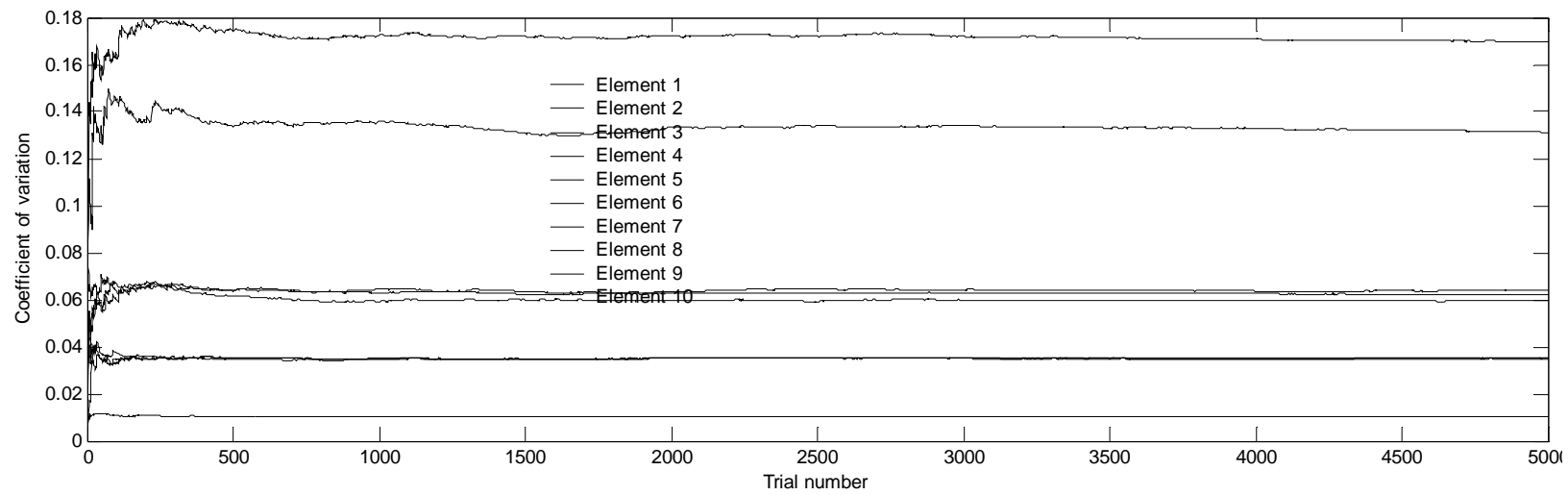
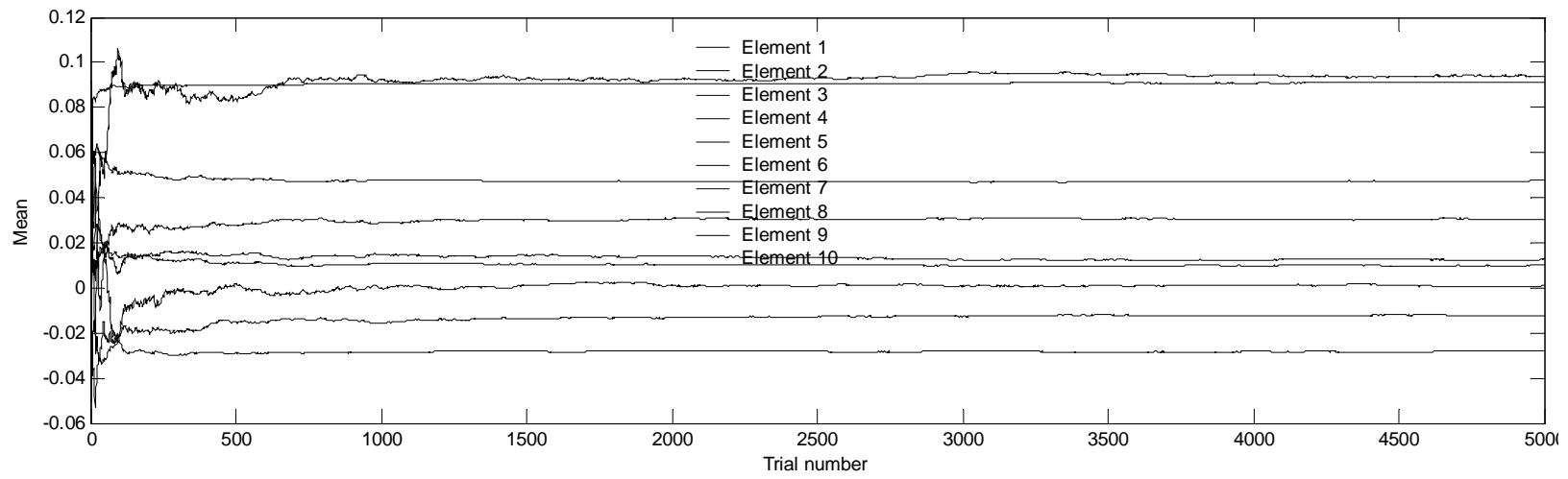


**Figure 4.13** Variation in mean and COV with respect to trail number of MCS for 1% measurement noise

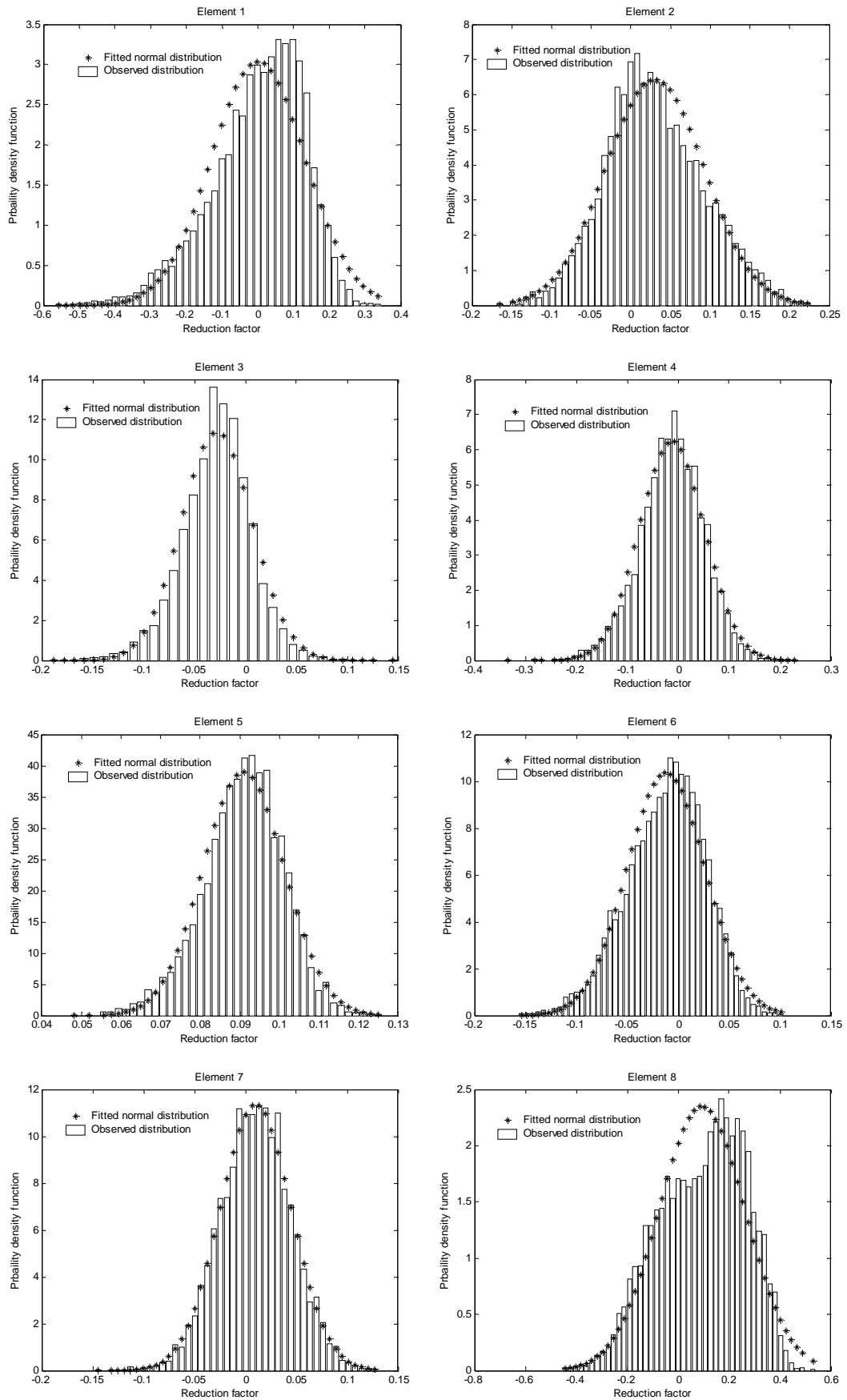


**Figure 4.14 Probability density functions of reduction factors in MCS method for 1% measurement noise**

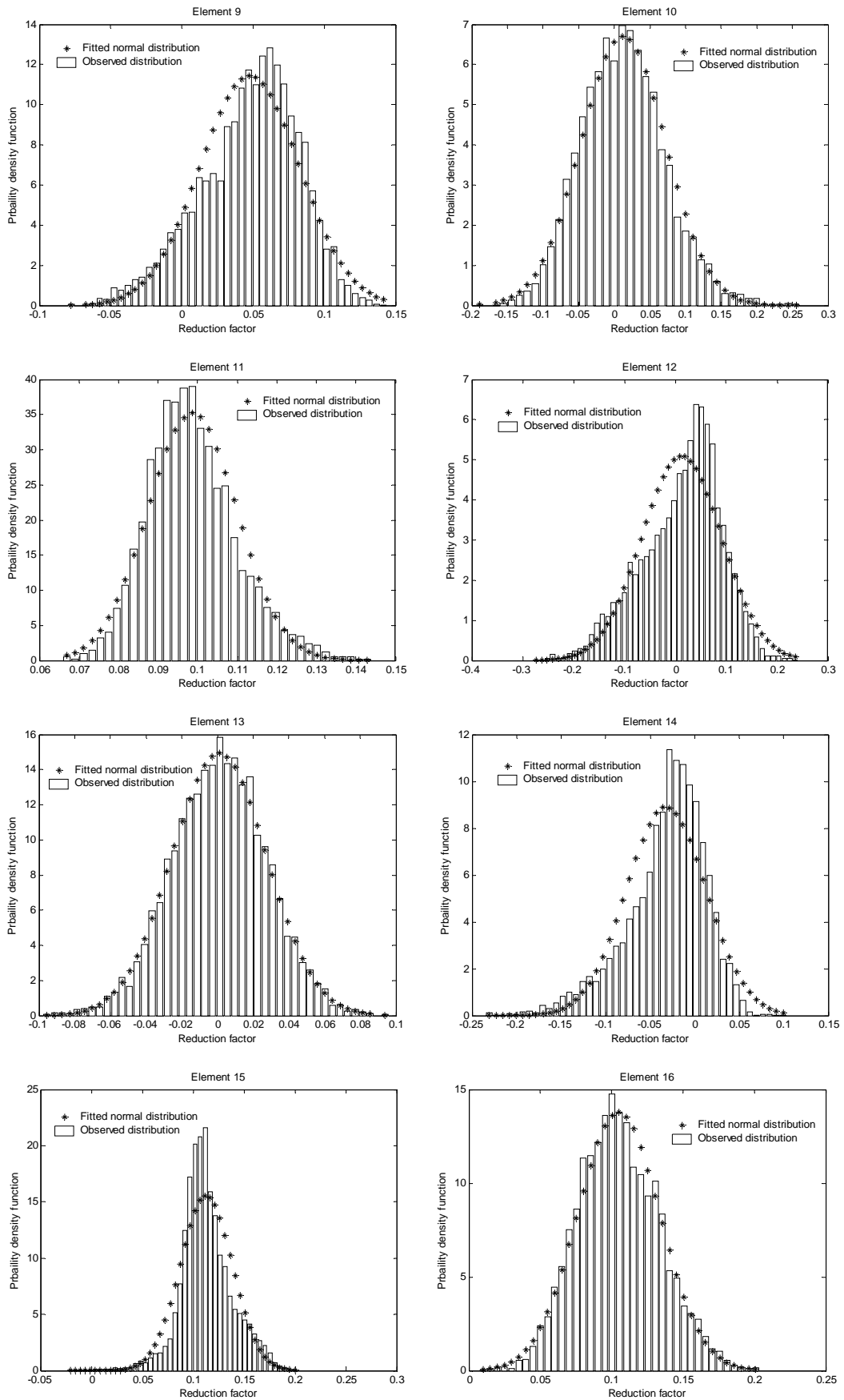


**Figure 4.14 Probability density functions of reduction factors in MCS method for 1% measurement noise (Cont'd)**

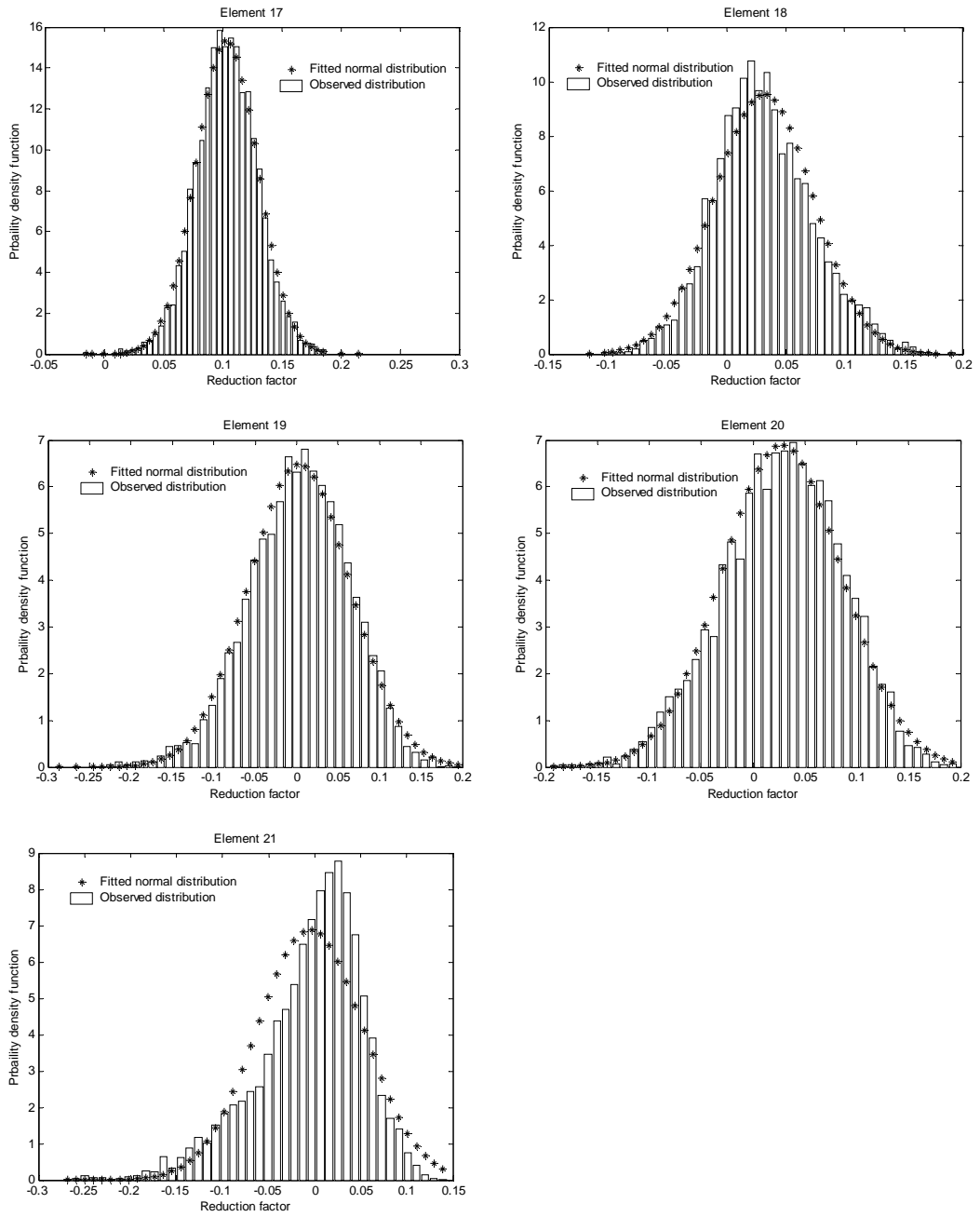


**Figure 4.14 Probability density functions of reduction factors in MCS method for 1% measurement noise (Cont'd)**

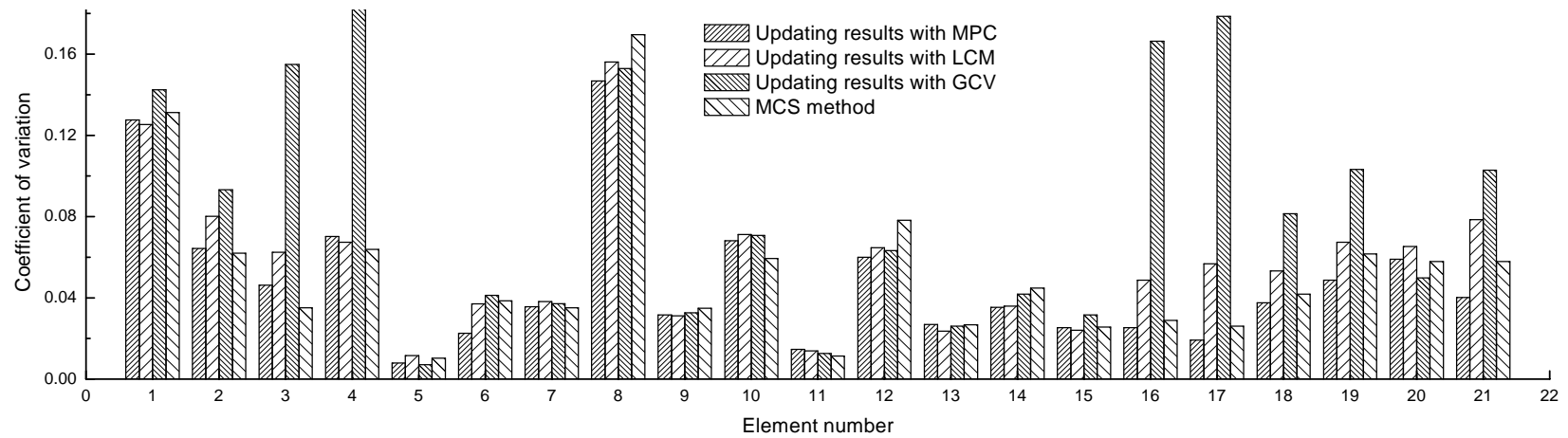
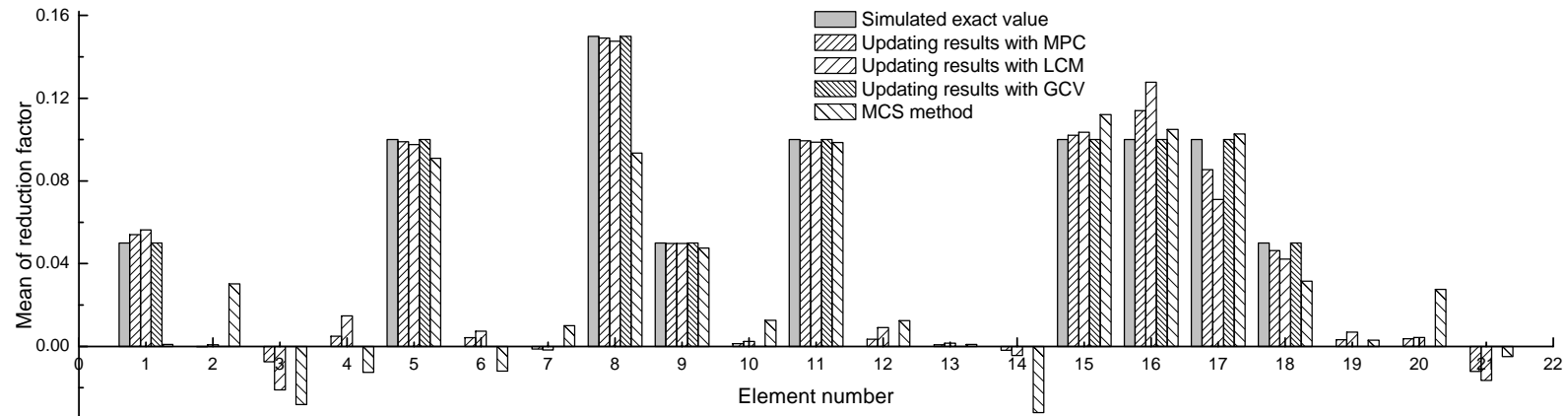


**Figure 4.15 Comparison of perturbation method and MCS method for 1% measurement noise:**  
**(a) mean of reduction factor; (b) COV**

fitted normal distributions whose mean and standard deviation are estimated from MCS samples. Goodness-of-fit test on the hypothesized normal distribution of updated parameters is performed in terms of Kolmogorov-Smirnov (K-S) test and Chi-Squared test (Kottegoda and Rosso 1997). Results show that the hypothesized normal distributions of most updating parameters are accepted with a confidence level of 95%, implying that they can be well approximated with a normal distribution. **Figure 4.15** presents a comparison of the statistics of updating parameters between the perturbation method and the MCS method. It is seen that the results from the perturbation method are generally in accordance with those obtained from the MCS method.

Now we look back the plot of probability density functions of updating parameters shown in **Figure 4.15**. From these diagrams, two observations are made:

- (i) The PDFs of some updating parameters with a large COV seem to have a tendency to bifurcate the way in which two or more peaks exist. As mentioned previously, the bifurcation into several peaks in the plot of PDF may be attributed to many local minima in the identification problem whereby many simulation runs are attracted. More local minima a nonlinear least squares problem poses, more peaks may appear in the plot of PDF of estimator (updating parameter) when local optimization methods such as gradient-based methods are used.
- (ii) The probability density function for each updating parameter is often peaked at particular value(s) which deviates from the mean of sample sequences, or rather, the summits of observed PDF and fitted normal PDFs separate with each other. Partially caused by the existence of local minima

in the identification problem, the separation between the observed peak of PDF plot and the mean value is attributed to the nonlinear relation between modal properties and updating parameters as elaborated in the following paragraph.

**Figure 4.16** illustrates the map of probability density function between the known input (measured modal frequency) and the unknown estimator (updating parameter) in the case of single input and single output. Due to the nonlinearity between input and estimator, it is clear that the probability density function of estimator is essentially non-normal even when the PDF of input is normal. The non-normality in estimator causes the deviation of the mean of the MCS results from the peak of PDF (or the simulated exact value). As shown in **Figure 4.16** when the input  $y$  (modal frequency) concentrates on a single value the estimator  $x$  (updating parameter) will take a fixed value; otherwise, as the standard deviation of  $y$  increases, the mean of estimator  $x$  value will shift away from its original mean value, and vice versa. Larger standard deviation in  $y$  value, larger shifts in  $x$  value away from its original mean value. **Figure 4.17** illustrates the nonlinear relationship between the first six modal frequencies and the first updating parameter, which implies the possible separation of means and summits of PDFs of updating parameters in **Figure 4.14**.

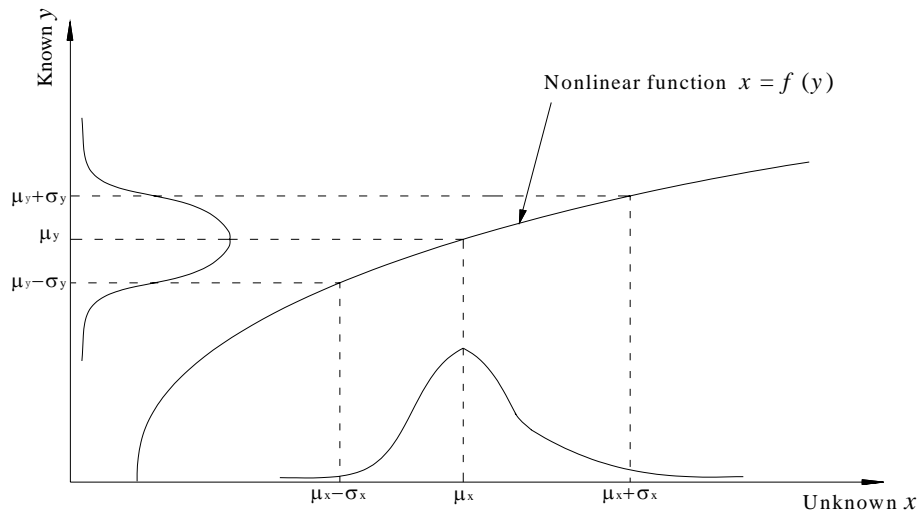


**Figure 4.16** Map of probability density function between input and output

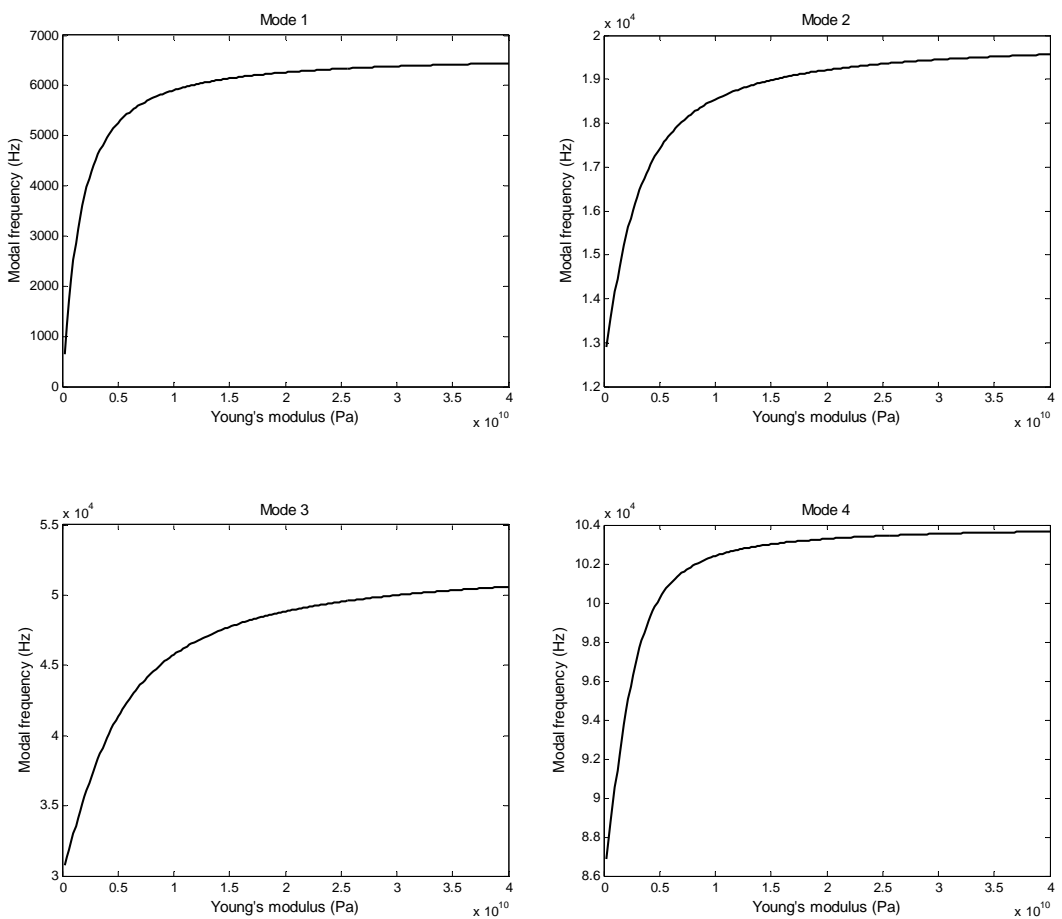


**Figure 4.17** Relationship between the first six modal frequencies and the first updating parameter

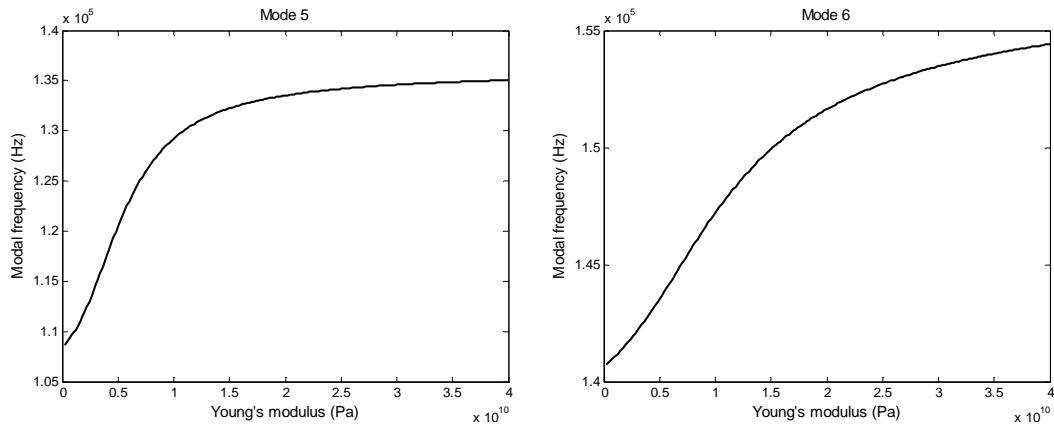


**Figure 4.17 Relationship between the first six modal frequencies and the first updating parameter (Cont'd)**

#### 4.4.2.3 Effect of Uncertainty Level

The effect of the level of measurement noise is further addressed for the perturbation method and the MCS method. As the perturbation method generally produces solutions with acceptable accuracy for nonlinear least squares problems only at small level of measurement noise, it is important to investigate the accuracy of the perturbation method with respect to noise level. It should be noted that in the first-order perturbation method the means of updating parameters remain constant for varying noise levels while the standard deviations of the updating parameters will vary linearly with noise levels.

The stochastic model updating using the perturbation method and the MCS method are carried out at different uncertainty levels from 0.1% to 3%, where 5,000 MCS trials are again used to obtain the means and variances of updating parameters. **Figure 4.18** illustrates the sample sequences, PDFs and CDFs of updating parameters for both element 1 and element 8 using the MCS method when the uncertainty level is 0.1%. As expected, the normality is more preserved than those in

the case of 1% uncertainty level. **Figure 4.19** shows the variation in sample means of reduction factors with uncertainty levels. In the considered range of noise levels, the reduction factors may gradually decrease or decrease with the increasing uncertainty levels; also the rate of change of reduction factors is different for different elements. The smaller value of the rate of change indicates that the computed reduction factor is more robust to measurement noise. Due to the nonlinearity between updating parameters and modal properties as illustrated in **Figures 4.16** and **4.17**, it is easy to understand that the mean of updating parameter will vary with the noise levels. **Figure 4.20** shows the variation in COVs of updating parameters using the MCS method with respect to the noise level.

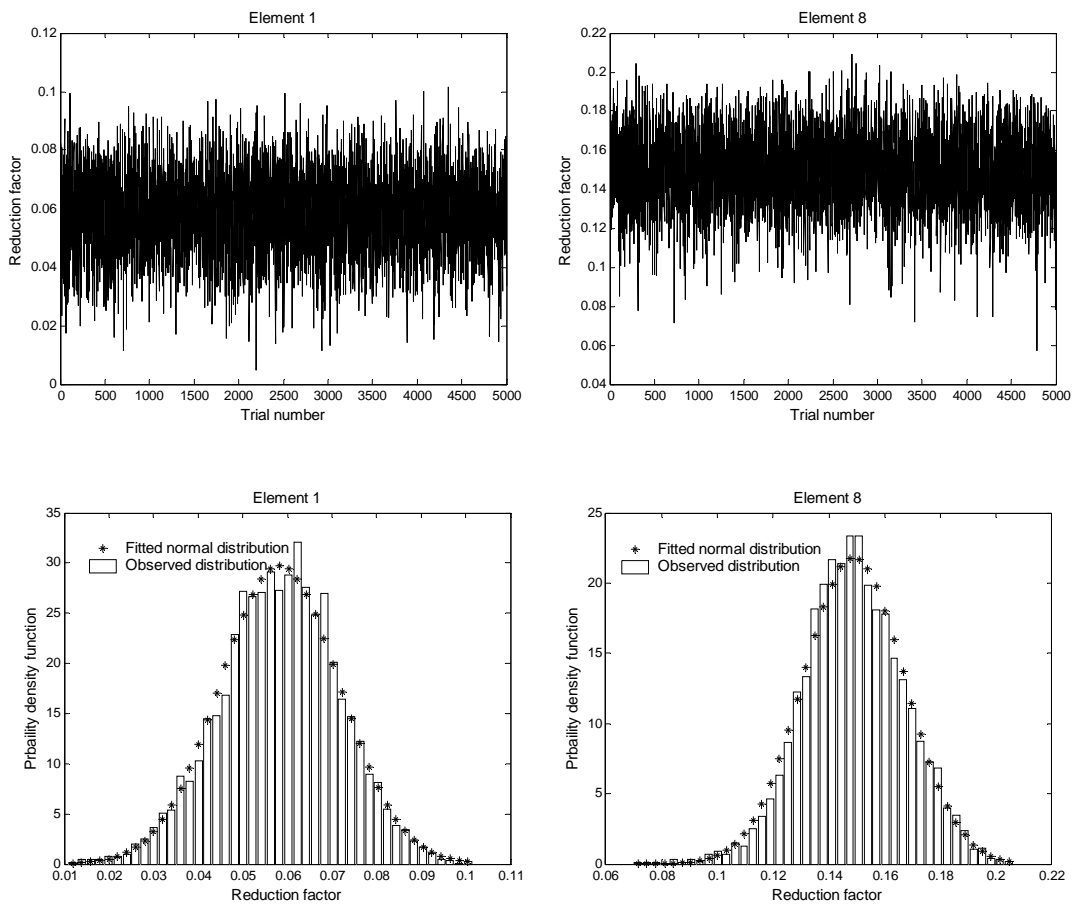


**Figure 4.18** Sample sequences, PDFs, and CDFs of elements 1 and 8 for 0.1% measurement noise

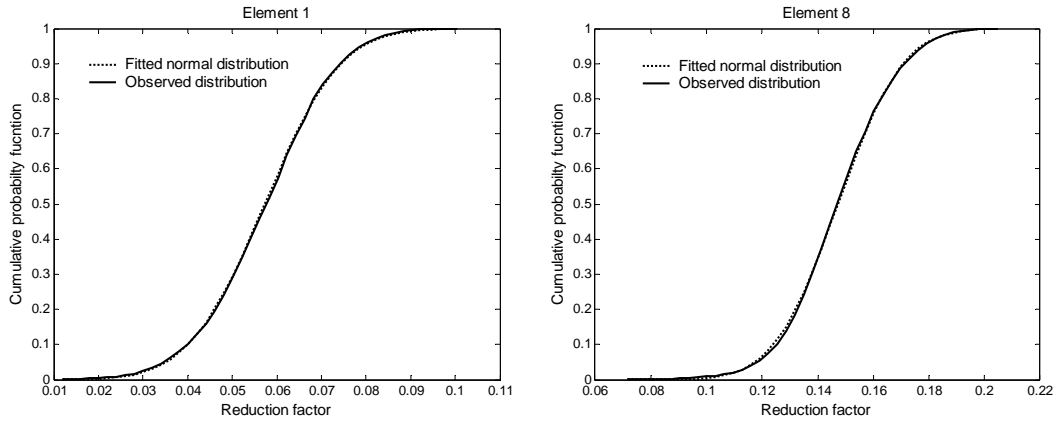
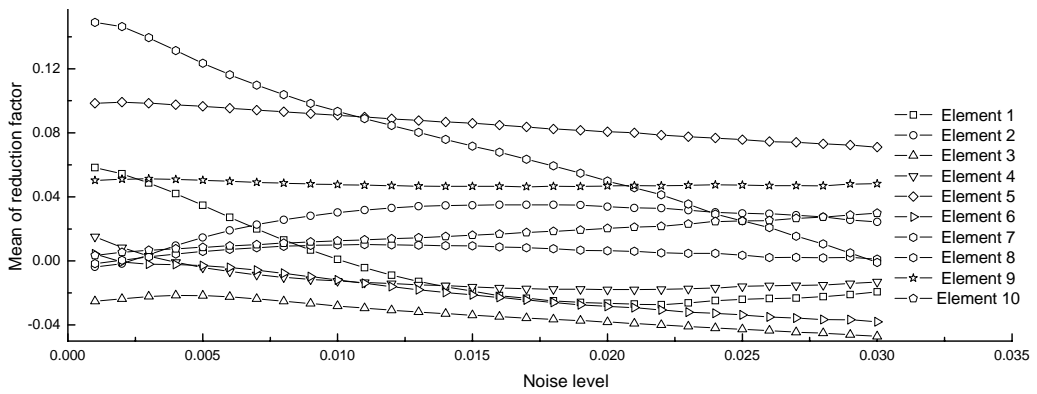
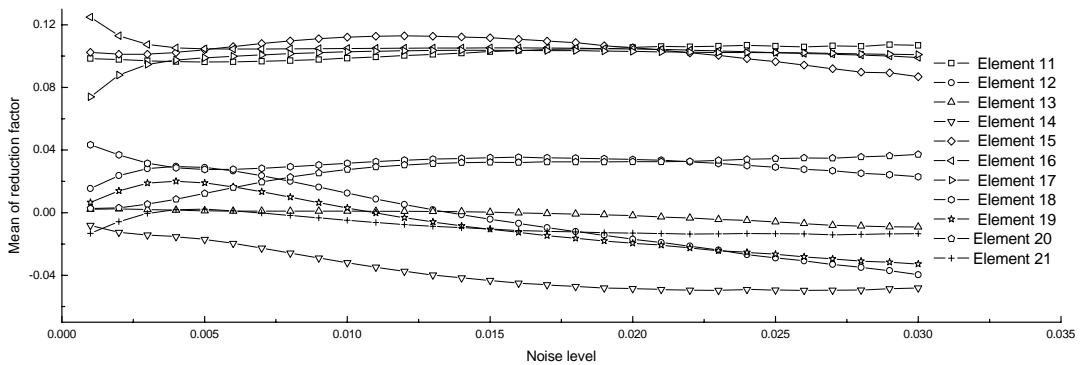


**Figure 4.18 Sample sequences, PDFs, and CDFs of elements 1 and 8 for 0.1% measurement noise (Cont'd)**

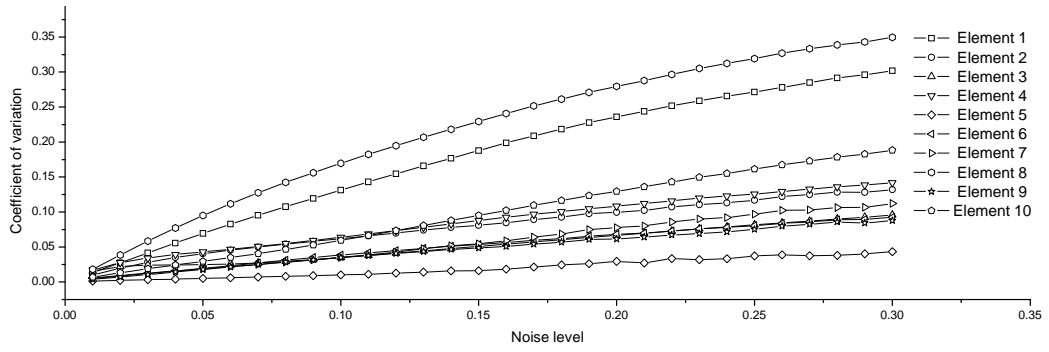


(a)

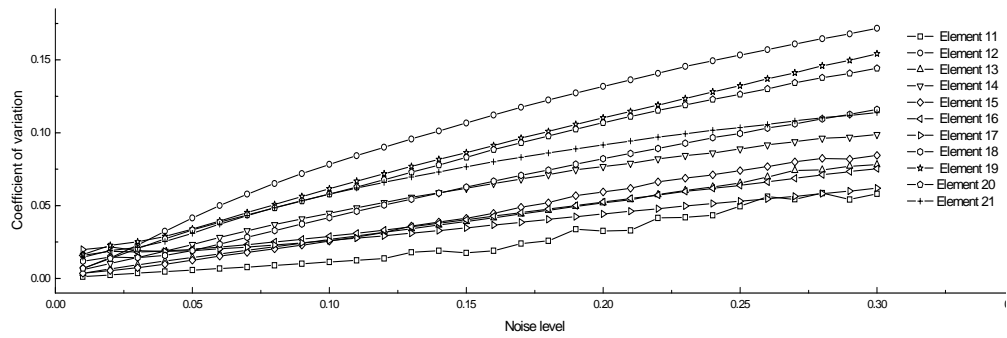


(b)

**Figure 4.19 Variation in mean of reduction factors with respect to noise level: (a) elements 1-10; (b) elements 11-21**



(a)



(b)

**Figure 4.20 Variation in COVs of updating parameters versus noise level: (a) elements 1-10; (b) elements 11-21**

**Figure 4.21** illustrates the evolution of PDFs of updating parameters with uncertainty level. As expected, the geometry of the PDF of updating parameters becomes increasingly complex with increase of noise level. **Figure 4.22** compares the coefficients of variation obtained from the MCS method and the perturbation method under different noise levels. Note that small offset between the MCS results and the perturbation results for some updating parameters appears even at the extremely small uncertainty level (0.1%). It may be attributed to the effect of regularization method. It was known that the perturbation method results in linear relations between COVs of updating parameters and uncertainty level (or COV) of measured modal properties as the first-order Taylor series expansion is employed for approximation; whereas the MCS method produces nonlinear relations. In general,

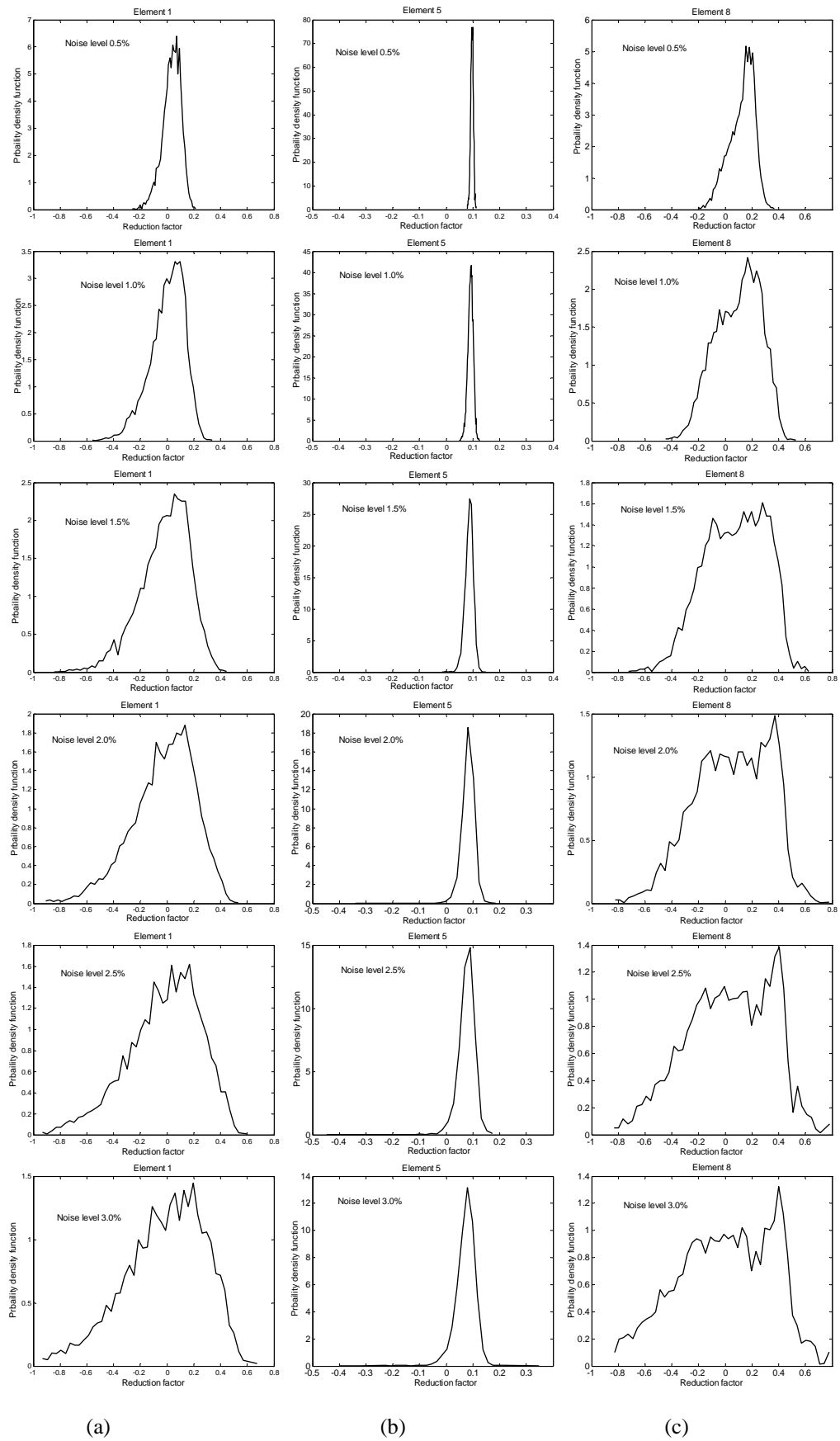


**Figure 4.21 Probability distribution functions of reduction factors at different noise levels: (a) element 1; (b) element 5; (c) element 8**

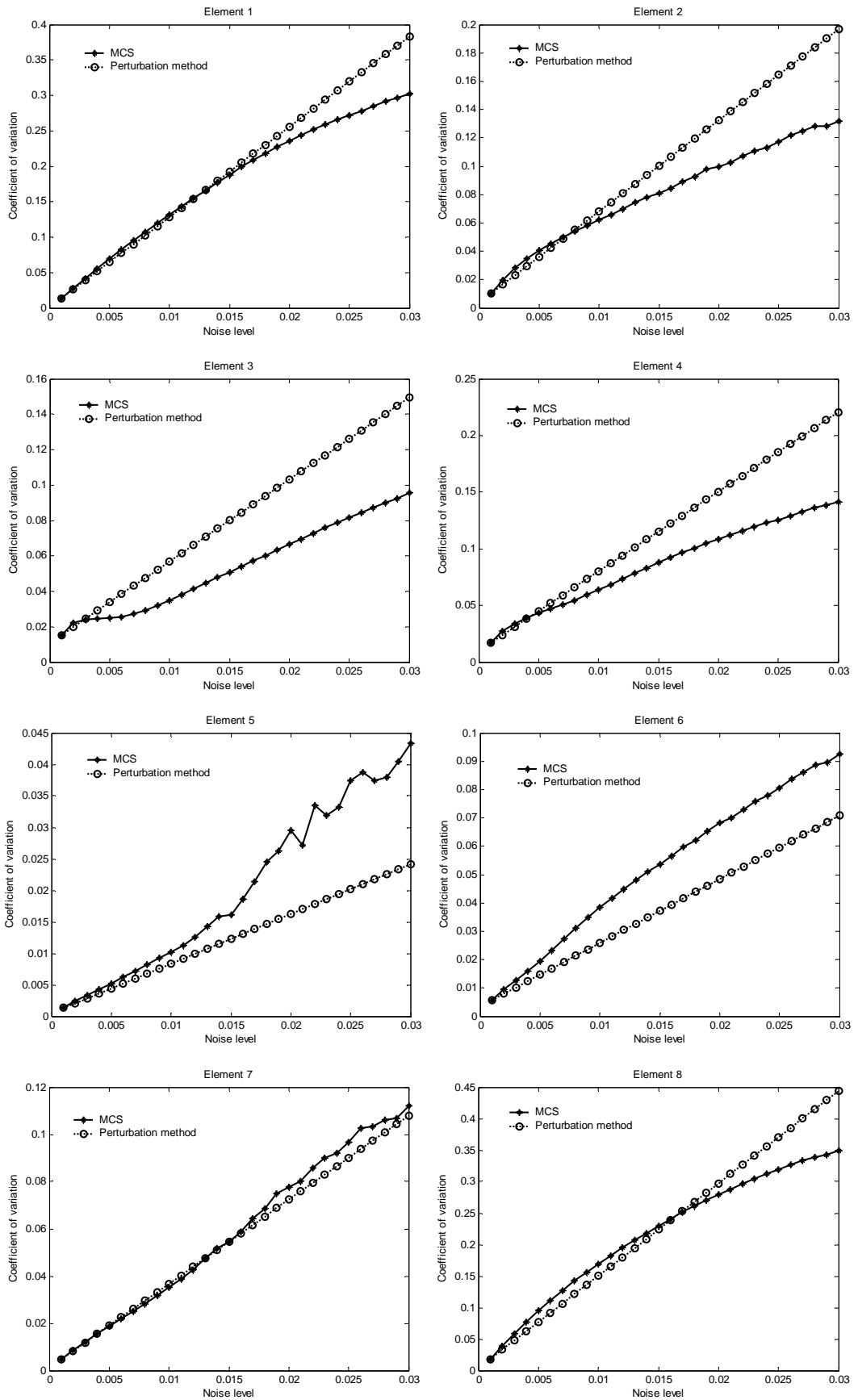


**Figure 4.22 Comparison of COVs between perturbation method and MCS method under different noise levels**

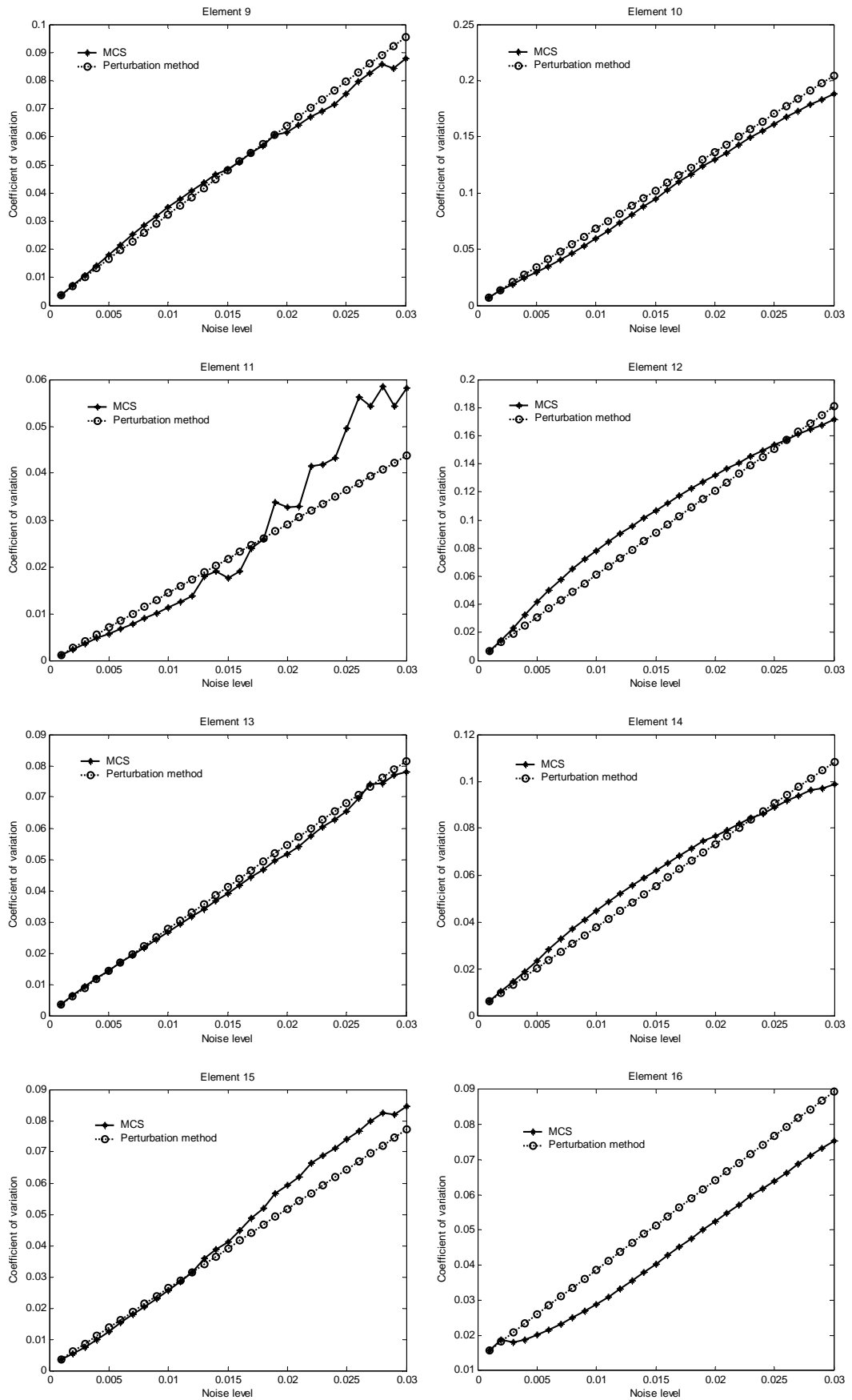


**Figure 4.22 Comparison of COVs between perturbation method and MCS method under different noise levels (Cont'd)**

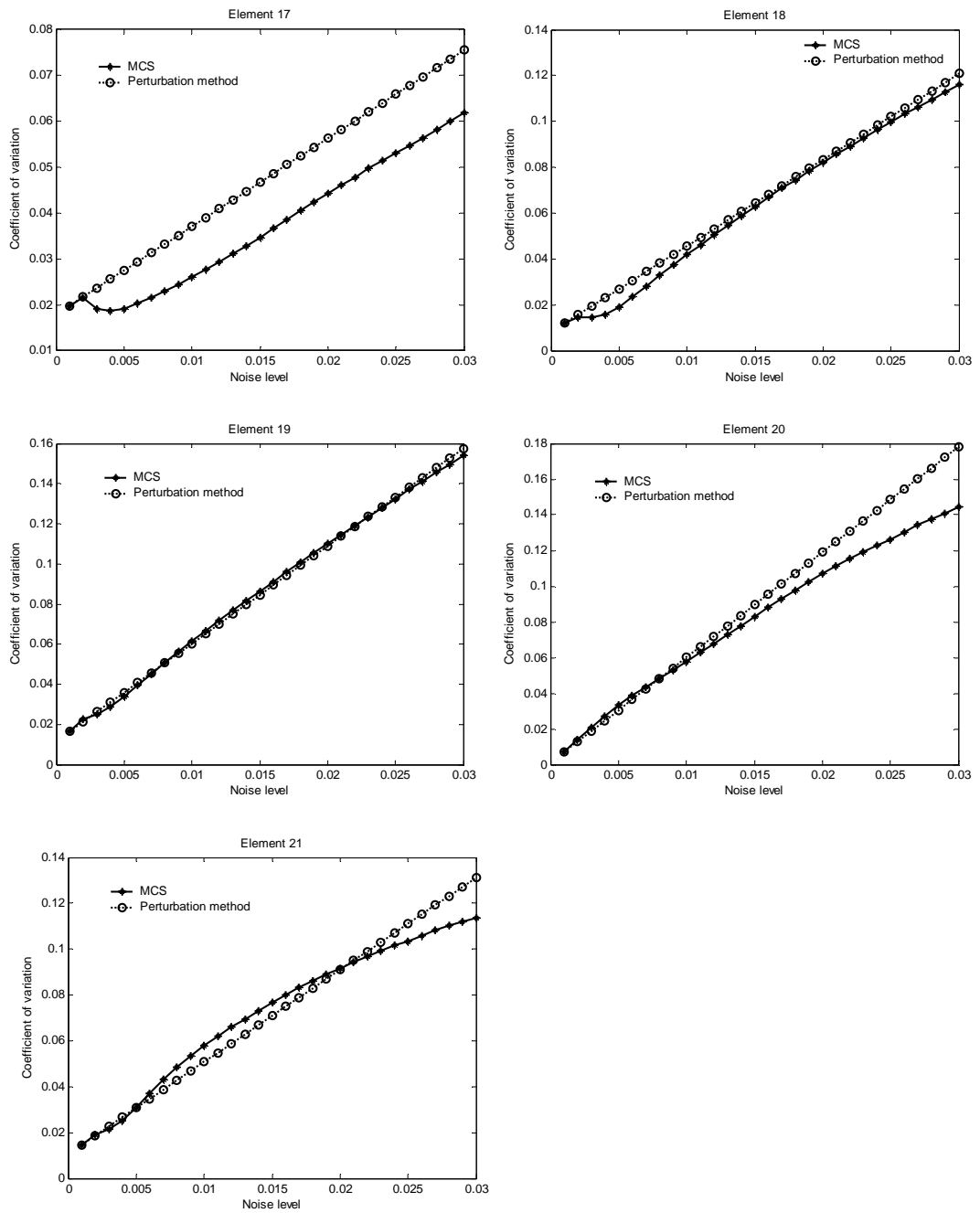


**Figure 4.22 Comparison of COVs between perturbation method and MCS method under different noise levels (Cont'd)**

the deviation of results between the perturbation method and the MCS method increases with the uncertainty level. **Figure 4.23** shows the average relative errors between the MCS method and the perturbation methods.

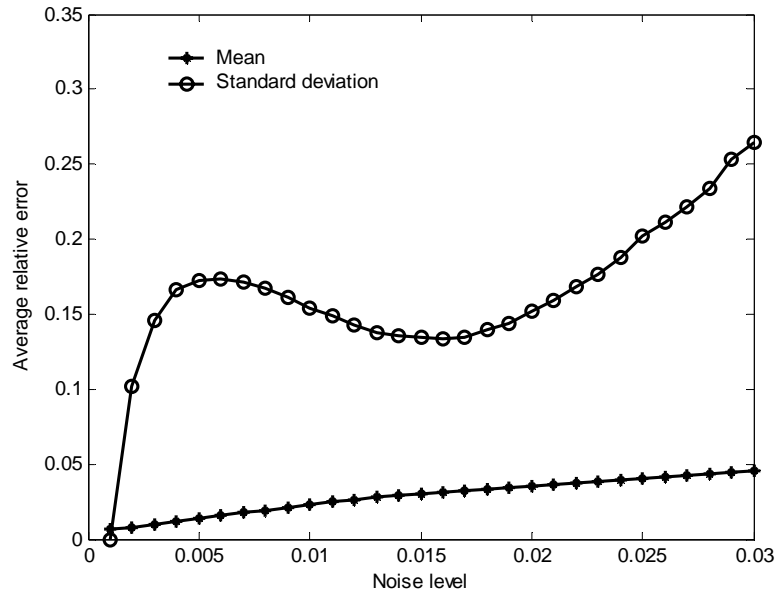


**Figure 4.23 Average relative errors between MCS method and perturbation method**

#### 4.4.2.4 Effect of Random Modal Properties

Because the measured uncertain modal properties do not have equal influence on the statistics of updating parameters, it is of significant importance to identify the modal variables that contribute notably to the statistics of updating parameters. This can be accomplished with the experimental sensitivity of updating parameters with respect to a random variable  $X_j$ , normalized with its standard deviation, as

$$\gamma_{ij} = \frac{\partial \theta_i}{\partial X_j} \sigma_{X_j} \quad (4.35)$$

where  $\gamma_{ij}$  refers to as the normalized sensitivity index (NSI) of updating parameter  $\theta_i$  with respect to basic random variable  $X_j$ ; and  $\sigma_{X_j}$  the standard deviation of random variable  $X_j$ . Taking average over all updating parameters, one gets the average normalized sensitivity index (ANSI) as

$$\gamma_j = \frac{1}{m} \sum_{i=1}^m \frac{\partial \theta_i}{\partial X_j} \sigma_{x_j} \quad (4.36)$$

where  $\gamma_j$  represents the contribution of the  $j$ th random variables to the statistics of updating parameters.

As NSI and ANSI combine the effect of both experimental sensitivity to a random variable and its uncertainty (standard deviation), these two quantities could be helpful to select measurement points (component of mode shape) and to identify the most significant random variables. It is straightforward to see that large values in NSI and ANSI could produce large standard deviation of updating parameters, thus making the model updating and damage detection results unreliable. In order to reduce the standard deviation of updating results, the modal properties that have small values of NSI and ANSI should be used for FE model improvement and damage detection.

The NSI and ANSI for all updating parameters are listed in **Table 4.3**. It is observed that the NSIs of eigenvalues are many orders larger than those of eigenvectors, indicating that the statistics of updating parameters are predominantly caused by the uncertainty in eigenvalues. It is widely accepted that the accuracy of measured modal frequencies can be considerably higher than that of mode shapes. This implies that the weighting scheme used in the study (relative ratio of weight for eigenvalues to weight for eigenvector is 10) takes advantage of attenuating the effect of uncertainty in mode shapes but at a cost of more ill-conditioning in the solution course.

On account of the magnitudes of NSIs and ANSIs of eigenvalues and eigenvectors being of several orders difference, they are separately visualized. **Figure 4.24** shows

NSIs of the measured modal properties with respect to all updating parameters, and **Figure 4.25** illustrates NSIs of the eigenvectors with a clearer presentation of significance of each mode shape component. Similarly ANSIs of the eigenvalues and eigenvectors are shown in **Figure 4.26**. It is seen that both NSIs and ANSIs for high-order eigenvalues and eigenvectors may have relatively large values, implying that the high-order modal properties may significantly contribute to the uncertainty in updating parameters and therefore leading to unreliable model improvement and damage detection results.

The commonly acknowledged thumb-of-rule indicates that the high-order modes should be used for model updating as well as damage detection because they have large damage sensitivity. Here the damage sensitivity is referred to as the sensitivity of modal properties with respect to updating parameters. On the other hand, the uncertainties existing in high-order modes may be significantly larger than those in low-order modes. **Figure 4.27** shows the damage sensitivity  $S$  for eigenvalues and eigenvectors, respectively. As expected, the high-order modes have relatively larger sensitivity coefficients than the low-order modes do. However, as discussed in the above paragraph, the inclusion of high-order modes does not necessarily improve the accuracy of updating results as they might have larger uncertainty than low-order ones.

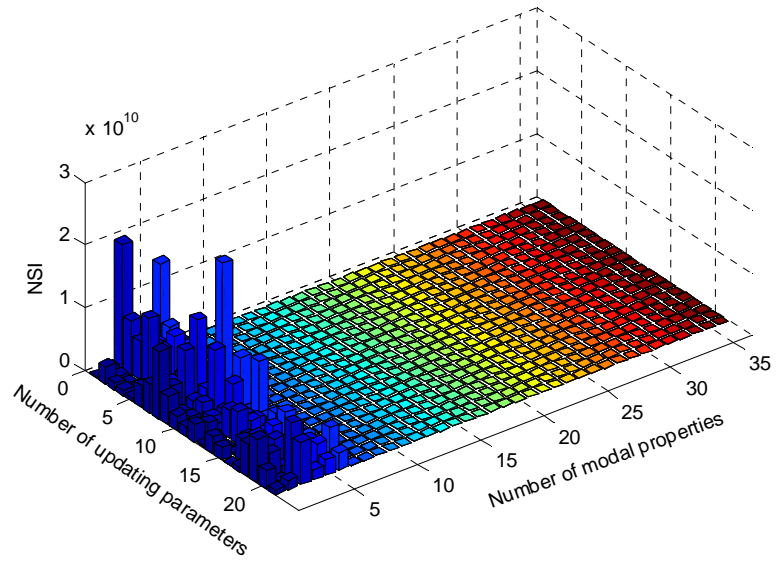


**Figure 4.24 Illustration of NSI of eigenvalues and eigenvectors**

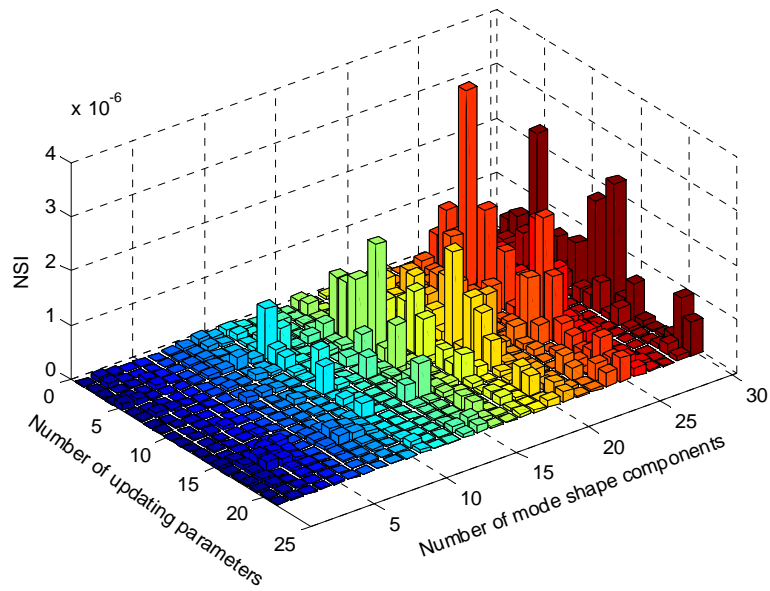


**Figure 4.25 Illustration of NSI of eigenvectors**

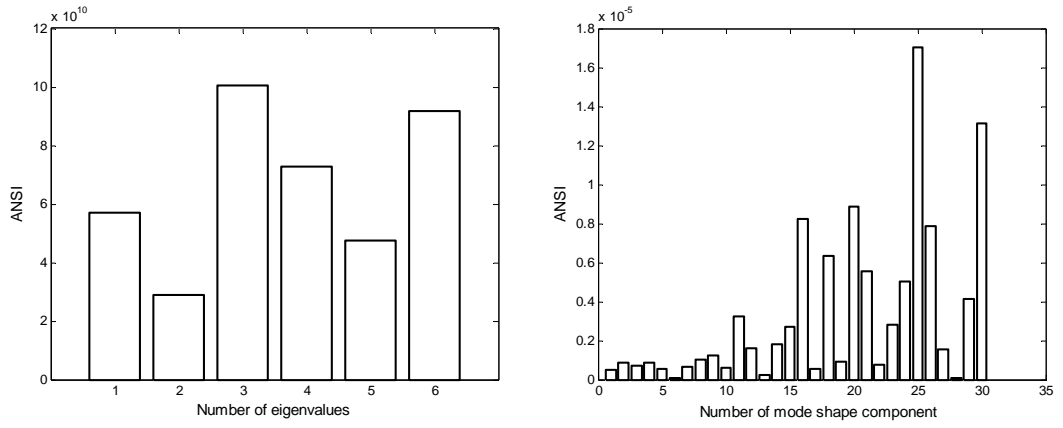


**Figure 4.26 Illustration of ANSI of modal properties:  
(a) eigenvalues; (b) eigenvectors**

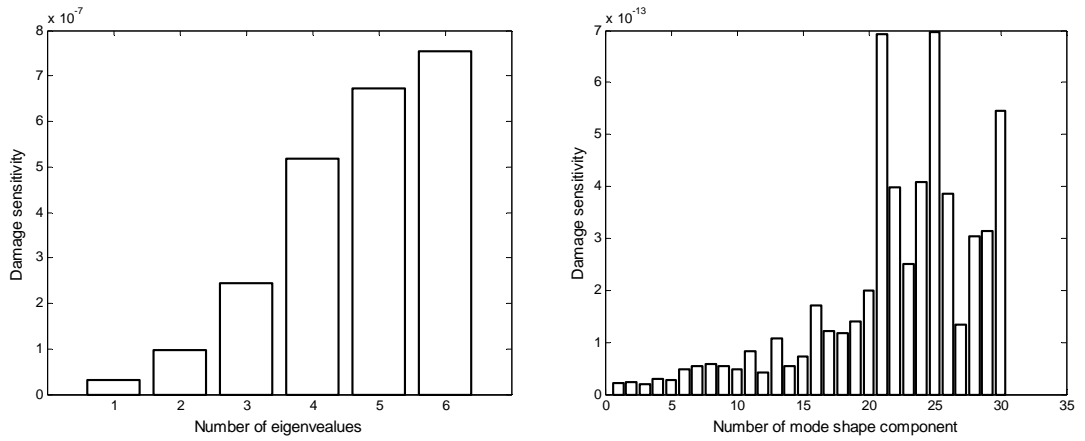


**Figure 4.27 Illustration of damage sensitivity of modal properties:  
(a) eigenvalues; (b) eigenvectors**

**Table 4.3 Summary of normalized sensitivity index and average normalized sensitivity index**

$\theta_i$	$z_i$	1 ( $\times 10^8$ )	2 ( $\times 10^8$ )	3 ( $\times 10^8$ )	4 ( $\times 10^8$ )	5 ( $\times 10^8$ )	6 ( $\times 10^8$ )	7 ( $\times 10^8$ )	8 ( $\times 10^8$ )	9 ( $\times 10^8$ )	10 ( $\times 10^8$ )	11 ( $\times 10^8$ )	12 ( $\times 10^8$ )	13 ( $\times 10^8$ )	14 ( $\times 10^8$ )	15 ( $\times 10^8$ )	16 ( $\times 10^8$ )	17 ( $\times 10^8$ )	18 ( $\times 10^8$ )
1	1.82	8.65	198.30	34.54	61.11	144.22	1.53	8.41	3.40	0.58	0.47	0.24	2.62	6.08	12.31	6.04	9.93	5.51	
2	27.46	5.61	85.30	66.76	34.69	52.96	1.18	7.57	1.95	0.92	0.52	0.08	1.99	4.83	9.36	4.37	13.15	3.83	
3	10.83	3.36	61.36	48.01	27.95	39.27	1.55	0.76	2.31	7.06	2.46	0.64	5.97	6.35	1.73	0.12	5.77	7.81	
4	8.94	3.76	107.4	50.10	63.77	38.72	1.90	1.64	1.45	6.68	2.86	0.66	5.27	4.81	2.67	1.07	8.68	8.12	
5	6.56	2.85	2.91	7.45	10.14	5.46	12.06	10.62	2.30	1.73	1.07	2.87	6.54	9.39	22.10	10.66	93.13	47.24	
6	33.80	3.67	12.96	0.60	20.92	15.99	0.91	0.14	0.37	0.05	0.37	0.03	0.46	0.23	0.12	0.28	28.66	4.82	
7	45.26	16.21	6.06	49.17	8.46	15.01	4.50	8.81	5.42	2.42	0.73	1.60	5.74	2.46	11.06	5.57	24.56	6.10	
8	107.10	44.77	93.84	134.60	39.87	210.36	0.30	0.29	0.47	0.41	0.63	0.01	0.59	0.07	0.48	0.50	7.12	6.40	
9	45.30	12.62	22.95	32.94	12.13	5.49	1.76	2.98	0.99	0.54	0.61	1.12	9.77	10.74	7.79	2.30	3.83	51.90	
10	23.43	13.72	27.95	105.10	7.71	77.06	0.04	0.16	3.14	0.030	0.01	0.03	0.26	2.16	0.68	0.33	0.10	0.52	
11	15.53	0.01	15.27	19.48	0.68	2.51	0.02	2.04	3.65	7.71	4.37	0.15	0.06	2.56	9.22	2.63	51.03	7.44	
12	28.15	23.32	4.088	69.65	11.04	89.70	0.270	0.36	0.50	0.53	0.32	0.04	0.15	0.04	0.07	0.12	2.33	0.62	
13	3.78	3.27	44.94	21.23	16.58	10.89	1.89	2.10	0.11	4.14	4.11	0.39	0.19	2.03	4.54	0.20	14.06	2.64	
14	26.52	2.57	52.57	29.44	3.76	25.12	0.19	0.24	0.53	0.44	0.56	0.017	0.44	0.27	0.01	1.34	3.94	1.79	
15	18.54	1.58	20.51	0.80	22.17	36.24	4.86	6.08	1.82	10.93	12.72	0.81	5.02	6.35	0.76	7.16	26.52	0.46	
16	0.17	32.32	31.23	0.62	1.97	23.53	2.79	8.34	18.34	15.15	6.03	0.22	7.64	20.18	15.75	6.24	1.50	0.33	
17	7.34	34.35	4.281	3.87	12.75	6.83	2.70	7.49	16.61	13.83	5.34	0.18	6.79	18.16	14.63	5.87	0.98	0.44	
18	52.58	17.32	44.46	1.78	18.71	15.76	4.04	6.58	1.04	5.99	2.53	0.69	4.70	3.81	5.78	3.04	4.29	2.04	
19	69.91	40.16	10.67	34.71	37.80	14.94	3.31	4.83	0.60	4.00	2.04	0.46	3.14	2.37	3.74	1.89	5.33	1.63	
20	28.74	4.96	89.21	0.39	40.85	58.73	1.64	3.11	2.82	0.29	3.18	0.05	0.68	1.47	1.26	0.68	10.04	1.20	
21	6.98	13.73	67.94	16.20	23.84	27.85	1.117	1.76	1.16	1.30	2.36	0.09	0.24	0.27	0.25	0.67	6.12	1.12	
ANSI	568.7	288.8	1004	727.4	476.9	916.5	48.55	84.31	68.95	84.71	53.31	10.35	68.26	104.6	124.3	61.08	321.1	161.9	

**Table 4.3 Summary of normalized sensitivity index and average normalized sensitivity index (Cont'd )**

$\theta_i$ \ $z_i$	19 ( $\times 10^{-8}$ )	20 ( $\times 10^{-8}$ )	21 ( $\times 10^{-8}$ )	22 ( $\times 10^{-8}$ )	23 ( $\times 10^{-8}$ )	24 ( $\times 10^{-8}$ )	25 ( $\times 10^{-8}$ )	26 ( $\times 10^{-8}$ )	27 ( $\times 10^{-8}$ )	28 ( $\times 10^{-8}$ )	29 ( $\times 10^{-8}$ )	30 ( $\times 10^{-8}$ )	31 ( $\times 10^{-8}$ )	32 ( $\times 10^{-8}$ )	33 ( $\times 10^{-8}$ )	34 ( $\times 10^{-8}$ )	35 ( $\times 10^{-8}$ )	36 ( $\times 10^{-8}$ )
1	1.22	12.03	0.50	16.81	0.34	5.49	0.20	7.23	2.47	0.25	0.17	1.06	2.71	12.74	0.17	0.049	0.38	1.27
2	1.02	10.02	2.38	22.31	0.08	12.17	1.10	7.62	35.13	1.76	5.27	25.09	63.55	6.36	5.01	0.20	14.02	45.95
3	0.85	2.09	6.62	4.74	0.075	15.17	2.11	46.55	10.02	4.02	10.68	17.06	121.3	1.81	2.57	0.42	28.99	62.98
4	1.07	1.78	6.80	5.74	0.59	18.29	2.42	52.31	3.51	2.53	16.24	0.38	87.13	3.57	0.59	0.34	21.55	44.50
5	3.64	14.96	26.79	104.4	14.48	51.05	5.74	32.37	68.91	17.73	43.18	102.9	364.1	87.00	12.09	0.37	61.38	237.3
6	0.29	1.63	4.26	105.1	4.00	28.88	1.53	7.77	2.91	0.27	4.20	1.44	3.16	41.43	10.59	0.52	2.70	10.74
7	0.03	7.20	8.69	122.3	6.34	63.87	5.14	90.23	45.81	9.51	49.08	22.24	165.3	82.35	29.85	1.73	38.71	67.62
8	0.47	0.81	4.23	7.94	0.51	1.56	0.06	5.54	3.04	0.77	0.20	4.93	14.68	48.68	3.11	0.58	12.45	19.29
9	3.66	19.31	51.21	208.2	7.61	84.81	7.10	48.49	102.2	9.27	21.4	54.71	108.5	59.60	6.36	0.89	29.6	77.43
10	0.05	0.20	0.40	26.48	1.78	114.2	2.22	19.49	3.46	0.10	4.83	3.42	18.34	1.93	0.14	0.01	1.61	5.15
11	4.44	39.17	9.13	80.18	2.36	72.71	9.31	178.1	18.74	1.64	2.62	10.42	82.34	181.2	42.48	0.35	25.72	178.3
12	0.24	3.47	6.46	4.24	0.18	4.32	0.32	14.25	16.05	2.49	0.93	15.34	90.48	4.14	2.41	0.09	25.11	32.24
13	0.77	0.34	6.28	25.27	3.31	36.91	12.80	115.5	111.2	11.14	33.27	113.1	216.7	113.1	8.43	0.37	56.75	231.9
14	0.19	4.81	29.78	9.83	1.41	22.64	5.94	98.64	30.41	3.74	11.24	37.34	117.3	31.53	2.56	0.13	12.51	30.79
15	2.73	31.54	62.53	9.88	6.70	50.22	17.46	56.58	7.58	1.75	12.52	0.58	42.63	22.70	11.23	2.02	31.78	67.43
16	0.15	4.52	4.50	9.76	1.36	9.33	2.88	10.77	5.34	1.21	1.35	9.59	30.29	29.11	0.34	0.38	5.64	10.91
17	0.09	3.42	3.18	4.57	0.74	3.28	1.72	5.07	2.77	0.61	0.55	4.94	15.19	11.29	0.54	0.17	2.26	4.27
18	0.15	3.12	2.52	25.31	0.10	14.15	4.33	41.35	26.81	0.08	33.23	15.37	25.22	6.27	2.66	0.12	2.82	7.63
19	0.24	3.58	4.13	24.45	0.69	15.86	4.78	35.20	12.33	1.50	22.21	4.56	59.61	4.41	1.60	0.33	8.86	18.76
20	0.94	9.73	18.21	7.05	1.84	4.87	2.87	1.01	25.14	5.11	2.49	32.59	33.08	24.27	6.97	0.37	21.90	97.24
21	0.61	7.71	13.16	1.61	1.51	6.95	3.96	13.39	18.79	2.94	4.65	25.22	42.90	15.92	3.79	0.02	9.89	63.32
ANSI	22.83	181.4	271.8	826.2	55.97	636.7	93.98	887.5	552.6	78.40	280.3	502.2	1705	789.4	153.5	9.451	414.6	1315

#### 4.4.3 Uncertainty due to Measurement Noise and Natural Randomness

The last case studied is the stochastic model updating using the uncertain model properties arising from both the natural randomness of structure and measurement noise. Similarly, the natural randomness of structure is simulated by means of temperature-caused variability in Young's modulus of each member and the measurement noise in each modal parameter is modeled by a normally distributed random variable with zero mean. In order to obtain the covariance of stochastic modal properties, it is assumed that the Young's modulus and measurement noise are uncorrelated random variables. In practice, the covariance of measured modal properties can be readily estimated from a series of measured modal properties obtained by the monitoring system (Ko *et al.* 2003). Making use of the statistical independence between Young's modulus and measurement noise, the covariance of simulated experimental modal properties is expressed as

$$\text{Var}(\tilde{\mathbf{z}}, \tilde{\mathbf{z}}) = \text{Var1} + \text{Var2} \quad (4.37)$$

where  $\text{Var1} = \mathbf{S}_d \boldsymbol{\Sigma}_E \mathbf{S}_d^T$ , is the covariance caused by natural randomness of Young's modulus; and  $\text{Var2} = (1\%)^2 \text{diag}(\bar{z}_1^2 \quad \dots \quad \bar{z}_i^2 \quad \dots \quad \bar{z}_n^2)$  represents the covariance in modal properties due to measurement noise.

##### 4.4.3.1 Stochastic Model Updating Using Perturbation and MCS Methods

Both the perturbation method and the MCS method have been applied to conduct the stochastic model updating. A summary of the stochastic model updating results using these two methods is shown in Table 4.4 together with the updating results for the previous two cases. The model updating results are also illustrated in **Figure 4.28**. Despite the simultaneous presence of uncertainties in both natural randomness and

measurement noise, the updating results from the perturbation method still agree with those from the MCS method. It is observed that the means of reduction factors obtained in this case are approximately the average of those obtained in the previous two cases, and that the COV (or standard deviation) of updating parameters obtained in this case are approximately squared root of those obtained in the previous two cases. That is

$$\mu_3 = \frac{(\mu_1 + \mu_2)}{2} \quad (4.38)$$

$$\sigma_3 = \sqrt{\sigma_1^2 + \sigma_2^2} \quad (4.39)$$

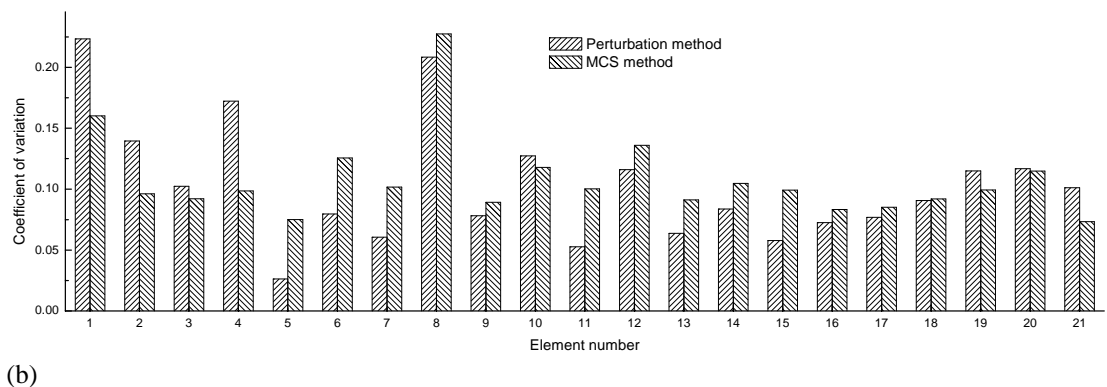
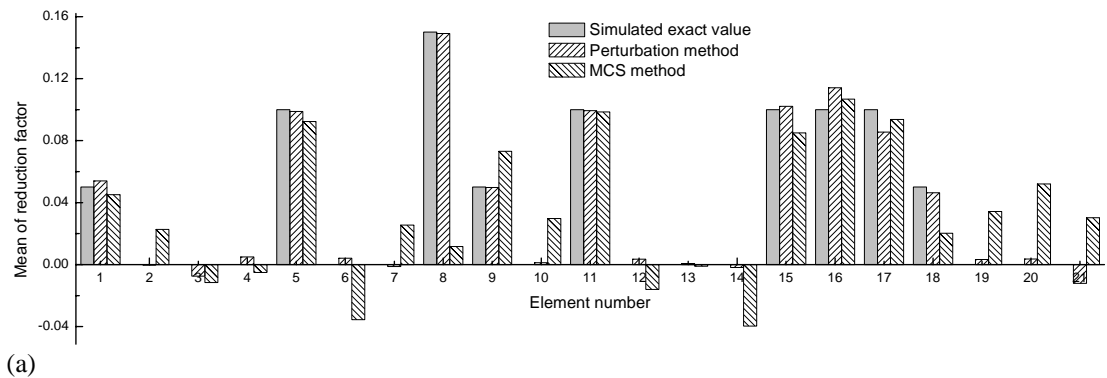


**Figure 4.28 Comparison of perturbation method with MCS method for 10% randomness and 1% measurement noise (case study 1): (a) mean of reduction factor; (b) COV**

**Table 4.4 Comparison of MCS method with perturbation method for three cases**

<i>Element No.</i>	<i>Simulated damage (%)</i>	<i>Case 1 (Natural randomness)</i>				<i>Case 2 (Noise)</i>				<i>Case 3 (Natural randomness + noise)</i>			
		<i>Perturbation</i>		<i>MCS</i>		<i>Perturbation</i>		<i>MCS</i>		<i>Perturbation</i>		<i>MCS</i>	
		<i>Mean</i>	<i>COV</i>	<i>Mean</i>	<i>COV</i>	<i>Mean</i>	<i>COV</i>	<i>Mean</i>	<i>COV</i>	<i>Mean</i>	<i>COV</i>	<i>Mean</i>	<i>COV</i>
1	5	5.40	0.184	6.122	0.116	5.40	0.128	0.97	0.131	5.40	0.224	4.51	0.160
2	0	-0.02	0.124	1.745	0.089	-0.02	0.064	3.02	0.062	-0.02	0.139	2.27	0.096
3	0	-0.74	0.091	0.143	0.091	-0.74	0.046	-2.8	0.035	-0.74	0.102	-1.16	0.092
4	0	0.50	0.157	0.599	0.088	0.50	0.070	-1.25	0.064	0.50	0.172	-0.50	0.099
5	10	9.89	0.025	9.579	0.077	9.89	0.008	9.09	0.010	9.89	0.026	9.23	0.075
6	0	0.43	0.076	-2.041	0.116	0.43	0.022	-1.20	0.038	0.43	0.080	-3.55	0.126
7	0	-0.12	0.049	1.834	0.102	-0.12	0.036	1.00	0.035	-0.12	0.060	2.54	0.102
8	15	14.91	0.148	6.752	0.186	14.91	0.147	9.35	0.170	14.91	0.208	1.17	0.228
9	5	4.98	0.071	6.871	0.088	4.98	0.032	4.76	0.035	4.98	0.078	7.31	0.089
10	0	0.13	0.108	2.201	0.110	0.13	0.068	1.26	0.059	0.13	0.127	2.98	0.118
11	10	9.94	0.051	9.583	0.103	9.94	0.015	9.86	0.011	9.94	0.053	9.84	0.100
12	0	0.35	0.099	-1.493	0.116	0.35	0.060	1.25	0.078	0.35	0.116	-1.60	0.136
13	0	0.08	0.058	-0.314	0.092	0.08	0.027	0.10	0.027	0.08	0.064	-0.11	0.091
14	0	-0.19	0.076	-2.112	0.101	-0.19	0.035	-3.20	0.045	-0.19	0.084	-3.96	0.105
15	10	10.21	0.052	9.057	0.096	10.21	0.025	11.21	0.026	10.21	0.058	8.49	0.099
16	10	11.41	0.068	10.513	0.086	11.41	0.025	10.49	0.029	11.41	0.072	10.68	0.083
17	10	8.54	0.074	9.101	0.086	8.54	0.019	10.27	0.026	8.54	0.077	9.37	0.085
18	5	4.64	0.082	3.436	0.093	4.64	0.038	3.16	0.042	4.64	0.091	2.04	0.092
19	0	0.32	0.104	1.886	0.093	0.32	0.049	0.30	0.062	0.32	0.115	3.43	0.099
20	0	0.37	0.101	3.443	0.111	0.37	0.059	2.76	0.058	0.37	0.117	5.21	0.115
21	0	-1.20	0.093	0.753	0.080	-1.20	0.040	-0.49	0.058	-1.20	0.101	3.02	0.073

#### 4.4.3.2 Second-Stage Bayesian Updating

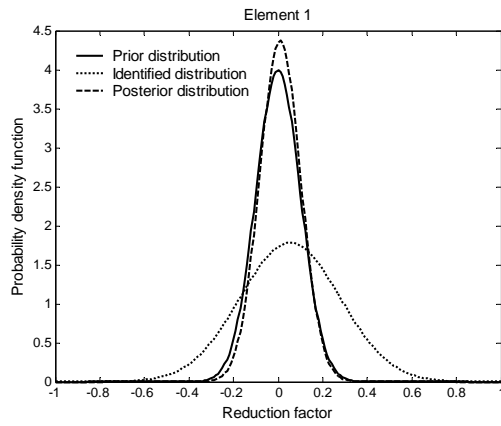
After conducting the first-stage stochastic model updating, the updating results corresponds to the experimentalist's knowledge and confidence on the estimates of updating structural parameters. When the prior knowledge of structural parameters, which embodies the analyst's confidence, is available, the identified statistics of structural parameters from the first-stage updating can be further updated to achieve a posterior distribution function by means of Bayesian theorem. It should be noted that although the use of Bayesian theorem for model updating is quite natural in theoretical consideration, objections to this have been raised that the selection of the priors is an extremely controversial aspect of the method since it is a subjective judgment. Also the selection of prior distributions will significantly affect the posterior distributions.

For illustration, it is assumed that all updating parameters comply with a normal distribution with mean of 200 GPa and COV of 0.1. Table 4.5 summarizes the posterior statistics of updating parameters. Some results are also illustrated in **Figure 4.29**. For all updating parameters, the posterior distribution functions of structural parameters are sharper than both the prior distribution function and the identified distribution function. This is expected because the variance of a variable decreases when more information is utilized. The Bayesian estimator gives rise to more confidence in the information with small variance. When the variance in the prior distribution is smaller than that in the identified distribution, the Bayesian estimator is closer to the prior distribution than to the identified distribution as shown in **Figure 4.29(a)**; when the variance in the prior distribution is larger than that in the identified distribution, the Bayesian estimator is closer to the identified distribution

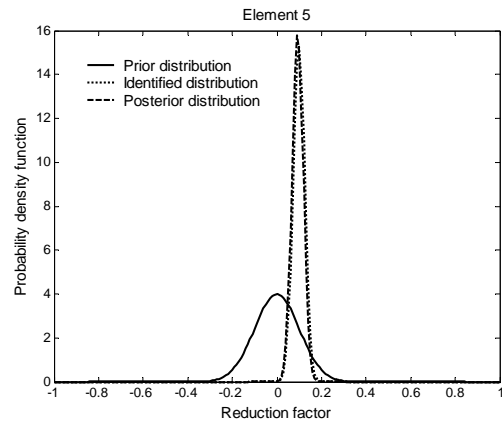
than to the prior distribution as shown in **Figure 4.29(b)**; and when the variance in the prior distribution is identical with that in the identified distribution, the Bayesian estimator is balanced between the prior distribution and the identified distribution as shown **Figure 4.29(c-d)**.

**Table 4.5 Summary of prior, identified, and posterior distribution parameters**

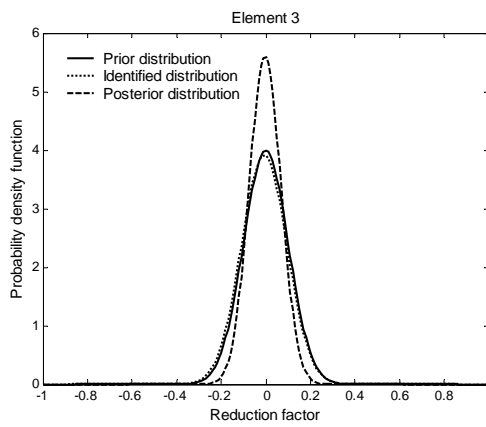
<i>Element No.</i>	<i>Prior statistics</i>		<i>Identified statistics</i>		<i>Posterior statistics</i>	
	<b>Mean</b>	<b>COV</b>	<b>Mean</b>	<b>COV</b>	<b>Mean</b>	<b>COV</b>
1	0	0.1	0.054	0.224	0.009	0.091
2	0	0.1	0.000	0.139	0.000	0.081
3	0	0.1	-0.007	0.102	-0.004	0.071
4	0	0.1	0.005	0.172	0.002	0.086
5	0	0.1	0.099	0.026	0.093	0.025
6	0	0.1	0.004	0.080	0.003	0.062
7	0	0.1	-0.001	0.060	0.000	0.052
8	0	0.1	0.149	0.208	0.028	0.090
9	0	0.1	0.050	0.078	0.031	0.062
10	0	0.1	0.001	0.127	0.000	0.079
11	0	0.1	0.099	0.053	0.077	0.047
12	0	0.1	0.003	0.116	0.001	0.076
13	0	0.1	0.000	0.064	0.001	0.054
14	0	0.1	-0.002	0.084	-0.001	0.064
15	0	0.1	0.102	0.058	0.076	0.050
16	0	0.1	0.114	0.072	0.075	0.058
17	0	0.1	0.085	0.077	0.054	0.061
18	0	0.1	0.046	0.091	0.025	0.067
19	0	0.1	0.003	0.115	0.001	0.075
20	0	0.1	0.004	0.117	0.002	0.076
21	0	0.1	-0.012	0.101	-0.006	0.071



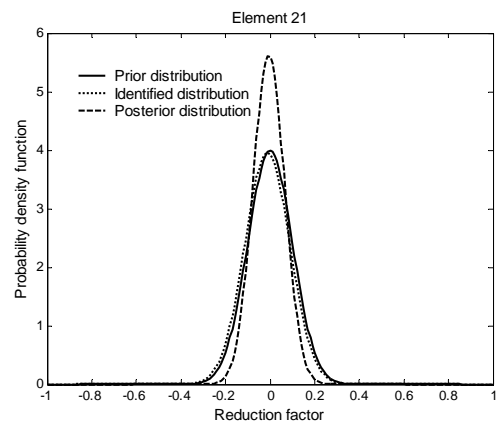
(a)



(b)



(c)



(d)

**Figure 4.29 Prior, identified and posterior PDFs of structural parameters:  
(a) element 1; (b) element 5; (c) element 3; (d) element 21**

## 4.5 Case Study 2: A Statically Indeterminate Truss Bridge

The first example shown in section 4.4 is a statically determinate bridge where failure of any member will lead to the collapse of the whole structural system. Provided in this section is the stochastic model updating of a statically indeterminate structure which could continuously carry the required load when a single member

fails. The two examples are given in this chapter for consistency with the subsequent analysis of structural reliability in the following chapters.

Illustrated in **Figure 4.30** is the geometry configuration of the statically indeterminate truss bridge. Likewise, each member of the bridge is modelled as a planar truss element. An analytical FE model is established which has been correlated with the modal properties of as-built or undamaged state of the bridge, and therefore this baseline model is representative of the bridge without damage. In this analytical model as shown in **Figure 4.30**, a total of 31 planar truss elements, each with two DOFs at every node, are used. The material properties used in this analytical model are as follows: mass density  $\rho = 7800 \text{ kg/m}^3$ , area of cross section for each member  $A = 10^{-2} \text{ m}^2$ , and the Young's modulus  $E = 200 \text{ GPa}$ .

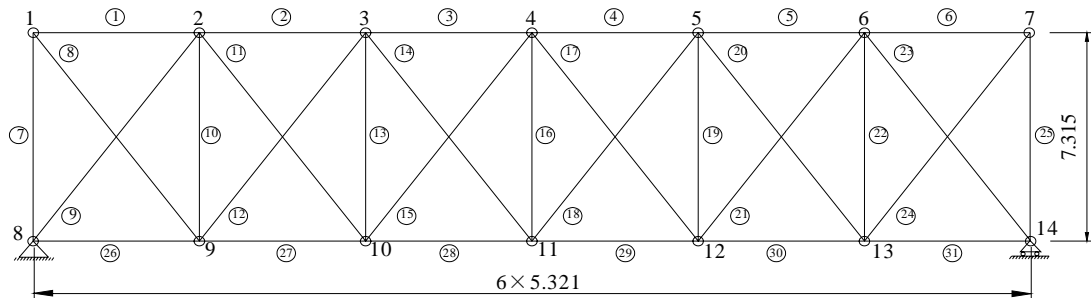


**Figure 4.30** Geometry configuration of statically indeterminate truss bridge

Similar to the first example, another FE model with the same topology as the baseline model is constructed to provide the simulated experimental modal properties by artificially reducing Young's modulus of each member to different levels to different levels, as shown in **Figure 4.31**. The modal properties computed from this FE model serve as the 'measured' modal properties corresponding to the damaged

structure. In order to simulate incomplete measurement, only five vertical modal displacements for each of the eigenvectors, namely vertical modal displacements at nodes 9, 10, 11, 12 and 13 as shown in **Figure 4.31**, are assumed to be available throughout this numerical study.

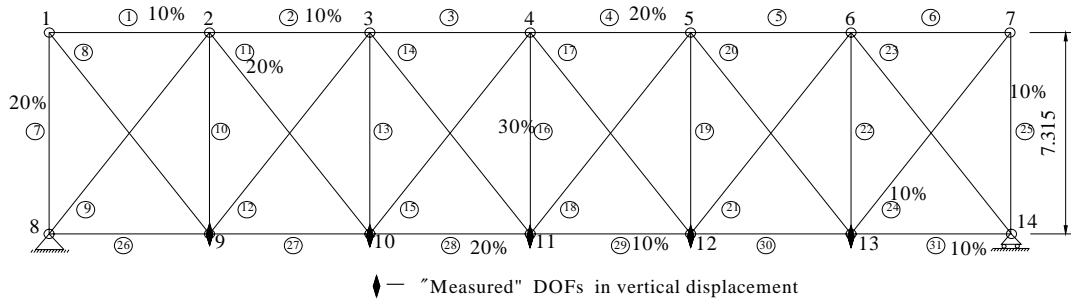
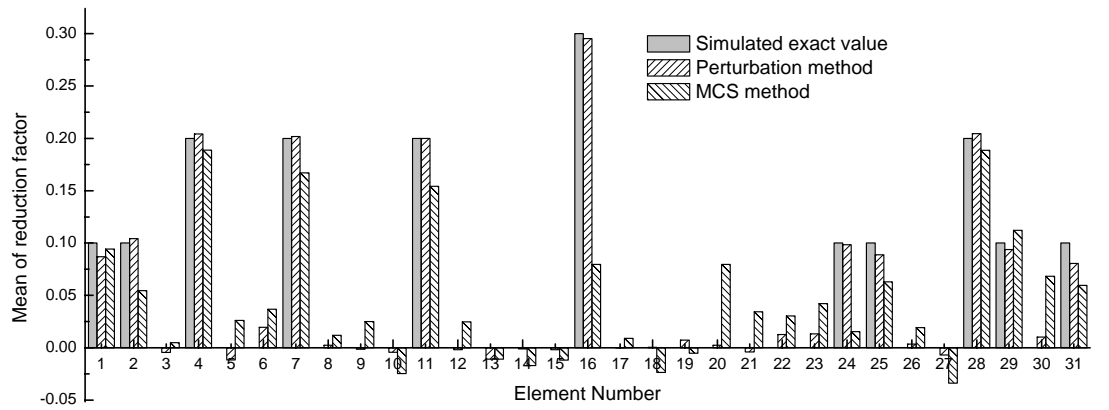


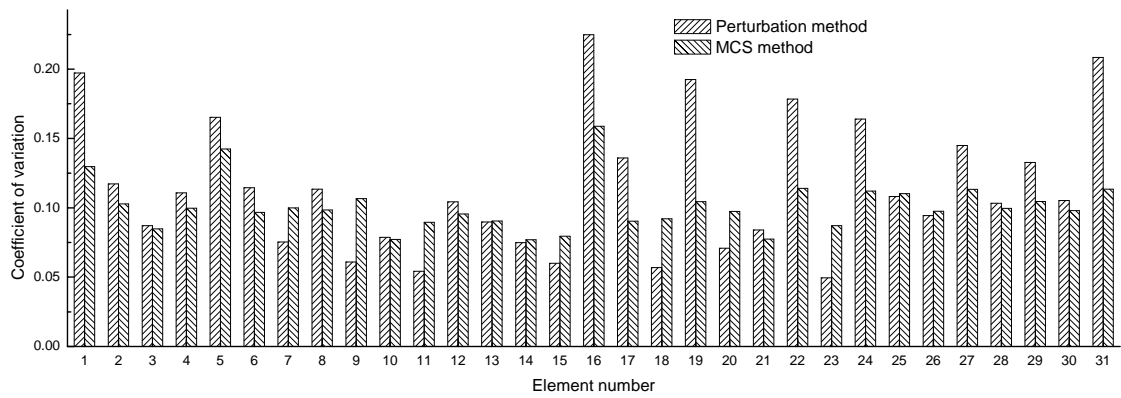
**Figure 4.31 Finite element model and simulated reduction factor of Young's modulus for statically indeterminate truss bridge**

The first-stage stochastic model updating is performed to identify the statistics of updating parameters using the uncertain modal properties. The first six modes are first used for stochastic model updating. It is found that COVs of updating parameters become considerably large, which are meaningless updating results. Then, the first seven modes are then used for the improvement of identification accuracy. For brevity, only the identified results for the last case with uncertainties in both natural randomness and measurement noise are presented here.

**Figure 4.32** compares the stochastic model updating results using the perturbation method and the MCS method. Once more, the perturbation method gives acceptable approximation to the means and COVs of updating parameters in comparison with the results of the MCS method.



(a)



(b)

**Figure 4.32 Comparison of perturbation method with MCS method for 10% natural randomness and 1% measurement noise (case study 2): (a) mean of reduction factor; (b) COV**

When the prior distributions of updating parameters are available, they can be combined with the above identified distributions of updating parameters to obtain the posterior distribution functions as illustrated in **Figure 4.33**. In this numerical example, the prior distributions of all the updating parameters are assumed as a normal distribution with mean of 200 GPa and COV of 0.1.

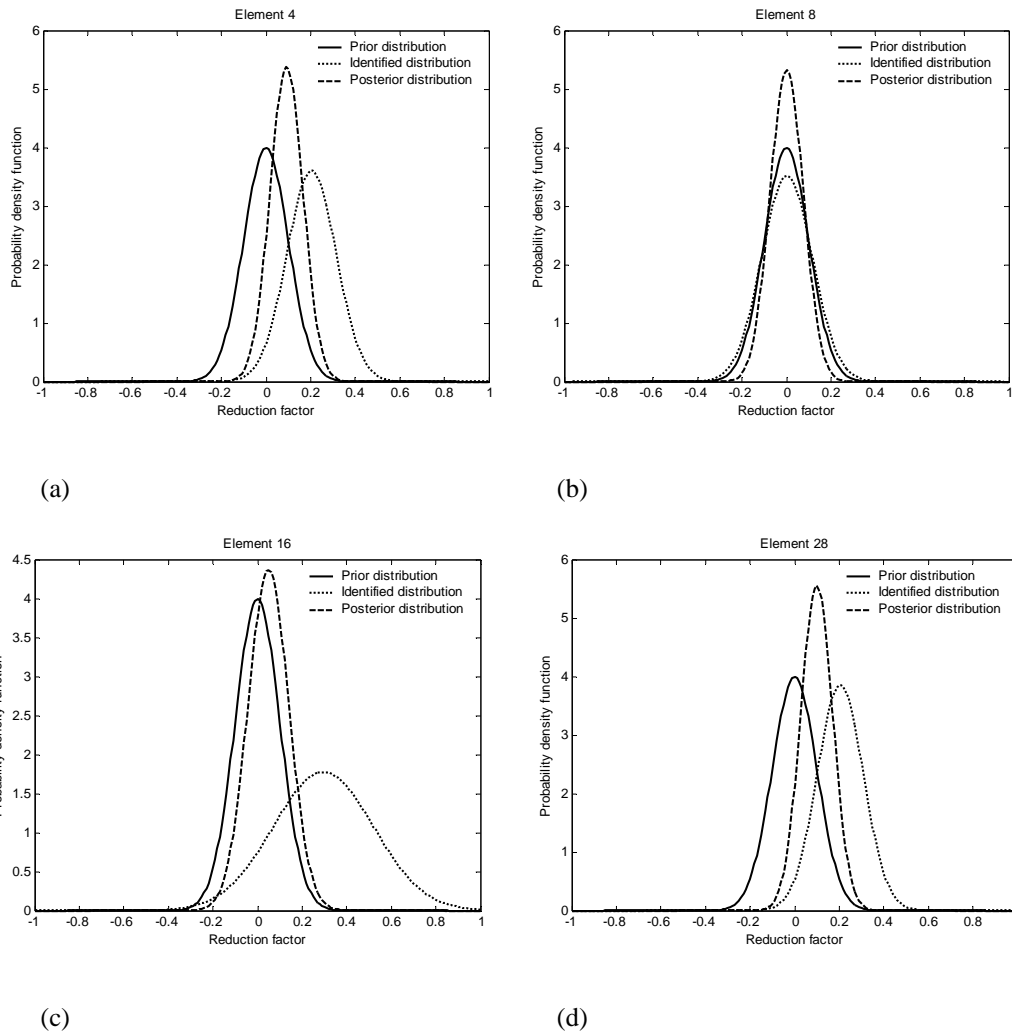


**Figure 4.33 Prior, identified and posterior PDFs of structural parameters: (a) element 4; (b) element 8; (c) element 16; (d) element 28**

## 4.6 Summary

A novel two-stage approach for stochastic FE model updating was presented in this chapter. The proposed approach involves a first-stage stochastic FE model updating from statistics of measured modal properties and a second-stage Bayesian updating. It is able to incorporate the knowledge and confidence about the measurement data from experimentalists and about the FE model from analysts. An improved

perturbation method and the MCS method are employed for the first-stage model updating, and the accuracy of the improved perturbation method for three types of uncertainties are compared with the MCS method through numerical studies of two truss bridges. Furthermore, based on the improved method, two indices were proposed to identify the most significant variables which considerably contribute to the variance of updating parameters. As the model updating and damage detection are not an end in the framework of structural health monitoring, the method developed in this chapter lay the base for the studies in the following chapters with the intention of the reliability-based condition assessment of bridge structures.

The numerical studies conclude the following points: i) for each type of uncertainties studied, the improved perturbation method generates satisfactory model updating results when that the uncertainty does not exceed a certain level (say 2%) but may be less accurate in the case of high uncertainty; ii) neglecting the correlations of modal parameter may result in an unreliable estimation of the covariance matrix of updating parameters; (iii) with the increase of uncertainty level, the geometry of updating parameter PDFs becomes more complicated and the PDFs could have several distinct peaks; iv) some high-order modal components significantly contribute to the updating parameter variance, indicating the limitations of the commonly acknowledged rule-of-thumb methods in the selection of the relevant modes in model updating and damage detection.

## **Chapter 5**

### **DEVELOPMENT OF COMPUTER CODE FOR LINEAR FE RELIABILITY ANALYSIS**

#### **5.1 Introduction**

The design and analysis of modern structures is performed in the face of numerous uncertainties. These uncertainties arise due to the inherent variability present in nature and due to the imperfect state of our knowledge. Furthermore, it may also arise due to the improper modelling of actual structural behaviour. Under the conditions of the uncertainty, it is essential to recognize that any structure always has a non-zero, albeit small, probability of failure or of not performing as intended. It is therefore impossible to guarantee the satisfactory performance of a structure.

Employing the concept of probability, the method of structural reliability computes the probability that a structure does not perform as intended by taking into account the uncertainties in both the structure and its external loadings, and then a rational analysis and design will be achieved by reducing the computed failure probability to an acceptable level. In the general theory and method of structural reliability, the uncertainties in a structure and its external loadings are characterized by continuous random variables with known distributions and then many approximation methods, such as the first-order reliability method (FORM) and the second-order reliability method (SORM), can be used to compute the probability that the random variables

fall into a predefined failure domain (Rackwitz 2001). Due to the rational basis and mathematical background, methods of structural reliability have gained increasing acceptance in academic circles and are beginning to be acknowledged and used by engineering practitioners (Estes and Frangopol 2005).

For large-scale and complex structures, their performance can be predicted only by numerical techniques, since no closed-form solution for response of the realistic structures is available. The most commonly used numerical technique for analyzing the response of a structure is the finite element (FE) method. In order to analyze the failure probability of a realistic structure with numerous uncertainties, the structural reliability method must be performed in connection with the FEM. The combination of the reliability method with the FE technique is often referred to as the finite element reliability method (FERM) in the literature (Haldar and Mahadevan 2000; Sudret and Der Kiureghian 2002).

The aim of this chapter is to describe the basic theory of structural reliability analysis and the approximation methods for computing the component failure probability, and to develop a computer code for the linear FERM by linking the well-established FORM/SORM with the FE technique. The contents presented in this chapter pave the way for the reliability-based condition assessment of existing structures to be addressed in the next chapter. The remaining of this chapter is organized as follows. The theory and method of structural component reliability is first outlined. It consists of the selection of random variables, formulation of limit-state function, and computation of failure probability. Two well-established methods, namely FORM and SORM, are employed to compute the probability of failure. Linear FERM is then presented for the analysis of failure probability of realistic structures. In compliance

with the reliability analysis, the FE technique is employed to compute the structural responses involved in the predefined limit-state function and the response gradients with respect to the random variables. Several numerical examples are provided for illustration of the FE reliability analysis.

## **5.2 First- and Second-Order Reliability Methods**

### **5.2.1 Fundamentals of Structural Reliability**

The structural reliability problems of interest here are based on two fundamental assumptions. First, the uncertainties in the structure and its external loadings are assumed to be time-invariant and modelled by continuous random variables. These random variables include the load-related, resistance-related, and geometry-related quantities (Nowak and Collins 2000). The set of basic random variables describing these uncertainties are represented by a random vector  $\mathbf{x} = (x_1 \ \cdots \ x_n)^T$ . Second, the structure may fail in any of a finite number of failure modes, and with respect to each mode it is either in a safe state or in a failure state. The evaluation of the failure probability for a single failure mode (or a single limit-state function) is called *component* reliability analysis. The probability due to the combination of numerous failure modes requires a *system* reliability analysis, for which the component failure probability is the basic ingredient. Present study will focus on component reliability analysis. Details on system reliability can be found in references (Ditlevsen 1979; Madsen *et al.* 1986; Ditlevsen and Madsen 1996; Melchers 1999). The term *failure* is used in a general sense. It may denote the physical failure of a structure or its member, or the exceeding of a serviceability limit state. In other words, the reliability analysis can be formulated for both the safety and serviceability limit states.

Structural limit states are usually defined in terms of the structural responses and the response thresholds. The structural responses, denoted by a vector  $\mathbf{y}$ , are functions of the basic random variables, that is

$$\mathbf{y} = \mathbf{y}(\mathbf{x}) \quad (5.1)$$

For example, the limit-state function may be expressed as  $g(\mathbf{x}) = y_0 - y(\mathbf{x})$  with  $y_0$  being the predefined response threshold. However, for large-scale and complex structures, the analytical expression in Equation (5.1) between structural responses and random variables seldom exists. In that case, the reliability analysis should be integrated with the FE technique for computing the required ingredients, including the response  $y(\mathbf{x})$  and the response gradients  $\partial y / \partial \mathbf{x}$ .

Classical reliability methods deal with the explicitly given limit-state function  $g(\mathbf{x})$ . The limit-state surface  $g(\mathbf{x}) = 0$  divides the outcome space of  $\mathbf{x}$  into a safe set (or domain) and a failure set (or domain). In general, the set with  $g(\mathbf{x}) > 0$  defines the safe domain and the set with  $g(\mathbf{x}) < 0$  defines the failure domain as illustrated in **Figure 5.1**. Thus, the probability of failure (denoted as the shaded area in **Figure 5.1**) associated with the prescribed limit-state function  $g(\mathbf{x})$  is the probability that the random variables fall in the failure domain and is given by an  $n$ -fold integral, namely

$$p_f = \int \cdots \int_{g(\mathbf{x}) < 0} f_{X_1, X_2, \dots, X_n}(x_1, x_2, \dots, x_n) dx_1 dx_2 \cdots dx_n \quad (5.2)$$

which may also be written as

$$p_f = \int_{g(\mathbf{x}) < 0} f_{\mathbf{x}}(\mathbf{x}) d\mathbf{x} \quad (5.3)$$

where  $f_{x_1, x_2, \dots, x_n}(x_1, x_2, \dots, x_n)$  denotes the joint probability density function (PDF) of random vector  $\mathbf{x}$ . An alternative to failure probability  $p_f$  as a measure of safety is the reliability index  $\beta$  defined as

$$\beta = \Phi^{-1}(1 - p_f) = -\Phi^{-1}(p_f) \quad (5.4)$$

in which  $\Phi^{-1}(\cdot)$  is the inverse cumulative distribution function (CDF) of the standard normal variate.

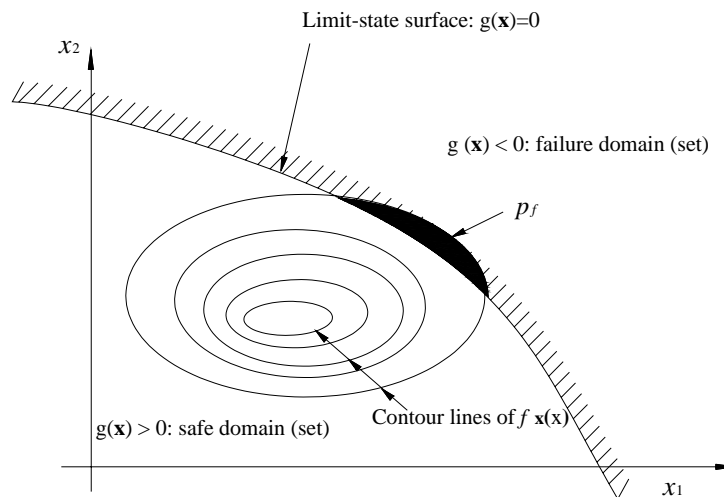


**Figure 5.1 Safe and failure sets separated by limit-state surface**

Although the expression in Equation (5.3) for computing the failure probability appears simple, direct analytical computation of this probability integral for most limit-state functions with a large number of random variables is a formidable task. Furthermore, straightforward numerical integration techniques are generally also impractical when the limit-state function is complicated and the number of random variables is large. Over the past decades, a number of approximation methods have been developed to compute this probability integral as summarized by Melchers

(1999). The present study employs two widely used methods: the first-order reliability method and the second-order reliability method, which have been proved satisfactory for most of engineering problems (Rackwitz 2001).

In general, the computation of failure probability using FORM and SORM encompasses the following four steps: (1) transformation of the random variables in the original  $\mathbf{x}$ -space into the standard normal  $\mathbf{u}$ -space; (2) determination of the nearest point, often called the design point, in the failure surface to the origin in the  $\mathbf{u}$ -space; (3) approximation of the failure surface in the  $\mathbf{u}$ -space around the design point; and (4) computation of the failure probability corresponding to the approximating failure surface. Common to FORM and SORM are the first two steps. The difference lies in that a tangent hyperplane is used to approximate the limit-state surface around the design point in the case of FORM while a quadratic surface is employed to approach the limit-state surface when using SORM. These steps are explained in the following sections.

### ***5.2.2 Transformation to Standard Normal Space***

One of the major developments in the approximation methods of structural reliability is the invention of a generally applicable method for transformation of a random vector  $\mathbf{x}$  into a standard normal vector  $\mathbf{u}$ , thus enabling the reliability analysis for random variables with arbitrary distribution types. The standard normal space is defined by a set of independent and standard normal variates  $\mathbf{u}$  having zero means and unit covariance matrix and the following joint PDF:

$$f_{\mathbf{u}}(\mathbf{u}) = \phi_n(\mathbf{u}) = \frac{1}{(2\pi)^{n/2}} e^{-\frac{1}{2}\mathbf{u}^T\mathbf{u}} \quad (5.5)$$

In principle, a one-to-one transformation between the original  $\mathbf{x}$ -space and the  $\mathbf{u}$ -space

$$\mathbf{u} = \mathbf{T}(\mathbf{x}) \quad (5.6)$$

can always be established for the random variables having strictly increasing continuous CDF for each argument, although it may not be unique. As the algorithm to find the design point requires iterative scheme, both transformation and the inverse of transformation are required. The inverse of transformation is expressed as

$$\mathbf{x} = \mathbf{T}^{-1}(\mathbf{u}) \quad (5.7)$$

Suppose the random variables  $\mathbf{x}$  are normally distributed with mean vector  $\boldsymbol{\mu}_x$  and covariance matrix  $\boldsymbol{\Sigma}$ . In this case, a convenient form of the transformation to the standard normal space is

$$\mathbf{u} = \mathbf{L}^{-1}\mathbf{D}^{-1}(\mathbf{x} - \boldsymbol{\mu}_x) \quad (5.8)$$

where the diagonal matrix  $\mathbf{D}$  contains the standard deviation of each random variable,  $\mathbf{D} = \text{diag}(\sigma_i)$ ;  $\mathbf{L}$  is the lower triangular matrix obtained from Cholosky decomposition of the correlation matrix  $\mathbf{R}$  of random vector such that  $\mathbf{R} = \mathbf{L}\mathbf{L}^T$ ; and the relation between covariance matrix and correlation matrix is  $\boldsymbol{\Sigma} = \mathbf{D}\mathbf{R}\mathbf{D}$ . The inverse of Equation (5.8) then becomes

$$\mathbf{x} = \boldsymbol{\mu}_x + \mathbf{L}\mathbf{D}\mathbf{u} \quad (5.9)$$

and the Jacobian matrix of the transformation needed to compute the gradient of limit-state function in the  $\mathbf{u}$ -space is obtained as

$$\mathbf{J}_{\mathbf{u},\mathbf{x}} = \mathbf{L}^{-1}\mathbf{D}^{-1} \quad (5.10)$$

Now suppose that the random variables  $\mathbf{x}$  are statistically independent non-normal variables such that  $f(\mathbf{x}) = f_1(x_1)f_2(x_2)\cdots f_n(x_n)$  where  $f_i(x_i)$  denotes the marginal PDF of  $x_i$ . The needed transformation is diagonal (each variable is transformed independently of other variables) and has the form

$$u_i = \Phi^{-1}(F_i(x_i)) \quad i = 1, 2, \dots, n \quad (5.11)$$

where  $F_i(x_i) = \int_{-\infty}^{x_i} f_i(x_i)dx_i$  denotes the marginal CDF of  $x_i$ ; and  $\Phi^{-1}(\cdot)$  is the inverse CDF of the standard normal variate. **Figure 5.2** shows a graphical representation of this transformation. Each point  $(x_i, u_i)$  on the curve is obtained by equating the cumulative probabilities  $F_i(x_i)$  and  $\Phi(u_i)$ . The corresponding inverse of the transformation in this case is written as

$$x_i = F_i^{-1}(\Phi(u_i)) \quad i = 1, 2, \dots, n \quad (5.12)$$

As  $x_i$  is non-normal, both transformations in Equations (5.11) and (5.12) are nonlinear. Following the above method, all random variables can be sequentially transformed to the  $\mathbf{u}$ -space. As the random variables are statistically independent, the Jacobian matrix of the transformation to the  $\mathbf{u}$ -space is a diagonal matrix having the elements

$$\mathbf{J}_{\mathbf{u},\mathbf{x}} = \text{diag} \left[ \frac{f_i(x_i)}{\varphi(u_i)} \right] \quad (5.13)$$

where  $\varphi(u) = (2\pi)^{-1/2} \exp(-u^2/2)$  is the standard normal PDF of univariate.

In the more general case of statistically dependent non-normal variables, the required transformation is necessarily coupled. Two methods, namely *Nataf model*

(Der Kiureghian and Liu 1986) and *Rosenblatt transformation* (Ditlevsen 1981; Hobenbichler and Rackwitz 1981), are available to transform the original variables to the standard normal uncorrelated ones.

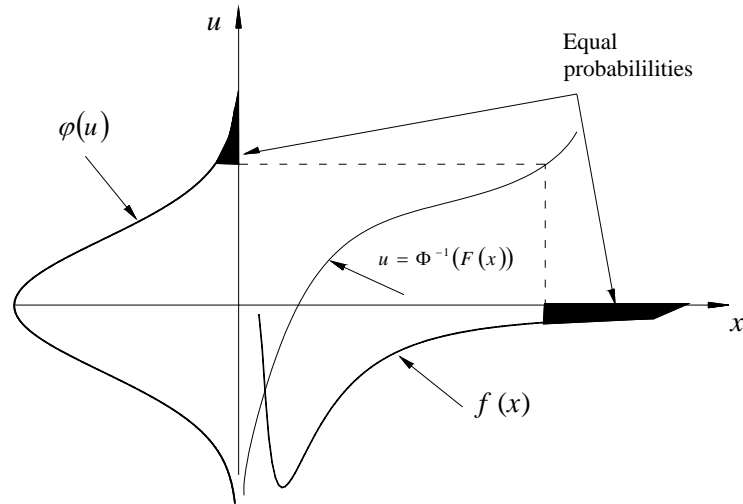


**Figure 5.2 Transformation to standard normal space for a single random variable**

The one-to-one transformation  $\mathbf{u} = \mathbf{T}(\mathbf{x})$  maps the limit-state surface in the  $\mathbf{x}$ -space,  $\{\mathbf{x} \mid g(\mathbf{x}) = 0\}$ , into the limit-state surface in the  $\mathbf{u}$ -space,  $\{\mathbf{u} \mid G(\mathbf{u}) = 0\}$ , as illustrated in **Figure 5.3**. The transformation preserves the probability content,  $p_f$ , of failure domain in the original  $\mathbf{x}$ -space and thus the failure probability integral may be expressed as

$$p_f = \int_{g(\mathbf{x}) < 0} f_{\mathbf{x}}(\mathbf{x}) d\mathbf{x} = \int_{G(\mathbf{u}) < 0} \phi_n(\mathbf{u}) d\mathbf{u} \quad (5.14)$$

The standard normal space has three important properties: (1) the probability density function is rotationally symmetric about the origin; (refer Figure 5.3; (2) the probability density decays exponentially with the square of the distance from the

origin; and (3) the probability contents of some simple sets in this space are available for arbitrary dimensions. From the first two points, it follows that the contribution to the probability integral in Equation (5.14) comes mostly from the region around the point on the failure surface that is nearest to the origin. The last property is used to construct simple approximations to the probability integral. These approximations are achieved by replacing the limit-state surface with an approximating surface fitted at the nearest point, for which the probability content is readily known.

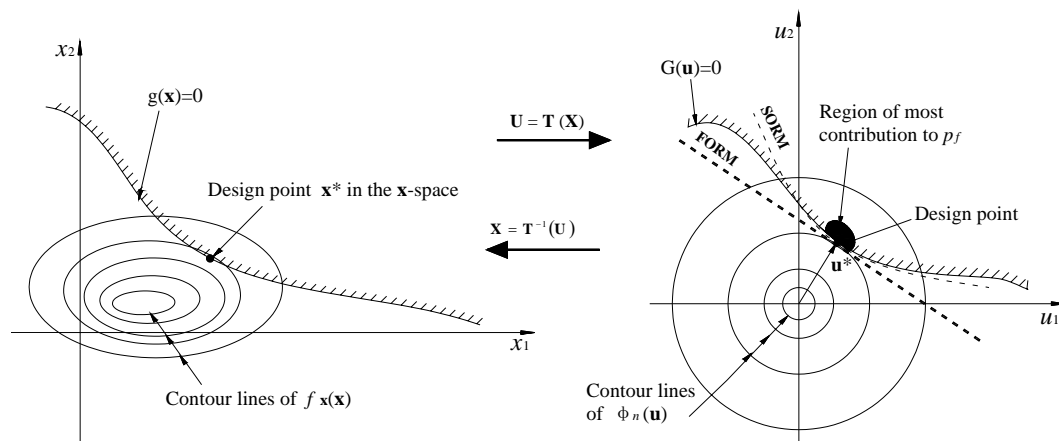


**Figure 5.3 One-to-one mapping from x-space to u-space**

### 5.2.3 Determination of Design Point

One major effort in the development of reliability methods is to find the minimum-distance point from the limit-state surface to the origin in the standard normal space. This point is also known as the mostly likely failure point (MLFP) or design point or also  $\beta$ -point in the literature. The finding of the design point requires the solution of a constrained optimization problem in the standard normal space, namely

$$\text{Minimize } \frac{1}{2} \mathbf{u}^T \mathbf{u} \quad \text{subject to } G(\mathbf{u}) = 0 \quad (5.15)$$

Many algorithms are available to solve this problem. The HL-RF method, originally proposed by Hasofer and Lind (1974) for second-moment reliability analysis and later extended by Rackwitz and Fiessler (1978) to take into account the distribution information transformation, is currently the most widely used method for solving the optimization problem in structural reliability. The HL-RF method is a simple gradient-based algorithm with the following recursive formula

$$\mathbf{u}^{(k+1)} = \frac{1}{\|\nabla G(\mathbf{u}^{(k)})\|_2^2} [\nabla G(\mathbf{u}^{(k)}) \cdot \mathbf{u}^{(k)} - G(\mathbf{u}^{(k)})] \nabla G(\mathbf{u}^{(k)})^T \quad (5.16)$$

where  $\nabla G = [\partial G / \partial u_1 \quad \dots \quad \partial G / \partial u_n]$  denotes the gradient row vector of  $G(\mathbf{u})$ . The algorithm starts at an initial point  $\mathbf{u}^{(1)}$  (usually  $\mathbf{u}^{(1)} = \mathbf{T}(\mathbf{x}^{(1)})$ ) where the limit-state function and its gradient vector are computed. After substituting these values into the recursive formula, a new iteration point  $\mathbf{u}^{(2)}$  is obtained. If convergence has not been reached, a new iteration cycle is performed and the process is continued until the difference in point coordinates between two successive iterations is less than a threshold. The algorithm is illustrated in **Figure 5.4**. It should be noted that the above iteration process is performed in the transformed  $\mathbf{u}$ -space; however, it is usually more convenient to compute the limit-state function and its gradient in the original space rather than in the standard normal space. For this purpose, each iteration point  $\mathbf{u}^{(k)}$  is first mapped back into the original space by the one-to-one inverse of transformation in Equation (5.7), and then the value of limit-state function and its gradient at the iteration point  $\mathbf{x}^{(k)}$  in the original space are evaluated. Next, making use of the chain

rule of differential calculus, the gradient of the limit-state surface in the standard normal space is obtained from

$$\nabla G(\mathbf{u}) = \nabla g(\mathbf{x}) \mathbf{J}_{\mathbf{x}, \mathbf{u}} \quad (5.17)$$

in which  $\mathbf{J}_{\mathbf{x}, \mathbf{u}} = [\partial x_i / \partial u_j]$  denotes the Jacobian matrix of the probability transformation in Equation (5.6) and  $\mathbf{J}_{\mathbf{x}, \mathbf{u}} = \mathbf{J}_{\mathbf{x}, \mathbf{u}}^{-1}$ .

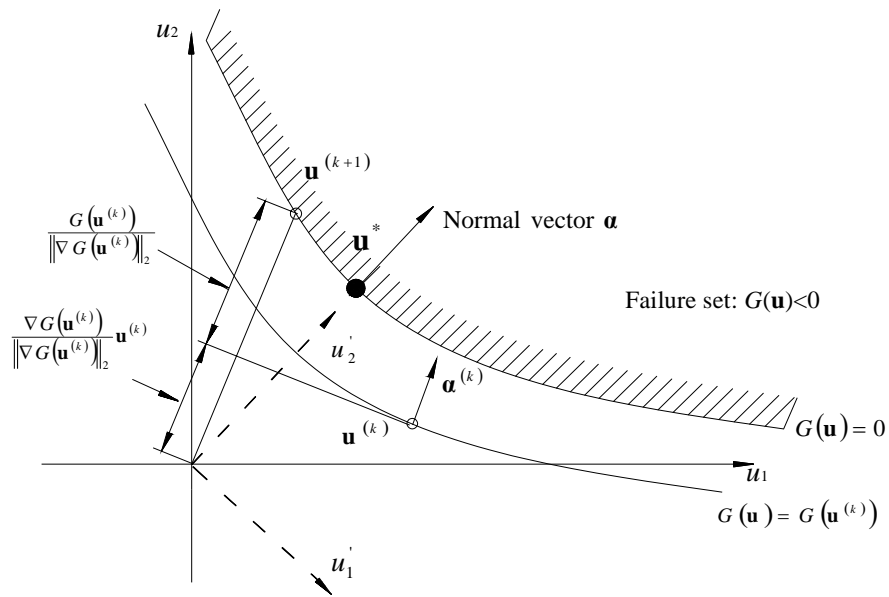


**Figure 5.4 HL-RF algorithm for finding design point in u-space**

The algorithm implementation of the HL-RF method is as follows:

- (1) Assume initial guesses of the design point  $\mathbf{x}^{(1)}$  in the original space. Typically, the initial values may be assumed to be the mean values (or the medians) of random variables; and let  $k = 1$ ;
- (2) Evaluate the value of limit-state function  $g(\mathbf{x})$ , its gradient  $\nabla g(\mathbf{x})$ , and Jacobian matrix  $\mathbf{J}_{\mathbf{x}, \mathbf{u}}$  at the point  $\mathbf{x}^{(k)}$ ;

- (3) Compute the gradient  $\nabla G(\mathbf{u})$  in the standard normal space using Equation (5.17) and then determine the next iteration point  $\mathbf{u}^{(k+1)}$  according to Equation (5.16);
- (4) Check the convergence criterion; if not satisfied, map the iteration point  $\mathbf{u}^{(k+1)}$  to the original space using inverse of the transformation, namely  $\mathbf{x}^{(k+1)} = \mathbf{T}^{-1}(\mathbf{u}^{(k+1)})$ , rerun to step 2; otherwise stop.

#### 5.2.4 First-Order Reliability Method

From the foregoing second property in the  $\mathbf{u}$ -space, it follows that the design point  $\mathbf{u}^*$ , which is the point on the failure surface  $\{\mathbf{u} \mid G(\mathbf{u}) = 0\}$  closest to the origin, has the highest probability density among all failure points in the standard normal space. As a result, the main contribution to the probability integral comes from the neighborhood of the design point  $\mathbf{u}^*$ , provided that the limit-state surface is not strongly distorted and there is only one design point. In such a case, the limit-state surface in the neighborhood of design point can be well approximated by a tangent hyperplane for which the probability content is readily available.

In the first-order reliability method, the limit-state surface is approximated by the tangent hyperplane at design point (Hasofer and Lind 1974; Rackwitz and Fiessler 1978; Ditlevsen 1981; Hobenbichler and Rackwitz 1981), namely, the limit-state surface in the  $\mathbf{u}$ -space is replaced by its first-order Taylor series expansion at  $\mathbf{u}^*$  as

$$G(\mathbf{u}) = G(\mathbf{u}^*) + \nabla G(\mathbf{u}^*)(\mathbf{u} - \mathbf{u}^*) \quad (5.18)$$

where  $\nabla G(\mathbf{u}^*)$  is the gradient  $G(\mathbf{u})$  evaluated at the design point  $\mathbf{u}^*$ . The first-order estimate of failure probability,  $p_{f1}$ , is then equal to the probability content defined by the linearized failure domain, as given by

$$P_{f1} = \int_{\nabla G(\mathbf{u}^*)} \phi(\mathbf{u}) d\mathbf{u} = \Phi(-\beta) \quad (5.19)$$

where  $\Phi(\cdot)$  is the CDF of the standard normal variate; and  $\beta$ , called the first-order reliability index, corresponds to the distance from the origin to the approximating tangent hyperplane in the  $\mathbf{u}$ -space and is given by

$$\beta = \boldsymbol{\alpha} \cdot \mathbf{u}^* = -\frac{\nabla G(\mathbf{u}^*)}{\|\nabla G(\mathbf{u}^*)\|_2} \cdot \mathbf{u}^* \quad (5.20)$$

in which  $\boldsymbol{\alpha}$  is the normal row vector (directional cosine) at the design point, directing towards the failure domain as shown in **Figure 5.4**.

The first-order reliability method provides a satisfactory approximation of the exact failure probability if the transformed limit-state surface in the  $\mathbf{u}$ -space is flat or nearly flat. Non-flatness in this surface may arise from the nonlinearity in the limit-state function  $g(\mathbf{x})$  and the nonlinearity in distribution information transformations when  $\mathbf{x}$  has a non-normal distribution. In such a case, a higher-order approximating surface, such as a quadratic surface, may be used to improve the accuracy of the approximation as described in the following section.

### 5.2.5 Second-Order Reliability Method

In the second-order reliability method, the limit-state surface is approached by a second-order surface fitted to the design point. Such an approximation was first investigated by Fiessler *et al.* (1979). However, their results, which are derived for the general quadratic surfaces, are too cumbersome for practical use and the resulting probability integrals can only be solved numerically. After that, it soon became obvious that a parabolic approximation to the limit-state surface is more

preferred, for which the probability content is much easier to compute (Breitung 1984; Der Kiureghian *et al.* 1987; Tvedt 1990).

As its name implies, the second-order reliability method involves a second-order approximation to the limit-state surface. Making use of  $G(\mathbf{u}) = 0$  at the design point, the second-order Taylor series expansion of the limit-state function  $G(\mathbf{u})$  at the design point  $\mathbf{u}^*$  is expressed as

$$\begin{aligned}
 G(\mathbf{u}) &= \nabla G(\mathbf{u}^*) (\mathbf{u} - \mathbf{u}^*) + \frac{1}{2} (\mathbf{u} - \mathbf{u}^*)^T \mathbf{H} (\mathbf{u} - \mathbf{u}^*) \\
 &= \|\nabla G(\mathbf{u}^*)\|_2 \left[ (\beta - \boldsymbol{\alpha} \mathbf{u}) + \frac{1}{2 \|\nabla G(\mathbf{u}^*)\|_2} (\mathbf{u} - \mathbf{u}^*)^T \mathbf{H} (\mathbf{u} - \mathbf{u}^*) \right] \quad (5.21)
 \end{aligned}$$

where  $\boldsymbol{\alpha}$  and  $\beta$  are defined earlier in Equation (5.20); and  $\mathbf{H}$  is the Hessian matrix evaluated at the design point having the elements  $H_{ij} = \partial^2 G(\mathbf{u}) / \partial u_i \partial u_j$   $i, j = 1, \dots, n$ .

To construct the approximating paraboloid, the coordinates of standard normal space are first rotated through an orthogonal transformation

$$\mathbf{u}' = \mathbf{Q} \mathbf{u} \quad (5.22)$$

such that the new  $u'_n$  axis coincides with the normal vector at the design point  $\boldsymbol{\alpha}$ , as illustrated in **Figure 5.4** (the dash line) in the case of two random variables. This is achieved by selecting the  $n$ -th row of the transformation matrix  $\mathbf{Q}$  as the directional cosine of limit-state function at the design point, i.e.  $Q_{nj} = \alpha_j$  ( $j = 1, \dots, n$ ). The remaining rows of  $\mathbf{Q}$  are determined by a suitable orthogonalization scheme, such as the Gram-Schmidt orthogonalization procedure. In other words, this rotation positions the design point on the  $u'_n$  axis of rotated space  $\mathbf{u}'$  such that the coordinates

of the design point are  $[0 \ \cdots \ 0 \ \beta]^T$ . After doing that and keeping only second-order term in  $\mathbf{u}'_{n-1}$ , the limit-state surface in Equation (5.21) is then rewritten in terms of a parabolic approximation in the rotated standard normal space  $\mathbf{u}'$ , as

$$u'_n = \beta + \frac{1}{2} \mathbf{u}'_{n-1 T} \mathbf{A} \mathbf{u}'_{n-1} \quad (5.23)$$

where the matrix  $\mathbf{A}$  is of the size  $(n-1) \times (n-1)$ , whose elements, denoted as  $a_{ij}$ , are computed as

$$A_{ij} = \frac{(\mathbf{Q} \mathbf{H} \mathbf{Q}^T)_{ij}}{\|\nabla G(\mathbf{u}^*)\|_2} \quad (i, j = 1, \dots, n-1) \quad (5.24)$$

Equation (5.23) represents a paraboloid with its apex at the design point. In the special case where the coordinate axes  $u'_i, i = 1, 2, \dots, n-1$  coincide with the principal axes of the paraboloid, the matrix  $\mathbf{A}$  will be diagonal and the paraboloid becomes

$$u'_n = \beta + \frac{1}{2} \sum_{i=1}^{n-1} \kappa_i (u'_i)^2 \quad (5.25)$$

where  $\kappa_i$ 's are the principal curvatures needed to compute the probability content for a paraboloid. In the more general case, Equation (5.25) can be obtained through an additional orthogonal rotation of the  $\mathbf{u}'_{n-1}$  space with each column of the rotation matrix being the eigenvector of matrix  $\mathbf{A}$ , and in that case the  $\kappa_i$ 's are the eigenvalues of the matrix  $\mathbf{A}$ . The paraboloid in Equation (5.25) is tangent to the limit-state surface at the design point and its principal curvatures match those of the limit-state surface at the design point. Thus the approximating paraboloid is also termed as the curvature-fitted paraboloid.

The paraboloid defined in Equation (5.23) is only approximate to the complete second-order surface around the design point since only second-order terms in  $\mathbf{u}'_{n-1}$  are kept. However, the probability content associated with the above-defined paraboloid is much easier to compute. Because the standard normal space is rotationally symmetric, this probability, denoted as  $p_{f_2}$ , is completely defined by  $\beta$  and the set of curvatures  $\kappa_i$ ,  $i=1, \dots, n-1$ . Several formulae available for computing the probability content for the paraboloid are provided in the following.

A simple closed-form formula was presented by Breitung (1984) using the theory of asymptotic analysis, as

$$p_{f_2}^{\text{Breitung}} \cong \Phi(-\beta) \prod_{i=1}^{n-1} (1 + \beta \kappa_i)^{-0.5} \quad (5.26)$$

where  $\kappa_i$  denotes the principal curvatures of paraboloid at the design point, and  $\beta$  is the reliability index determined using FORM. Breitung proved that this second-order probability estimate approaches asymptotically the first-order estimate and the true failure probability when  $\beta$  is sufficiently large and  $\beta \kappa_i$  remains constant. For small  $\beta$  values, the approximation was slightly modified by Hohenbichler and Rackwitz (1988) as

$$p_{f_2}^{\text{H-R}} = \Phi(-\beta) \prod_{i=1}^{n-1} \left( 1 + \frac{\phi(-\beta)}{\Phi(-\beta)} \kappa_i \right)^{-0.5} \quad (5.27)$$

Tvedt derived a three-term approximation to probability content of the paraboloid by a power series expansion in terms of  $\mathbf{u}'_{n-1} \mathbf{A} \mathbf{u}'_{n-1}$ , neglecting the terms of the order higher than two (Madsen *et al.* 1986). The resulting formula is

$$p_{f_2}^{\text{Tvedt1}} = p_{f_2}^{\text{Breitung}} + A_1 + A_2 \quad (5.28)$$

where

$$A_1 = [\beta\Phi(-\beta) - \phi(\beta)] \left\{ \prod_{i=1}^{n-1} (1 + \beta\kappa_i)^{-0.5} - \prod_{i=1}^{n-1} (1 + (1 + \beta)\kappa_i)^{-0.5} \right\} \quad (5.29)$$

$$A_2 = (\beta + 1) [\beta\Phi(-\beta) - \phi(\beta)] \left\{ \prod_{i=1}^{n-1} (1 + \beta\kappa_i)^{-0.5} - \operatorname{Re} \left[ \prod_{i=1}^{n-1} (1 + (i + \beta)\kappa_i)^{-0.5} \right] \right\} \quad (5.30)$$

where  $\operatorname{Re}(\cdot)$  is real part of the quantity in the parentheses; and  $i = \sqrt{-1}$ .

Tvedt (1990) further derived an exact result for probability content of the paraboloid in the form of the single-fold integral, which is more complex to evaluate. Tvedt's exact formula is

$$p_{f_2}^{\text{Tvedt2}} = \varphi(\beta) \operatorname{Re} \left\{ i \left( \frac{2}{\pi} \right)^{0.5} \int_0^{i\infty} \left[ \frac{1}{s} e^{\frac{(s+\beta)^2}{2}} \prod_{i=1}^{n-1} (1 - \kappa_i s)^{-0.5} \right] ds \right\} \quad (5.31)$$

In summary, computing the second-order estimate of failure probability according to the above formulae involves the following steps after determining the design point

- (1) Construct the orthogonal matrix  $\mathbf{Q}$  with  $\boldsymbol{\alpha}$  as its last row;
- (2) Evaluate the Hessian matrix  $\mathbf{H}$  at the design point in the standard normal space by the finite difference method;
- (3) Calculate the matrix  $\mathbf{A}$  and then determine its eigenvalues;
- (4) Compute the second-order approximation of the failure probability using either formula described above.

### 5.2.6 Parameter Sensitivity Measures

An important feature of FORM is that it provides measures of the reliability index sensitivity and the first-order failure probability sensitivity with respect to the basic random variables and with respect to the parameters defining the probability distributions. The first set of such sensitivity measures is with respect to the variation of the design point  $\mathbf{u}^*$  in the standard normal space. This sensitivity measure is given by the normal vector at the design point, namely

$$\frac{\partial \beta}{\partial \mathbf{u}^*} = \boldsymbol{\alpha}^T \quad (5.32)$$

where  $\partial \beta / \partial \mathbf{u}^* = [\partial \beta / \partial u_1^* \ \cdots \ \partial \beta / \partial u_n^*]^T$  denotes the column vector of partial derivatives, providing a measure of relative importance of each standard normal variates  $u_i$ . According to the chain rule of differentiation, the reliability index sensitivity with respect to the design point in the original  $\mathbf{x}$ -space which is given by  $\mathbf{x}^* = \mathbf{T}^{-1}(\mathbf{u}^*)$ , is

$$\frac{\partial \beta}{\partial \mathbf{x}^*} = \boldsymbol{\alpha}^T \mathbf{J}_{\mathbf{u},\mathbf{x}} \quad (5.33)$$

However, it is noted that the sensitivity in Equation (5.33) depends on the units of basic variables  $x_i$ . Therefore, to compare the relative importance of each variable, Der Kiureghian and Ke (1985) defined the unit dimensionless vector as

$$\boldsymbol{\gamma} = \frac{\boldsymbol{\alpha}^T \mathbf{J}_{\mathbf{u},\mathbf{x}} \mathbf{D}}{\|\boldsymbol{\alpha}^T \mathbf{J}_{\mathbf{u},\mathbf{x}} \mathbf{D}\|_2} \quad (5.34)$$

where  $\mathbf{D}$  is the diagonal matrix of standard deviations of the variables  $\mathbf{x}$ .

Other sensitivity measures of reliability index are with respect to the parameter  $\theta$  in distribution function of  $\mathbf{x}$ . The reliability index sensitivity with respect to distribution parameter  $\theta$  is given by

$$\frac{\partial \beta}{\partial \theta} = \boldsymbol{\alpha} \frac{\partial \mathbf{u}}{\partial \theta} = \boldsymbol{\alpha} \frac{\partial \mathbf{T}(\mathbf{x})}{\partial \theta} \quad (5.35)$$

Of particular interest among the sensitivities to the distribution parameters are the sensitivity vectors with respect to the mean vector,  $\boldsymbol{\mu} = \{\mu_1 \ \cdots \ \mu_n\}$ , and the standard deviation vector  $\boldsymbol{\sigma} = \{\sigma_1 \ \cdots \ \sigma_n\}$  of the random variables. When scaled by the diagonal matrix of standard deviations, these sensitivity vectors are expressed as

$$\boldsymbol{\delta} = \text{diag}(\boldsymbol{\sigma}) \frac{\partial \beta}{\partial \boldsymbol{\mu}} \quad \boldsymbol{\eta} = \text{diag}(\boldsymbol{\sigma}) \frac{\partial \beta}{\partial \boldsymbol{\sigma}} \quad (5.36)$$

which represent dimensionless variation in  $\beta$  with respect to variation in the mean and standard deviation of each variable. The former vector gives the relative importance of the random variables in terms of their central values; whereas the latter gives the relative importance with respect to their variability.

The sensitivities of the first-order failure probability with respect to the above-mentioned quantities are readily obtained by the chain rule of differentiation to Equation (5.19). For example, the first-order failure probability sensitivity with respect to the distribution parameter is obtained as

$$\frac{\partial p_{f_1}}{\partial \theta} = -\varphi(\beta) \frac{\partial \beta}{\partial \theta} \quad (5.35)$$

All above sensitivity measures have been shown useful to reduce the number of random variables, as FORM/SORM is presently limited to several hundreds up to about a thousand basic random variables (Rackwitz 2001). When the variability of a random variable has a relatively small influence on reliability index, then that variable can be replaced with a deterministic quantity, such as mean value or median value, thus reducing the dimension of basic random variables. The above sensitivity measures are also useful in the structural design and condition assessment (Melchers 1999). They can be used to identify the variables or parameters which have major contributions to the failure probability, thus providing an effective means to improve the design. These measures also help in gaining insights into the complex behaviour of structural systems.

### **5.3 Linear FE Reliability Analysis Method**

As discussed in the previous section, the first- and second-order structural reliability methods require the computation of structural response involved in the limit-state function and the response gradient. When the limit-state function is explicitly given, the computation of the limit-state function and its gradient at a particular point is straightforward. However, for a realistic structure, the structural response involved in the limit-state function can only be numerically solved by the FE technique as the relation between structural response and random structural parameters is not analytically known. For example, for a large-scale bridge, it is difficult to express analytically the displacement of a node in terms of random structural parameters such as Young's modulus and cross-section areas. In addition, in such a case the response gradient needs also to be computed numerically by the FE technique. Therefore, in order to analyze the failure probability for a realistic structure, the FE

technique should be embedded into the reliability method to compute the structural response and response gradient. The flowchart of FERM is outlined in **Figure 5.5**. The use of the FE technique for computing structural response (nodal displacement and internal force) and its gradient is briefly explained in the next two sections.

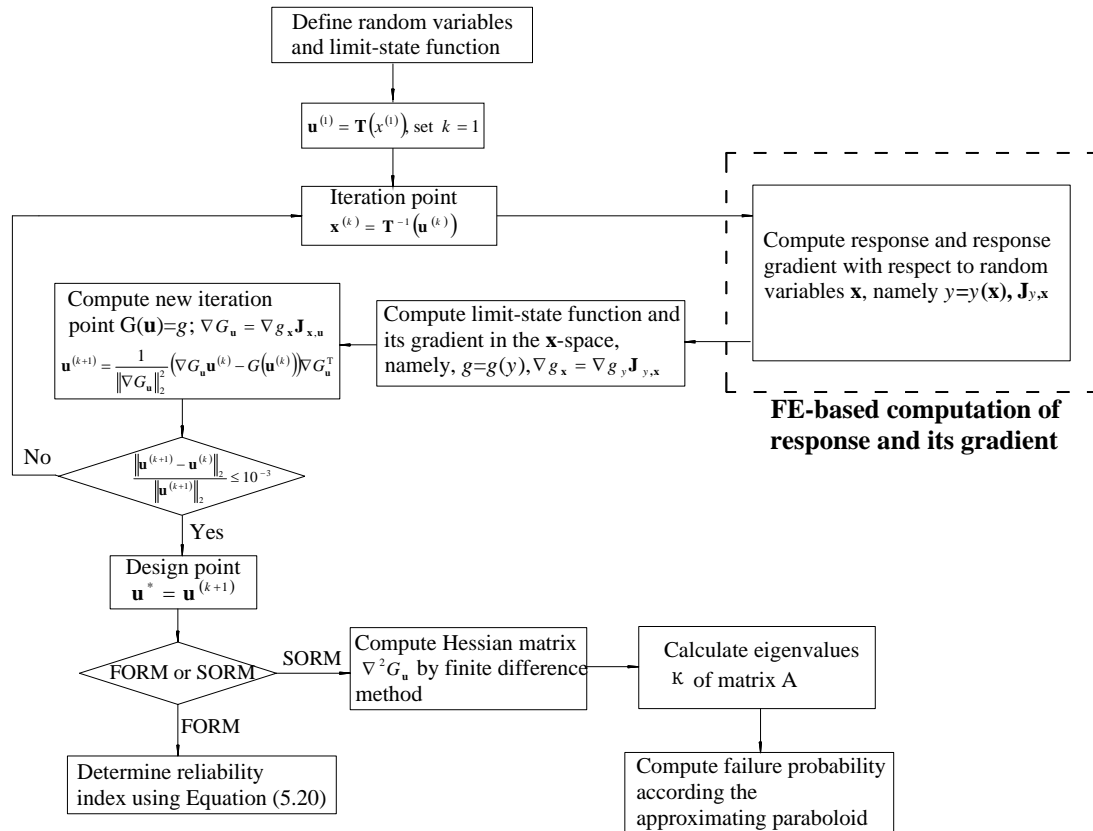


**Figure 5.5 Flowchart of FE reliability method**

### 5.3.1 Computation of Response

The static equilibrium equation for a constrained linear elastic structure is expressed as

$$\mathbf{K}(\mathbf{x})\mathbf{y}(\mathbf{x}) = \mathbf{p}(\mathbf{x}) \quad (5.36)$$

where  $\mathbf{x}$  represents a random vector consisting of both the stiffness-related and load-related variables such as Young's modulus, area of cross-section, moment of inertia, and external loadings;  $\mathbf{K}$  is the global stiffness matrix in terms of the stiffness-related structural parameters;  $\mathbf{p}$  is the equivalent random nodal load vector; and the displacement vector  $\mathbf{y}$  is a function of the random vector  $\mathbf{x}$ . For a specific realization of the random vector  $\mathbf{x}$ , standard procedures are available to assemble Equation (5.36) and to solve for the nodal displacements (Bathe 1996).

After determining the nodal displacements, the internal forces of each element can also be obtained. **Figure 5.6** illustrates a general planar truss element connecting with two nodes  $i$  and  $j$ , where  $u$  and  $v$  are the nodal displacements in the global coordinate system  $XY$  and  $\bar{u}$  is the nodal displacement in the local coordinate system. The member forces of a truss element are given by

$$\begin{Bmatrix} F_i^e \\ F_j^e \end{Bmatrix} = \frac{EA}{L} \begin{bmatrix} 1 & -1 \\ -1 & 1 \end{bmatrix} \begin{Bmatrix} \bar{u}_i \\ \bar{u}_j \end{Bmatrix} \quad (5.37)$$

where  $F_i^e$  and  $F_j^e$  are internal forces at both ends of element  $e$ ;  $EA$  and  $L$  are the axial rigidity and length of element  $e$ , respectively; and  $\bar{u}_i$  and  $\bar{u}_j$  are the nodal displacements in the local coordinate system. As the nodal displacements solved from Equation (5.36) are in the global coordinate system, it is required to transform them into the local coordinate system as

$$\begin{Bmatrix} \bar{u}_i \\ \bar{u}_j \end{Bmatrix} = \begin{bmatrix} l_{\bar{x}x} & l_{\bar{x}y} & 0 & 0 \\ 0 & 0 & l_{\bar{x}x} & l_{\bar{x}y} \end{bmatrix} \begin{Bmatrix} u_i \\ v_i \\ u_j \\ v_j \end{Bmatrix} \quad (5.38)$$

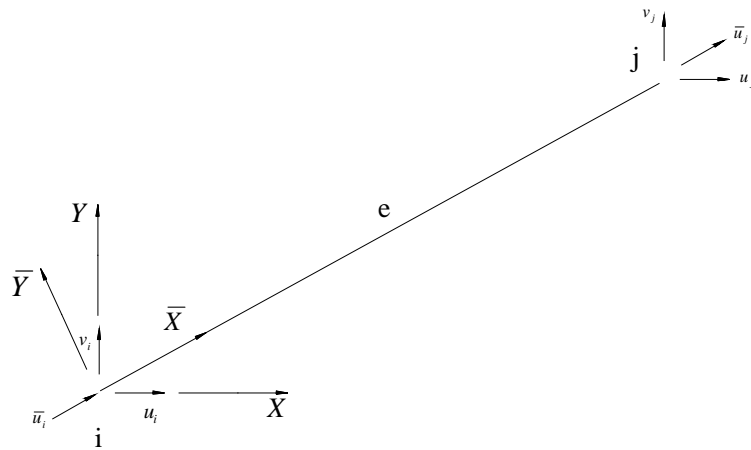


**Figure 5.6 Illustration of a planar truss element**

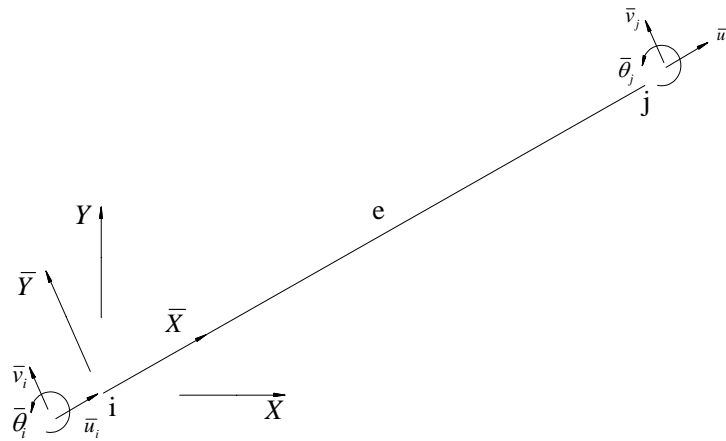


**Figure 5.7 Illustration of a planar frame element**

where  $l_{\bar{x}x}$  and  $l_{\bar{x}y}$  are the directional cosines between local  $\bar{X}$ -axis and global coordinate system  $XY$ . Substituting Equation (5.38) into Equation (5.37) allows evaluation of the axial forces of truss members.

**Figure 5.7** shows a general planar frame element with two nodes, for which the member forces are given by

$$\begin{Bmatrix} F_{Xi}^e \\ F_{Yi}^e \\ M_{\theta i} \\ F_{Xj}^e \\ F_{Yj}^e \\ M_{\theta j} \end{Bmatrix} = \begin{bmatrix} \frac{EA}{L} & 0 & 0 & -\frac{EA}{L} & 0 & 0 \\ & \frac{12EI}{L^3} & \frac{6EI}{L^2} & 0 & -\frac{12EI}{L^3} & \frac{6EI}{L^2} \\ & & \frac{4EI}{L} & 0 & -\frac{6EI}{L^2} & \frac{2EI}{L} \\ & & & \frac{EA}{L} & 0 & 0 \\ & & & & \frac{12EI}{L^3} & -\frac{6EI}{L^2} \\ & & & & & \frac{4EI}{L} \end{bmatrix} \begin{Bmatrix} \bar{u}_i \\ \bar{v}_i \\ \bar{\theta}_i \\ \bar{u}_j \\ \bar{v}_j \\ \bar{\theta}_j \end{Bmatrix} \quad (5.39)$$

Symmetry

where  $EA$  and  $EI$  are the axial and flexural rigidities of element  $e$ ;  $L$  is the element length; and  $\bar{u}$ ,  $\bar{v}$ , and  $\bar{\theta}$  are the nodal displacements in the local coordinate system. Similar to truss elements, the transformation of such nodal displacements to the nodal displacements in the local coordinate system reads as

$$\begin{Bmatrix} \bar{u}_i \\ \bar{v}_i \\ \bar{\theta}_i \\ \bar{u}_j \\ \bar{v}_j \\ \bar{\theta}_j \end{Bmatrix} = \begin{bmatrix} l_{xx} & l_{xy} & 0 & 0 & 0 & 0 \\ l_{xx} & l_{xy} & 0 & 0 & 0 & 0 \\ 0 & 0 & 1 & 0 & 0 & 0 \\ 0 & 0 & 0 & l_{xx} & l_{xy} & 0 \\ 0 & 0 & 0 & l_{xx} & l_{xy} & 0 \\ 0 & 0 & 0 & 0 & 0 & 1 \end{bmatrix} \begin{Bmatrix} u_i \\ v_i \\ \theta_i \\ u_j \\ v_j \\ \theta_j \end{Bmatrix} \quad (5.40)$$

After presenting Equation (5.40) into Equation (5.39), the member forces of planar frame elements are obtained.

### 5.3.2 Computation of Response Gradient

Taking derivatives of both sides of Equation (5.36) with respect to the  $k$ th random variable  $x_k$ , one obtains the nodal displacement gradients, as

$$\frac{\partial \mathbf{y}}{\partial x_k} = \mathbf{K}^{-1} \left( \frac{\partial \mathbf{p}}{\partial x_k} - \frac{\partial \mathbf{K}}{\partial x_k} \mathbf{y} \right) \quad (5.41)$$

where

$$\frac{\partial \mathbf{y}}{\partial x_k} = \begin{Bmatrix} \frac{\partial y_1}{\partial x_k} \\ \frac{\partial y_2}{\partial x_k} \\ \vdots \\ \frac{\partial y_N}{\partial x_k} \end{Bmatrix}; \quad \frac{\partial \mathbf{K}}{\partial x_k} = \begin{bmatrix} \frac{\partial k_{11}}{\partial x_k} & \frac{\partial k_{12}}{\partial r_k} & \dots & \frac{\partial k_{1N}}{\partial x_k} \\ \frac{\partial k_{21}}{\partial x_k} & \frac{\partial k_{21}}{\partial r_k} & \dots & \frac{\partial k_{2N}}{\partial x_k} \\ \vdots & \vdots & \ddots & \vdots \\ \frac{\partial k_{N1}}{\partial x_k} & \frac{\partial k_{n1}}{\partial x_k} & \dots & \frac{\partial k_{NN}}{\partial x_k} \end{bmatrix} \quad (5.42)$$

with  $N$  being the number of degrees of freedom. In the case that  $x_k$  is the stiffness-related variable, the derivatives of the external loadings with respect to  $x_k$  will be zero; otherwise, the derivatives of stiffness matrix  $\mathbf{K}$  with respect to  $x_k$  will vanish. Only back-substitution is required for solving Equation (5.41) as the global stiffness matrix  $\mathbf{K}$  has been decomposed during solving Equation (5.36). Making use of the correlation between internal forces and nodal displacements given in Equations (5.37) and (5.39), we can obtain the gradient of the internal forces with respect to the random variables.

In the above two sections, the expressions of nodal displacement and its gradient have been derived, both of which are essential for analyzing the failure probabilities associated with the displacement limit-state function. Likewise, both the derived expressions of internal force and its gradient are indispensable to determine the failure probabilities associated with the stress limit-state function.

## 5.4 Numerical Examples

In this section, four examples are provided to demonstrate the reliability analysis using the developed computer code for the linear FERM. The first example involves the computation of failure probability defined by a linear limit-state function. In this

example, the nonlinearity in the limit-state function in standard normal space arises from the probability transformation. In the second example, the failure probability defined by a nonlinear limit-state function is computed. The last two examples address the reliability analysis for two truss bridges, namely a statically determinate truss and a statically indeterminate one, in which the displacement and stress limit-state functions are considered. For each example in study, the failure probability is computed by FORM/SORM and verified by the Monte Carlo simulation.

#### **5.4.1 Example 1: Reliability for a Linear Limit-State Function**

First, the failure probability defined by a linear limit-state function with five random variables is calculated. The limit-state function is given as

$$g(\mathbf{x}) = x_1 + 2x_2 + 2x_3 + x_4 - 5x_5 - 5x_6 \quad (5.43)$$

where  $x_i$ 's ( $i = 1, 2, \dots, 6$ ) are statistically independent random variables following the Lognormal distribution. The random variables  $x_1$  to  $x_4$  have the same mean of 150 and standard deviation of 15;  $x_5$  has a mean of 50 and a standard deviation of 15;  $x_6$  has a mean of 60 and a standard deviation of 18. The unit of each quantity is kN.m. Failure occurs when the limit-state function  $g(\mathbf{x}) < 0$ .

As described earlier, even the limit-state function in the original  $\mathbf{x}$ -space  $g(\mathbf{x})$  is linear, the corresponding limit-state function in the standard normal space  $G(\mathbf{u})$  becomes nonlinear due to the nonlinearity in probability transformation of the Lognormal distribution to the normal one. Starting with the initial design point at the mean value and following each step of FORM/SORM, the iteration converges to the solution point  $\mathbf{u}^* = [-0.1906, -0.3744, -0.3744, -0.1906, 1.3734, 1.9521]^T$ , which

corresponds to  $\mathbf{x}^* = [146.44, 143.78, 143.78, 146.44, 71.67, 101.93]^T$  in the original  $\mathbf{x}$ -space. After finding the design point, the failure surface is approximated either by a hyperplane or by a paraboloid at the design point, and the corresponding failure probabilities are computed according to the approximating failure surfaces. The first- and second-order failure probabilities and the reliability indices are summarized in Table 5.1. The exact failure probability and corresponding reliability index are obtained as  $9.293 \times 10^{-3}$  and 2.354, respectively, by performing the Monte Carlo simulation. It is seen that both FORM and SORM give a very accurate approximation of the true failure probability.

**Table 5.1 Failure probability and reliability index for example 1 ( $p_f \times 10^{-3}$ )**

<i>Parameter</i>	<i>FORM</i>				<i>SORM</i>					
	$p_{f_1}$	$\beta_1$	$p_{f_2}^{\text{Breitung}}$	$\beta_2^{\text{Breitung}}$	$p_{f_2}^{\text{H-R}}$	$\beta_2^{\text{H-R}}$	$p_{f_2}^{\text{Tvedt1}}$	$\beta_2^{\text{Tvedt1}}$	$p_{f_2}^{\text{Tvedt2}}$	$\beta_2^{\text{Tvedt2}}$
Value	6.954	2.460	9.092	2.362	9.604	2.342	9.336	2.352	9.230	2.356

Table 5.2 gives the sensitivities of the first-order failure probability and the reliability index with respect to distribution parameters, namely the mean and standard deviation. The larger the mean value of the first four random variables, the lower the probability that the limit-state function is larger than zero. This implies that  $\partial p_{f_1} / \partial \mu < 0$  for these four variables. While for the last two variables, the larger their mean values, the higher of failure probability. Thus,  $\partial p_{f_1} / \partial \mu$  is positive for the last two random variables. The values of  $\partial p_{f_1} / \partial \sigma$  for all the variables take negative values. This is explained as that the standard deviation of the limit-state function increases with the increase in the standard deviation of each variable, resulting in an increase in the failure probability.

Now it is assumed that the last two variables follow the type I extreme value distributions (EVD) for the largest value which is commonly used to model environmental loads such as wind loadings and temperature loadings. Following the HL-RF algorithm, the design point in the original  $\mathbf{x}$ -space is determined as [146.70, 144.26, 144.26, 146.70, 69.65, 104.43]<sup>T</sup>. Table 5.3 summarizes the FORM and SORM results. The exact failure probability and corresponding reliability index in this case are  $11.049 \times 10^{-3}$  and 2.289, respectively. Although both FORM and SORM give satisfactory results, the relative error in this case (6.1% for FORM) is larger than that when the random variables following the Lognormal distribution (4.5% for FORM). The reason is that the nonlinearity in the probability transformation in this case is more significant than that in the previous case.

**Table 5.2 Sensitivities of failure probability and reliability index with respect to distribution parameters**

<i>Variable</i>	$\partial p_{f_1} / \partial \mu$	$\partial p_{f_1} / \partial \sigma$	$\partial \beta_1 / \partial \mu$	$\partial \beta_1 / \partial \sigma$
1	$-1.032 \times 10^{-4}$	$2.892 \times 10^{-5}$	$5.329 \times 10^{-3}$	$-1.493 \times 10^{-3}$
2	$-2.063 \times 10^{-4}$	$9.273 \times 10^{-5}$	$1.065 \times 10^{-2}$	$-4.787 \times 10^{-3}$
3	$-2.063 \times 10^{-4}$	$9.273 \times 10^{-5}$	$1.065 \times 10^{-2}$	$-4.787 \times 10^{-3}$
4	$-1.032 \times 10^{-4}$	$2.892 \times 10^{-5}$	$5.329 \times 10^{-3}$	$-1.493 \times 10^{-3}$
5	$5.129 \times 10^{-4}$	$7.460 \times 10^{-4}$	$-2.648 \times 10^{-2}$	$-3.851 \times 10^{-2}$
6	$4.658 \times 10^{-4}$	$1.357 \times 10^{-3}$	$-2.405 \times 10^{-2}$	$-7.007 \times 10^{-2}$

**Table 5.3 Failure probability and reliability index when following type I EVD for the largest value ( $p_f \times 10^{-3}$ )**

<i>Parameter</i>	<i>FORM</i>				<i>SORM</i>					
	$p_{f_1}$	$\beta_1$	$p_{f_2}^{\text{Breitung}}$	$\beta_2^{\text{Breitung}}$	$p_{f_2}^{\text{H-R}}$	$\beta_2^{\text{H-R}}$	$p_{f_2}^{\text{Tvedt1}}$	$\beta_2^{\text{Tvedt1}}$	$p_{f_2}^{\text{Tvedt2}}$	$\beta_2^{\text{Tvedt2}}$
Value	7.579	2.429	10.822	2.297	11.759	2.267	11.272	2.281	10.900	2.294

### 5.4.2 Example 2: Reliability for a Nonlinear Limit-State Function

The reliability analysis for a nonlinear limit-state function is conducted in this example, where the limit-state function is defined as

$$g(\mathbf{x}) = 1.7 - \frac{x_2}{1000x_3} - \left(\frac{x_1}{200x_3}\right)^2 - \frac{x_5}{1000x_6} - \left(\frac{x_4}{200x_6}\right)^2 \quad (5.44)$$

where  $x_i$ 's ( $i = 1, 2, \dots, 6$ ) are statistically independent random variables following the Lognormal distribution as summarized in Table 5.4.

Table 5.5 summarizes the failure probability and reliability index results for this example obtained by FORM/SORM. Following the Monte Carlo simulation, the exact failure probability and reliability index are obtained as  $1.910 \times 10^{-1}$  and 0.874, respectively. It is seen that both the FORM and SORM results are fairly satisfactory.

**Table 5.4 Distribution type and its parameters**

<i>Variable</i>	<i>Distribution type</i>	<i>Mean</i>	<i>Standard deviation</i>	<i>Coefficient of variation</i>
1	Lognormal	500	100	0.2
2	Lognormal	2000	600	0.3
3	Lognormal	5	1.5	0.3
4	Lognormal	450	180	0.4
5	Lognormal	1800	720	0.4
6	Lognormal	4.5	0.9	0.2

**Table 5.5 Failure probability and reliability index results ( $p_f \times 10^{-1}$ )**

<i>Parameter</i>	<i>FORM</i>				<i>SORM</i>					
	$P_{f_1}$	$\beta_1$	$P_{f_2}^{\text{Breitung}}$	$\beta_2^{\text{Breitung}}$	$P_{f_2}^{\text{H-R}}$	$\beta_2^{\text{H-R}}$	$P_{f_2}^{\text{Tvedt1}}$	$\beta_2^{\text{Tvedt1}}$	$P_{f_2}^{\text{Tvedt2}}$	$\beta_2^{\text{Tvedt2}}$
Value	1.350	1.103	1.790	0.919	2.121	0.799	2.044	0.826	1.938	0.864

### 5.4.3 Example 3: Reliability for a Statically Determinate Truss

The above two examples are concerned with the reliability analysis with explicitly given limit-state functions. Addressed in this example is the reliability analysis for a statically determinate truss bridge through the linear FERM in which both structural response and its gradient are obtained by a numerical manner. For this bridge, the failure of a single member leads to the collapse of the whole bridge.

The truss bridge, as illustrated in **Figure 5.8**, is a simply-supported pin-jointed steel bridge consisting of top members, bottom members, vertical members and diagonal members. In the FE model, a total of 21 planar truss elements, each with two DOFs at every node, are used. Each member has the same area of cross-section  $A = 10^{-2} \text{ m}^2$  and the same mass density  $\rho = 7800 \text{ kg/m}^3$ . The Young's modulus for each member is assumed to be a random variable following the Lognormal distribution with a mean of 200GPa and a standard deviation of 20GPa. The bridge is subject to five vertical loadings and one horizontal loading, all of which are also random variables following the Lognormal distribution. The five vertical loadings have the same mean of 120 kN and standard deviation of 24 kN; and the horizontal loading has a mean of 60 kN and a standard deviation of 12 kN. As a result, a total of 27 random variables are included in this problem. The bridge is considered failure when the vertical displacement at node 9 exceeds a threshold  $v_0$ . Thus the limit-state function is formulated as

$$g(\mathbf{x}) = v_0 - v_9(\mathbf{x}) \quad (5.45)$$

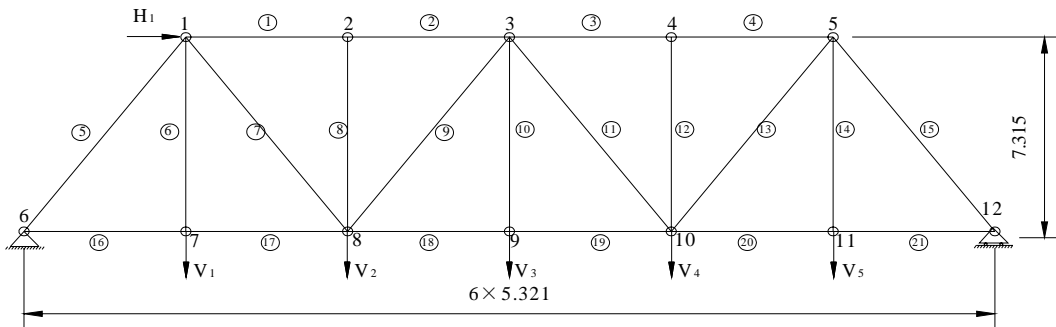


**Figure 5.8 Example of statically determinate truss bridge**

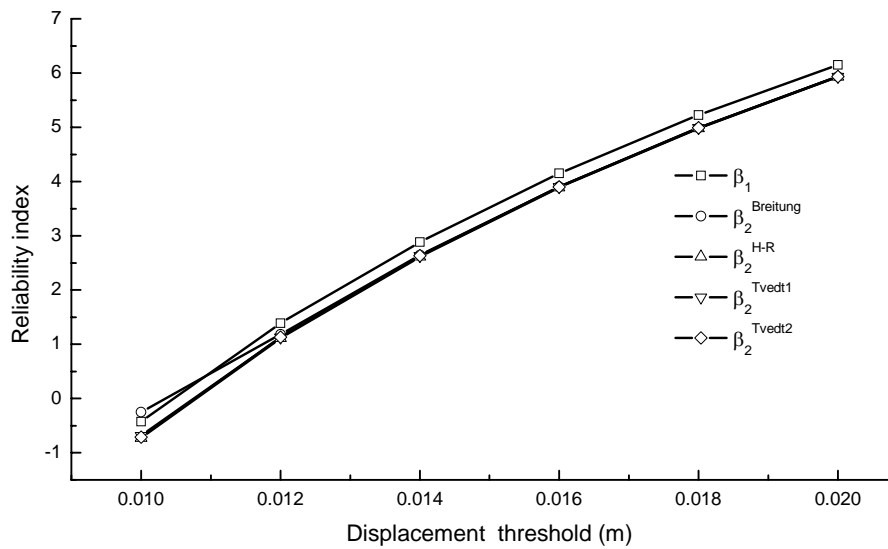


**Figure 5.9 Variation of reliability index with displacement threshold for statically determinate truss bridge**

Making use of the linear FERM, both FORM and SORM are performed for a variety of the threshold  $v_0$  ranging from 0.01 m to 0.02 m. **Figure 5.9** shows the variation of the first- and second-order reliability index versus the displacement threshold. For each threshold, the FORM and SORM results are in a close agreement. This indicates that the vertical displacement at node 9 is almost a linear function of the random variables and the resulting limit-state surface is nearly flat in the standard normal

space, at least at the neighborhood of the design point. In addition, each reliability index grows almost linearly with the displacement threshold.

**Table 5.6 Comparison of mean-value point and design point**

<i>Variable</i>	<i>Mean value</i>	<i>Design point</i>	<i>Variable</i>	<i>Mean value</i>	<i>Design point</i>
$x_1$	$2 \times 10^{11}$	$1.865 \times 10^{11}$	$x_{15}$	$2 \times 10^{11}$	$1.817 \times 10^{11}$
$x_2$	$2 \times 10^{11}$	$1.865 \times 10^{11}$	$x_{16}$	$2 \times 10^{11}$	$1.942 \times 10^{11}$
$x_3$	$2 \times 10^{11}$	$1.870 \times 10^{11}$	$x_{17}$	$2 \times 10^{11}$	$1.942 \times 10^{11}$
$x_4$	$2 \times 10^{11}$	$1.870 \times 10^{11}$	$x_{18}$	$2 \times 10^{11}$	$1.783 \times 10^{11}$
$x_5$	$2 \times 10^{11}$	$1.828 \times 10^{11}$	$x_{19}$	$2 \times 10^{11}$	$1.783 \times 10^{11}$
$x_6$	$2 \times 10^{11}$	$1.978 \times 10^{11}$	$x_{20}$	$2 \times 10^{11}$	$1.946 \times 10^{11}$
$x_7$	$2 \times 10^{11}$	$1.882 \times 10^{11}$	$x_{21}$	$2 \times 10^{11}$	$1.946 \times 10^{11}$
$x_8$	$2 \times 10^{11}$	$1.978 \times 10^{11}$	$x_{22}$	$6 \times 10^4$	$6.219 \times 10^4$
$x_9$	$2 \times 10^{11}$	$1.943 \times 10^{11}$	$x_{23}$	$1.2 \times 10^5$	$1.348 \times 10^4$
$x_{10}$	$2 \times 10^{11}$	$1.892 \times 10^{11}$	$x_{24}$	$1.2 \times 10^5$	$1.581 \times 10^5$
$x_{11}$	$2 \times 10^{11}$	$1.932 \times 10^{11}$	$x_{25}$	$1.2 \times 10^5$	$2.143 \times 10^5$
$x_{12}$	$2 \times 10^{11}$	$1.978 \times 10^{11}$	$x_{26}$	$1.2 \times 10^5$	$1.581 \times 10^5$
$x_{13}$	$2 \times 10^{11}$	$1.871 \times 10^{11}$	$x_{27}$	$1.2 \times 10^5$	$1.348 \times 10^5$
$x_{14}$	$2 \times 10^{11}$	$1.978 \times 10^{11}$			

For each of the cases studied, the coordinates of design point  $\mathbf{x}^*$  define the most likely failure values of the basic variables in the failure set. As an example, Table 5.6 lists the most likely values of the basic variables and **Figure 5.10** illustrates the corresponding deformed configuration of the truss bridge when  $v_0 = 0.016$  m superimposed with the undeformed configuration for comparison. As expected, the values of the most likely failure point for the resistance-related variables  $x_1$  to  $x_{21}$  are below their mean values, and those for the load-related variables are above their mean values. The dimensionless sensitivities of the failure probability and reliability index as formulated in Equation (5.35) are summarized in Table 5.7. The zero sensitivity values imply that the corresponding distribution parameters completely do not affect reliability index, which helps to reduce the number of random variables.

Similar to the first example, the sensitivities  $\partial p_{f_i} / \partial \mu$  take positive values for the resistance-related variables and become negative in the case of load-related variable, Again, all the sensitivities  $\partial p_{f_i} / \partial \sigma$  are negative.

**Table 5.7 Sensitivities of failure probability and reliability index with respect to distribution parameters**

<i>Variable</i>	$\sigma \partial p_{f_i} / \partial \mu$	$\sigma \partial \beta_1 / \partial \sigma$	<i>Variable</i>	$\sigma \partial p_{f_i} / \partial \sigma$	$\sigma \partial \beta_1 / \partial \sigma$
$x_1$	0.686	-0.339	$x_{15}$	1.016	-0.649
$x_2$	0.686	-0.339	$x_{16}$	0.207	-0.053
$x_3$	0.656	-0.315	$x_{17}$	0.207	-0.053
$x_4$	0.656	-0.315	$x_{18}$	1.265	-0.936
$x_5$	0.935	-0.565	$x_{19}$	1.265	-0.936
$x_6$	0	0	$x_{20}$	0.181	-0.044
$x_7$	0.576	-0.255	$x_{21}$	0.181	-0.044
$x_8$	0	0	$x_{22}$	-0.336	-0.027
$x_9$	0.200	-0.051	$x_{23}$	-0.756	-0.396
$x_{10}$	0.515	-0.213	$x_{24}$	-1.359	-2.279
$x_{11}$	0.265	-0.076	$x_{25}$	-1.660	-10.114
$x_{12}$	0	0	$x_{26}$	-1.358	-2.279
$x_{13}$	0.648	-0.309	$x_{27}$	-0.755	-0.396
$x_{14}$	0	0			

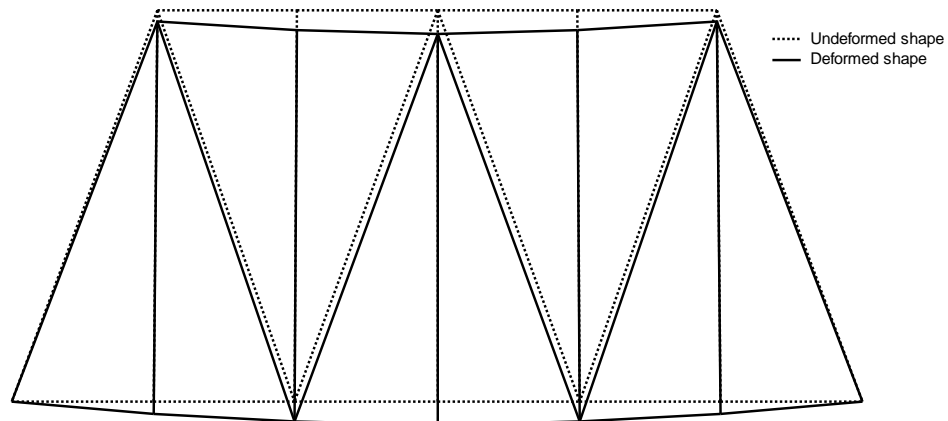


**Figure 5.10 Deformed shape at design point for statically determinate truss bridge**

#### 5.4.4 Example 4: Reliability for a Statically Indeterminate Truss

In this example, the reliability analysis for a statically indeterminate truss bridge is conducted. **Figure 5.11** shows the statically indeterminate truss bridge in study. Similarly, each member of the bridge is modelled as a planar truss element, and a total of 31 planar truss elements are used to model the bridge. Each member in the bridge has the same area of cross-section  $A = 10^{-2} \text{ m}^2$  and the same mass density  $\rho = 7800 \text{ kg/m}^3$ . The Young's modulus for each member is assumed to be a random variable following the Lognormal distribution with a mean of 200 GPa and standard deviation of 60 GPa. The truss bridge is subject to five vertical loadings and seven horizontal loadings, all of which are random variables following the type I EVD for the largest value and are uncorrelated. The five vertical loadings have the same mean of 240 kN and the same standard deviation of 4.8 kN; and the seven horizontal loadings have the same mean of 120 kN and the same standard deviation of 1.2 kN. As a result, a total of 43 random variables are included in this problem. Two types of the limit states, namely the displacement and stress limit states, are considered in this example.

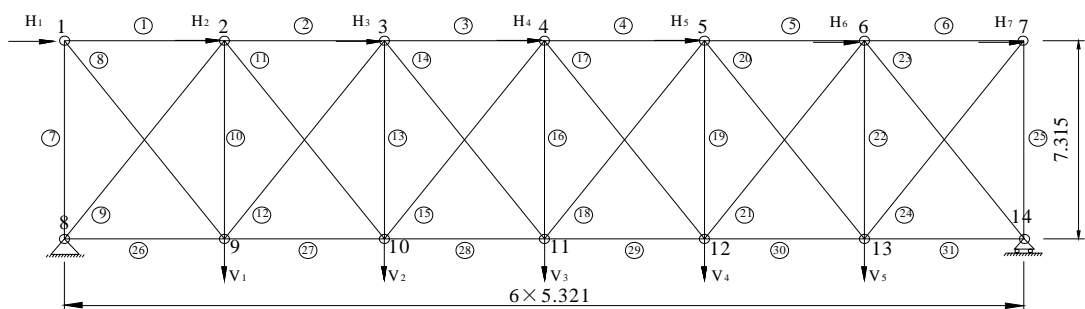


**Figure 5.11 Example of statically indeterminate truss bridge**

The first limit state studied is that the vertical displacement at node 11 exceeds a threshold  $v_0$ . Thus, the limit-state function in this case is formulated as

$$g_1(\mathbf{x}) = v_0 - v_{11}(\mathbf{x}) \quad (5.45)$$

The resulting first- and second-order reliability indices are illustrated in **Figure 5.12** for a series of prescribed threshold  $v_0$ . The FORM and SORM results are again in a close agreement and each reliability index grows linearly with the displacement threshold. **Figure 5.13** shows the deformed shape at the design point superimposed with the undeformed shape for  $v_0 = 0.03$  m. **Figure 5.14** presents the corresponding dimensionless reliability index sensitivities with respect to the distribution parameters of each variable. Similarly, the reliability index sensitivities have positive values for the mean of the resistance-related variables, and become negative for the mean of the load-related variables.

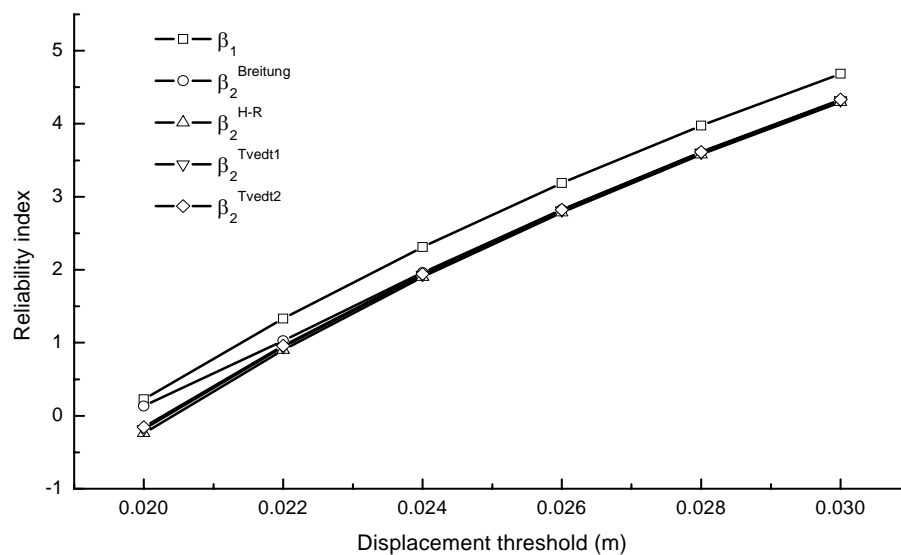


**Figure 5.12** Variation of reliability index with displacement threshold for statically indeterminate truss bridge

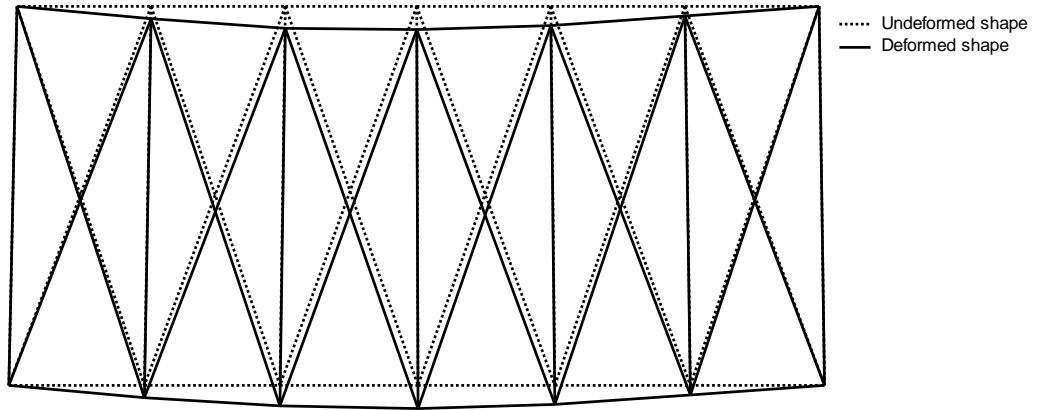


**Figure 5.13 Deformed shape at design point  $s$  for statically indeterminate truss bridge**

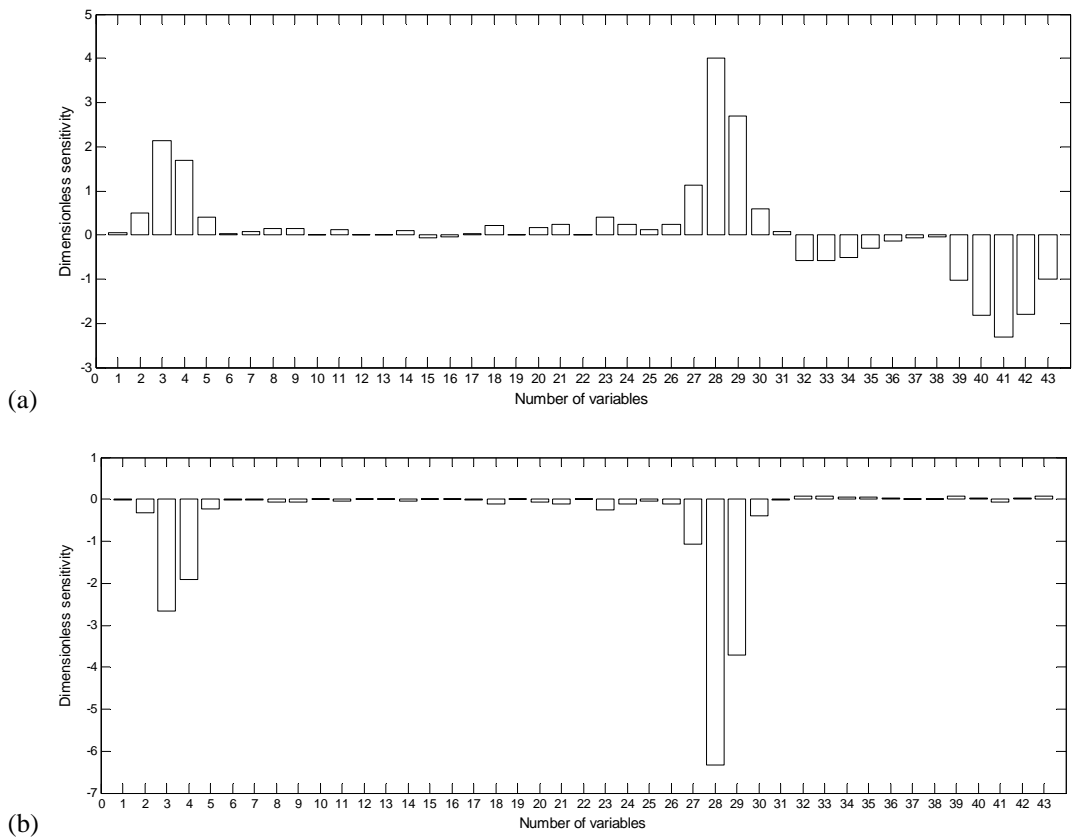


**Figure 5.14 Dimensionless reliability index sensitivity with respect to distribution parameters for displacement limit-state function: (a) mean; (b) standard deviation**

**Table 5.8 Comparison of mean-value point and design point for displacement and stress limit states**

<i>Variable</i>	<i>Mean value</i>	<i>Design point</i>		<i>Variable</i>	<i>Mean value</i>	<i>Design point</i>	
		<i>Displacement</i>	<i>Stress</i>			<i>Displacement</i>	<i>Stress</i>
$x_1$	$2 \times 10^{11}$	$1.882 \times 10^{11}$	$1.909 \times 10^{11}$	$x_{23}$	$2 \times 10^{11}$	$1.67 \times 10^{11}$	$1.910 \times 10^{11}$
$x_2$	$2 \times 10^{11}$	$1.633 \times 10^{11}$	$2.016 \times 10^{11}$	$x_{24}$	$2 \times 10^{11}$	$1.760 \times 10^{11}$	$1.920 \times 10^{11}$
$x_3$	$2 \times 10^{11}$	$1.119 \times 10^{11}$	$7.463 \times 10^{10}$	$x_{25}$	$2 \times 10^{11}$	$1.835 \times 10^{11}$	$1.918 \times 10^{11}$
$x_4$	$2 \times 10^{11}$	$1.220 \times 10^{11}$	$2.031 \times 10^{11}$	$x_{26}$	$2 \times 10^{11}$	$1.764 \times 10^{11}$	$1.938 \times 10^{11}$
$x_5$	$2 \times 10^{11}$	$1.673 \times 10^{11}$	$1.902 \times 10^{11}$	$x_{27}$	$2 \times 10^{11}$	$1.38 \times 10^{11}$	$1.738 \times 10^{11}$
$x_6$	$2 \times 10^{11}$	$1.899 \times 10^{11}$	$1.916 \times 10^{11}$	$x_{28}$	$2 \times 10^{11}$	$8.166 \times 10^{10}$	$2.989 \times 10^{11}$
$x_7$	$2 \times 10^{11}$	$1.864 \times 10^{11}$	$1.906 \times 10^{11}$	$x_{29}$	$2 \times 10^{11}$	$1.007 \times 10^{11}$	$1.755 \times 10^{11}$
$x_8$	$2 \times 10^{11}$	$1.816 \times 10^{11}$	$1.896 \times 10^{11}$	$x_{30}$	$2 \times 10^{11}$	$1.590 \times 10^{11}$	$1.933 \times 10^{11}$
$x_9$	$2 \times 10^{11}$	$1.822 \times 10^{11}$	$1.930 \times 10^{11}$	$x_{31}$	$2 \times 10^{11}$	$1.868 \times 10^{11}$	$1.915 \times 10^{11}$
$x_{10}$	$2 \times 10^{11}$	$1.916 \times 10^{11}$	$1.919 \times 10^{11}$	$x_{32}$	$1.2 \times 10^5$	$1.197 \times 10^5$	$1.199 \times 10^5$
$x_{11}$	$2 \times 10^{11}$	$1.835 \times 10^{11}$	$2.018 \times 10^{11}$	$x_{33}$	$1.2 \times 10^5$	$1.197 \times 10^5$	$1.199 \times 10^5$
$x_{12}$	$2 \times 10^{11}$	$1.916 \times 10^{11}$	$1.928 \times 10^{11}$	$x_{34}$	$1.2 \times 10^5$	$1.197 \times 10^5$	$1.199 \times 10^5$
$x_{13}$	$2 \times 10^{11}$	$1.907 \times 10^{11}$	$2.077 \times 10^{11}$	$x_{35}$	$1.2 \times 10^5$	$1.196 \times 10^5$	$1.198 \times 10^5$
$x_{14}$	$2 \times 10^{11}$	$1.855 \times 10^{11}$	$2.334 \times 10^{11}$	$x_{36}$	$1.2 \times 10^5$	$1.196 \times 10^5$	$1.198 \times 10^5$
$x_{15}$	$2 \times 10^{11}$	$1.963 \times 10^{11}$	$2.105 \times 10^{11}$	$x_{37}$	$1.2 \times 10^5$	$1.196 \times 10^5$	$1.198 \times 10^5$
$x_{16}$	$2 \times 10^{11}$	$1.942 \times 10^{11}$	$2.111 \times 10^{11}$	$x_{38}$	$1.2 \times 10^5$	$1.196 \times 10^5$	$1.198 \times 10^5$
$x_{17}$	$2 \times 10^{11}$	$1.888 \times 10^{11}$	$1.878 \times 10^{11}$	$x_{39}$	$2.4 \times 10^5$	$2.396 \times 10^5$	$2.402 \times 10^5$
$x_{18}$	$2 \times 10^{11}$	$1.770 \times 10^{11}$	$2.041 \times 10^{11}$	$x_{40}$	$2.4 \times 10^5$	$2.399 \times 10^5$	$2.413 \times 10^5$
$x_{19}$	$2 \times 10^{11}$	$1.915 \times 10^{11}$	$1.919 \times 10^{11}$	$x_{41}$	$2.4 \times 10^5$	$2.401 \times 10^5$	$2.415 \times 10^5$
$x_{20}$	$2 \times 10^{11}$	$1.803 \times 10^{11}$	$1.935 \times 10^{11}$	$x_{42}$	$2.4 \times 10^5$	$2.399 \times 10^5$	$2.407 \times 10^5$
$x_{21}$	$2 \times 10^{11}$	$1.757 \times 10^{11}$	$1.889 \times 10^{11}$	$x_{43}$	$2.4 \times 10^5$	$2.396 \times 10^5$	$2.399 \times 10^5$
$x_{22}$	$2 \times 10^{11}$	$1.912 \times 10^{11}$	$1.920 \times 10^{11}$				

Then a stress limit state is considered. The failure criterion is the exceeding of the axial stress of member 28 over 150 MPa, and therefore the limit-state function is

$$g_2(\mathbf{x}) = 150 - s_{28}(\mathbf{x}) \quad (5.46)$$

where  $s_{28}$  is the axial stress of member 28. Similarly the reliability analyses are performed by FORM. Table 5.8 compares the design point and the mean-value point for the displacement and stress limit states. For the displacement limit state, it is

apparent that values of all resistance-related variables at the design point are below their respective mean values. However, for the stress limit state, some of them are below their mean values and some of them are above the mean values. This is because an increase in the mean of some variables causes the increase in the axial stress of member 28, thus they have a positive effect on the failure of this member. It is further substantiated in **Figure 5.15** which shows the dimensionless reliability index sensitivities with respect to the mean of the basic variables. For example, the dimensionless reliability index sensitivity with respect to the mean of the 3rd variable takes a positive value, implying that the decrease of the mean will reduce the reliability index. Thus any structural damage in the third member (corresponding to the third random variable) could significantly change the stress reliability index of member 28. More detailed analysis of the effect of structural damage on reliability index will be made in the next chapter addressing the reliability-based condition assessment based on the stochastic model updating results.

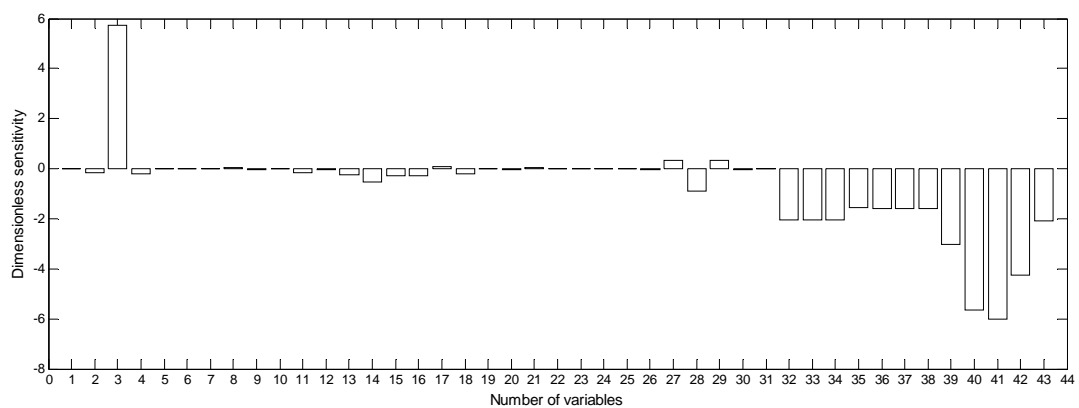


**Figure 5.15 Dimensionless reliability index sensitivity with respect to means of variables for stress limit state**

## 5.5 Summary

In this chapter, the fundamental concepts of reliability methods were first outlined. The popular approximation methods like FORM/SORM were described in detail. The key ingredients of reliability methods including the transformation of the basic random variables into a standard normal space, determination of the design point, approximation of the failure surface and computation of the probability content were discussed. The reliability index sensitivity to distribution parameter was also explained. To analyze the failure probability of large-scale structures with uncertain parameters, the reliability method must be accompanied with the FE technique with the help of which structural responses and response gradients are computed. Based on the established structural reliability method and the FE technique, a computer program for linear FE reliability analysis was developed. This program is able to compute the failure probability defined by both displacement and stress limit-state functions. It is capable of dealing with the various distributions of random variables and provides the reliability index sensitivity to distribution parameters. The developed code will be used to perform the reliability-based condition assessment of existing structures based on stochastic model updating results.

Four examples are provided to demonstrate the reliability analysis using both the explicitly and implicitly defined limit-state functions. The results indicate that both FORM and SORM perform satisfactorily in all the examples. The sensitivity measures of reliability index to distribution parameters are important to identify the significant variables affecting structural reliability.

## **Chapter 6**

# **RELIABILITY-BASED CONDITION ASSESSMENT OF BRIDGES USING STOCHASTIC FE MODEL UPDATING RESULTS**

### **6.1 Introduction**

Engineering structures continuously deteriorate and accumulate damage during their service life due to material degradation and unexpected catastrophic events. Such deterioration and accumulated structural damage will adversely affect the safety and performance of structures. Accordingly, after a period of operation, the condition of an existing structure may be very different from that of the as-built one and the analytical model used for analysis and assessment of structural performance and safety is therefore in need of continuous updating and improvement to incorporate the effect of deterioration and structural damage in the model. For bridge structures, the present demand to carry the ever increasingly heavier vehicles may also differ significantly from that adopted in design. As a result, it is of vital importance to reevaluate structural safety and performance after a period of operation by using the collected data on the structure and external loadings to which the structure may be subject. Due to structural complexity and incomplete data, predicting the reliability for a realistic civil engineering structure is much more difficult than for an idealized system in design stage.

In bridge engineering community, instrumentation-based monitoring has been an accepted technology for surveilling and assessing structural health and condition (Aktan *et al.* 1997; Ko and Ni 2005; Wang 2005). With this innovative technology, the monitoring data can be obtained and used to modify an initial analytical model so that the updated analytical model is more accurate in representing the present structural condition than the initial one. Many FE model improvement algorithms and structural damage detection methods have been developed during the past several decades and some of them have got successful applications in practice. While the development of bridge structural health monitoring systems for model improvement and damage detection has now attained some degree of maturity, the application of monitoring data for instructing bridge inspection, maintenance, and management is still in its infancy. A gap between health monitoring technologies and bridge inspection, maintenance and management exercises exists currently which impedes bridge managers to benefit from the monitoring system. From the monitoring data, the bridge managers want to get answers to the serviceability and safety reliability issues of the structure: (i) has the load capacity or resistance of the structure changed? (ii) what is the probability of failure of structural members and the whole structural system? (iii) how much life is still out there? Indicators of these performance issues are indeed needed to enable the bridge authorities to allocate resources towards inspection, maintenance and rehabilitation of the structure.

In comparison with the myriad of literature addressing on FE model improvement algorithms and structural damage detection methods, research efforts devoted to above issues are very few. As structural reliability is the major decision factor throughout the life cycle of civil engineering structures, methodologies that accept the processed monitoring data as input and produce as output the reliability of the

concerned structure are indeed desirable. The prominent work is due to Yao and his colleagues (Yao 1979; Yao 1983; Natke and Yao 1988; Yao and Natke 1994; Wong and Yao 2001). They proposed a holistic view where health monitoring, damage detection, and reliability evaluation are defined as the sequential components in a value chain. In order to cater for the reliability analysis of instrumented structures, the symptom-based reliability method compatible with health monitoring technologies was introduced in their study. Following this study, Stubbs *et al.* (1998; 2000) developed a methodology to continuously assess the safety of civil engineering structures in which structural damage was first identified using the measurement data of modal parameters and reliability method was then applied to the possibly damaged structure to determine the failure probability and reliability index. However, as discussed earlier, the deterministic model updating approach lacks the capability in accounting for the uncertainties in measurement data, such as measurement errors and inherent randomness. In response to this problem, an improved perturbation method and the MCS method have been applied for statistical identification of structural parameters and Bayesian updating is further implemented to incorporate the prior information if available, as presented in Chapter 4.

The objective of this chapter is to develop a systematic methodology from identifying the statistics of updating parameters, assessing the component reliability index, to making decision on bridge inspection and maintenance using long-term monitoring data. As consistent with reliability analysis, the updating parameters in the FE model are treated as random variables and their statistics are identified from the measured modal parameters taking into account uncertainties; and the updating parameter statistics may be further revised through Bayesian updating when the prior knowledge of structural parameters is available. Making use of the stochastically

updated FE model, structural reliability analysis is then performed to obtain the failure probabilities and reliability indices associated with the predefined limit-state functions using the developed code for linear FE reliability analysis. The established correspondence between reliability index value and required maintenance action is finally used to decide maintenance/repair strategy. Following the proposed approach, health monitoring technology is able to provide quantitative information for bridge inspection and maintenance. Case studies of a statically determinate truss bridge and a statically indeterminate truss bridge are provided to demonstrate the proposed approach.

## **6.2 Probabilistic Approach for Health Monitoring and Condition Assessment**

**Figure 6.1** shows the flowchart of the proposed methodology. Following this methodology, stochastic FE model updating is first performed using the statistics of the measured modal parameters obtained from long-term monitoring systems. In this study, the improved perturbation method described in Chapter 4 is used to achieve the stochastically updated FE model obtained. Making use of this model, structural reliability analysis is then carried out to obtain the reliability indices and failure probabilities for predefined limit-state functions under expected future loads. The established correspondence between reliability index and required maintenance strategy is finally used to decide an appropriate inspection/maintenance action. These steps are explained in detail in the following sections.

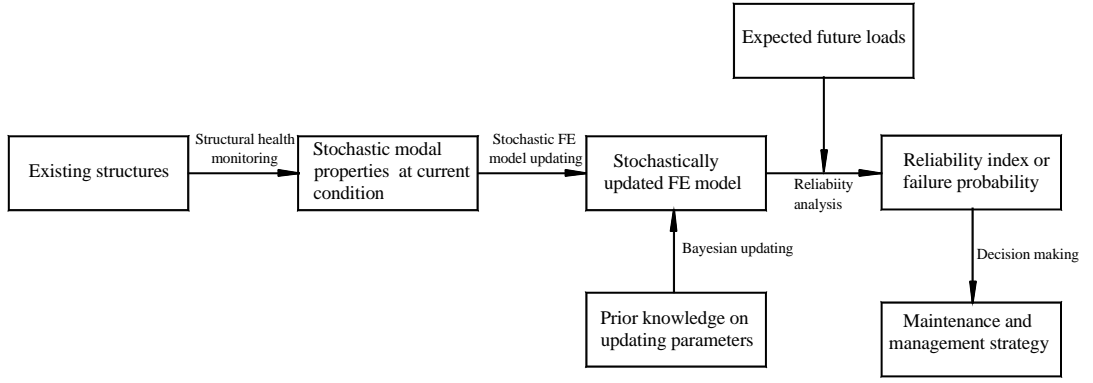


**Figure 6.1 Probabilistic approach for health monitoring and condition assessment**

### 6.2.1 Stochastic FE Model Updating

The content of stochastic FE model updating is briefed for completeness. In FE model updating using measured modal parameters, the identification of structural parameters is formulated in terms of an optimization problem where structural parameters are sought so that the updated FE model can reproduce as closely as possible the measurement data. The objective function is defined as a sum of the weighted squared error

$$J(\boldsymbol{\theta}) = \tilde{\boldsymbol{\varepsilon}}^T \mathbf{W} \tilde{\boldsymbol{\varepsilon}} = \|\mathbf{W}_\varepsilon (\tilde{\mathbf{z}} - \mathbf{z}(\boldsymbol{\theta}))\|_2^2 \quad \text{with } \tilde{\boldsymbol{\varepsilon}} = \tilde{\mathbf{z}} - \mathbf{z}(\boldsymbol{\theta}) \quad (6.1)$$

where  $\tilde{\boldsymbol{\varepsilon}}$  is the output error of modal parameters;  $\tilde{\mathbf{z}}$  and  $\mathbf{z}(\boldsymbol{\theta}) \in R^n$  are vectors of the experimental and analytical modal parameters with  $n = n_f \times (n_m + 1)$ ;  $n_f$  and  $n_m$  are the numbers of measured natural frequencies and measured coordinates of each mode shape, respectively;  $\boldsymbol{\theta} \in R^m$  is a vector consisting of  $m$  updating parameters;  $\mathbf{W}_\varepsilon = \mathbf{W}^{1/2}$  is the diagonal weighting matrix; and the subscript  $T$  represents the transpose of

matrix/vector. In order to obtain a unique solution, the number of known modal data  $n$  should be not less than the number of unknown updating parameters  $m$ .

In practice, the measured modal parameters are uncertain due to natural randomness and measurement errors. In order to take into consideration the uncertainties in measured modal parameters, stochastic FE model updating should be used. The uncertainties in measured modal parameters are assumed herein as normally distributed independent random variables with known statistics. In this study, the measured uncertain modal properties are expressed as the summation of a deterministic part and a random part, that is

$$\tilde{z}_i = \bar{z}_i + Y_i \quad (i = 1, 2, \dots, n) \quad (6.2)$$

where  $\bar{z}_i$  is the mean of the measured modal parameter  $\tilde{z}_i$ ;  $Y_i$  represents the uncertainties in the measured modal parameters due to natural randomness and measurement noise.

With the use of the first-order perturbation method and after some manipulations, the mean and covariance of the updated structural parameters at each iteration step are obtained as

$$\bar{\boldsymbol{\theta}}^{(k+1)} = \bar{\boldsymbol{\theta}}^{(k)} + \Delta \bar{\boldsymbol{\theta}}^{(k)} \quad (6.3)$$

$$\begin{aligned} \text{Var}(\boldsymbol{\theta}^{(k+1)}, \boldsymbol{\theta}^{(k+1)}) = & \left[ \frac{\partial \boldsymbol{\theta}^{(k)}}{\partial \mathbf{Y}} \right] \boldsymbol{\Sigma}_Y \left[ \frac{\partial \boldsymbol{\theta}^{(k)}}{\partial \mathbf{Y}} \right]^T + \left[ \frac{\partial \boldsymbol{\theta}^{(k)}}{\partial \mathbf{Y}} \right] \boldsymbol{\Sigma}_Y \left[ \frac{\partial \Delta \boldsymbol{\theta}^{(k)}}{\partial \mathbf{Y}} \right]^T \\ & + \left[ \frac{\partial \Delta \boldsymbol{\theta}^{(k)}}{\partial \mathbf{Y}} \right] \boldsymbol{\Sigma}_Y \left[ \frac{\partial \boldsymbol{\theta}^{(k)}}{\partial \mathbf{Y}} \right]^T + \left[ \frac{\partial \Delta \boldsymbol{\theta}^{(k)}}{\partial \mathbf{Y}} \right] \boldsymbol{\Sigma}_Y \left[ \frac{\partial \Delta \boldsymbol{\theta}^{(k)}}{\partial \mathbf{Y}} \right]^T \end{aligned} \quad (6.4)$$

in which the quantities have been defined in Chapter 4.

After calculating the updating parameter statistics from the perturbation algorithm, the posterior statistics of structural parameters will be obtained using Bayesian theorem in the case when the prior knowledge on the updating parameters is available. Assume that the structural parameter  $\theta$  was known a *prior* to have a normal distribution with a mean of  $\mu_1$  and a standard deviation of  $\sigma_1$  before performing FE model updating, and with the measurement data the structural parameter is also identified as a normal distribution with a mean of  $\mu_2$  and a standard deviation of  $\sigma_2$ . According to Bayesian theorem, the mean  $\mu$  and standard deviation  $\sigma$  of the structural parameter posterior distribution are obtained as

$$\mu = \frac{\mu_1(\sigma_2)^2 + \mu_2(\sigma_1)^2}{(\sigma_1)^2 + (\sigma_2)^2} \quad (6.5)$$

$$\sigma = \sqrt{\frac{(\sigma_1)^2(\sigma_2)^2}{(\sigma_1)^2 + (\sigma_2)^2}} \quad (6.6)$$

### 6.2.2 Structural Reliability Evaluation

During the life cycle, the health and condition of a structure may deteriorate from material degradation such as fatigue or corrosion, or from structural damage induced in structural members or joints by a severe loading event such as strong wind loads or earthquakes. In other cases, the structure may also be rehabilitated after observing the distress in the structure. All these changes in condition of the structure may lead to a significant change in the structural reliability. Therefore, it is of paramount significance to reevaluate the performance and safety of an existing structure for a certain period.

In the proposed approach, the reassessment of structural reliability is made based on stochastic FE model updating results. After obtaining the identified material property parameters, expected external loading parameters, and the limit-state function  $g(\mathbf{x})$  in terms of a random vector  $\mathbf{x} = (x_1 \ \cdots \ x_n)^T$ , the failure probability associated with the limit-state function  $g(\mathbf{x})$  is defined as the probability that the random vector falls in the failure domain  $g(\mathbf{x}) < 0$ , and is given by the following  $n$ -fold integral

$$p_f = \int \cdots \int_{g(\mathbf{x}) < 0} f_{x_1, x_2, \dots, x_n}(x_1, x_2, \dots, x_n) dx_1 dx_2 \cdots dx_n \quad (6.7)$$

where  $f_{x_1, x_2, \dots, x_n}(x_1, x_2, \dots, x_n)$  denotes the joint PDF of basic random variables  $\mathbf{x}$ .

An alternative to failure probability  $p_f$  as a measure of safety is the reliability index  $\beta$  obtained as

$$\beta = \Phi^{-1}(1 - p_f) = -\Phi^{-1}(p_f) \quad (6.8)$$

in which  $\Phi^{-1}(\cdot)$  is the inverse of the standard normal cumulative distribution function (CDF).

The first-order reliability method (FORM) can be used to compute the probability integral defined in Equation (6.7). FORM uses a linearized hyperplane at the design point in the transformed standard normal space  $\mathbf{u}$  to approach the limit-state surface  $G(\mathbf{u}) = 0$ , and the first-order estimate of failure probability,  $p_{f1}$ , is then equal to the probability content for this linearized failure domain in  $\mathbf{u}$ -space. That is

$$p_{f1} = \int_{\nabla G(\mathbf{u}^*) \cdot (\mathbf{u} - \mathbf{u}^*) \leq 0} \phi(\mathbf{u}) d\mathbf{u} = \Phi(-\beta) \quad (6.9)$$

where  $\Phi(\cdot)$  is the CDF of the standard normal variate; and the reliability index  $\beta$  corresponds to the distance from the origin to the approximating tangent hyperplane and is given by

$$\beta = \boldsymbol{\alpha} \cdot \mathbf{u}^* = -\frac{\nabla G(\mathbf{u}^*)}{\|\nabla G(\mathbf{u}^*)\|_2} \cdot \mathbf{u}^* \quad (6.10)$$

where  $\boldsymbol{\alpha}$  is the normal row vector (directional cosine) at the design point  $\mathbf{u}^*$  directing towards the failure domain. For reliability analysis of a realistic structure, the reliability analysis must be performed in parallel with the FE technique to compute structural response and response gradient needed for searching the design point.

An important feature of FORM is that it provides sensitivity measures of the reliability index or the first-order estimate of failure probability with respect to the random variables. Such sensitivities of the reliability index and the failure probability with respect to the parameters  $\theta$  in the distribution function of  $\mathbf{x}$ , are given, respectively, by

$$\frac{\partial \beta}{\partial \theta} = \boldsymbol{\alpha} \frac{\partial \mathbf{u}}{\partial \theta} = \boldsymbol{\alpha} \frac{\partial \mathbf{T}(\mathbf{x})}{\partial \theta} \quad (6.11)$$

$$\frac{\partial p_{f_i}}{\partial \theta} = -\varphi(\beta) \frac{\partial \beta}{\partial \theta} \quad (6.12)$$

Of particular interests among the sensitivities to the distribution parameters are those with respect to the mean vector  $\boldsymbol{\mu} = \{\mu_1 \ \cdots \ \mu_n\}$  and the standard deviation vector  $\boldsymbol{\sigma} = \{\sigma_1 \ \cdots \ \sigma_n\}$  of the random variables. When scaled by the diagonal matrix of standard deviations, these sensitivity vectors read as

$$\delta = \text{diag}(\sigma) \frac{\partial \beta}{\partial \boldsymbol{\mu}} \quad \boldsymbol{\eta} = \text{diag}(\sigma) \frac{\partial \beta}{\partial \boldsymbol{\sigma}} \quad (6.13)$$

which represent dimensionless variation in  $\beta$  with respect to variation in the mean and standard deviation of each variable. The former vector gives relative importance of the random variables in terms of their central values; whereas the latter gives relative importance with respect to their variances.

### 6.2.3 Decision Making on Maintenance

In the past, the inspection/maintenance of bridge structures was conducted without using reliability- or risk-informed approaches. The traditional technologies for bridge inspection/maintenance may not be ensuring necessary serviceability and cost-effective maintenance and management of structures. Nowadays, research efforts are being made towards the application of reliability-based or risk-informed approaches to maintenance optimization of structures, with the aim of reducing the operation and maintenance expenditures while still providing the structure with a high value of reliability index (Frangopol and Hearn 1996).

When the reliability indices of structural components are obtained at regular intervals, it is possible to decide bridge inspection/maintenance strategy because several researchers have investigated this issue and proposed the correspondence between reliability index value and required maintenance action (Frangopol *et al.* 2001; Lark and Flaig 2005). Table 6.1 shows such a correspondence adopted in the present study (Frangopol *et al.* 2001). **Figure 6.2** illustrates the bridge reliability level versus bridge age assuming no maintenance is made. Note that a new bridge structure is not necessary in excellent condition (state 5) and that the linear bridge reliability profile

represents an approximation to the nonlinear reliability degradation that might exist in reality. According to this correspondence, no action is required when the existing reliability index is larger than 9.0; inspection may become necessary if the reliability index lies in the range from 6.0 to 9.0; possible strengthening in advance may reduce the life-cycle costs if the reliability index is further degraded; and finally immediate action, such as reducing the loads or rehabilitation of the structure, is required when the estimated reliability index falls below 4.6. Thus a linkage among the structural health monitoring, bridge reliability assessment, and decision making on bridge maintenance has been established, with which the health monitoring technology is able to provide quantitative information on maintenance and management exercises.

**Table 6.1 Relation between reliability index and maintenance action**

<i>Safety state</i>	<b>5</b>	<b>4</b>	<b>3</b>	<b>2</b>	<b>1</b>
Reliability index	$\beta > 9.0$	$9.0 > \beta > 8.0$	$8.0 > \beta > 6.0$	$6.0 > \beta > 4.6$	$4.6 > \beta$
Attribute for Safety	excellent	very good	Good	fair	unacceptable
Maintenance Action	no action	preventive inspection	detailed inspection	possible strengthening	rehabilitation

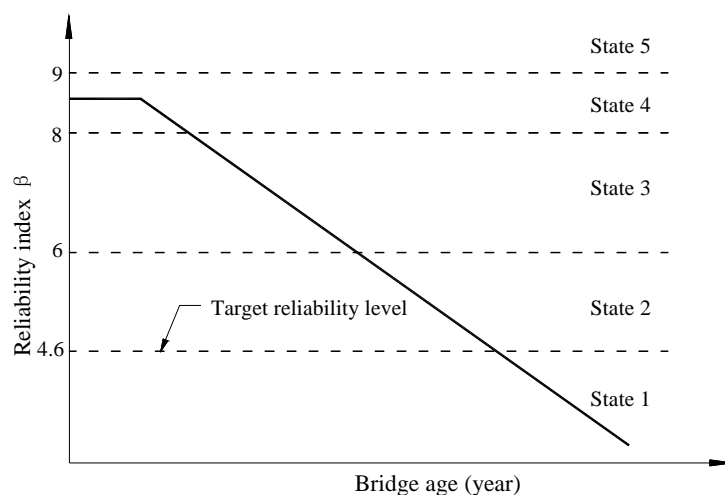


**Figure 6.2 Bridge reliability profile without maintenance and management (after Frangopol *et al.* 2001)**

It should be pointed out that while the establishment of the correspondence between reliability index and optimum maintenance action is possible but the development of such a correspondence is not necessarily straightforward and is still faced with several difficulties (Frangopol 1999; Frangopol *et al.* 2001). In order to achieve the optimum strategy that ensures an adequate level of reliability at the lowest possible life-cycle cost, life-cycle cost analysis is required to integrate with structural reliability analysis for each of the possible inspection/maintenance strategies. Issues such as target reliability level, whole life performance (reliability) assessment, and optimum inspection/maintenance strategies for bridges have to be analyzed and solved from a life-cycle cost perspective (Ang and De Deon 1997; Melchers 1999).

## **6.3 Applications**

### ***6.3.1 Example 1: A Statically Determinate Truss Bridge***

A statically determinate truss bridge is used as the first example to illustrate the proposed methodology. The truss bridge, as shown in **Figure 6.3**, is a simply-supported pin-jointed steel bridge consisting of top members, bottom members, vertical members and diagonal members. An analytical model (nominal model) is assumed for structural analysis and condition assessment; this model may also represent the bridge without structural damage as used in the previous chapters. In the nominal model as shown in **Figure 6.4**, a total of 21 planar truss elements, each with two DOFs at every node, are used. The material properties used in this model are as follows: mass density  $\rho = 7800 \text{ kg/m}^3$ , area of cross section  $A = 10^{-2} \text{ m}^2$  for each member, and the Young's modulus  $E = 200 \text{ GPa}$  for each member.

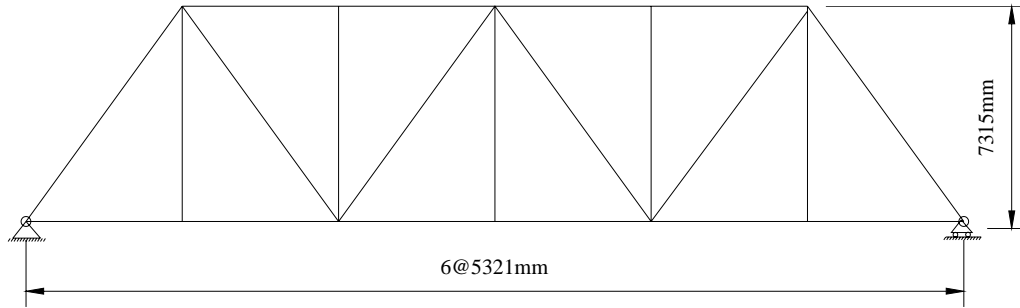


**Figure 6.3 Configuration of statically determinate truss bridge**

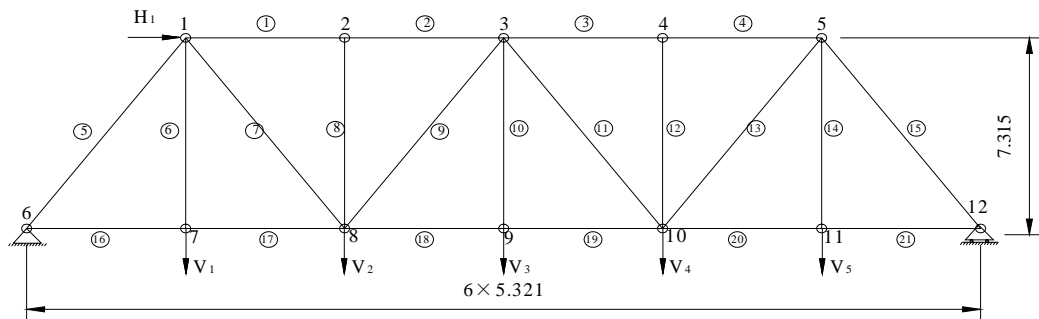


**Figure 6.4 Nominal model for statically determinate truss bridge**

After a period of service, the structure may experience some extent of structural damage. Thus another analytical FE model with the same topology as the nominal model is constructed to represent the present condition of the bridge with structural damage through reducing Young's modulus of each member in the nominal model to different levels, as illustrated in **Figure 6.5**. However, in practice the structural parameter values in the damaged bridge are not exactly known. Nevertheless, when the testing data such as modal parameters are available, FE model updating can be performed by adjusting the structural parameter values in the nominal model to obtain an updated model which reproduce as closely as possible the testing data. Generally the updated model provides a better representation of the damaged

structure than the nominal model. In all, three analytical models are available to represent the bridge, namely the nominal model, the actual model, and the updated model. The nominal model does not account for possible damage appearing in the bridge and therefore it may not be able to reflect satisfactorily the behaviour of the damaged bridge; the actual model is the exact representation of the structural behaviour but it is unknown in practice; and the updated model presumably gives a better representation of the structure as the model has been calibrated to the testing data. In the following, the failure probability and reliability index results obtained from the three models will be presented and compared.

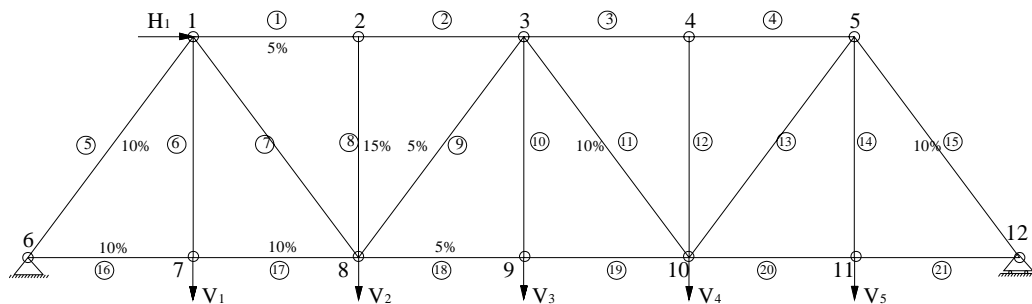


**Figure 6.5 Actual model for statically determinate truss bridge**

In this study the reliability of the structure to expected future static loadings will be considered. The loadings include five vertical loadings and one horizontal loading, all of which are random variables and follow the Lognormal distribution. The five vertical loadings have the same mean of 120 kN and the same standard deviation of 24 kN, and the horizontal loading has a mean of 60 kN and a standard deviation of 12 kN. The loadings are also shown in **Figures 6.4** and **6.5**. The failure probability and reliability index corresponding to a displacement limit-state function are considered in this example. The displacement limit state assumes that the bridge will fail (or unserviceable) when the vertical displacement at node 9 exceeds 0.02 m.

Two cases are investigated. The first case considers that all the structural parameters in the damaged bridge are deterministic. Therefore, for this case, the structural parameters in the nominal and actual models are deterministic, and the structural parameters in the updated model are random due to the uncertainty in modal parameters where the uncertainty is caused only by measurement noise. In order to incorporate the temperature effect on Young's modulus, the second case assumes that the structural parameters in the damaged bridge are independent and normally distributed random variables, all of which have the same coefficient of variation (COV) of 0.1. Thus, in this case, the structural parameters in the nominal and actual models are also regarded as independent and normally distributed random variables with the same COV of 0.1, and the structural parameters in the updated model are random as the modal parameters used for updating are uncertain not only because of measurement noise but also due to natural randomness. For both cases, the detailed information on the statistics of structural parameters in the updated model has been provided in Tables 4.4 and 4.5, and is not repeated herein. For each analytical model the failure probability and reliability index associated with the displacement limit-state function are determined by FORM. The results for the two cases are tabulated in Tables 6.2 and 6.3.

The reliability index and failure probability for case 1 are provided in Table 6.2. As expected, the updated model gives an improved representation of the actual damaged bridge, and therefore provides a more accurate estimate to the actual failure probability than the nominal model. However, this is not necessarily the case when the variance of structural parameters in the updated model is very large which is likely to occur when uncertainties in the modal parameters were considerably notable. For example, should if the standard deviations of structural parameters in the updated

model be doubled and their means remain unchanged, the resulting reliability index is now computed as 3.594 which would provide a less accurate estimate than the nominal model. With the reliability index computed from the updated model and following the correspondence given in Table 6.1, the bridge state is characterized by ‘State 3’, indicating that detailed inspection may be necessary. Additionally, the elements mostly contributing the failure probability and therefore deserving detailed inspection may be identified from sensitivity analysis where the sensitivities of reliability index with respect to the distribution parameters (means and standard deviations) in the updating parameters are of concern. The sensitivity coefficients provided in Table 5.7 can be used for ranking inspection priority of all elements when a detailed inspection exercise is to be executed. Thus, a complete methodology from statistical model updating using measurement data of modal parameters, reliability evaluation using the updated model, to decision making on inspection and maintenance strategies based on the reliability index has been developed.

**Table 6.2 Failure probability for displacement limit state (case 1)**

	<i>Nominal model</i>	<i>Updated model</i>	<i>Actual model</i>
Reliability index	6.648	6.264	6.316
Failure probability	$1.428 \times 10^{-11}$	$1.878 \times 10^{-10}$	$1.339 \times 10^{-10}$

To generate the situation where the reliability index falls below 4.6, three elements with the largest sensitivity coefficients and another three elements with the smallest ones are selected according to the reliability index sensitivity provided in Table 5.7, and the damage extent of each of these elements, in turn, is assumed to become progressively severe. More precisely, the means of updating parameters for these selected elements are gradually reduced while keeping their standard deviations

unchanged. The reliability index is then recomputed and is illustrated in **Figure 6.6**. As consistent with the sensitivity analysis, it is shown that the reliability index drops rapidly when the damage level of the element with the largest sensitivity coefficient is gradually severe. From **Figure 6.6**, reliability indices will fall below 4.6 when the damage extent of the elements 5, 15, and 18 approaches approximately 70%, respectively, and the damage in each of another three elements does not significantly alter the reliability index. Nevertheless, it should be noted that the requirement of reliability index associated with other limit states, such as stress limit state, might have been violated when the elements have experienced severe structural damage. The probability due to the combination of numerous limit states (or failure modes) requires a system reliability analysis, which is out of the scope of the present study. Details on system reliability can be found in references (Ditlevsen 1979; Madsen *et al.* 1986; Ditlevsen and Madsen 1996; Melchers 1999). **Figure 6.6** shows that the reliability index profile can be well approximated by a straight line at the small level of damage.

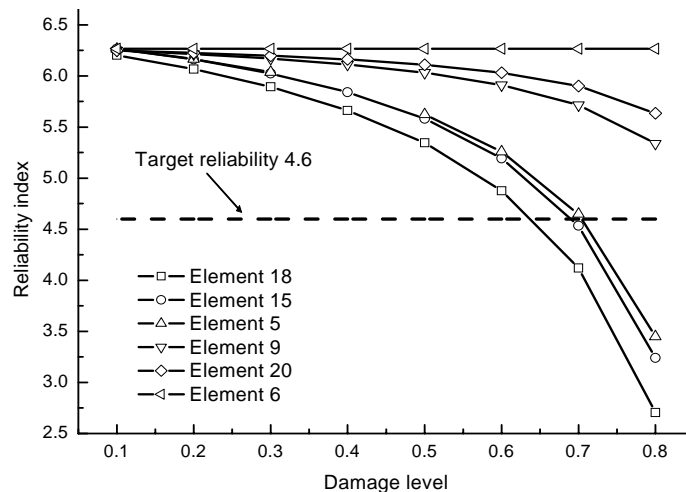


**Figure 6.6 Reliability index profile versus damage level**

The reliability index and failure probability for case 2 are analyzed and the results are provided in Table 6.3. In this case, two updated models are used for reliability analysis. The updated model 1 is the statistically updated model from the first-stage updating; it is further revised to achieve the updated model 2 by incorporating the prior information of structural parameters through Bayesian theorem. The statistics of structural parameters in the updated model 1 and in the updated model 2 are given in columns 4~5 and columns 6~7 of Table 4.5, respectively. As shown in columns 3 and 4 of Table 6.3, the updated models again give the improved estimate to the failure probability than the nominal model. By comparing column 3 with column 4, it is seen that the updated model 1 produces a closer result to the failure probability than the updated model 2, indicating that Bayesian updating is not effective in this case. In this study, the application of Bayesian updating does improve the estimate to the actual failure probability in the case where the variance of structural parameters in updated model 1 is considerably large. Likewise, with the reliability index and following Table 6.1, the bridge state is also characterized by ‘State 3’.

**Table 6.3 Failure probability for displacement limit state (case 2)**

	<i>Nominal model</i>	<i>Updated model 1</i>	<i>Updated model 2</i>	<i>Actual model</i>
Reliability index	6.457	6.121	6.340	6.124
Failure probability	$5.345 \times 10^{-11}$	$4.660 \times 10^{-10}$	$1.145 \times 10^{-10}$	$4.552 \times 10^{-10}$

### **6.3.2 Example 2: A Statically Indeterminate Truss Bridge**

The first example illustrated in above section is the reliability analysis of a statically determinate truss bridge where failure of any member will lead to collapse of the whole structural system. Presented in this section is the reliability-based condition

assessment of a statically indeterminate truss bridge. **Figure 6.7** shows the geometry configuration of the statically indeterminate truss bridge. Likewise, each member of the bridge is modelled as a planar truss element. An analytical model (nominal model) is assumed for structural analysis and condition assessment. In this nominal model as shown in **Figure 6.7**, a total of 31 planar truss elements, each with two DOFs at every node, are used. The material properties used in this model are as follows: mass density  $\rho = 7800 \text{ kg/m}^3$ , area of cross section  $A = 10^{-2} \text{ m}^2$  for each member, and the Young's modulus of  $E = 200 \text{ GPa}$  for each member.

Likewise, in order to represent the present condition of the bridge with structural damage, another analytical FE model with the same topology as the nominal model is constructed through reducing Young's modulus of each member in the nominal model to different levels, as shown in **Figure 6.8**. The measurement data of modal parameters from this damaged bridge are assumed available, and they are used to implement stochastic model updating to achieve an updated model. Similarly, three analytical models are available to represent the bridge, namely the nominal model, the actual model, and the updated model, and all of which are used for reliability analysis. To avoid lengthy presentation, only the random structure incorporating the behaviour of temperature-dependent Young's modulus is studied. The structural parameters in the nominal model and the actual model are assumed as independent and normally distributed random variables with the same COV of 0.1, and the structural parameters in the updated model are random because the modal parameters used for updating are uncertain due to both measurement noise and natural randomness. The statistics of updating parameters in the updated model are adopted from section 4.5 of Chapter 4. In the following, the reliability index for each of the three models will be obtained and compared. The resulting reliability index is then

utilized to determine the appropriate inspection and maintenance strategy using the correspondence given in Table 6.1.

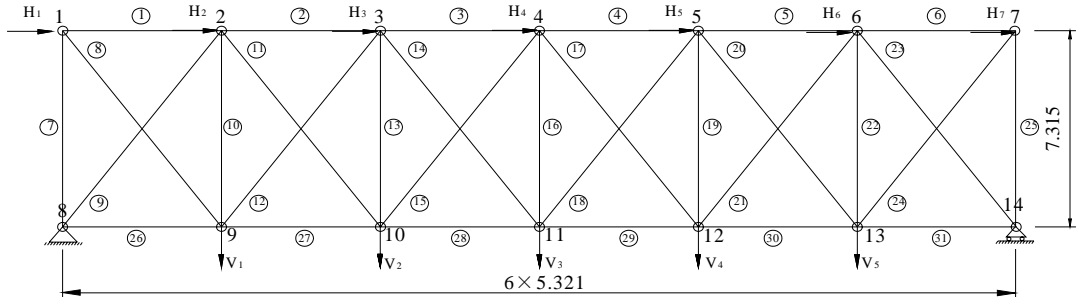


**Figure 6.7 Configuration of statically indeterminate truss bridge**

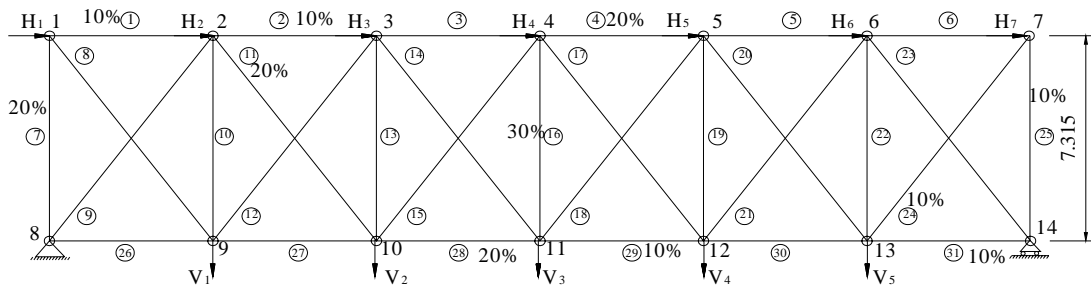


**Figure 6.8 Actual model for statically indeterminate truss bridge**

The reliability of the structure to expected future static loadings will be considered for both displacement and stress limit states. The displacement limit state assumes that the bridge will fail when the vertical displacement at node 11 exceeds 0.03 m; whereas in the stress limit state the member is considered failure when the axial stress exceeds 150 MPa. The truss is subject to five vertical loadings and seven horizontal loadings, all of which are random variables following the Lognormal distribution and are uncorrelated. The five vertical loadings have the same mean of

240 kN and the same standard deviation of 48 kN, and the seven horizontal loadings have the same mean of 120 kN and the same standard deviation of 24 kN. The loadings are schematically shown in **Figures 6.7** and **6.8**. For each model, the failure probabilities and reliability indices defined by the displacement and stress limit-state functions are determined using FORM. The results are given in Tables 6.4 and 6.5.

The reliability index and failure probability corresponding to the displacement limit-state function are provided in Table 6.4. Similar to the first example, two updated models are used for reliability analysis. The updated model 1 is the statistically updated model from the first-stage updating; and it is further revised to achieve the updated model 2 by incorporating the prior information of structural parameters using Bayesian theorem. Once again, the updated models are shown to provide an improved representation of actual damaged bridge, and therefore provide more accurate estimates to the actual failure probability than the nominal model. It is interesting to note: i) the nominal model always gives a larger reliability index value than the actual model as it ignores the structural damage which adversely affects the performance and safety of the structure; ii) the updated model 1 (without application of the Bayesian updating) always produce a smaller reliability index value than the actual model because the variances of updating parameters in this model are larger than true values due to the presence of both measurement noise and natural randomness, thus yielding a conservative estimate of reliability index. However, when the measurement noise is significant, the variances of updating parameters will be very large and therefore the resulting reliability index will be too conservative and unreliable; and iii) the performance of updated model 2 is significantly affected by the prior information. With the reliability index computed from the updated model 1 and following Table 6.1, the bridge state is characterized by ‘State 1’, indicating

**Table 6.4 Failure probability for displacement limit state**

	<i>Nominal model</i>	<i>Updated model 1</i>	<i>Updated model 2</i>	<i>Actual model</i>
Reliability index	5.577	4.508	5.293	4.590
Failure probability	$1.226 \times 10^{-8}$	$3.269 \times 10^{-6}$	$6.022 \times 10^{-8}$	$2.208 \times 10^{-6}$

**Table 6.5 Failure probability for stress limit state**

<i>Element No.</i>	<i>Nominal model</i>	<i>Updated model 1</i>	<i>Actual model</i>
1	12.517	12.538	12.560
2	8.372	8.580	8.582
3	6.562	6.314	6.324
4	6.727	6.786	6.789
5	8.746	8.694	8.716
6	12.717	12.489	12.522
7	12.846	13.161	12.871
8	11.652	11.962	12.587
8	11.892	11.714	11.719
10	13.565	13.285	13.299
11	12.202	13.058	13.260
12	13.250	13.805	13.907
13	13.508	9.158	10.056
14	9.774	9.708	9.725
15	13.895	9.351	9.664
16	10.059	9.334	13.203
17	13.011	9.055	12.834
18	13.315	13.058	13.069
19	13.303	13.918	13.934
20	12.284	11.194	13.148
21	11.323	11.058	11.263
22	12.796	7.290	13.071
23	10.420	10.185	10.187
24	11.321	7.416	11.265
25	11.996	7.458	11.861
26	7.406	7.321	7.321
27	4.722	4.488	4.514
28	3.753	4.025	4.011
29	5.055	4.932	4.958
30	8.556	8.596	8.591
31	13.95	8.031	12.970

immediate action such as rehabilitation is required. Similarly, the sensitivity coefficients illustrated in **Figure 5.14** provide the priority of structural members to be rehabilitated.

The reliability index and failure probability corresponding to the stress limit-state function for each element are analyzed and the results are tabulated in Table 6.5. In general the updated model provides a better estimate to the actual reliability index than the nominal model. However, there are cases where the situation is reversed. With the obtained reliability index, each component can be characterized according to Table 6.1.

## **6.4 Summary**

An issue of great concern with bridge health monitoring systems is how to use the monitoring data to aid the bridge authorities in decision making. The information generated by monitoring systems must be channeled towards the goal to support the bridge managers in making financial decision. In this chapter, a systematic approach was proposed to bridge the gap currently existing between health monitoring technologies and bridge inspection/maintenance exercises. As consistent with structural reliability analysis, this unified approach begins with the statistical identification of structural parameters using modal parameters, and then proceeds to the determination of reliability index on the basis of the statistical identification results. Finally this approach makes use of the established correspondence between reliability index and required maintenance action to decide maintenance and repair strategy. Following the proposed approach, structural health monitoring system is able to provide quantitative information for bridge inspection and maintenance.

Two examples are provided for demonstration of the proposed methodology. For each example, the failure probabilities and reliability indices with respect to the nominal, updated, and actual models, are computed and compared. The results indicate that: (i) the reliability index obtained from the updated model is much closer to true reliability index than that obtained from the nominal model in the case of low uncertainty in measured modal parameters; in the case of high uncertainty, the updated model may become unreliable as the reliability index computed from the nominal model rather than from the updated model is closer to the true value; (ii) the nominal model always gives a larger reliability index value than the actual model, as it ignores structural damage which adversely affects the reliability of structure; (iii) the updated model from the first-stage updating always produces a smaller reliability index value than the actual model, because the variances of updating parameters in the model are larger than the actual ones due to the simultaneous occurrence of measurement noises and natural randomness.

## Chapter 7

# MODELLING OF TEMPERATURE-FREQUENCY CORRELATION USING COMBINED PCA AND SVR TECHNIQUE

### 7.1 Introduction

Recent advances in sensing, data acquisition, computing, communication, data and information management, have made it possible to implement long-term structural health monitoring systems for obtaining objective indices on structural conditions and guiding management and maintenance of large-scale bridges (Pines and Aktan 2002; Casciati 2003; Koh *et al.* 2003; Fujino and Abe 2004; Wong 2004; Wang 2005). The core of a structural health monitoring system is the diagnostic algorithms for detection of the presence, location, and extent of structural damage followed by evaluating the impact of the damage on structural performance and reliability. Among various diagnostic algorithms, the vibration-based damage detection technique, which achieves the capabilities in identifying the presence, location, and severity of structural damage through examining the changes in modal parameters, has been shown to be one of the most promising methods (Doebbling *et al.* 1998; Sohn *et al.* 2004).

However, it has been recognized recently that the performance of vibration-based diagnostic algorithms in locating and quantifying local-level structural damage

suffers from the fact that changes in modal parameters are also caused by varying environmental and operational conditions for in-service large-scale civil structures. In reality, civil engineering structures are subject to varying environmental and operational conditions such as traffic, wind, humidity, solar-radiation and most important, temperature. These environmental effects cause changes in physical parameters such as Young's modulus, structural mass, boundary conditions, and thermal-induced internal forces for redundant structures, and thereby induce changes in modal parameters, which may yield false indication of damage when vibration-based damage detection algorithms are applied. For practical implementation and reliable performance of the damage detection algorithms, it is of paramount importance to characterize normal variability of modal parameters due to environmental and operational conditions, and to discriminate such normal variability from abnormal changes in modal parameters caused by structural damage. When the effects of normal environmental changes are well understood or quantified, it is possible to achieve reliable and accurate damage identification through incorporating the environmental effect models into the damage detection algorithms in either a statistical or deterministic way (Worden *et al.* 2002; Kim *et al.* 2004).

Considerable research efforts have been made on investigating the influence of environmental conditions on modal frequencies of bridges via field measurements and dynamic tests (Robert and Pearson 1996; Abdel Wahab and De Roeck 1997; Farrar *et al.* 1997; Cornwell *et al.* 1999; Sohn *et al.* 1999; Alampalli 2000; Lloyd *et al.* 2000; Rohrman *et al.* 2000; Bolton *et al.* 2001; Peeters and De Roeck 2001; Ko *et al.* 2003). Most of these investigations indicated that temperature was the critical source causing variability of modal parameters, and the changes in modal frequencies caused by temperature might reach up to 4% or more in highway bridges.

Although a lot of field measurements and observations have been made, very few studies addressed the modelling of environmental effects on modal properties. Based on field measurement data of temperature and modal frequency, Sohn *et al.* (1999) proposed a linear adaptive model (multivariate regression model) to represent the frequency variations caused by temperature for the Alamosa Canyon Bridge. Peeters and De Roeck (2001) derived an auto-regressive and moving average (ARMA) model using long-term measurement data to formulate the relation between temperature and modal frequency for the Z24 Bridge. These linear regression models were generally acceptable in reproducing the measurement data, but their generalization capability in predicting unseen data was not satisfactory. Both studies showed that the measured temperatures from different locations of a structure are highly correlated, and the correlated features could seriously deteriorate the generalization performance of regression model. Therefore, selecting appropriate feature vectors from all candidate variables was essential for improving the model performance.

In this chapter, a method that utilizes the attractive merits of principal component analysis (PCA) for extracting predominant feature vectors and support vector regression (SVR) for data-based statistical learning is proposed for modelling temperature-caused variability of structural modal frequencies with the use of long-term measurement data. PCA is first performed to extract principal components (PCs) from the measured temperatures. SVR analysis is then conducted on the extracted PCs and the measured modal frequencies to formulate empirical models quantifying the effect of temperature on modal frequencies. Research efforts have been made on properly choosing the hyper-parameters to formulate SVR models with good generalization performances and comparing the prediction capability of the

formulated models with and without considering temporal correlation. With the use of long-term monitoring data from the cable-stayed Ting Kau Bridge, the generalization performance of the formulated SVR models with the hyper-parameters determined by a grid search method with cross validation and a heuristic method, respectively, is examined. Both ‘dynamic’ and ‘static’ SVR models with and without considering thermal inertia effect are formulated. The PCA-based SVR model is compared with the SVR model which is trained by directly using measurement data in terms of model accuracy and computational costs, and with a multivariate linear regression (MLR) model in terms of model accuracy and adaptability. Both hypothesis test and goodness-of-fit test are adopted to assess the model performance.

## **7.2 Presentation of Method**

### ***7.2.1 Overview of Combined PCA and SVR Method***

**Figure 7.1** shows the flowchart of the proposed PCA-SVR method for modelling temperature-frequency correlation based on long-term measurement data. Following this method, the PCs of temperature measurement data are first extracted by projecting the original data to eigenvectors of its covariance matrix, and the extracted PCs together with frequency measurement data are then fed into a support vector algorithm to formulate SVR models. Since the performance of a SVR model depends on a proper setting of its hyper-parameters, a key issue in applying SVR in practice is how to select these parameters to achieve good generalization performances. Unfortunately, the existing SVR packages, e.g. LIBSVM (Hsu *et al.* 2003), require SVR hyper-parameters to be specified *a priori* by users. In the present study, a grid search method with cross validation and a heuristic method are explored to determine

the optimal SVR hyper-parameters, while the number of PCs is selected by trial-and-error. The outer and inner blocks illustrated in **Figure 7.1** indicate the process to loop over the number of PCs and to loop over the hyper-parameters, respectively. When the grid search method is used, the SVR models are formulated using the training data for a wide spectrum of SVR hyper-parameters, and the prediction errors are obtained by comparing the predicted values and the target values for new validation data following a  $k$ -fold cross-validation scheme. Then the optimal hyper-parameters for a specific number of PCs are determined which produce the minimal prediction error. By repeating this process from taking only the first PC to taking all the PCs, the optimal number of PCs is determined with the global smallest prediction error and the hyper-parameters are finally selected as the optimal values corresponding to the optimal number of PCs. When the heuristic method is adopted, the hyper-parameters are determined from empirical formulae and then used to formulate SVR models for a given number of PCs. By comparing the prediction errors obtained using different number of PCs, the optimal number of PCs and the optimal hyper-parameters are determined which achieve the smallest prediction error.

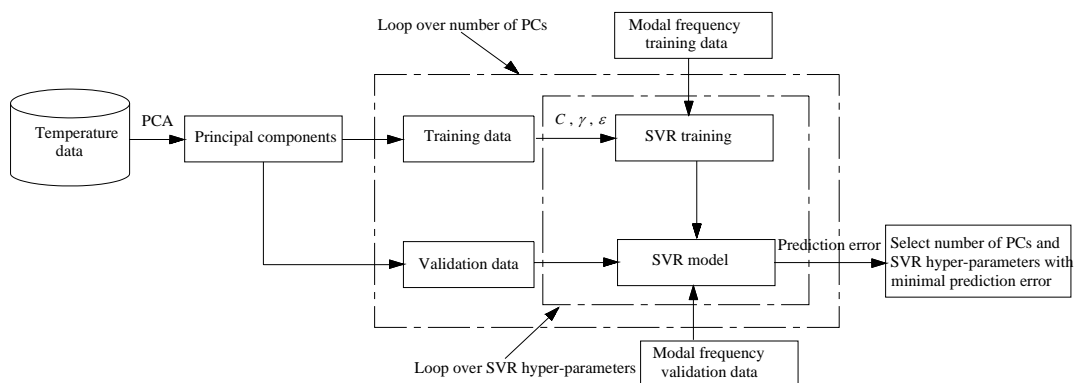


**Figure 7.1 Flowchart of the combined PCA-SVR method**

### 7.2.2 PCA for Extracting Feature Vectors

In multivariate regression, the highly correlated data could result in a multicollinearity problem and are prone to producing unstable regression estimates (Rencher 2002). It is desired to reduce the data to a smaller subset of predominant feature vectors that give rise to more stable estimate of regression coefficients. When large-scale bridges such as suspension bridges and cable-stayed bridges are instrumented with long-term monitoring systems, temperature sensors are usually installed at different structural parts (deck, tower, cable, etc.) for temperature measurement of various materials (steel, concrete, asphalt, air, etc.) (Wong 2004). As a result, a large number of temperature measurement data from different locations of a bridge are available and some of the data may be closely correlated. PCA provides a powerful mathematical tool to select predominant feature vectors (Jolliffe 2002). It also has the capability of eliminating measurement noise (Ni *et al.* 2006).

Using an orthogonal projection, the original set of correlated variables (temperature measurement data) in an  $n$ -dimensional space can be transformed into a new set of uncorrelated variables, the so-called principal components, in a  $p$ -dimensional orthogonal space such that  $p \leq n$ . This process seeks to project the high-dimensional data into a new low-dimensional set of Cartesian coordinates  $(z_1, z_2, \dots, z_p)$ . The new coordinates have the following properties:  $z_1$  is the linear combination of the original coordinate  $x_i (i = 1, 2, \dots, n)$  with maximal variance,  $z_2$  is the linear combination that explains most of the remaining variance and so on. The calculation of the orthogonal matrix can be described as follows: given the  $j$ th measurement data set  $\{\mathbf{x}\}_j = (x_{j1}, x_{j2}, \dots, x_{jn})^T$ ,  $j = 1, 2, \dots, m$  where the subscript T denotes

transposition and  $m$  is the total number of measurements, the  $n \times n$  dimension covariance matrix  $\mathbf{C}$  is formed as

$$\mathbf{C} = \sum_{j=1}^m \{\mathbf{x}\}_j \{\mathbf{x}\}_j^T \quad (7.1)$$

The singular value decomposition on the covariance matrix is conducted as

$$\mathbf{C} = \mathbf{U}\mathbf{\Lambda}\mathbf{U}^T \quad (7.2)$$

where  $\mathbf{U}$  is the orthogonal eigenvector matrix with  $\mathbf{U}^T\mathbf{U} = \mathbf{I}$ ; and  $\mathbf{\Lambda}$  is the eigenvalue or singular value matrix which has the form of

$$\mathbf{\Lambda} = \begin{bmatrix} \lambda_1 & 0 & \cdots & 0 \\ 0 & \lambda_2 & \vdots & 0 \\ \vdots & \vdots & & \vdots \\ 0 & 0 & \cdots & \lambda_n \end{bmatrix} \quad (7.3)$$

with  $\lambda_1 \geq \lambda_2 \geq \cdots \geq \lambda_n \geq 0$ . The transformation to the PCs is then applied as

$$\{\mathbf{z}\}_j = \mathbf{U}^T(\{\mathbf{x}\}_j - \{\bar{\mathbf{x}}\}) \quad (7.4)$$

where  $\{\bar{\mathbf{x}}\}$  is the vector of means of  $\mathbf{x}$ -data. It can be shown that the covariance matrix of  $\{\mathbf{z}\}_j$  ( $j = 1, 2, \dots, m$ ) has the expression

$$\mathbf{C}_z = \sum_{j=1}^m \{\mathbf{z}\}_j \{\mathbf{z}\}_j^T = [\mathbf{\Lambda}] = \begin{bmatrix} \lambda_1 & 0 & \cdots & 0 \\ 0 & \lambda_2 & \vdots & 0 \\ \vdots & \vdots & & \vdots \\ 0 & 0 & \cdots & \lambda_n \end{bmatrix} \quad (7.5)$$

which implies that the vectors  $\{\mathbf{z}\}_j$  ( $j = 1, 2, \dots, m$ ) are uncorrelated.

From the dimensionality reduction point of view, PCA works by discarding those linear combinations of the data which contribute least to the overall variance or range of the data set. In practice, the smallest eigenvalue will not vanish due to measurement noise, i.e., none of components can be completely described by the linear combinations of the remaining components. Nevertheless when the input data are highly correlated, the eigenvalue of the covariance matrix  $\mathbf{C}$  will decrease drastically. The proportion of variance explained by the first  $p$  eigenvalues is defined as

$$\text{Prop}_p = \frac{\sum_{i=1}^p \lambda_i}{\sum_{j=1}^n \lambda_j} \quad (7.6)$$

then the transformation to the first  $p$  principal components is

$$\{\tilde{\mathbf{z}}\}_j = \tilde{\mathbf{U}}_{n \times p}^T (\{\mathbf{x}\}_j - \{\bar{\mathbf{x}}\}) \quad (7.7)$$

In the above formulation, PCA is conducted on the set  $\{\mathbf{x}\}_j$  which consists of the temperature data measured at the same time. The SVR models formulated using such obtained PCs will be the ‘static’ regression models for correlation between the instant temperature and the instant frequency. As the change of modal frequency may lag behind the temperature change due to thermal inertia effect, ‘dynamic’ regression models which account for temporal correlation presumably possess stronger prediction capability. When continuously measured data are available, ‘dynamic’ SVR models can be formulated using the PCs extracted from the following augmented temperature vector

$$\{\mathbf{t}\}_i = \{\mathbf{x}_{i-1}^T \quad \mathbf{x}_i^T\}^T \quad (7.8)$$

where  $\{\mathbf{x}\}_i$  is the set of temperature data measured at the  $i$ th time step, and  $\{\mathbf{x}\}_{i-1}$  is the set of temperature data measured at the  $(i-1)$ th time step. Such obtained ‘dynamic’ SVR models will relate the current output (modal frequency) with not only the current input (temperature) but also the input in the previous time step.

### 7.2.3 SVR for Data-Based Statistical Learning

SVR provides a new statistical learning algorithm for regression estimate which employs the structural risk minimization (SRM) principle rather than the commonly used empirical risk minimization (ERM) principle (Vapnik 1999; Smola and Schölkopf 2004). In SVR, an upper bound on the generalization error,  $R(f)$ , is minimized as opposed to ERM which minimizes the error on the training data set,  $R_{emp}(f)$ . This formulation equips SVR with a greater potential to generalize the input-output relation and predict the unseen data more accurately. In this study, we apply SVR technique to formulate regression models by use of the PCs of temperature measurement data and the corresponding frequency measurement data for each vibration mode.

Consider a set of  $m$  measurement data set  $S = \{(\mathbf{x}_1, y_1), (\mathbf{x}_2, y_2), \dots, (\mathbf{x}_m, y_m)\}$ , such that  $\mathbf{x}_i \in R^p$  is a  $p$ -dimensional vector of input variables (features) and  $y_i \in R$  the corresponding scalar output (target). The objective is to find a regression function,  $y = f(\mathbf{x})$ , such that it minimizes the error of predicting new data set  $S_1$ , which is derived from the same joint probability distribution  $P(\mathbf{x}, y)$  as the training data set. To fulfill the stated goal, SVR considers the following linear estimation function

$$f(x) = \langle \mathbf{w}, \mathbf{x} \rangle + b \quad (7.9)$$

where  $\mathbf{w}$  denotes the weighting vector;  $b$  is a constant known as bias;  $\langle *, * \rangle$  denotes the inner product. As opposed to the ERM principle which minimizes the error on the training data set,  $R_{emp}(f)$ , the SRM principle which minimizes an upper bound on the generalization error,  $R(f)$ , is adopted in SVR to avoid over-fitting and thereby improve generalization performance. The relationship between the structural risk  $R(f)$  and the empirical risk  $R_{emp}(f)$  can be expressed as (Burges 1998)

$$R(f) \leq R_{emp}(f) + \lambda \|\mathbf{w}\|^2 = \frac{1}{m} \sum_{i=1}^m L(f(\mathbf{x}_i) - y_i) + \lambda \|\mathbf{w}\|^2 \quad (7.10)$$

where  $\lambda$  is a regularization parameter;  $\|\mathbf{w}\|^2 = \langle \mathbf{w}, \mathbf{w} \rangle$  is the Euclidean norm; and  $L(f(\mathbf{x}_i) - y_i)$  is some kind of cost function measuring the empirical risk of the training data. There are various kinds of loss functions with respect to different noise conditions, such as Huber's robust loss, polynomial,  $\varepsilon$ -insensitive, and Gaussian (Smola and Schölkopf 2004). The commonly used loss function is the  $\varepsilon$ -insensitive loss function expressed as

$$L(f(\mathbf{x}) - y) = \begin{cases} |f(\mathbf{x}) - y| - \varepsilon & \text{for } |f(\mathbf{x}) - y| \geq \varepsilon \\ 0 & \text{otherwise} \end{cases} \quad (7.11)$$

where  $\varepsilon$  is a parameter representing the radius of tube located around the regression function as illustrated in **Figure 7.2**. The region enclosed by the tube is known as the  $\varepsilon$ -insensitive zone. In **Figure 7.2**, the values with excess positive and negative deviations are depicted by  $\xi$  and  $\xi^*$ , respectively, which are termed as slack variables. The optimization criterion penalizes those data points whose values of  $y$  lie more than  $\varepsilon$  distance away from the fitted function  $f(\mathbf{x})$ . By substituting the  $\varepsilon$ -insensitive loss function into Equation (7.10), the optimization object becomes

$$\text{minimize } \frac{1}{2}\|\mathbf{w}\|^2 + C\sum_{i=1}^m(\xi_i + \xi_i^*) \quad (7.12)$$

$$\text{subject to } \begin{cases} y_i - \langle \mathbf{w}, \mathbf{x}_i \rangle - b \leq \varepsilon + \xi_i \\ \langle \mathbf{w}, \mathbf{x}_i \rangle + b - y_i \leq \varepsilon + \xi_i^* \\ \xi_i, \xi_i^* \geq 0 \end{cases} \quad (7.13)$$

where the positive constant  $C$ , which combines the effect of  $m$  and  $\lambda$ , determines the trade-off between the flatness of  $f(\mathbf{x})$  and the empirical error.

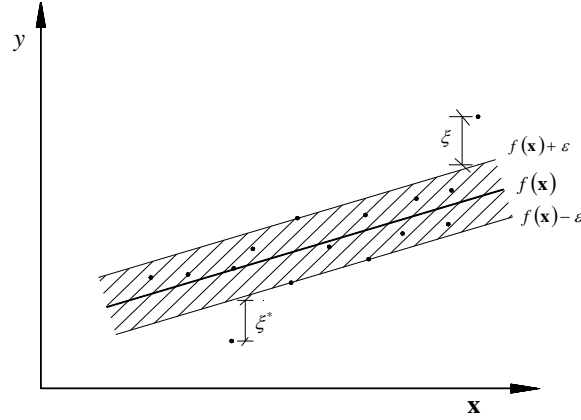


**Figure 7.2**  $\varepsilon$ -insensitive loss function for linear SVR

The solution to the optimization problem of Equation (7.12) under constraints of Equation (7.13) is given by the saddle point of the Lagrange function

$$\begin{aligned} L = & \frac{1}{2}\|\mathbf{w}\|^2 + C\sum_{i=1}^m(\xi_i + \xi_i^*) - \sum_{i=1}^m \alpha_i(\varepsilon + \xi_i - y_i + \langle \mathbf{w}, \mathbf{x}_i \rangle + b) \\ & - \sum_{i=1}^m \alpha_i^*(\varepsilon + \xi_i^* + y_i - \langle \mathbf{w}, \mathbf{x}_i \rangle - b) - \sum_{i=1}^m (\eta_i \xi_i + \eta_i^* \xi_i^*) \end{aligned} \quad (7.14)$$

where  $\alpha_i, \alpha_i^*, \eta_i, \eta_i^*$  are Lagrange multipliers (dual variables). It follows from the saddle point condition that the partial derivatives of  $L$  with respect to primal variables  $(\mathbf{w}, b, \xi_i, \xi_i^*)$  have to vanish for optimality. That is,

$$\partial_b L = \sum_{i=1}^m (\alpha_i^* - \alpha_i) = 0 \quad (7.15)$$

$$\partial_w L = \mathbf{w} - \sum_{i=1}^m (\alpha_i - \alpha_i^*) \mathbf{x}_i = 0 \quad (7.16)$$

$$\partial_{\xi_i} L = C - \alpha_i - \eta_i = 0 \quad (7.17)$$

$$\partial_{\xi_i^*} L = C - \alpha_i^* - \eta_i^* = 0 \quad (7.18)$$

Substituting Equations (7.15) to (7.18) into Equation (7.14) yields the following dual optimization problem

$$\text{minimize } -\frac{1}{2} \sum_{i,j=1}^m (\alpha_i - \alpha_i^*) (\alpha_j - \alpha_j^*) \langle \mathbf{x}_i, \mathbf{x}_j \rangle - \varepsilon \sum_{i=1}^m (\alpha_i + \alpha_i^*) + \sum_{i=1}^m y_i (\alpha_i - \alpha_i^*) \quad (7.19)$$

$$\text{subject to } \begin{cases} \sum_{i=1}^m (\alpha_i - \alpha_i^*) = 0 \\ 0 \leq \alpha_i, \alpha_i^* \leq C \end{cases} \quad (7.20)$$

The dual variables  $\eta_i, \eta_i^*$  have been eliminated in deriving Equation (7.19) through conditions in Equations (7.17) and (7.18). Thus the solution for  $\alpha_i, \alpha_i^*$  is obtained from the above optimization problem after specifying the parameters  $C$  and  $\varepsilon$ . The weighting vector in Equation (7.16) can be rewritten as

$$\mathbf{w} = \sum_{i=1}^m (\alpha_i - \alpha_i^*) \mathbf{x}_i \quad (7.21)$$

and therefore

$$f(\mathbf{x}) = \sum_{i=1}^m (\alpha_i - \alpha_i^*) \langle \mathbf{x}_i, \mathbf{x} \rangle + b \quad (7.22)$$

This is the so-called support vector expansion, where  $\mathbf{w}$  is completely described as a linear combination of the training samples  $\mathbf{x}_i$ . The parameter  $b$  in Equation (7.22) is calculated using the Karush-Kuhn-Tucker (KKT) conditions which state that at the optimal solution the product between dual variables and constraints has to vanish.

For the above problem, the KKT conditions give rise to

$$\alpha_i (\varepsilon + \xi_i - y_i + \langle \mathbf{w}, \mathbf{x}_i \rangle + b) = 0 \quad (7.23)$$

$$\alpha_i^* (\varepsilon + \xi_i^* + y_i - \langle \mathbf{w}, \mathbf{x}_i \rangle - b) = 0 \quad (7.24)$$

and

$$(C - \alpha_i) \xi_i = 0 \quad (7.25)$$

$$(C - \alpha_i^*) \xi_i^* = 0 \quad (7.26)$$

From Equations (7.23) to (7.26) the parameter  $b$  is obtained as

$$b = y_i - \langle \mathbf{w}, \mathbf{x}_i \rangle - \varepsilon \quad \text{for } \alpha_i \in (0, C) \quad (7.27)$$

$$b = y_i - \langle \mathbf{w}, \mathbf{x}_i \rangle + \varepsilon \quad \text{for } \alpha_i^* \in (0, C) \quad (7.28)$$

where  $\mathbf{x}_i$  refer to those samples located at the tube bound. Furthermore, from Equations (7.23) and (7.24), for all samples inside the  $\varepsilon$  tube, their Lagrange coefficients become zero. The samples with nonzero coefficients are called support vectors.

The power of SVR lies in its ability to transform data to a high-dimensional feature space endowed with an inner product. The above derived linear SVR algorithm can be easily extended to nonlinear regression with the aid of kernel methods (Müller *et al.* 2001). The kernel methods map the input data in original space  $R^P$ , which is a low-dimension space, into a much higher-dimensional feature space  $F$  using a nonlinear mapping  $\phi$ , i.e.,  $\mathbf{z}_i = \phi(\mathbf{x}_i)$ . The linear support vector algorithm is then conducted in the feature space, which represents nonlinear support vector algorithm in the original space. For some nonlinear mappings  $\phi$ , such as polynomial, sigmoidal and radial-basis functions, there exists a highly effective trick for calculating inner products in the feature space using a kernel function

$$K(\mathbf{x}_i, \mathbf{x}_j) = \langle \phi(\mathbf{x}_i), \phi(\mathbf{x}_j) \rangle \quad (7.29)$$

A significant merit of this formulation is that for certain classes of mapping functions  $\phi(\mathbf{x}_i)$ , the kernel function  $K(\mathbf{x}_i, \mathbf{x}_j)$  for inner products in the feature space can be expressed explicitly without probing real characteristics of the feature space. In this way we can avoid dealing directly with the high-dimensional space and excessive computations that result from the space transformation. By using different kernel functions for inner product evaluations, various types of nonlinear models in the original space could be constructed. Three common choices for kernel functions are listed as follows.

(i) Polynomial kernel function

$$K(\mathbf{x}_i, \mathbf{x}_j) = (\langle \mathbf{x}_i, \mathbf{x}_j \rangle + c)^d, \quad c > 0 \quad (7.30)$$

(ii) Radial basis kernel function (RBF)

$$K(\mathbf{x}_i, \mathbf{x}_j) = \exp\left(-\gamma \|\mathbf{x}_i - \mathbf{x}_j\|^2\right), \quad \gamma > 0 \quad (7.31)$$

(iii) Sigmoidal kernel function

$$K(\mathbf{x}_i, \mathbf{x}_j) = \tanh(\gamma \langle \mathbf{x}_i, \mathbf{x}_j \rangle + c), \quad \gamma > 0, c > 0 \quad (7.32)$$

where  $\gamma$ ,  $c$ , and  $d$  are kernel parameters.

Substituting  $K(\mathbf{x}_i, \mathbf{x}_j)$  for  $\langle \mathbf{x}_i, \mathbf{x}_j \rangle$  in Equation (7.19) allows to rewriting the support vector algorithm as

$$\text{minimize} \quad -\frac{1}{2} \sum_{i,j=1}^m (\alpha_i - \alpha_i^*)(\alpha_j - \alpha_j^*) K(\mathbf{x}_i, \mathbf{x}_j) - \varepsilon \sum_{i=1}^m (\alpha_i + \alpha_i^*) + \sum_{i=1}^m y_i (\alpha_i - \alpha_i^*) \quad (7.33)$$

$$\text{subject to} \quad \begin{cases} \sum_{i=1}^m (\alpha_i - \alpha_i^*) = 0 \\ 0 \leq \alpha_i, \alpha_i^* \leq C \end{cases} \quad (7.34)$$

The expression of  $\mathbf{w}$  is accordingly obtained as

$$\mathbf{w} = \sum_{i=1}^m (\alpha_i - \alpha_i^*) K(\mathbf{x}_i) \quad (7.35)$$

and therefore

$$f(\mathbf{x}) = \sum_{i=1}^m (\alpha_i - \alpha_i^*) K(\mathbf{x}_i, \mathbf{x}) + b \quad (7.36)$$

The difference of nonlinear support vector algorithm from linear support vector algorithm lies in that  $\mathbf{w}$  and  $f(\mathbf{x})$  is no longer explicitly given.

The kernel parameters in Equations (7.30) to (7.32) and the parameters  $\varepsilon$  and  $C$  in Equation (7.33), referred to as SVR hyper-parameters, need to be specified *a priori*.

After doing that, the model parameters  $\alpha_i$ ,  $\alpha_i^*$  and  $b$  in Equation (7.36) are determined using training data  $(\mathbf{x}_i, y_i)$  by solving the constrained optimization problem defined in Equation (7.33) and (7.34). In the present study, the sequential minimal optimization (SMO) algorithm (Platt 1999; Shevade *et al.* 2000) has been employed to solve the quadratic programming (QP) convex problem of Equation (7.33). For the problem in concern, only a subset of the coefficients  $(\alpha_i^* - \alpha_i)$  will be nonzero in most cases. Making use of the sparseness, the SMO algorithm decomposes a large QP problem into a series of small QP sub-problems of size two (two variables). Each sub-problem can be analytically solved without use of a QP solver. The SMO algorithm is efficient to deal with large-size sparse data sets.

#### ***7.2.4 Determination of SVR Hyper-Parameters***

A key issue of applying SVR for ‘real-world’ problems is how to set the hyper-parameter values to achieve good generalization performances for SVR models trained by given data sets. In the present study, a grid search method and a heuristic method are utilized to determine the optimal values of SVR hyper-parameters. When using the grid search method, a series of SVR models are first trained by assuming a wide spectrum of SVR hyper-parameters. If all available data are used to train the SVR models, the trained models are expected to simulate (reproduce) the training data well but may perform poorly in generalizing (predicting) unseen data. A cross-validation scheme is performed to circumvent this over-fitting problem. The total measurement data are divided into  $k$  subsets of equal size. Each subset is tested by feeding the data into the SVR models trained on the remaining  $(k - 1)$  subsets for each combination of the hyper-parameters. This procedure is repeated until all

subsets have been used for a validation test. Then the mean squared error (MSE) is calculated from each omitted subset and is averaged over all subsets. The optimal values of SVR hyper-parameters are determined which produce the minimal average MSE. MSE for each subset of validation data is defined as

$$\text{MSE} = \frac{1}{l} \sum_{j=1}^l (y_{pj} - y_{rj})^2 \quad (7.37)$$

where  $y_{pj}$  and  $y_{rj}$  denote the  $j$ th model-predicted value and the target value, respectively; and  $l$  is the number of validation data.

A heuristic method has been proposed by Cherkassky and Ma (2004) for practical selection of SVR hyper-parameters to achieve good model performances. This method provides empirical formulae for analytic parameter selection directly from the training data and the estimated noise level. When using the RBF kernel function, they obtained the following formulae:

$$C = \max(|\bar{y} + 3\sigma_y|, |\bar{y} - 3\sigma_y|) \quad (7.38)$$

$$\varepsilon = 3\sigma \sqrt{\frac{\ln m}{m}} \quad (7.39)$$

$$\gamma = \frac{1}{2} [(0.1 \sim 0.5) \times r]^{2/p} \quad (7.40)$$

where  $\bar{y}$  and  $\sigma_y$  are the mean and the standard deviation of the  $y$  data for training;  $\sigma$  is the standard deviation of the noise in the  $y$  data;  $p$  is the dimension of input variables; and  $r$  is the range of each feature. The above empirical formulae have been validated only using simulation data; their applicability to ‘real-world’ data will be examined in the present study.

### 7.3 Experimental Data

The Ting Kau Bridge in Hong Kong, as shown in **Figure 7.3**, is a multi-span cable-stayed bridge with three monoleg towers supporting two main spans of 448 m and 475 m respectively and two side spans of 127 m each. After completing its construction in 1998, the bridge has been instrumented with a long-term structural health monitoring system by the Hong Kong SAR Highways Department (Wong 2004). This system consists of more than 230 sensors of various types, including accelerometers, displacement transducers, strain gauges, anemometers, temperature sensors, weigh-in-motion sensors and global positioning systems. A total of 83 temperature sensors (five categories) have been installed at different locations of the bridge to measure: (i) steel-girder temperature, (ii) temperature inside concrete deck, (iii) temperature in tower legs, (iv) temperature in asphalt pavement, and (v) atmosphere temperature. Likewise, 24 uni-axial accelerometers, 20 bi-axial accelerometers and one tri-axial accelerometer (a total of 67 channels) have been installed on the deck of two main spans and two side spans, the longitudinal stabilizing cables, the top of three towers, and the base of central tower to monitor ground excitation and dynamic response of the bridge. The deployment of temperature sensors and accelerometers is illustrated in **Figure 7.3**.

One-year (the year of 1999) continuous measurement data from all the sensors installed on the bridge have been collected to establish a database in the Hong Kong Polytechnic University for damage detection related research (Wang 2003). The measurement data were acquired with sampling rates of 25.6 Hz and 0.07 Hz for acceleration and temperature, respectively. With a careful inspection of the

measurement data, a total of 770-hour data from all the temperature sensors and accelerometers were selected after removing the signals which were not triggered or likely to be abnormal even at one signal channel. They are composed of 185-hour data in February, 35-hour data in March, 95-hour data in June, 208-hour data in July, 95-hour data in August, and 152-hour data in December.

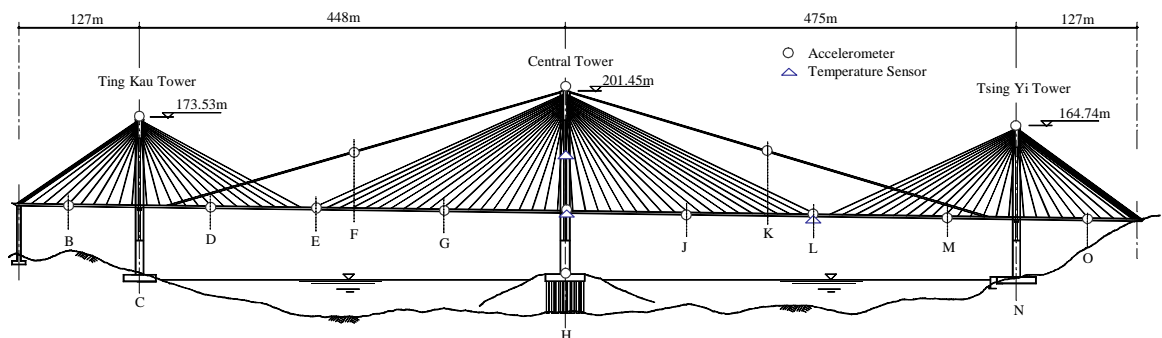


**Figure 7.3 Deployment of temperature sensors and accelerometers on Ting Kau Bridge**

### 7.3.1 Measurement Data of Temperature

For each of the five temperature monitoring categories, four sensors are selected after sensitivity and correlation analysis among the data sequences from all the temperature sensors. As a result, a total of 20 temperature sensors are chosen to provide data for modeling of the temperature-frequency relationship. Statistical analysis of the hourly-average temperatures has been conducted to obtain minimum and maximum values and histograms of the measured temperatures. It is observed that the measured temperatures on the bridge range from 2.83 to 53.46 °C. The average temperatures in one-hour duration for the 20 selected sensors are plotted in **Figure 7.4**.

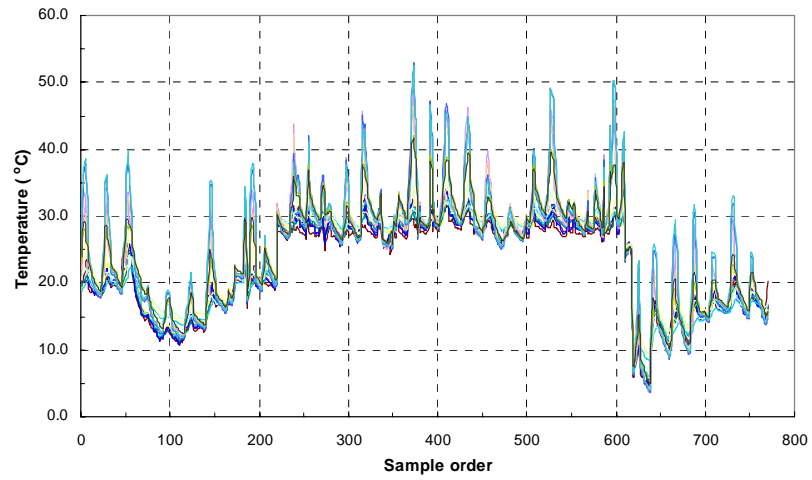
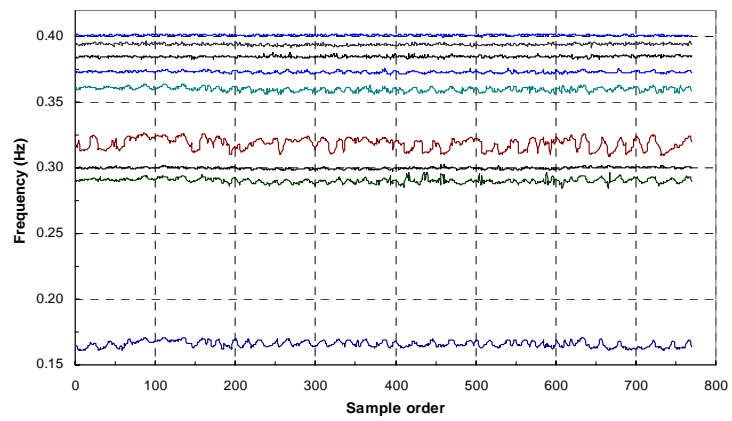
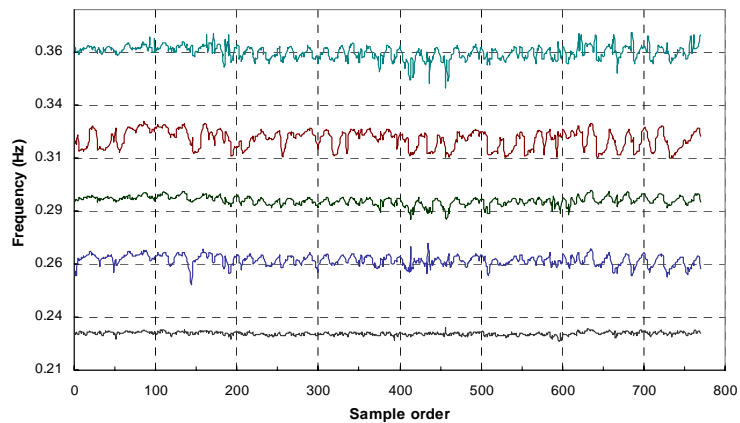


**Figure 7.4 Variation of hourly-average temperatures from 20 temperature sensors**



(a)



(b)

**Figure 7.5 Variation of measured modal frequencies: (a) from vertically oriented accelerometers; (b) from laterally oriented accelerometers**

### 7.3.2 *Measurement Data of Modal Frequency*

An automatic modal identification program has been developed for continuous extraction of modal parameters from ambient vibration measurements (Ni *et al.* 2005). This program employs the Complex Modal Indication Function (CMIF) algorithm and uses simultaneously all the measured data from 67 accelerometer channels for output-only modal identification. With the 770-hour data, the program automatically identifies modal parameters of the bridge at one-hour intervals.

**Figure 7.5** shows the variation of the identified modal frequencies from vertically and laterally oriented accelerometers, respectively. Table 7.1 summarizes the statistics of identified modal frequencies. For the Ting Kau Bridge, it is found that the first ten modes lie in the frequency range of 0.1 to 0.4 Hz, indicating closely spaced modes in this bridge. Except that the first mode is almost a purely vertical mode, all other modes are coupled modes with participation of both vertical and lateral modal components. Variance of the measured frequencies for the first ten modes is between 0.20% and 1.43%. The standard deviation given in the table represents the absolute error (variability) of the measured modal frequencies. The larger value of standard deviation for the 6th mode indicates that this mode exhibits a relatively large frequency variation, as observed in **Figure 7.5** where the 6th mode has a wider frequency band. It means that the 6th mode is sensitive to environmental change. It is also possible that there exist two close modes within that frequency band. These effects may mask the modal change caused by structural damage, and therefore must be well understood before reliable use of vibration-based damage identification algorithms.

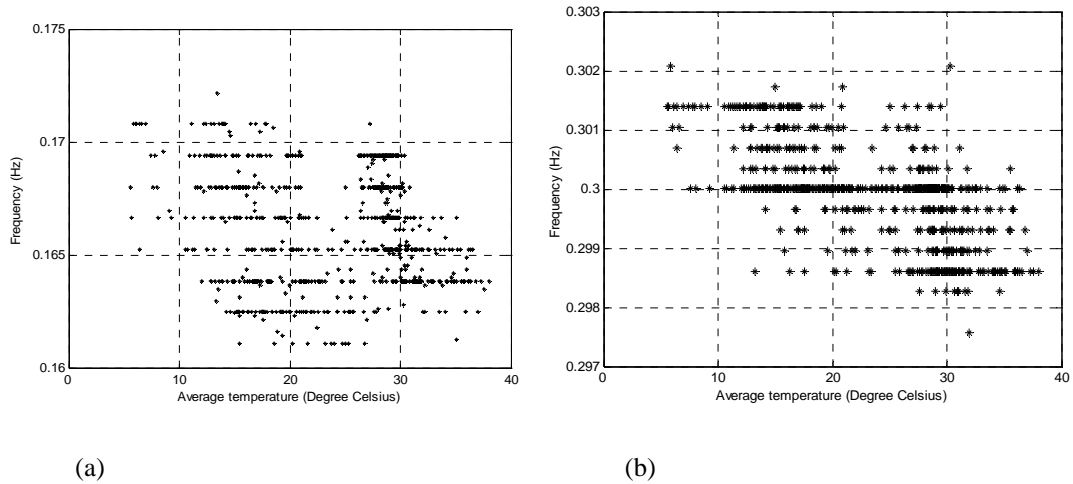


**Figure 7.6 Modal frequency versus hourly-average temperature:  
(a) 1st mode; (b) 5th mode**

Figure 7.6 illustrates the measured frequency versus the hourly-average temperature from all 20 sensors for the first and fifth modes, respectively. For all the measured modes, an overall decrease in modal frequency with the increase of temperature is observed. However, the temperature-frequency plotting is far from a linear relationship and highly dispersed. It implies that linear regression models should be incompetent for characterizing such a scattered relation.

**Table 7.1 Statistics of identified modal frequencies**

<i>Mode</i>	<i>Frequency range (Hz)</i>	<i>Average frequency (Hz)</i>	<i>Standard deviation (<math>10^{-3}</math>)</i>	<i>Variance (%)</i>	<i>Description</i>
1	0.150-0.175	0.1659	2.378	1.43	Predominantly vertical mode
2	0.215-0.235	0.2273	0.783	0.34	Coupled torsional & lateral mode
3	0.245-0.275	0.2618	2.506	0.96	Predominantly lateral mode
4	0.275-0.305	0.2902	2.036	0.70	Coupled lateral & torsional mode
5	0.290-0.308	0.2999	0.746	0.25	Predominantly vertical mode
6	0.305-0.335	0.3186	4.302	1.35	Coupled torsional & lateral mode
7	0.340-0.370	0.3600	1.675	0.47	Predominantly vertical mode
8	0.369-0.381	0.3731	0.840	0.23	Predominantly vertical mode
9	0.380-0.390	0.3849	0.685	0.18	Predominantly torsional mode
10	0.388-0.402	0.3942	0.791	0.20	Coupled lateral & torsional mode

## 7.4 Model Development

In this section, SVR models are first trained using the original temperature data to compare the performance of the models with their hyper-parameters determined by the grid search method and the heuristic method, respectively. Then both ‘static’ and ‘dynamic’ SVR models are formulated using 87-hour continuously measured data to examine the influence of temporal correlation on model accuracy. Next, SVR models are developed using PCA-compressed data and their performances are compared with those trained directly using the original measurement data in terms of model accuracy and computational costs. The PCA-based SVR model is also compared with a MLR model obtained using the same training data. Finally, both hypothesis test and goodness-of-fit test are conducted to assess the performance of the formulated SVR model. In this study, a normalization of the training and validation data has been made to achieve a fixed feature range  $[-1, 1]$  ( $r = 2$ ).

### 7.4.1 Training and Validation Using Original Data

SVR models are first trained directly using the original measurement data. The grid search method is first implemented to determine the optimal SVR hyper-parameters ( $C, \gamma, \varepsilon$ ). The grid points are generated by dividing the intervals of  $C \sim (2^{-10}, 2^{-9}, \dots, 2^3)$ ,  $\gamma \sim (2^{-15}, 2^{-14}, \dots, 2^5)$  and  $\varepsilon \sim (0, 1 \times 10^{-4}, \dots, 10^{-3})$ . For each combination (grid point) of the hyper-parameters, SVR models are trained using the original temperature and frequency data and evaluated by a 10-fold cross validation scheme. The total 770-hour measurement data have been used. Because they were not continuously measured, only ‘static’ SVR models can be formulated. All the formulation and validation are performed on a 2.8 GHz Pentium IV processor

running of Windows XP, with a total CPU time of about 1,254 minutes. **Figure 7.7** shows the average MSE versus the regularization parameter  $C$  and the kernel parameter  $\gamma$  under different values of the insensitive loss coefficient  $\varepsilon$  in the case of the first modal frequency. It is seen that MSE varies significantly with  $C$  and  $\gamma$ . Furthermore, there exists a dependency between  $C$  and  $\gamma$  for a good model with small MSE; for example, a small  $C$  should be accompanied by a large  $\gamma$  and vice versa. This inverse dependency can be justified from Equations (7.12) and (7.31). As the regularization parameter  $C$  is used to take a trade-off between the model complexity and the empirical error, small model errors should be accommodated by a ‘flat’ kernel, thus enforcing a large value of the kernel parameter  $\gamma$  according to Equation (7.31).

**Figure 7.8** illustrates the variation of minimal MSE with  $\varepsilon$ , where the minimal MSE is obtained by picking up the valley of the previous MSE versus  $(C, \gamma)$  surface for each  $\varepsilon$ . It is observed that the variation of MSE with  $\varepsilon$  is relatively smooth, particularly in the range of  $\varepsilon$  from  $4 \times 10^{-4}$  to  $7 \times 10^{-4}$ . As a result, it can be reasonably assumed that the selection of  $\varepsilon$  can be independent of  $C$  and  $\gamma$ . Such an observation coincides with the performance of  $\nu$  in the  $\nu$ -SVR formulation in which the MSE exhibits a relatively flat curve in terms of hyper-parameter  $\nu$  (Chalimourda *et al.* 2004). The SVR model with the smallest MSE is obtained when  $\varepsilon$  is approximately equal to 0.0006. In this way the optimal SVR hyper-parameters are finally determined as  $C = 0.03125$ ,  $\gamma = 8.0$ , and  $\varepsilon = 0.0006$ , and the corresponding MSE is  $1.58 \times 10^{-6}$ .

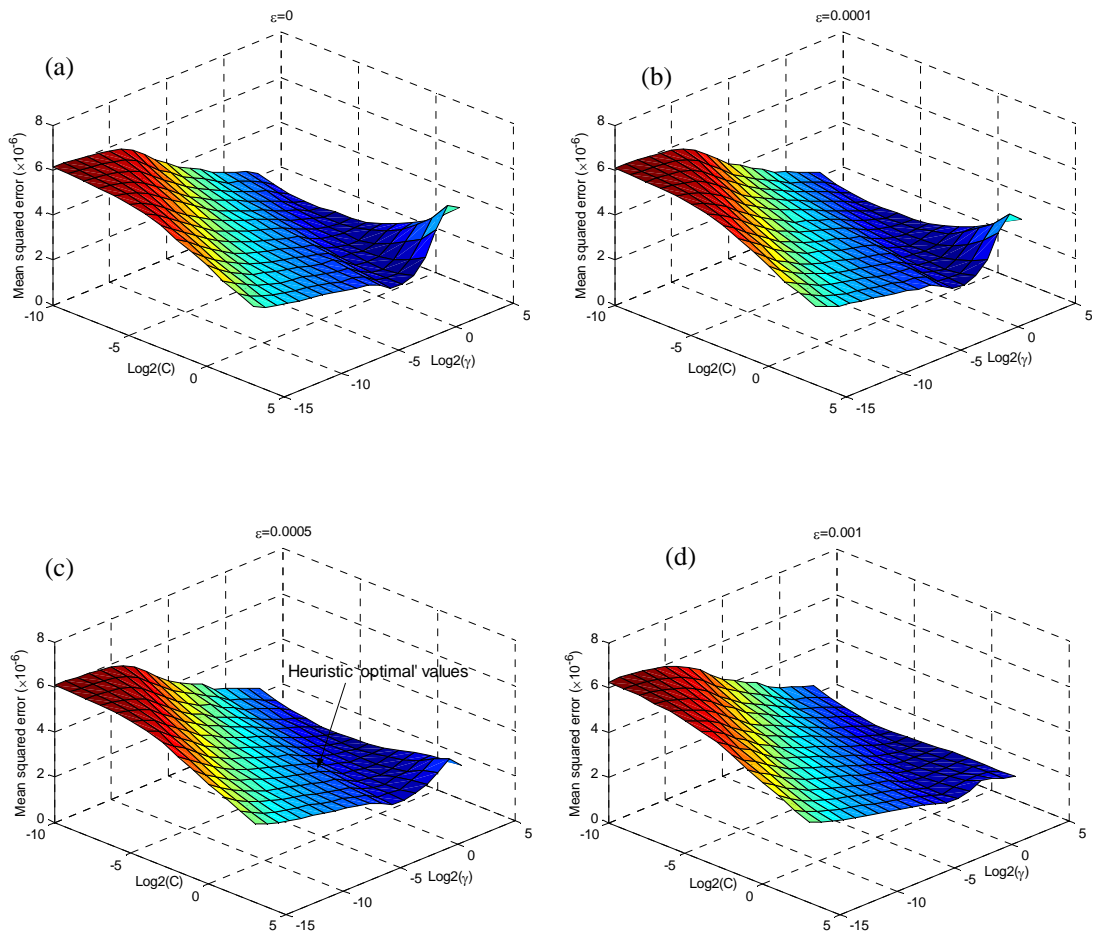


**Figure 7.7 MSE versus  $C$  and  $\gamma$  :**  
**(a)  $\varepsilon = 0$ ; (b)  $\varepsilon = 0.0001$ ; (c)  $\varepsilon = 0.0005$ ; (d)  $\varepsilon = 0.001$**

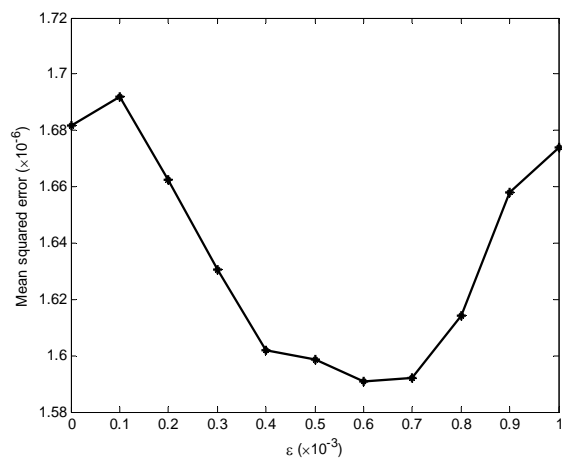


**Figure 7.8 Minimal MSE versus  $\varepsilon$**

SVR models are then formulated with the hyper-parameters determined by the heuristic method. With a general assumption that the noise level in measured modal frequency is 1% (Doebbling *et al.* 1998), the heuristic ‘optimal’ values of SVR hyper-parameters are obtained using Equations (7.38) to (7.40). They are listed in Table 7.2 and also shown in **Figure 7.7(c)** for comparison. It is found that the optimal values of  $\varepsilon$  obtained from the heuristic method and the grid search method agree very well but both  $C$  and  $\gamma$  deviate significantly from each other. This difference is attributed to the fact that the optimal values of  $C$  and  $\gamma$  were determined independently in the heuristic method while those obtained from the grid search method were found to be interdependent (a more detailed observation on the dependency between  $C$  and  $\gamma$  will be made later in formulating SVR models using PCA-compressed data). Making use of the heuristic ‘optimal’ values of the hyper-parameters, SVR models are trained again using the same original data and evaluated by 10-fold cross validation. The average MSE is obtained to be  $1.92 \times 10^{-6}$  in this case. It is therefore found that the difference of MSE values obtained from the two methods is relatively small although the heuristic ‘optimal’ values are quite different from those obtained by the grid search method. This indicates that there are a number of ‘nearly optimal’ hyper-parameter values with good model performances.

**Table 7.2 Heuristic optimal values of SVR hyper-parameters**

<i>Parameter</i>	$\bar{y}$ (Hz)	$\sigma_y$ (Hz)	$\sigma$ (Hz)	$m$	$p$	$r$	$C$	$\varepsilon$	$\gamma$
Value	0.1661	0.0025	0.0017	770	20	2	0.1735	0.0005	0.5~0.5873

#### 7.4.2 SVR Model Considering Thermal Inertia Effect

In order to examine the influence of temporal correlation on model performance, a ‘static’ SVR model (SVR1) without considering temporal correlation and a ‘dynamic’ SVR model (SVR2) with considering temporal correlation are formulated, respectively, using 87-hour continuously measured original data. The grid search method together with 10-fold cross validation is employed to determine the optimal values of SVR hyper-parameters. An augmented temperature vector defined as Equation (7.8) should be constructed in formulating the ‘dynamic’ SVR model. In 10-fold cross validation, the data measured in the last time step for the  $(i-1)$ th subset has been included to construct the first element of the augmented vector for the  $i$ th subset to keep temporal correlation.

The MSE values for SVR1 and SVR2 are obtained following the same approach as before. **Figures 7.9 and 7.10** show the average MSE versus the regularization parameter  $C$  and the kernel parameter  $\gamma$  under different values of the insensitive loss coefficient  $\varepsilon$  in the case of the first modal frequency for the ‘static’ regression model and the ‘dynamic’ regression model, respectively. **Figure 7.11** presents the resulting minimal MSE versus  $\varepsilon$  for the two models, from which the smallest MSE is determined to be  $2.24 \times 10^{-6}$  for SVR1 and  $1.08 \times 10^{-6}$  for SVR2, respectively. After specifying the optimal hyper-parameters which achieve the smallest MSE, the two models are tested by presenting the 87-hour measurement data, and the residual is obtained by the formula

$$e_i = y_{ri} - y_{pi} \quad (i = 1, 2, \dots, m) \quad (7.41)$$

where  $y_{pi}$  denotes the prediction value of the  $i$ th sample and  $y_{ri}$  represents the target (observation) value of the  $i$ th sample;  $m$  is equal to 87 in this case.

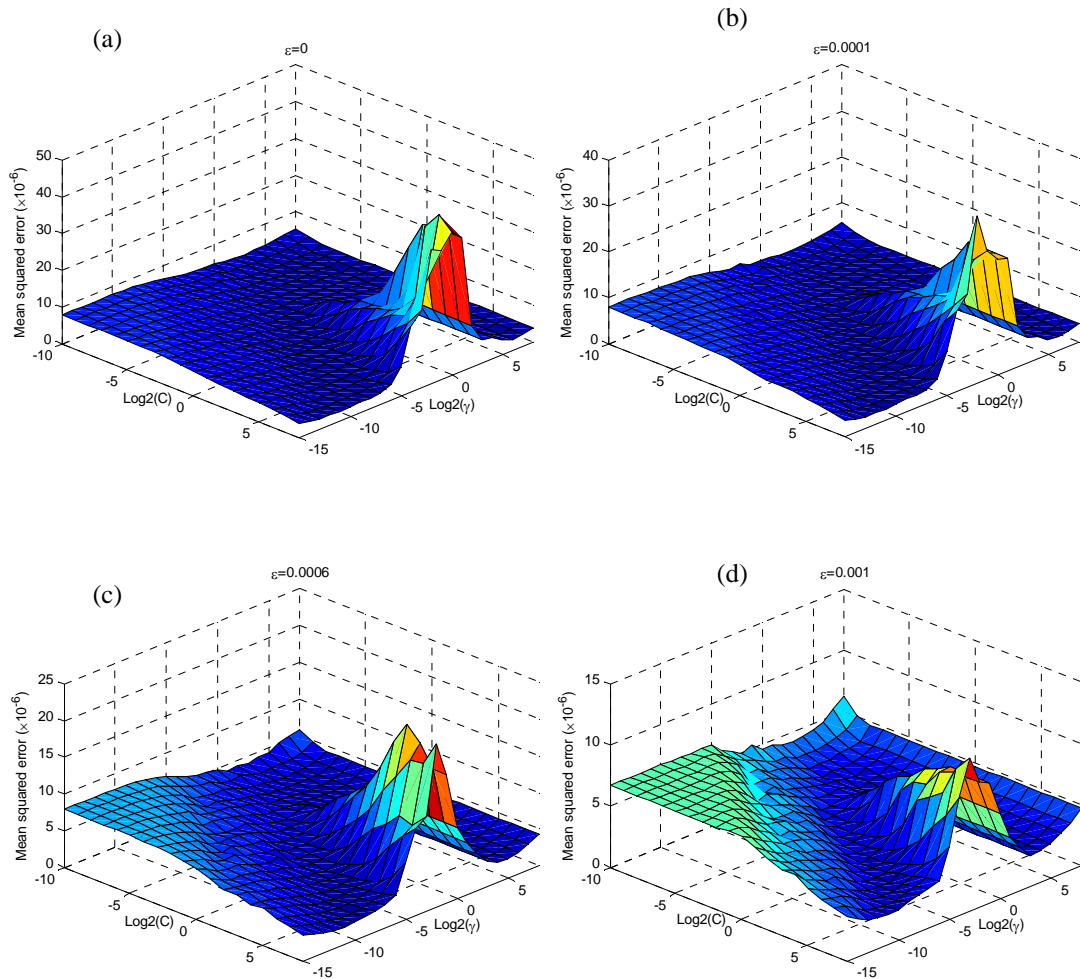


**Figure 7.9 MSE versus  $C$  and  $\gamma$  for SVR1:**  
**(a)  $\epsilon = 0$ ; (b)  $\epsilon = 0.0001$ ; (c)  $\epsilon = 0.0005$ ; (d)  $\epsilon = 0.001$**

**Figure 7.12** illustrates the residual sequences generated by SVR1 and SVR2, respectively. By comparing both MSE and residual obtained from the two models, it is concluded the ‘dynamic’ SVR model is superior to the ‘static’ SVR model. It validates that the change of modal frequency indeed lags behind the temperature variation, and ‘dynamic’ regression models incorporating thermal inertia effect are preferable to represent the temperature-frequency correlation when continuous

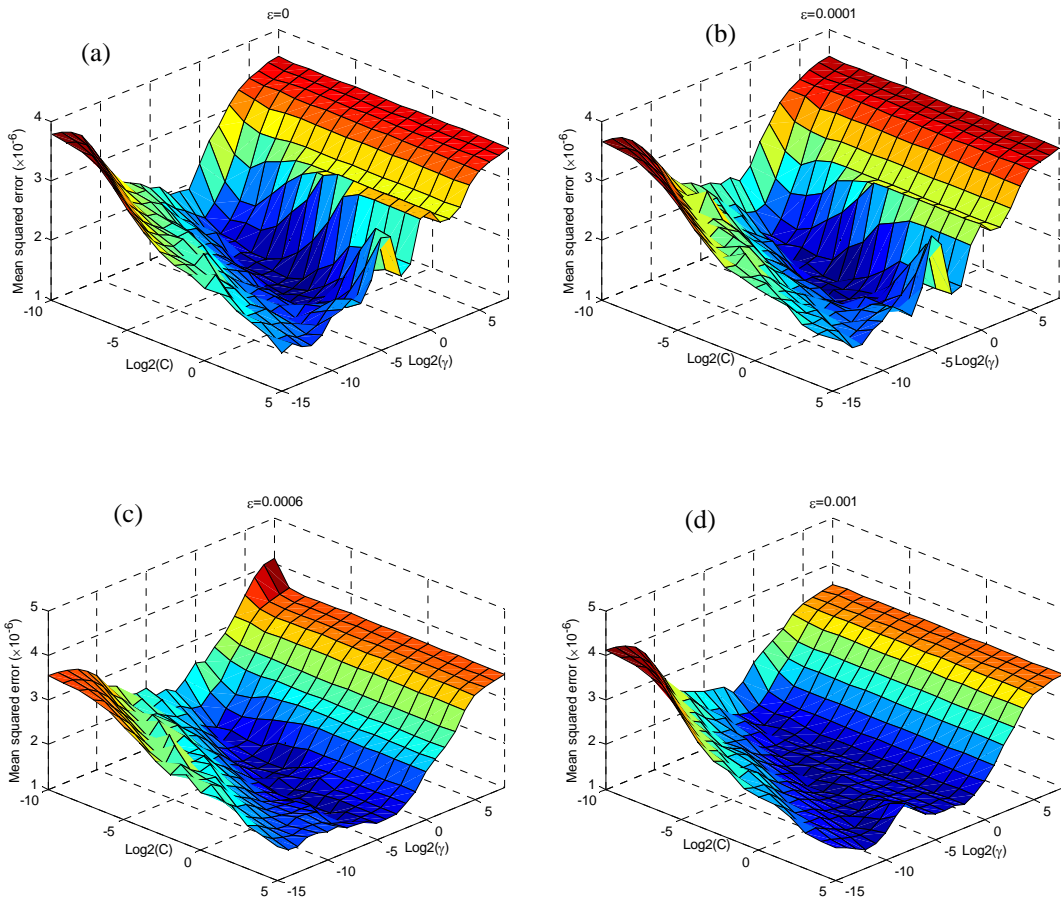


**Figure 7.10 MSE versus  $C$  and  $\gamma$  for SVR2:**  
**(a)  $\varepsilon = 0$ ; (b)  $\varepsilon = 0.0001$ ; (c)  $\varepsilon = 0.0005$ ; (d)  $\varepsilon = 0.001$**

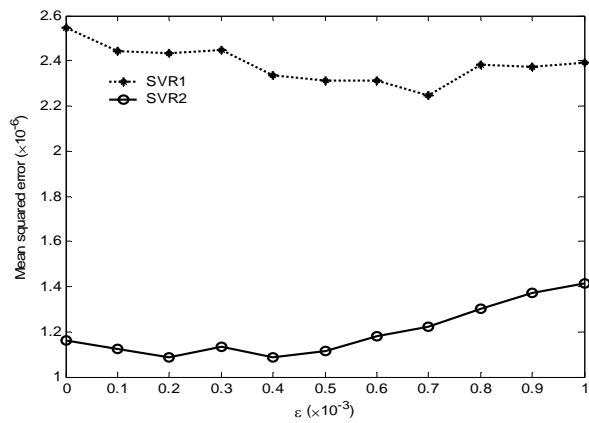


**Figure 7.11 Minimal MSE versus  $\varepsilon$  for SVR1 and SVR2**

measurement data are available. However, the long-term measurement data from an on-line monitoring system are usually discontinuous because of the existence of an automatic trigger system and abnormal signals.

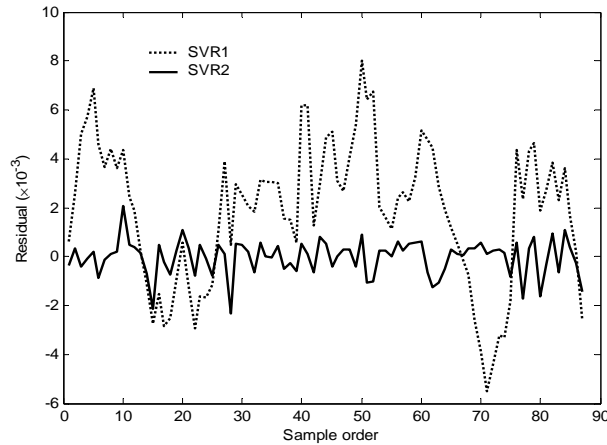


**Figure 7.12 Residual of SVR1 and SVR2**

### ***7.4.3 PCA-Based Compression of Temperature Data***

PCA is conducted on the total 770 sets of temperature measurement data from 20 sensors to extract predominant feature vectors. Table 7.3 summarizes the eigenvalues of covariance matrix for the 770 sets of temperature data, and **Figure 7.13** shows the graph of eigenvalues. It is found that the first two principal components account for 99.1% and the first 14 principal components account for 99.99% of the total variance. It comes to the conclusion that temperatures measured at different locations are heavily correlated. We can retain the first  $p$  components ( $p < 20$  in this case) as predominant feature vectors for dimension reduction of the input vectors used in regression.

**Figure 7.14** shows the measured frequency versus the first PC for the first and fifth vibration modes with the correlation coefficient being -0.1733 and -0.6142, respectively. Again the temperature-frequency plotting is considerably scattered. It indicates that one PC might be inadequate for charactering the correlation. However, instead of arbitrary selection of feature vectors from the original space, the selection of feature vectors in the transformed PC space is straightforward since the first several PCs represent the major variation in the original data.

**Table 7.3 Eigenvalues of covariance matrix for temperature data**

<i>No.</i>	<i>Eigenvalue</i>	<i>Proportion of variance</i>	<i>Cumulative proportion</i>
1	1042.368	0.947	0.94727
2	47.949	0.044	0.99085
3	3.106	0.003	0.99367
4	2.581	0.002	0.99602
5	0.951	$8.6 \times 10^{-4}$	0.99688
6	0.882	$8.0 \times 10^{-4}$	0.99768
7	0.798	$7.2 \times 10^{-4}$	0.99841
8	0.532	$4.8 \times 10^{-4}$	0.99889
9	0.444	$4.0 \times 10^{-4}$	0.99929
10	0.233	$2.1 \times 10^{-4}$	0.99951
11	0.198	$1.8 \times 10^{-4}$	0.99969
12	0.125	$1.1 \times 10^{-4}$	0.99980
13	0.061	$5.5 \times 10^{-5}$	0.99985
14	0.046	$4.2 \times 10^{-5}$	0.99990
15	0.039	$3.6 \times 10^{-5}$	0.99993
16	0.029	$2.6 \times 10^{-5}$	0.99996
17	0.022	$2.0 \times 10^{-5}$	0.99998
18	0.012	$1.1 \times 10^{-5}$	0.99999
19	0.009	$8.4 \times 10^{-6}$	1.00000
20	0.002	$1.8 \times 10^{-6}$	1.00000

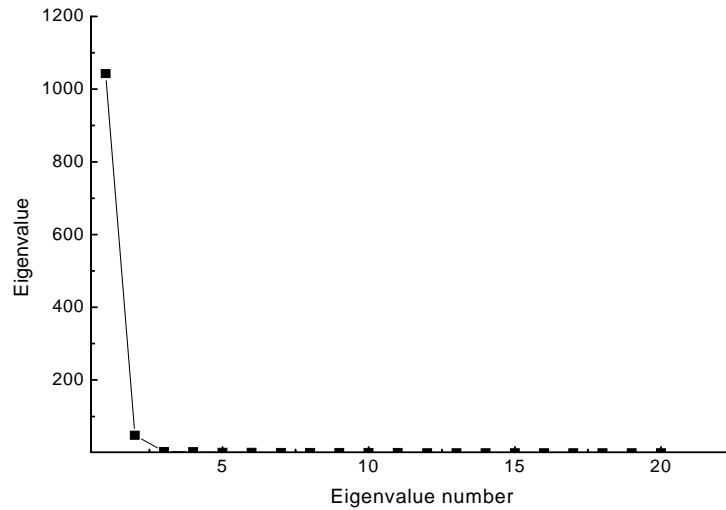


**Figure 7.13** Graph of eigenvalues of covariance matrix for temperature data

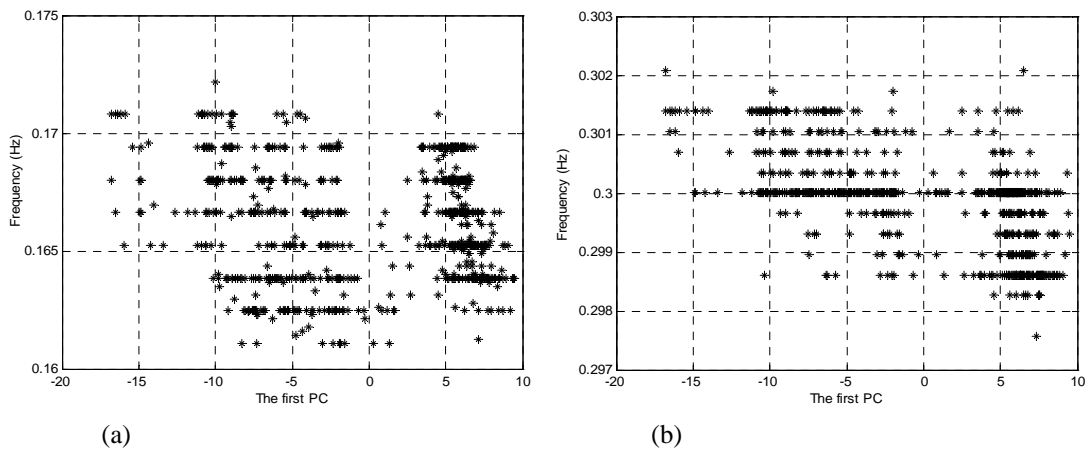


**Figure 7.14** Modal frequency versus the first PC: (a) 1st mode; (b) 5th mode

#### 7.4.4 Training and Validation Using PCA-Compressed Data

SVR models are now trained using the PCA-compressed feature vectors, and compared with those trained directly using the original measurement data in terms of model accuracy and computational costs. First, all the 20 normalized principal components are fed into the support vector algorithm for model formulation. So the

function of PCA in this case is just a coordinate transformation. Because PCA was conducted on the total 770-hour data which were intermittently measured, only the ‘static’ SVR model is trained. The grid search method with 10-fold cross validation is used again for choosing the optimal values of SVR hyper-parameters.

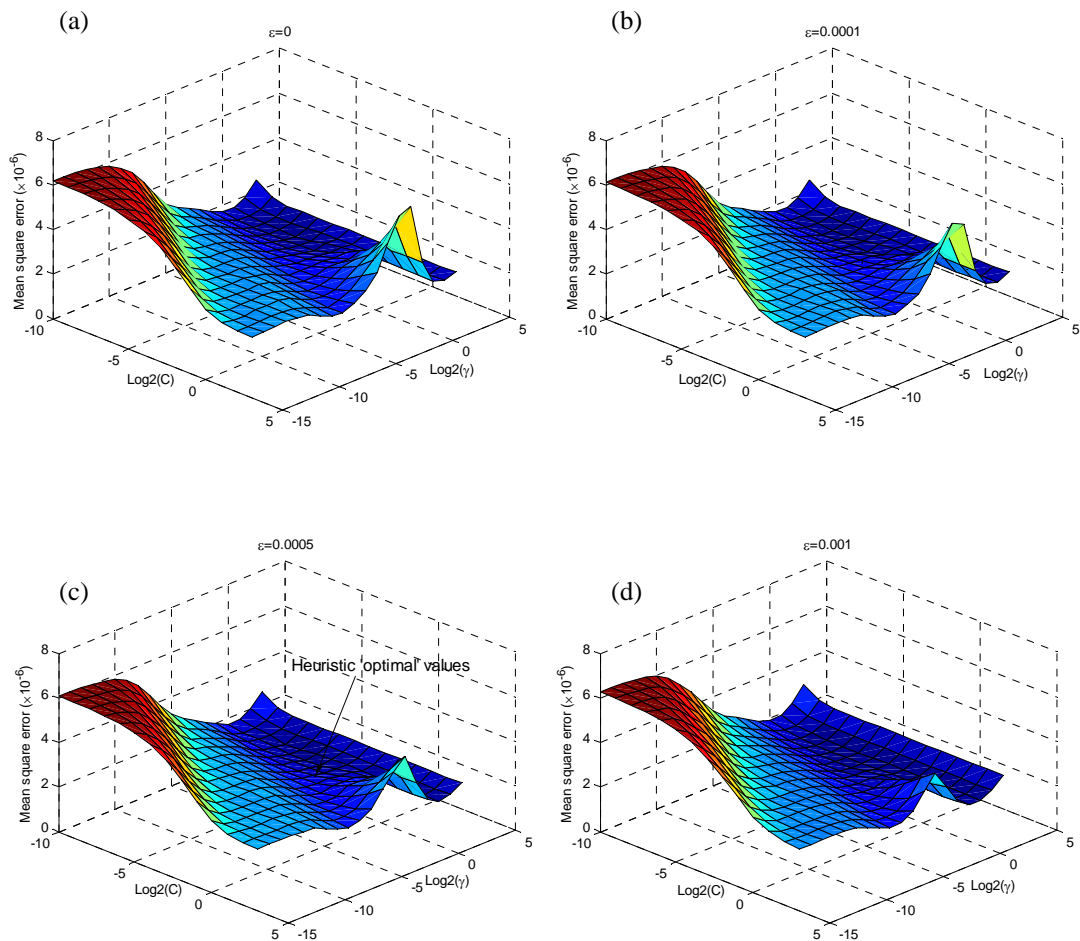


**Figure 7.15 MSE versus  $C$  and  $\gamma$  when using 20 PCs:  
 (a)  $\epsilon = 0$ ; (b)  $\epsilon = 0.0001$ ; (c)  $\epsilon = 0.0005$  (d)  $\epsilon = 0.001$**

**Figure 7.15** illustrates the average MSE versus  $C$  and  $\gamma$  under different values of  $\epsilon$  in the case of the first modal frequency. The MSE surface shows a similar dependency between  $C$  and  $\gamma$  as that in **Figure 7.7**. For a small value of  $\gamma$ , the SVR model has its optimal performance at large  $C$  values. This is further validated by

**Figure 7.16** which shows the optimal values of  $C$  for a series of given  $\gamma$  when  $\varepsilon = 0$ .

It is observed that the optimal  $C$  is approximately inversely proportional to  $\gamma$ .

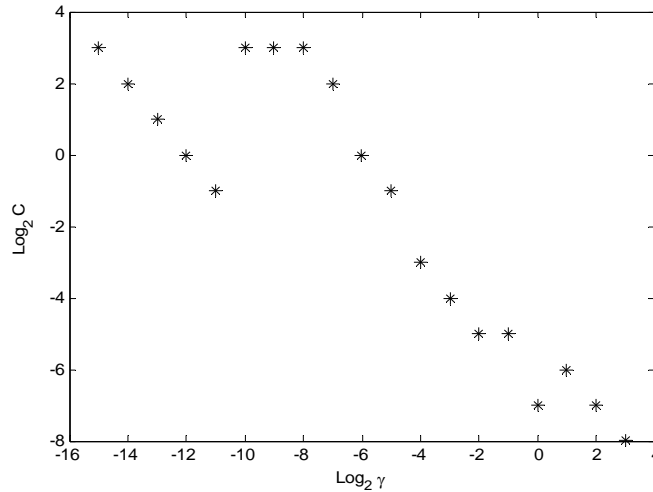


**Figure 7.16** Dependency between optimal  $C$  and  $\gamma$  for  $\varepsilon = 0$

**Figure 7.17** illustrates the variation of minimal MSE with  $\varepsilon$ , where the minimal MSE is obtained by picking up the valley of the MSE surface for each  $\varepsilon$ . From this figure the optimal values of SVR hyper-parameters are determined as  $C = 0.00781$ ,  $\gamma = 2.0$ , and  $\varepsilon = 0.0005$ , which achieve the smallest MSE of  $1.44 \times 10^{-6}$ . This smallest MSE value indicates an improvement of model performance even when using all 20 PCs. The optimal values of the parameters  $C$  and  $\gamma$  obtained in the PC space differ significantly from those obtained in the original data space because they depend on the distribution of the  $\mathbf{x}$  data, while the optimal value of the parameter  $\varepsilon$  remains almost unchanged as it depends on the noise level in the  $y$  data. For comparison, the ‘optimal’ values of SVR hyper-parameters obtained by the heuristic method are also indicated in **Figure 7.15**.

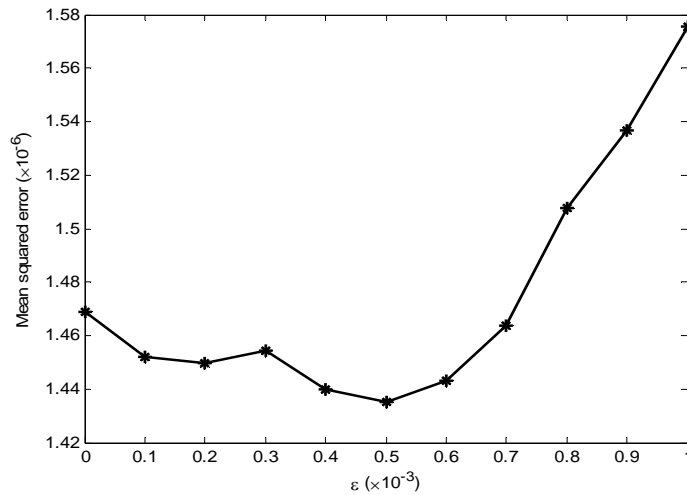


**Figure 7.17 Minimal MSE versus  $\epsilon$  when using 20 PCs**

Then the number of PCs is selected to achieve the optimal SVR model. By increasing the number of PCs from 1 to 20, SVR models are formulated with the optimal hyper-parameters resulting from the grid search method and the heuristic method, respectively, and the corresponding MSE values are evaluated using 10-fold cross validation as shown in Table 7.4. The CPU time for formulation and validation of each SVR model when using the grid search method is also provided in the table for comparison. It is observed that when the number of PCs is increased from one to six, MSE has a dramatic reduction. Then MSE has insignificant change with the increase in the number of PCs. It is therefore concluded that selecting the first six PCs as feature vectors will achieve a SVR model with favorable generalization performance. As the smallest MSE value ( $1.38 \times 10^{-6}$ ) is achieved when the first 16 PCs are included, the optimal SVR model is defined as SVR16 which incorporates the first 16 PCs and has the hyper-parameters  $C = 0.0156$ ,  $\gamma = 2.0$ , and  $\epsilon = 0.0004$ . The SVR16 model outperforms the SVR model trained using the original data in both model accuracy and computational costs.

**Table 7.4 Comparison of MSE values for different PCs**

<i>No. of PCs</i>	<i>Grid search method</i>			<i>Heuristic method</i>	
	$(C, \gamma, \epsilon)$	MSE ( $\times 10^{-6}$ )	CPU time (minutes)	$(C, \gamma, \epsilon)$	MSE ( $\times 10^{-6}$ )
1	(0.0313, 8, 0.0009)	4.64	264	(0.1735, 1.39, 0.0005)	5.12
2	(0.0625, 8, 0.0008)	3.54	398	(0.1735, 0.83, 0.0005)	3.93
3	(0.0625, 8, 0.0009)	2.46	452	(0.1735, 0.70, 0.0005)	2.97
4	(0.0156, 8, 0.0009)	2.20	460	(0.1735, 0.64, 0.0005)	2.75
5	(0.0313, 8, 0.0008)	1.97	480	(0.1735, 0.61, 0.0005)	2.60
6	(0.0313, 8, 0.0007)	1.66	517	(0.1735, 0.59, 0.0005)	2.60
7	(0.0313, 8, 0.0007)	1.70	1100	(0.1735, 0.58, 0.0005)	2.56
8	(0.0156, 8, 0.0007)	1.71	495	(0.1735, 0.57, 0.0005)	2.42
9	(0.0156, 8, 0.0005)	1.62	539	(0.1735, 0.56, 0.0005)	2.42
10	(0.0156, 8, 0.0006)	1.67	587	(0.1735, 0.55, 0.0005)	2.24
11	(0.0781, 8, 0.0005)	1.59	656	(0.1735, 0.55, 0.0005)	2.00
12	(0.0781, 4, 0.0005)	1.54	672	(0.1735, 0.54, 0.0005)	1.88
13	(0.0156, 2, 0.0006)	1.45	711	(0.1735, 0.54, 0.0005)	1.75
14	(0.0156, 2, 0.0006)	1.42	756	(0.1735, 0.54, 0.0005)	1.60
15	(0.0313, 2, 0.0004)	1.40	780	(0.1735, 0.54, 0.0005)	1.61
16	(0.0156, 2, 0.0004)	1.38	760	(0.1735, 0.53, 0.0005)	1.58
17	(0.0156, 2, 0.0005)	1.44	852	(0.1735, 0.53, 0.0005)	1.63
18	(0.0156, 2, 0.0004)	1.40	902	(0.1735, 0.53, 0.0005)	1.64
19	(0.0156, 2, 0.0004)	1.45	905	(0.1735, 0.53, 0.0005)	1.69
20	(0.0781, 2, 0.0005)	1.44	980	(0.1735, 0.50, 0.0005)	1.70

**7.4.5 Comparison between SVR and MLR Models**

In this section the SVR model is compared with a multivariate linear regression (MLR) model. We also include the first 16 PCs of temperature data in the formulation of the MLR model. The MLR model using the first 16 PCs is expressed by

$$y = w_0 + \sum_{i=1}^{16} w_i z_i \tag{7.42}$$

where  $z_i$  ( $i = 1, 2, \dots, 16$ ) are the PCs, and  $w_i$  ( $i = 0, 1, \dots, 16$ ) are unknown coefficients which are estimated using the measurement data by the least squares method.

**Figure 7.18** provides a comparison of the residual generated by the SVR model and the MLR model. In **Figure 7.18(a)**, the SVR model is SVR16 with the optimal hyper-parameters. It is seen that the SVR16 model notably outperforms the MLR model in prediction capability. The SVR model shown in **Figure 7.18(b)** is trained by using a linear kernel and taking a very large  $C$  ( $=10^3$ ) and zero  $\varepsilon$ . In this case the SVR model approximately reduces to a linear regression model, and the residual generated by this model matches well with that from the MLR model as shown in **Figure 7.18(b)**. It is therefore concluded that the SVR model performs much better and equips with more flexibility than the MLR model.

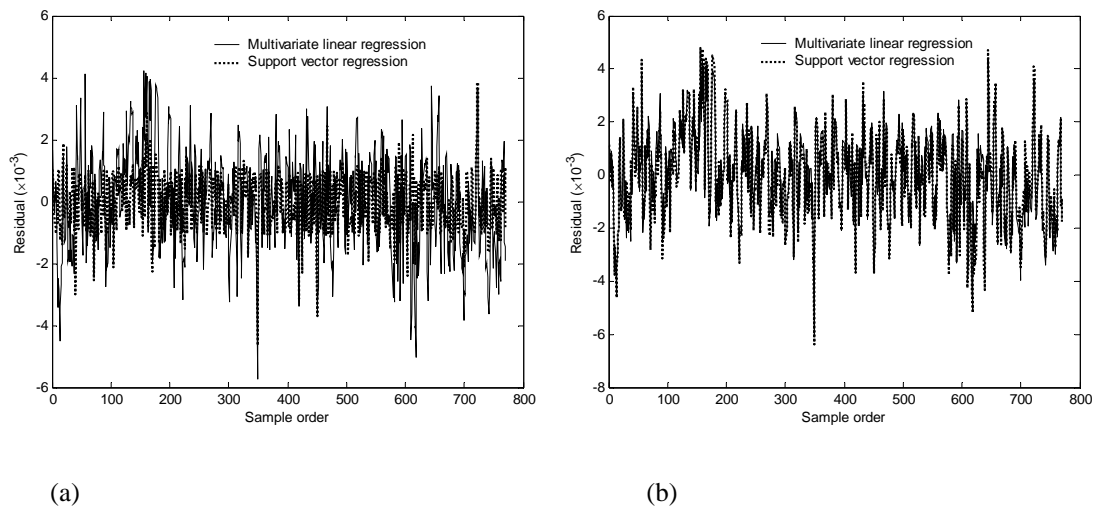


**Figure 7.18 Residual of SVR model and MLR model:**  
**(a) optimal SVR model; (b) linear SVR model with extremely large  $C$  and zero  $\varepsilon$**

#### 7.4.6 Assessment of Model Performance

The performance of the SVR16 model is assessed by different methods. **Figure 7.19** shows the modal frequency sequence predicted by the SVR16 model in comparison with the measured modal frequency sequence for the first mode. A favorable agreement between the predicted and measured results is observed. Similar observations are also obtained for the higher modes. Because of the discontinuous measurement data, the SVR16 model was formulated without considering temporal correlation. A more accurate SVR model is expected when continuous measurement data is available and temporal correlation is accounted for.

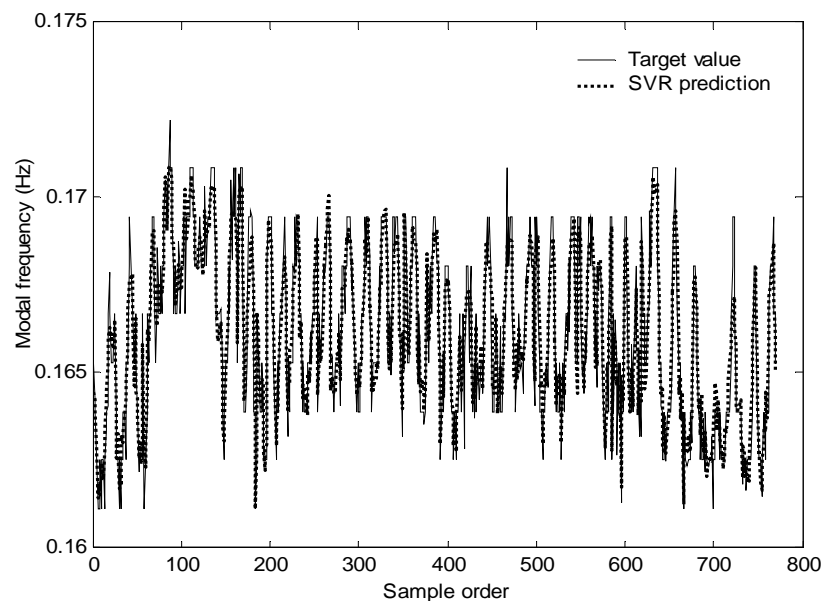


**Figure 7.19** Comparison between predicted and observed modal frequencies

A hypothesis test and a goodness-of-fit test are further conducted on the SVR16 model to provide more quantitative performance measures. It is generally assumed in statistical analysis that the measurement noise follows a normal distribution with

zero mean. As a result, if the residual generated by the model complies with a normal distribution with zero mean, it can be reasonably assumed that no useful information can be further extracted from the residual. The mean and the standard deviation of the residual are calculated by

$$\mu = \frac{1}{m} \sum_{i=1}^m e_i \quad (7.43)$$

$$s = \sqrt{\frac{1}{m-p} \sum_{i=1}^m e_i^2} \quad (7.44)$$

where  $m$  is the number of samples;  $p$  is the dimension of feature vectors, which is equal to sixteen for the SVR16 model.

In the hypothesis test, the hypothesis of interest is that the mean of the residual is equal to zero (null hypothesis), versus the alternative that it is not equal to zero:

$$H_0 : \mu = 0 \quad \text{vs} \quad H_1 : \mu \neq 0 \quad (7.45)$$

using the  $t$ -statistic

$$t = \frac{\mu - 0}{s / \sqrt{m}} \quad (7.46)$$

If  $H_0$  is true,  $t$  is distributed as  $t_{m-1}$ .  $H_0$  will be rejected if  $\left| \frac{\mu}{s / \sqrt{m}} \right| \geq t_{\alpha/2, m-1}$ , where

$t_{\alpha/2, m-1}$  is a critical value that can be found in the  $t$ -table (Rencher 2002). Table 7.5 shows the hypothesis test results for the residual generated by the SVR16 model, where the value of  $\alpha$  is taken as 0.05. The results indicate that  $H_0$  is accepted as the

absolute value of  $t$ -statistic is less than the critical value. The acceptance of  $H_0$  implies that the mean of the residual is equal to zero ( $\mu = 0$ ) in a statistical sense.

**Figure 7.20** shows the observed probability density function (PDF) and cumulative distribution function (CDF) of the residual and the corresponding theoretical curves produced by the best-fitted normal distribution. By conducting the Kolmogorov-Smirnov goodness-of-fit test (Kottegoda and Rosso 1997) on the observed PDF and CDF, the residual is shown to agree with a normal distribution. It is therefore concluded that the residual generated by the SVR16 model complies statistically with a normal distribution with zero mean.

**Table 7.5 Residual statistics and hypothesis test results**

<i>Item</i>	<i>Residual</i>		<i>t statistic</i>	<i>Critical value</i>
	Mean value	Standard derivation		
Value	$-3.76 \times 10^{-5}$	$7.13 \times 10^{-4}$	-1.46	1.96

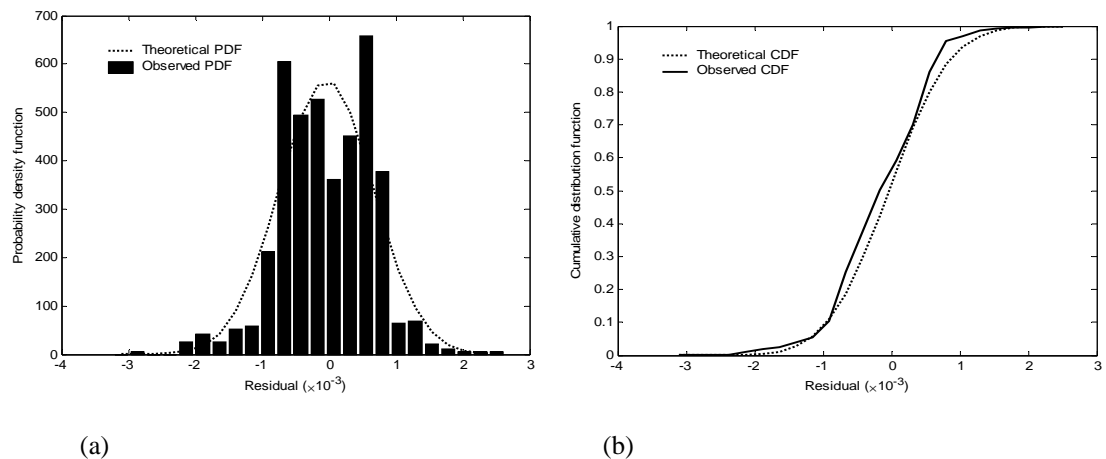


**Figure 7.20 Probability distribution of residual: (a) PDF; (b) CDF**

## 7.5 Summary

In this chapter, a combined PCA and SVR method is presented for modelling temperature-caused variability of structural modal frequencies based on long-term measurement data. Various types of vector, including original temperature vector, augmented temperature vector and principal components of original temperature vector, have been used as input feature for support vector regression. It has been shown that the SVR model trained using the PCA-compressed feature vector outperforms the SVR model trained using original data in both model accuracy and computational costs. When continuous measurement data are available, the ‘dynamic’ SVR model which is trained using augmented temperature vector to account for temporal correlation provides more accurate frequency prediction than the ‘static’ SVR model without considering temporal correlation. The PCA-based SVR model is superior to the MLR model in terms of generalization capability and model flexibility. The combined PCA and SVR method was proposed for modelling the temperature-frequency correlation in this study; however, the same approach can be applied to other data-based regression problems.

The influence of SVR hyper-parameters on the model performance has been studied in detail by the use of ‘real-world’ data acquired from a large-scale bridge. A grid search method with 10-fold cross validation has been applied to determine the optimal values of SVR hyper-parameters to achieve good generalization performances, and compared with the heuristic method proposed by Cherkassky and Ma (2004). It is shown that the optimal values of the hyper-parameters  $C$  and  $\gamma$  obtained from the two methods may deviate largely, but the difference in the corresponding MSE values is insignificant. For the problem in study, the grid search

method shows that there is an approximate inversely proportional relation between the optimal values of  $C$  and  $\gamma$ . This finding on the parameter interdependency shall be helpful for developing better empirical formulae to calculate the optimal hyper-parameters as the current heuristic formulae estimate the optimal hyper-parameters independently. This issue deserves further investigation.

## Chapter 8

# ASSESSMENT OF BRIDGE EXPANSION JOINTS USING LONG-TERM DISPLACEMENT AND TEMPERATURE MEASUREMENT

### 8.1 Introduction

Long-term structural health monitoring has become an important tool for diagnosing and prognosing structural performance and conditions in civil engineering community (Aktan *et al.* 2002; Ko and Ni 2005; Wang 2005). This is witnessed by tremendous growth in the implementation of long-term monitoring systems in bridge structures. Successful implementation and operation of structural health monitoring systems on bridges have been widely reported in different countries (Andersen and Pedersen 1994; Cheung *et al.* 1997; Barrish *et al.* 2000; Sumitro *et al.* 2001; Mufti 2002; Koh *et al.* 2003; Wang *et al.* 2003; Wong 2004; Wang 2005). When a bridge is instrumented with a structural health monitoring system, the bridge administrative authority and managers want to know how the monitoring system benefits the inspection, maintenance, and management of the bridge, and how to use the monitoring data for bridge health and condition assessment. Research attention has recently been paid to the use of monitoring data for improved operational efficiency of structures, safety/reliability enhancement, and lower maintenance costs (Chang 2003).

Expansion joints are important components in bridge structures which are used to accommodate bridge movements due to creep and shrinkage of concrete, temperature fluctuations, traffic loadings, and uneven settlement without imposing significant secondary stress to the superstructure (Dornsife 2000). The thermal movements of expansion joints due to temperature fluctuations are an important consideration in bridge design. Temperature in a deck cross-section can be divided into effective temperature which results in thermal movements and differential temperature (temperature gradient) which gives rise to internal forces and stresses for restrained structures. Bridge design codes in some countries have provided provisions related to the range of effective temperature, as well as the differential temperature for the calculation of structural response caused by thermal effects (e.g., British Standards Institution 1978; Hong Kong Highways Department Structures Division 1997; Canadian Standards Association 2000). Continuous monitoring of actual thermal movements at expansion joints and their comparison with design values can provide verification on the design. Likewise, since the service life of an expansion joint rely to a great extent on its accumulative displacement (the total displacement experienced by the expansion joint), an accurate prediction of the accumulative displacement based on measurement data will offer reliable information for decision making on prolonging or shortening the interval for replacement.

A long-term structural health monitoring system for a large-scale bridge usually includes the measurement of both displacement at expansion joints and temperature on one or several deck cross-sections (Cheung *et al.* 1997; Aktan *et al.* 2002; Wong 2004; Ku *et al.* 2005). In this chapter, a procedure for condition assessment based on long-term monitoring of expansion joint displacement and bridge temperature is presented and applied to the cable-stayed Ting Kau Bridge with the use of one-year

measurement data. A regression analysis is first conducted to establish the normal correlation pattern with an appropriate confidence interval, which will be used for anomaly alarming if the future monitoring data disobeys the normal pattern. Making use of the established correlation pattern and extreme value analysis, the maximum thermal movements of expansion joints and the extreme temperatures are predicted and compared with the corresponding design values for verification and actual safety reserve checking. Finally, annual or daily-average accumulative displacements of expansion joints are estimated by using the measurement data, which will provide information to justify or amend the scheduled interval for replacement of expansion joints.

## **8.2 Presentation of Procedure**

### **8.2.1 Establishment of Normal Correlation Pattern**

Temperature in a bridge deck cross-section can be divided into the differential temperature and the effective temperature (Li *et al.* 2004; Fu and DeWolf 2004). The differential temperature refers to temperature differences between the top surface and other levels in that cross-section, and will result in the temperature-induced internal forces and bending stresses in continuous structures. The current design code for highway bridges in Hong Kong specifies both positive temperature profile and reverse temperature profile across the section for design of thermal effects of differential temperature. Four types of differential temperatures are defined in the code for different types of construction and materials used. The effective temperature is an average of temperature distributed along the cross-section. According to the definition, the effective temperature can be expressed as

$$T = \frac{1}{A} \iint_A \bar{T}(x, y) dx dy \quad (8.1)$$

where  $A$  is the area of the cross-section;  $\bar{T}(x, y)$  is a two-dimensional temperature over the cross-section.

For the measurement of temperature on a deck cross-section, the cross-section section is usually divided into a number of sub-areas, and sensors are deployed to measure the temperature in each sub-area. On the assumption that the temperature in all locations of a sub-area is the same, the effective temperature can be obtained by weighted averaging of the temperatures measured at all sub-areas, where the weighting is the ratio of each sub-area to the total area of the cross-section. That is

$$T = \sum_{i=1}^k \frac{A_i}{A} \bar{T}_i \quad (8.2)$$

where  $A_i$  is the  $i$ th sub-area;  $\bar{T}_i$  is the measured temperature at the  $i$ th sub-area; and  $k$  is the number of sub-areas divided for the cross-section.

The thermal movement due to effective temperature  $T$  can be calculated by

$$\Delta_T = \alpha L (T - T_0) \quad (8.3)$$

where  $\alpha$  is the coefficient of thermal expansion, which can be taken as  $12 \times 10^{-6}$  per °C for structural steel and  $9 \times 10^{-6}$  per °C for concrete;  $L$  is the expansion length of structure subject to thermal variation; and  $T_0$  is the reference temperature.

Provided the maximum and minimum effective temperatures  $T_{\max}$  and  $T_{\min}$  for a certain return period, the design allowable displacements at expansion joints accounting for thermal effects are obtained as

$$\Delta_{\text{temp}} = \alpha L (T_{\max} - T_{\min}) \quad (8.4)$$

It should be noted that for long-span cable-stayed bridges, the expansion length  $L$  is usually difficult to accurately determine since it is affected by the presence of stay cables and cross girders. In addition, temperatures are not uniformly distributed along the bridge length. With the measurement data of displacement at expansion joints and effective temperature in a deck cross-section, a regression analysis can be carried out by assuming the following linear relationship

$$\Delta = \beta_1 T + \beta_0 \quad (8.5)$$

where  $\Delta$  is the displacement of an expansion joint; and  $T$  is the effective temperature at a deck cross-section. The regression coefficients  $\beta_1$  and  $\beta_0$  can be obtained by the least-squares method as

$$\beta_1 = \frac{S_{\Delta T}}{S_{TT}} \quad (8.6)$$

$$\beta_0 = \bar{\Delta} - \beta_1 \bar{T} \quad (8.7)$$

where  $S_{TT}$  is the variance of the measured temperature sequence;  $S_{\Delta T}$  is the covariance between the measured displacement and temperature sequences; and  $\bar{T}$  and  $\bar{\Delta}$  are means of the measured temperature and displacement sequences, respectively.

The residual of the regression model, which is defined as the difference between the observed and predicted values, is calculated by

$$e_i = \Delta_i - (\beta_1 T_i + \beta_0) \quad (8.8)$$

and the variance of the residual is obtained as

$$\hat{\sigma}^2 = \frac{1}{n-2} \sum_{i=1}^n (\Delta_i - \beta_1 T_i - \beta_0)^2 \quad (8.9)$$

where  $n$  is the number of samples.

For real applications, an interval under a certain confidence level is necessary to account for the inherent uncertainties due to randomness in the measurement data, incompleteness of the empirical model, and so on. The upper and lower bounds of an interval under a confidence of  $1 - \alpha$  for the predicted output  $\Delta_0$  at a given input  $T_0$  are described as

$$\hat{\Delta}_0 \pm t_{n-2, \alpha/2} \hat{\sigma} \sqrt{1 + \frac{1}{n} + \frac{(T_0 - \bar{T})^2}{S_{TT}}} \quad (8.10)$$

where  $\hat{\Delta}_0 = \beta_0 + \beta_1 T_0$ ; and  $t_{n-2, \alpha/2}$  is a critical value which can be obtained from the  $t$ -table (Kottegoda and Rosso 1997).

With the measurement data of expansion joint displacement and bridge deck temperature, the regression model expressed in Equation (8.5) and bounds of the confidence interval described by Equation (8.10) can be readily obtained. Once the normal correlation pattern is established, the newly measured displacement and temperature data can be fed into the established model for anomaly detection of the expansion joints. By substituting the design maximum and minimum effective

temperatures into the regression model, the displacement range of expansion joints due to temperature variation is predicted. Then a design validation can be conducted by comparing the predicted displacement range with the corresponding design value.

### ***8.2.2 Prediction of Extreme Temperatures***

During the design of long-span bridges, it is of importance to estimate, as accurately as possible, the extreme temperatures with a certain return period. Overestimation of the extreme temperatures will lead to economical over-design, whereas underestimation may pose a danger to bridge safety and serviceability. With the long-term monitoring data, a reasonable estimation of the extreme temperatures can be made.

Extreme value analysis (EVA) has been widely used in various engineering fields where extreme values are of importance (Castillo 1988; Castillo *et al.* 2005). EVA is a statistical technique that concentrates on the behavior of the extreme observations instead of the complete sample population and allows the generalization of return periods of extreme events. In the present study, EVA technique is employed for the evaluation of extreme effective temperatures at bridge deck based on a set of maxima and minima of the measured temperatures, with the intention of estimating the magnitudes of thermal variables for a certain return period.

Given the samples of maxima and minima from original observations, EVA attempts to parametrically fit the data to one of the three limiting distributions, namely the Frechet distribution, the Gumbel distribution, and the Weibull distribution (Castillo 1988). Gumbel (1958) has observed that tails of the frequency distributions of most

climatic variables such as temperature fall off in an exponential manner, and the extreme values of these variables comply with the following Gumbel distribution

$$F(T) = \exp\left(-\exp\left(-\frac{T-\lambda}{\delta}\right)\right) \quad -\infty < T < +\infty \quad (8.11)$$

where  $\lambda, \delta$  are constants to be determined from measurement data. The formulated distribution model is then used to extrapolate extremes with a specified return period.

Rearranging Equation (8.11) leads to

$$T = \lambda - \delta \ln(-\ln F(T)) \quad (8.12)$$

Denoting the sample sequence of maxima or minima for the measured effective temperatures by  $T_1, T_2, \dots, T_k$  where  $T_i$ 's are increasingly ordered with  $T_1 \leq T_2 \leq \dots \leq T_k$  and  $k$  is the number of total samples, the cumulative probability of the sample  $T_i$  is estimated as

$$p_i = \frac{i}{k+1} \quad (8.13)$$

As  $p_i$  is a rational estimate of the limiting distribution function  $F(T_i)$ , it follows from Equation (8.12) that

$$T_i = \lambda - \delta \ln(-\ln p_i) \quad (8.14)$$

Thus the coefficients  $\lambda$  and  $\delta$  can be best fitted from the above equation with the use of the temperature samples  $T_i$  and the corresponding cumulative probabilities  $p_i$  ( $i = 1, 2, \dots, k$ ). Extreme temperatures with a return period of  $y$  years are then estimated by

$$T_R = \lambda - \delta \ln \left( -\ln \left( 1 - \frac{1}{ky} \right) \right) \quad (8.15)$$

or

$$T_R \approx \lambda + \delta R \quad (8.16)$$

where  $R = \ln(ky)$  is termed as the reduced variate.

Making use of the long-term temperature monitoring data and Equation (8.15), the maximum and minimum effective temperatures for a return period equal to the bridge design life can be predicted. Verification is then conducted by comparing the predicted extreme temperatures with the corresponding design values.

### 8.2.3 *Estimation of Accumulative Displacements*

As the service life and interval for replacement of an expansion joint rely to a great extent on the accumulative displacement that the expansion joint experienced, it is of significance to obtain the actual daily and annual accumulative displacement. Upon the assumption of linear evolution of the accumulative displacement with time, annual and daily-average accumulative displacements can be readily estimated from the continuous monitoring data. Suppose that the design value of daily accumulative displacement is  $D_d$  from which the scheduled interval for replacement of expansion joints is determined as  $N_d$  years. When the actual daily-average accumulative displacement is measured to be  $D_m$ , a reasonable alteration of the interval for replacement of expansion joints can be made by assuming a linear dependence of the required replacement interval on the accumulative displacement, i.e.,

$$N_m = \frac{D_d}{D_m} N_d \quad (8.17)$$

where  $N_m$  is the updated interval (years) for replacement of expansion joints. If  $D_m$  is less than  $D_d$  and no rupture and damage due to over-strength are observed in the expansion joints after  $N_d$  years, it can be considered to prolong the interval for replacement of expansion joints as  $N_m$  years.

### 8.3 Application to Ting Kau Bridge

#### 8.3.1 Measurement Data

The Ting Kau Bridge in Hong Kong, as shown in **Figure 8.1**, is a multi-span cable-stayed bridge with three towers supporting two main spans of 448 m and 475 m respectively and two side spans of 127 m each. Each of the three towers consists of a single reinforced concrete leg. The bridge deck comprises two separated composite beam- and-slab decks interconnected by cross girders as shown in **Figure 8.1(b)**. The bridge deck is supported by four planes of stay cables anchored at the tower tops. It is constrained laterally at the three towers and is fixed to the central tower longitudinally while being free with longitudinal movements at the other two towers. Additional longitudinal stabilizing cables have been used to stabilize the central tower.

After completing its construction in 1998, the bridge has been instrumented with a long-term structural health monitoring system by the Hong Kong SAR Highways Department (Wong 2004). This system consists of more than 230 sensors of various types, including anemometers, accelerometers, displacement transducers,

temperature sensors, strain gauges, weigh-in-motion sensors and global positioning system. The displacement transducers have been used for the measurement of displacements at two expansion joints located at two ends of the continuous deck. A total of 83 temperature sensors have been installed at different locations of the bridge to measure: (i) steel- girder temperature, (ii) temperature inside concrete deck, (iii) temperature in tower legs, (iv) temperature in asphalt pavement, and (v) atmosphere temperature. The deployment of displacement transducers and temperature sensors on the Ting Kau Bridge is illustrated in **Figure 8.1**. **Figure 8.2** shows the layout of a displacement transducer at the Tsing Yi abutment and temperature sensors on the deck cross-section nearly in the middle of the Tsing Yi main span. The displacement transducer was installed for the measurement of longitudinal movement of the expansion joint and a total of 51 temperature sensors were installed on the deck cross-section for the measurement of steel, concrete, asphalt and atmosphere temperature.

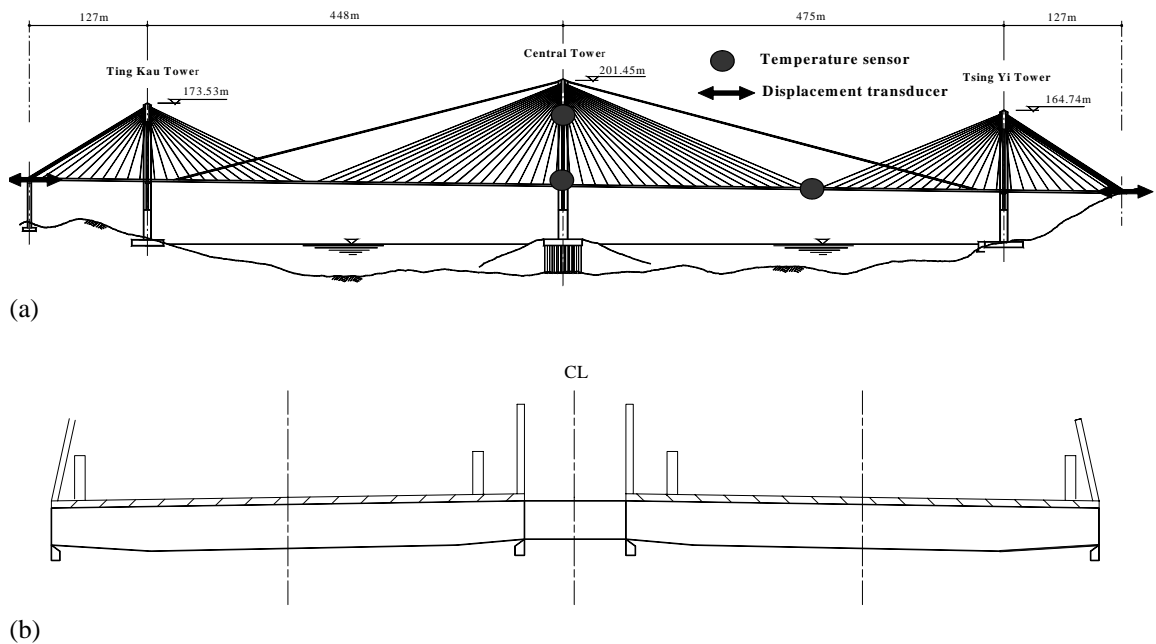


**Figure 8.1 Ting Kau Bridge: (a) elevation; (b) cross-section**

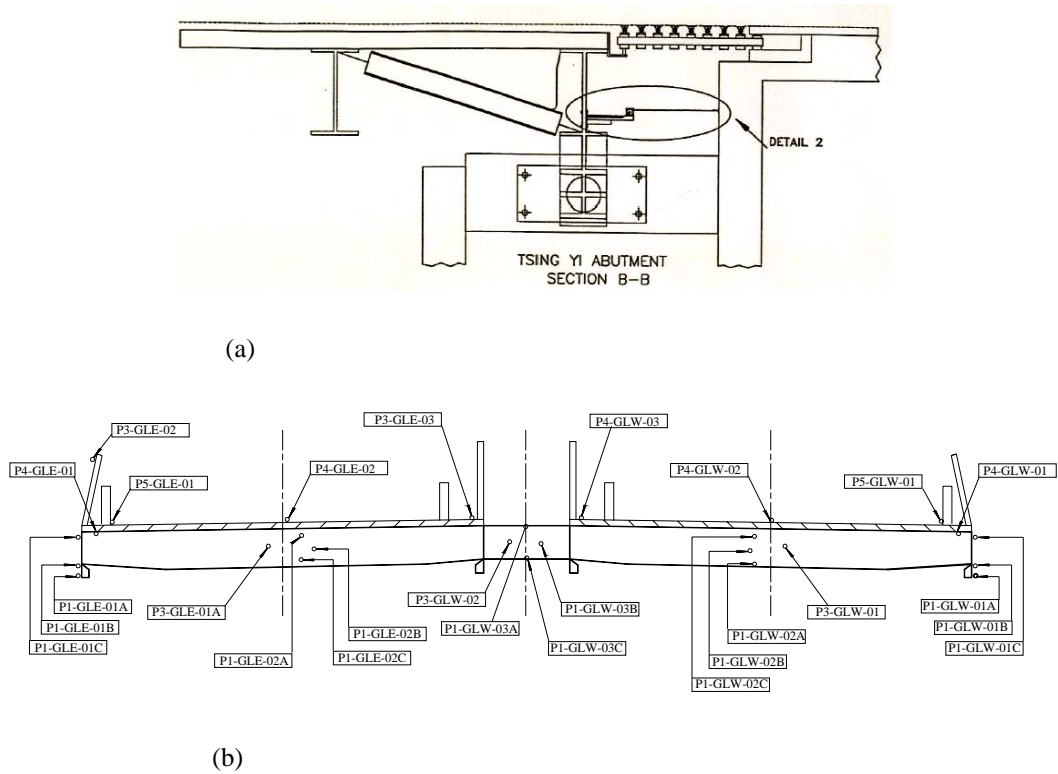


**Figure 8.2 Layout of sensors on Ting Kau Bridge: (a) displacement transducer at Tsing Yi abutment; (b) temperature sensors on deck cross-section**

Available for this study is one-year (the year of 1999) continuous measurement data from all sensors installed on the Ting Kau Bridge (Wang 2003). The data obtained in 1999 is used herein because they reflect the behavior of a healthy bridge. The temperature and displacement measurement data was acquired with the sampling rates of 0.07 Hz and 2.56 Hz respectively, from which the hourly-average values of the temperatures and displacements have been obtained. **Figure 8.3** shows the hourly-average temperatures for a 24-hour duration on the deck cross-section nearly in the middle of the Tsing Yi main span, which were obtained from 4 sensors in structural steel, 4 sensors in concrete, 4 sensors in atmosphere and 4 sensors in asphalt. The locations of these sensors on the cross-section are specified in **Figure 8.2(b)**. It is observed that in general the temperatures in asphalt are the highest and

the temperatures in atmosphere are the lowest. The temperatures measured at different locations on the same cross-section attain their maxima almost at the same hour.

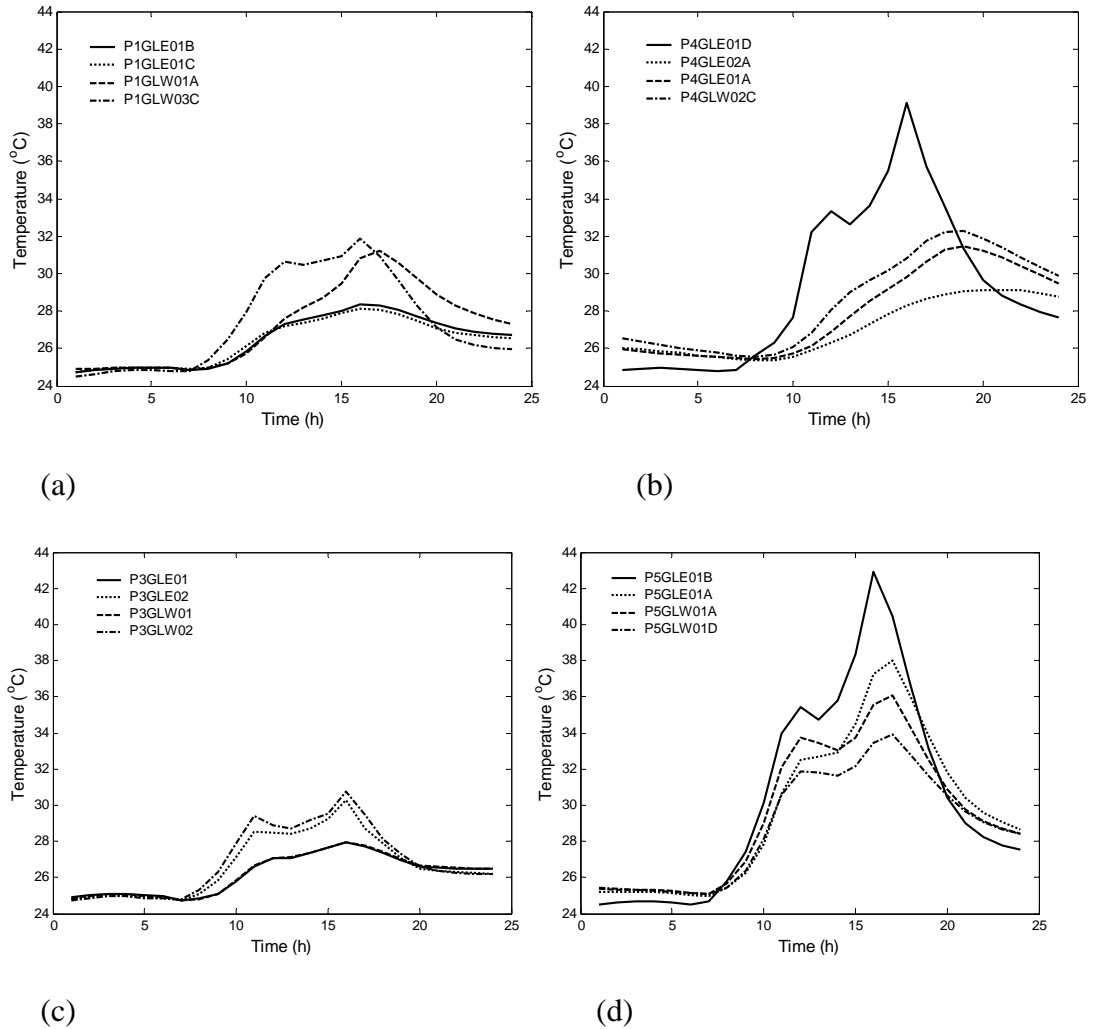


**Figure 8.3 Hourly-average temperatures on deck cross-section: (a) in structural steel; (b) in structural concrete; (c) in atmosphere; (d) in asphalt**

**Figure 8.4** illustrates the hourly-average displacements of expansion joints at the Ting Kau and Tsing Yi abutments for a 24-hour duration, where DSGAW01 denotes the displacement at the Ting Kau abutment and DSGPW01 denotes the displacement

at the Tsing Yi abutment. It is observed that the displacement change rates coincide with each other very well.

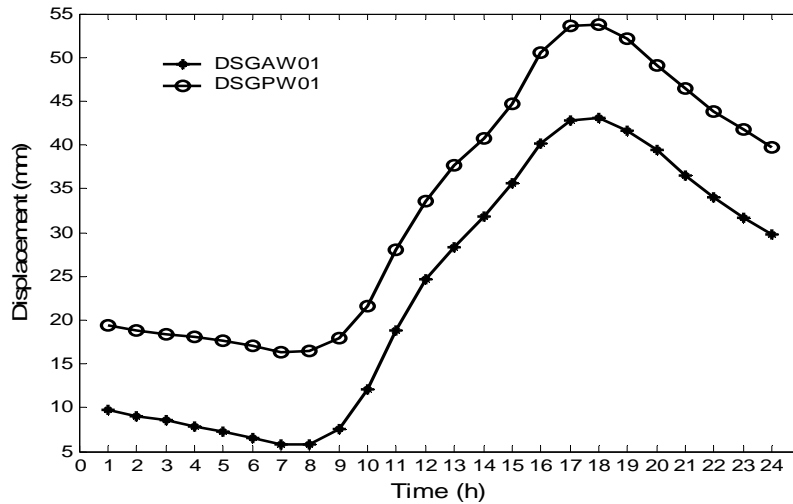


**Figure 8.4 Hourly-average displacements of expansion joints**

### 8.3.2 Analysis and Assessment

The measured displacements at the two expansion joints and the measured temperatures on the deck cross-section nearly in the middle of the Tsing Yi main span are used for analysis. According to the provision (Hong Kong Highways Department Structure Division 1997), the effective temperature on a deck cross-section should be estimated by using only the measured temperatures in structural components exclusive of those in asphalt and air. As a result, the measured temperatures from 39 sensors on the deck cross-section, including 15 in structural steel and 24 in concrete, are used to calculate the effective temperature. By dividing the cross-section into 39 sub-areas, the effective temperature can be readily estimated from Equation (8.2) making use of the measured temperatures from the 39 sensors.

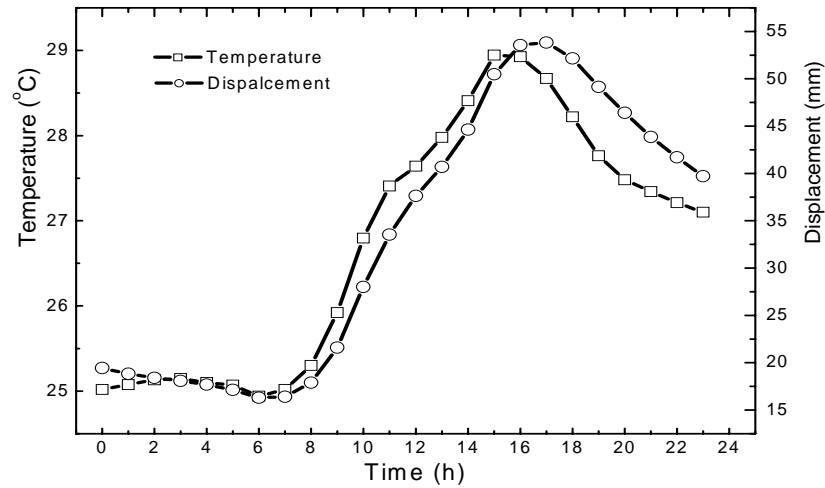


**Figure 8.5 Time histories of displacement and effective temperature**

After obtaining the effective temperature, a check on the correlation between the expansion joint displacement and the deck effective temperature is made. **Figure 8.5** shows the evolution of both the deck effective temperature and the expansion joint displacement at the Tsing Yi abutment with time. A good correlation is observed and it is therefore concluded that the temperature fluctuations mainly account for the movement of the expansion joint.

Before proceeding to the regression analysis, the one-year monitoring data were carefully screened to identify the outliers and eliminate unrealistic values. A total of 3400-hour data were finally selected for the regression analysis. Table 8.1 provides the regression parameters obtained from Equations (8.5) to (8.9), while **Figure 8.6** shows the measured and best-fitted relations between the displacement and effective temperature. It is known from Table 8.1 that the slopes of the linear regression functions are 8.13 mm/°C and 7.08 mm/°C for the expansion joints at the Ting Kau and Tsing Yi abutments, respectively. The regression functions are expressed as

$$\Delta = 8.13T - 192.46 \text{ (mm)} \quad \text{for Ting Kau abutment} \quad (8.18)$$

$$\Delta = 7.08T - 158.61 \text{ (mm)} \quad \text{for Tsing Yi abutment} \quad (8.19)$$

Design verification is made with Equations (8.18) and (8.19). Since the expansion lengths for spans at the left and right sides of the central tower are 575 m and 602 m, respectively, the corresponding thermal expansion coefficients are estimated as  $14.1 \times 10^{-6}$  per °C and  $11.8 \times 10^{-6}$  per °C, which are close to the design value of  $12.0 \times 10^{-6}$  per °C. The design maximum and minimum effective temperatures are 40 °C and -2 °C (Wong *et al.* 2002). By presenting these design values into Equations (8.18) and (8.19), the displacement range of the expansion joints due to temperature variation is calculated to be 341.46 mm and 297.36 mm for the Ting Kau and Tsing Yi abutments, respectively. They are very close to the design values of 339 mm and 297 mm.

**Table 8.1 Statistical parameters in regression analysis**

<i>Expansion joint</i>	<i>n</i>	$S_{TT}$ ( $^{\circ}\text{C}^2$ )	$S_{\Delta T}$ ( $\text{mm} \times ^{\circ}\text{C}$ )	$\bar{T}$ ( $^{\circ}\text{C}$ )	$\bar{\Delta}$ ( $\text{mm}$ )	$\beta_1$ ( $\text{mm}/^{\circ}\text{C}$ )	$\beta_0$ ( $\text{mm}$ )	$\sigma^2$ ( $\text{mm}^2$ )
Ting Kau side	3400	29.29	238.14	23.28	-3.15	8.13	-192.46	7.84
Tsing Yi side	3393	29.47	208.64	23.26	6.09	7.08	-158.61	7.59

The upper and lower bounds with a confidence level of 0.95 are also obtained from Equation (8.10) and illustrated in **Figure 8.6**. The bounds corresponding to an appropriate confidence level should be set to avoid false alarming. It is generally necessary to adjust the bounds after trial operation with the measurement data

obtained in the first few years. Once the normal correlation pattern is determined, new measurement data can be fed into it for anomaly detection of the expansion joints.

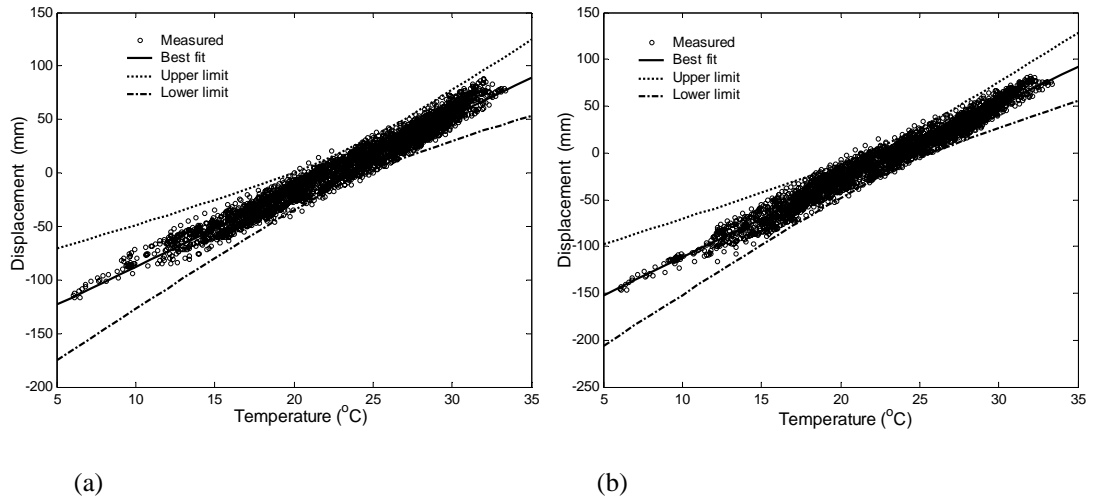


**Figure 8.6 Measured and fitted relations between displacement and effective temperature: (a) at the Ting Kau abutment; (b) at the Tsing Yi abutment**

To predict the extreme temperatures with a certain return period, the sequence of the measured effective temperature is first obtained as shown in **Figure 8.7** which comprises 3400 samples. EVA begins with the identification of peaks and valleys to generate extreme sequences on the basis of the total samples. As a rule of thumb, usually about  $0.5\%n$  peak and valley values are picked up to generate extreme sequences (Maes *et al.* 1992), where  $n$  is the total number of data points. Therefore the largest 17 ( $=0.5\% \times 3400$ ) peaks and the smallest 17 valleys of the measured temperature sequence are selected to form the maximum and minimum effective temperature sequences as shown in **Figure 8.8** for EVA. The Gumbel parameters  $\lambda$  and  $\delta$  are then obtained by least-squares fitting to Equation (8.14). Table 8.2 lists the identified parameters and **Figure 8.9** shows the measured and fitted relations

between the extreme temperature and reduced variate  $R$ . With the identified Gumbel parameters, the predicted extreme temperatures with a return period of  $y$  years are represented as

$$T_R = 32.61 + 0.31 \ln(8760y) \quad \text{for maximum temperature} \quad (8.20)$$

$$T_R = 7.71 - 0.82 \ln(8760y) \quad \text{for minimum temperature} \quad (8.21)$$

where 8,760 is the number of hours per year.

The design lifespan of the Ting Kau Bridge is 120 years. With Equations (8.20) and (8.21), the maximum and minimum effective temperatures for a return period of 120 years are predicted to be 36.9 °C and -3.6 °C, respectively. In comparison with these prediction values, the design maximum and minimum effective temperatures for bearing expansions are 40 °C and -2 °C with a return period of 120 years.

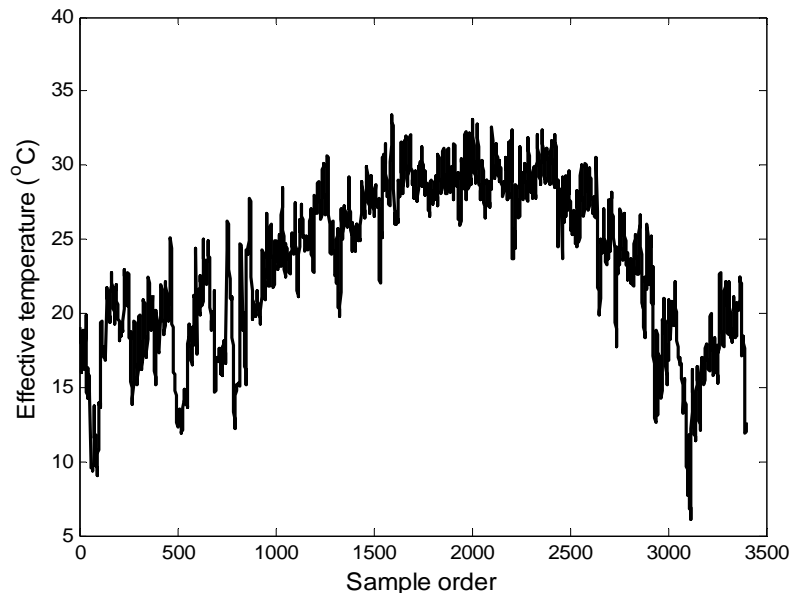


**Figure 8.7 Sequence of measured effective temperatures**

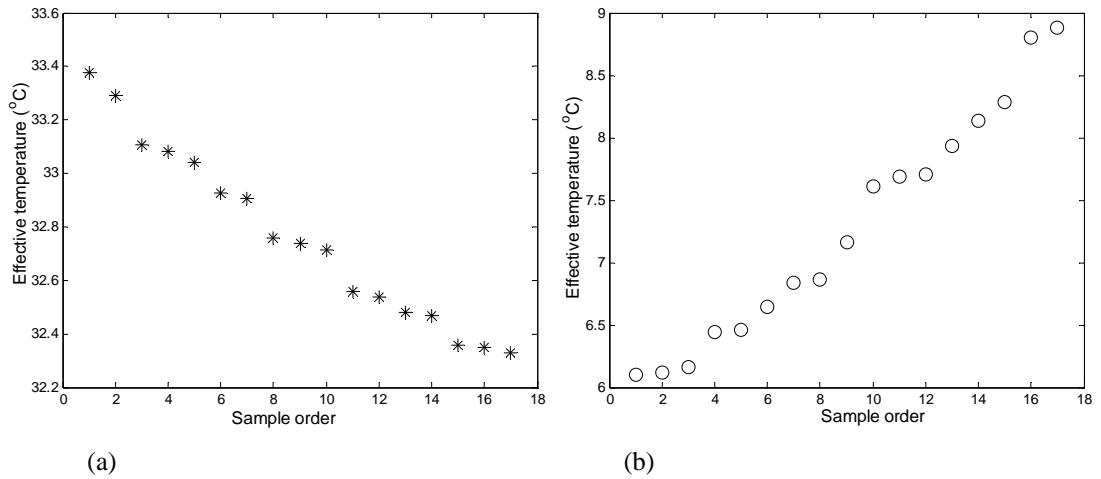


**Figure 8.8 Sequences of measured maximum and minimum effective temperatures: (a) maximum temperature; (b) minimum temperature**

**Table 8.2 Identified Gumbel parameters for extreme temperature prediction**

<i>Item</i>	$\lambda$	$\delta$
Maximum temperature	32.61	0.31
Minimum temperature	7.71	-0.82

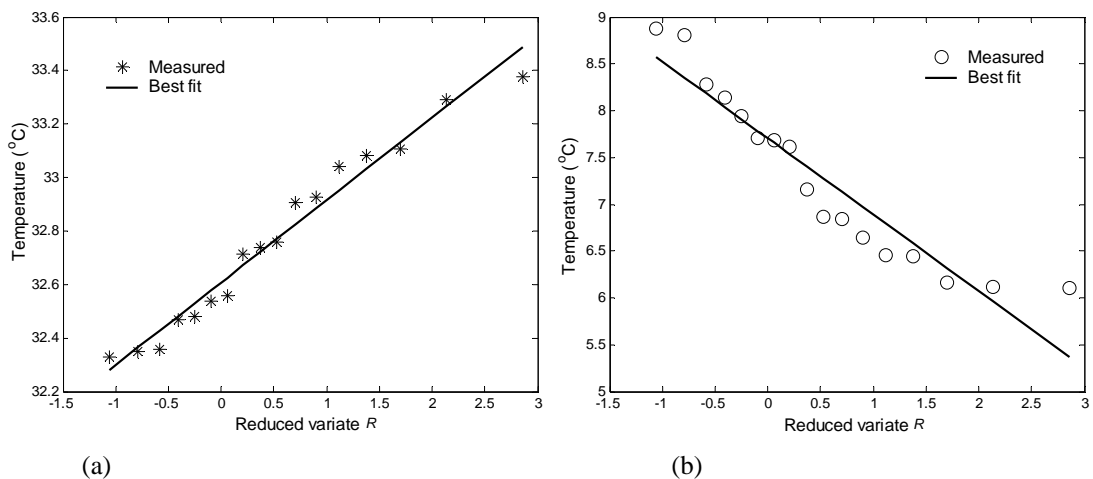


**Figure. 8.9 Measured and fitted relations between extreme temperature and reduced variate  $R$ : (a) maximum temperature; (b) minimum temperature**

**Figure 8.10** plots the measured instantaneous displacements of the expansion joints, from which the accumulative displacements are obtained as shown in **Figure 8.11**. It is found from **Figure 8.11** that the accumulative displacements increase with time in nearly linear proportion, with a rate of approximately 3.41 mm per hour for the Ting Kau abutment and 3.06 mm per hour for the Tsing Yi abutment, respectively. Hence the monthly or annual accumulative displacements can be easily estimated. The daily-average accumulative displacements are obtained from the measurement data as 81.82 mm and 73.48 mm for the Ting Kau and Tsing Yi abutments, respectively, which are much less than the design value of 120 mm. Following Equation (8.17), we obtain

$$N_m = \frac{120}{(81.82 + 73.48)/2} N_d \approx 1.5N_d \quad (8.22)$$

It is therefore expected that the service life of the expansion joints is longer than the design specification and the interval for replacement can be appropriately prolonged if no damage is observed in the expansion joints.

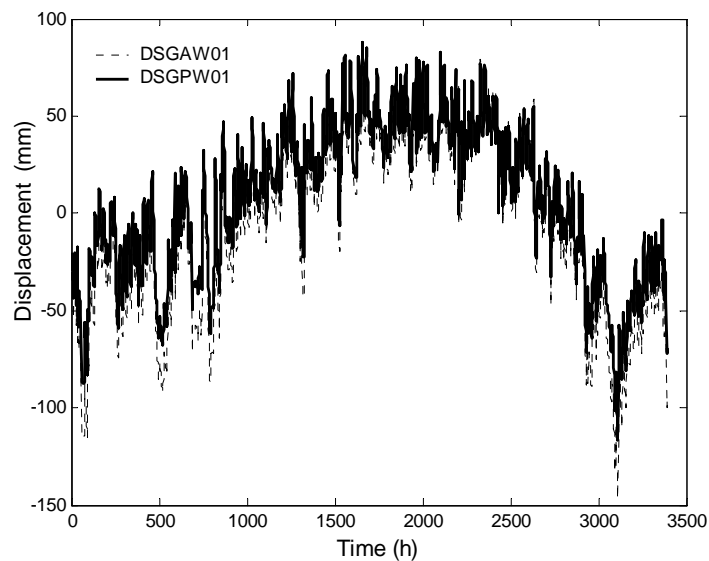


**Figure 8.10 Instantaneous displacements of expansion joints**

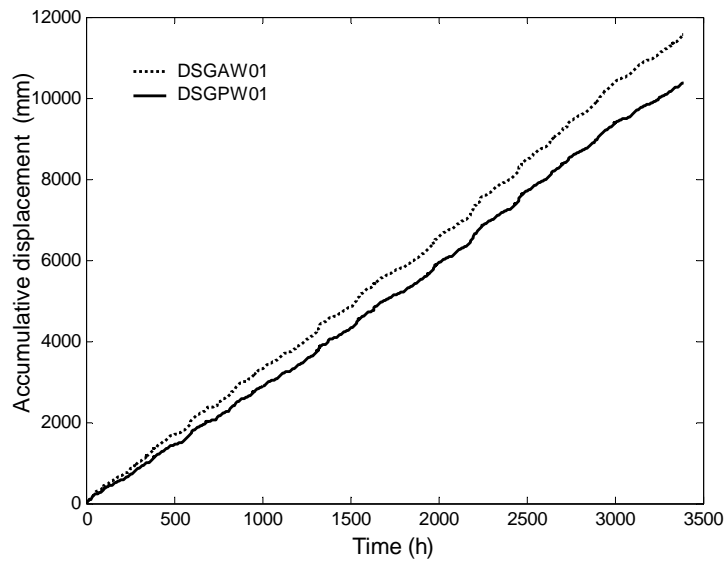


**Figure 8.11 Accumulative displacements of expansion joints**

## 8.4 Summary

An issue of great concern with bridge health monitoring systems is how to use the monitoring data for health and condition assessment of the instrumented bridges. In this study, a procedure for design verification and condition assessment of bridge expansion joints based on long-term monitoring of expansion joint displacement and bridge temperature was presented. It pursues the establishment and checking of the temperature-displacement pattern and the prediction and verification of the maximum displacement range, extreme temperature and accumulative movement. A case study of applying the procedure to the instrumented Ting Kau Bridge concludes the following points: (i) Movements of the expansion joints are highly correlated with the effective temperature. A linear regression model with an appropriate confidence interval can be formulated for condition alarming; (ii) Prediction results of the maximum displacement range and the extreme temperature agree well with the

design values, justifying the design assumptions; (iii) Accumulative displacements of the expansion joints are approximately in linear proportion to the service time, and it is therefore possible to predict the time taken to achieve a specified threshold value of accumulate displacements for making inspection and replacement. The measured daily-average accumulative displacements of the expansion joints in the bridge are much less than the design value.

## **Chapter 9**

### **CONCLUSIONS AND RECOMMENDATIONS**

#### **9.1 Conclusions**

Vibration-based damage detection and structural reliability evaluation, modelling of temperature-frequency correlation, and condition assessment of bridge expansion joints using long-term monitoring data are the subjects of this study. The research aim has been to i) develop a systematic approach from statistical identification of structural parameters to assessment of component reliability and condition based on long-term monitoring data; ii) propose a method for modelling the temperature-frequency correlation; and iii) present a procedure for condition assessment of bridge expansion joints.

In this study, a systematic approach for health monitoring and condition assessment has been developed. This approach enables both structural damage identification and monitoring-based reliability assessment to be explored in the probabilistic framework, taking into account uncertainty and randomness inherent in measurement data and structures. Additionally, a combined method of principal component analysis (PCA) and support vector machine (SVM) has been proposed for modelling the temperature-frequency correlation. A procedure for design verification and condition assessment of bridge expansion joints has also been achieved. The numerical

examples presented in this study are derived from bridge structures; however, most of the developed methods are general and can be used in connection with other engineering structures such as high-rise buildings and offshore platforms. The major contributions of the work are as follows.

**(i) Investigation of regularization methods for output-error-based FE model updating**

The treatment of the ill-conditioned and noisy system of equations is one of the critical problems for model updating, and has been tackled with the regularization methods in this study. The previous investigations focused on the application of regularization methods to equation-error-based model updating, the contribution of this stage of study lies in solving the ill-conditioned problem in output-error-based model updating using both modal frequency and mode shape information, and applying minimum product criterion (MPC) in model updating for the first time. The performances of regularization methods with regularization-parameter-selection methods have been rigorously examined and assessed through numerical studies. The specific findings and conclusions are as follows:

1. The regularization parameter obtained from MPC is close to that determined by L-curve method (LCM) in the case of a well-behaved L-curve; otherwise it is close to that determined by generalized cross validation (GCV). The LCM chooses the regularization parameter on the premise that the L-curve has a well-behaved L-shape. Unfortunately this is not guaranteed in model updating, and a poorly-posed L-curve could make LCM fail to choose an appropriate regularization parameter. MPC is able to select good regularization parameters for both Tikhonov regularization and truncated singular value decomposition

(SVD). Among various method combinations investigated, truncated SVD and Tikhonov regularization when working with MPC are the most robust techniques for output-error-based model updating;

2. In an output-error-based model updating approach, the singular value (SV) spectrum has a distinct gap separating large SVs from small ones for both the noise-free and the noisy data. It is different from equation-error-based model updating, where the SVs spread evenly over the SV spectrum when noisy modal data are utilized.

**(ii) Development of a procedure for stochastic FE model updating of structures**

The contribution of this study includes the development of an improved perturbation method and its combination with the Bayesian technique for stochastic model updating, and the formulation of two indices to identify the most relevant modal components which significantly contribute to the updating parameter variance. The developed procedure has been demonstrated on numerical studies with three types of uncertainty which frequently appear in measured modal parameters. The specific findings and conclusions are as follows:

1. For each type of uncertainties the improved perturbation method generates satisfactory model updating results when the uncertainty does not exceed a certain level (say 2%), however the results may be less accurate in the case of high uncertainty. It is found that neglecting the correlations of modal parameters may result in an unreliable estimation of the covariance matrix of updating parameters, hence highlighting the necessity to estimate the correlation among the modal parameters;

2. In the MCS method, the probability density functions (PDFs) of updating parameters can be well approximated with normal distributions in the case of low uncertainty. With the increase of uncertainty level, the geometry of updating parameter PDFs becomes more complicated due to the nonlinearity between updating parameters and modal parameters as well as the existence of many local minima for nonlinear least squares problems. In addition, the PDFs may have several distinct peaks.
3. The result from the two proposed indices indicates that some high-order modal components significantly contribute to the updating parameter variance. This implies that the commonly acknowledged rule-of-thumb method for selection of relevant modes in model updating and damage detection has significant limitations. They only assure the large damage sensitivity but neglect the uncertainties in these modes. Hence, the mode, which is sensitive to updating parameters while has large statistical uncertainties, might be not the best candidate for reliable model updating.

**(iii) Development of computer code for linear FE reliability analysis**

A computer program for linear FE reliability analysis has been developed. This program can compute the failure probability defined either by the displacement limit state or by the stress limit state in the context of finite element reliability analysis. It is capable of dealing with various distributions of random variables and provides reliability index sensitivity to distribution parameters.

Numerical examples have been provided to demonstrate the reliability analysis for both explicitly and implicitly defined limit state functions. The results have shown

that both first- and second-order reliability methods perform satisfactorily in all cases considered. It was revealed that the reliability index sensitivity to the distribution parameters is important in identifying the significant variables affecting structural reliability.

**(iv) Establishment of a systematic approach linking health monitoring technologies with bridge maintenance exercises**

The contribution of this study is the establishment of a systematic approach linking structural health monitoring technology and bridge inspection/maintenance exercise. Numerical examples with respect to the nominal, updated, and actual models have been provided to demonstrate the proposed approach. The specific findings and conclusions are as follows:

1. The reliability index obtained from the updated model is much closer to true reliability index than that obtained from the nominal model in the case of low uncertainty in measured modal parameters, hence ensuring the quality of the stochastically updated model. In the case of high uncertainty the updated model may be unreliable as the reliability index computed from the nominal model rather than from the updated model is closer to the true value;
2. The nominal model always gives a larger reliability index value than the actual model as it ignores structural damage. The updated model from the first-stage updating always produces a smaller reliability index value than the actual model, because structural parameter variances in the updated models are larger than the true values due to the simultaneous occurrence of measurement noises and natural randomness.

**(v) Formulation of nonlinear SVR models for characterizing temperature-frequency correlation**

The contribution of this study is the development of a method for modelling the temperature-frequency correlation based on long-term monitoring data. It utilizes the attractive merits of PCA for extracting predominant feature vectors and SVR for data-based statistical learning. The proposed method has been applied to characterize the temperature-frequency correlation with the use of one-year monitoring data from the cable-stayed Ting Kau Bridge. The specific findings and conclusions are as follows:

1. In both model accuracy and computational costs, the SVR model trained using the PCA-compressed feature vector outperforms the SVR model trained using original data. When continuous measurement data is available, the ‘dynamic’ SVR model trained using an augmented temperature vector to account for temporal correlation provides a more accurate frequency prediction than the ‘static’ SVR model which is trained without considering temporal correlation. The PCA-based SVR model is also superior to the multivariate linear regression (MLR) model in terms of generalization capability and model flexibility;
2. The optimal values of the hyper-parameters obtained using the grid search and the heuristic methods may deviate to a large extent, but the difference in the corresponding mean squared error values is insignificant. The grid search method shows that there is an approximate inversely proportional relation between the optimal values of the two hyper-parameters. This finding on the parameter interdependency is helpful for developing better empirical formulae to calculate the optimal hyper-parameters.

**(vi) Development of a methodology for condition assessment of bridge expansion joints**

The contribution of this study is the development of a general procedure for design verification and condition assessment of bridge expansion joints making use of long-term monitoring data of expansion joint displacement and bridge temperature. The procedure enables the establishment and checking of the temperature-displacement pattern and the prediction and verification of the maximum displacement range, extreme temperature and accumulative movement. The proposed procedure has been applied to the assessment of expansion joints in the cable-stayed Ting Kau Bridge with the use of one-year monitoring data. The specific findings and conclusions are as follows:

1. Movements of the expansion joints are highly correlated with bridge effective temperature. A linear regression model with an appropriate confidence interval can be readily formulated as a normal pattern. Alarms are raised when a future pattern deviates from the normal one;
2. Accumulative displacements of expansion joints are approximately in linear proportion to the service time. Therefore it is possible to predict the time taken to reach a specified threshold value of accumulated displacements for making inspection and replacement.

## **9.2 Recommendations**

In this PhD study, methods for stochastic model updating, damage identification and condition assessment of bridge structures making use of long-term monitoring data have been developed. However, there are some limitations on the developed methods:

i) the number of modes to produce a reliable stochastic model updating is determined by trial-and-error in this study; ii) the perturbation method may not give accurate stochastic model updating results in the case of high uncertainty level; iii) only the natural randomness caused by temperature-dependent Young's modulus is considered in this study, but in practice temperature variations also cause change in boundary conditions, structural configuration and internal forces; iv) the ingredients of the developed probabilistic method for bridge health monitoring and reliability assessment have been validated by numerical examples only and still need to be verified using the real-world data; and iv) the incorporation of the established temperature-frequency correlation model in damage detection algorithms is not addressed. The following recommendations are provided for further research and exploration.

**(i) Quantification of statistical uncertainties in other modal quantities**

The modal quantities used for FE model updating in the present study are basic modal parameters. Other modal quantities more sensitive to structural damage and updating parameters have been synthesized from the basic modal parameters for damage localization. They also have been used for model improvement and damage quantification. These modal quantities include such as mode shape curvature, strain mode shape, modal flexibility. Although being more sensitive to structural damage, the statistical uncertainties in these modal quantities may also be larger than those in basic modal parameters. For example, the mode shape curvature can be expressed approximately in terms of modal displacements as  $\kappa_i = (\phi_{i+1} - 2\phi_i + \phi_{i-1})$ . By assuming that each modal component is a statistically independent random variable and has the same standard deviation of  $\sigma_\phi$ , it is straightforward to obtain the standard

deviation in mode shape curvature as  $\sigma_\kappa = 6^{0.5}\sigma_\phi$ , hence indicating statistical uncertainty has been significantly amplified in the mode shape curvature. Therefore, in order to make a reasonable comparison of the model updating performance based on basic modal parameters and based on synthesized modal quantities, the statistical uncertainty in synthesized modal quantities must be quantified. After doing so, the stochastic method for model updating formulated in the present work should be employed to obtain the statistics of updating parameters. The modal quantity which produces the least statistical uncertainty of updating parameters from noisy measurement is finally determined as the best candidate for model updating and damage detection. This is still an unaddressed research field, yet meaningful and promising.

## (ii) Improvement of stochastic methods for FE model updating

This study employed an improved perturbation method and the MCS method for stochastic FE model updating. In the field of stochastic mechanics, several other stochastic methods, such as the Numan expansion method (Yamazaki *et al.* 1988), Polynomial chaos expansion method (Spanos and Ghanem 1989) and weighted integral method (Deodatis 1991), are available to obtain the statistics of response quantities, and have been proven more satisfactory than the perturbation method in the presence of high uncertainty. It would be of value to further explore the applicability of these methods to stochastic model updating.

Apart from the probabilistic descriptions of uncertainty in measured modal parameters, there are also alternative approaches such as fuzzy set theory, possibility

theory, interval analysis method, and evidence theory to depict such uncertainty. It is not very likely for a modal parameter to span all the values endowed by its probability distribution function. Instead, such a modal parameter generally falls into an interval with low and upper limits. In such cases, the interval analysis method would provide a better solution approach.

**(iii) Integrated research of structural health monitoring and structural reliability analysis**

The established linkage between structural health monitoring technologies and bridge inspection/maintenance exercises is still preliminary and in its infancy, more thorough research is required to completely realize the potential of this linkage to benefit bridge authorities from health monitoring technologies. The writer feels that this goal can be achieved by developing coordinated research programs involving participation of the researchers from both structural health monitoring and structural reliability disciplines.

**(iv) Interpretation of monitoring data in terms of structural condition and performance**

A long-term monitoring system accumulates a sizeable volume of measurement data regarding structural responses and imposed loadings. Ultimately these data must be channeled towards the goal of supporting bridge authorities in decision making. Integration of long-term monitoring data and reliability-based assessment techniques provide a viable approach for health and condition evaluation of bridge structures (Ko and Ni 2005). In the writer's opinion, this area deserves more research effort if bridge authorities are to be provided with more information useful for maintenance and management of bridge structures.

**(v) Incorporation of temperature-frequency model for damage detection under varying environmental conditions**

In this study, a stochastic FE model updating method has been proposed to take account of the varying environmental effect on model updating results, and then probabilistic approaches can be implemented for damage detection on the basis of stochastic model updating results (Xia *et al.* 2002; Xia and Hao 2003). An alternative approach for damage detection under varying environmental conditions is eliminating the changes in modal parameters due to temperature effect by using the formulated temperature-frequency model. This issue should be further studied.

## REFERENCES

- Abdalla, M. O., Grigoriadis, K. M., and Zimmerman, D. C.** (1998), “Enhanced structural damage detection using alternating projection methods”, *AIAA Journal*, 36, 1305-1311.
- Abdel Wahab, M. M.** (2001), “Effect of modal curvatures on damage detection using model updating”, *Mechanical Systems and Signal Processing*, 15, 439-445.
- Abdel Wahab, M. M., and De Roeck, G.** (1997), “Effect of temperature on dynamic system parameters of a highway bridge”, *Structural Engineering International*, 7, 266-270.
- Agbabian, M. S., Masri, S. F., Miller, R. K., and Caughey, T. K.** (1988), “A system identification approach to the detection of changes in structural parameters”, *Structural Safety Evaluation Based on System Identification Approach*, Friedrich Vieweg & Son, Wiesbaden, 341-356.
- Ahmadian, H., Gladwell, G. M. L., and Ismail, F.** (1997), “Parameter selection strategies in finite element model updating”, *Journal of Vibration and Acoustics*, ASME, 119, 37-45.
- Ahmadian, H., Mottershead, J. E., and Friswell, M. I.** (1998), “Regularization methods for finite element model updating”, *Mechanical Systems and Signal Processing*, 12, 47-64.
- Aktan, A. E., Catbas, F. N., Grimmelsman, K. A., Pervizpour, M., Curtis, J. M., Shen, K., and Qin, X.** (2002), “Health monitoring for effective management of infrastructure”, *Smart Structures and Materials 2002: Smart Systems for Bridges, Structures, and Highways*, Liu, S. C., and Pines, D. J., (editors), The

International Society for Optical Engineering, Bellingham, Washington, 17-29.

**Aktan, A. E., Farhey, D. N., Helmicki, A. J., Brown, D. L., Hunt, H. J., Lee, K. L., and Levi, A.** (1997), "Structural identification for condition assessment: experimental arts", *Journal of Structural Engineering*, ASCE, 123, 1674-1684.

**Alampalli, S.** (2000), "Effects of testing, analysis, damage, and environment on modal parameters", *Mechanical Systems and Signal Processing*, 14, 63-74.

**Allemang, R. J., and Brown, D. L.** (1982), "A correlation coefficient for modal vector analysis", *Proceedings of the 1st International Modal Analysis Conference*, Society for Experimental Mechanics, Bethel, 110-116.

**Alvin, K. F.** (1997), "Efficient computation of eigenvector sensitivities for structural dynamics", *AIAA Journal*, 35, 1760-1766.

**Andersen, E. Y., and Pedersen, L.** (1994), "Structural monitoring of the Great Belt East Bridge", *Strait Crossings* 94, Krokeborg, J. (editor), A.A. Balkema, Rotterdam, 189-195.

**Ang, A. H. S., and Tang, W. H.** (1975), *Probability Concepts in Engineering Planning and Design I: Basic Principals*, Wiley, New York.

**Ang, A. H. S., and De Leon, D.** (1997), "Determination of optimal target reliabilities for design and upgrading of structures", *Structural Safety*, 19, 91-103.

**Araki, Y., and Hjelmstad, K. D.** (2001), "Optimum sensitivity-based statistical parameters estimation from modal response", *AIAA Journal*, 39, 1166-1174.

**Arici, Y., and Mosalam, K. M.** (2005), "Statistical significance of modal parameters of bridge systems identified from strong motion data", *Earthquake Engineering and Structural Dynamics*, 34, 1323-1341.

- Askegaard, V., and Mossing, P.** (1988), “Long-term observation of RC-bridge using changes in natural frequencies”, *Nordic Concrete Research*, 7, 20-27.
- Banan, M. R., Banan, M. R., and Hjelmstad, K. D.** (1994a), “Parameter estimation of structures from static response I: computational aspects”, *Journal of Structural Engineering*, ASCE, 120, 3243-3258.
- Banan, M. R., Banan, M. R., and Hjelmstad, K. D.** (1994b), “Parameter estimation of structures from static response II: numerical simulation studies”, *Journal of Structural Engineering*, ASCE, 120, 3259-3283.
- Barrish, R. A., Jr., Grimmelman, K. A., and Aktan, A. E.** (2000), “Instrumented monitoring of the Commodore Barry Bridge”, *Nondestructive Evaluation of Highways, Utilities, and Pipelines IV*, Aktan, A. E., and Gosselin, S. R. (editors), The International Society for Optical Engineering, Bellingham, 112-126.
- Baruch, M.** (1978), “Optimization procedure to correct stiffness and flexibility matrices using vibration tests”, *AIAA Journal*, 16, 1208-1210.
- Baruch, M.** (1982), “Optimal correction of mass and stiffness matrices using measured modes”, *AIAA Journal*, 20, 1623-1626.
- Baruch, M.** (1984), “Methods of reference basis for identification of linear dynamic structures”, *AIAA Journal*, 22, 561-564.
- Baruch, M., and Bar Itzhack, I. Y.** (1978), “Optimal weighted orthogonalization of measured modes”, *AIAA Journal*, 16, 346-351.
- Bathe, K. J.** (1996), *Finite Element Procedures*, Prentice Hall, Englewood Cliffs, New Jersey.
- Beck, J. L., Au, S. K., and Vanik, M. V.** (2001), “Monitoring structural health using a probabilistic measure”, *Computer-Aided Civil and Infrastructure Engineering*, 16, 1-11.

- Beck, J. L., and Katafygiotis, L. S.** (1998), "Updating models and their uncertainties I: Bayesian statistical framework", *Journal of Engineering Mechanics*, ASCE, 124, 455-461.
- Ben-Haim, Y., and Prells, U.** (1993), "Selective sensitivity in the frequency domain - I: theory", *Mechanical Systems and Signal Processing*, 7, 461-475.
- Berman, A.** (1979), "Mass matrix correction using an incomplete set of measured modes", *AIAA Journal*, 17, 1147-1148.
- Berman, A., and Flannelly, W. G.** (1971), "Theory of incomplete models of dynamic structures", *AIAA Journal*, 9, 1481-1487.
- Berman, A., and Nagy, E. J.** (1983), "Improvement of a large analytical model using test data", *AIAA Journal*, 21, 1168-1173.
- Bernal, D.** (2002), "Load vectors for damage localization", *Journal of Engineering Mechanics*, ASCE, 128, 7-14.
- Bolton, R., Stubbs, N., Park, S., Choi, S., and Sikorsky, C.** (2001), "Documentation of changes in modal properties of a concrete box-girder bridge due to environmental and internal conditions", *Computer-Aided Civil and Infrastructure Engineering*, 16, 42-57.
- Brecolotti, M., Franceschini, G., and Materazzi, A. L.** (2004), "Sensitivity of dynamic methods for damage detection in structural concrete bridges", *Shock and Vibration*, 11, 383-394.
- Breitung, K.** (1984), "Asymptotic approximations for multinormal integrals", *Journal of Engineering Mechanics*, ASCE, 110, 357-366.
- British Standards Institute** (1978), *BS5400: Steel, Concrete, and Composite Bridges, Part 2: Specifications for Loads*, British Standards Institute, London, 20-22.

- Brownjohn, J. M. W., and Xia, P. Q.** (2000), “Dynamic assessment of curved cable-stayed bridge by model updating”, *Journal of Structural Engineering*, ASCE, 126, 252-260.
- Burges, C. J. C.** (1998), “A tutorial on support vector machines for pattern recognition”, *Data Mining and Knowledge Discovery*, 2, 121-167.
- Busby, H. R., and Trujillo, D. M.** (1997), “Optimal regularization of an inverse dynamics problem”, *Computers and Structures*, 63, 243-248.
- Canadian Standards Association** (2000), *Design of Highway Bridges*, Standard CAN/CSA-S6-00, Canadian Standards Association, Rexdale, Ontario.
- Carden, E. P., and Fanning, P.** (2004), “Vibration based condition monitoring: a review”, *Structural Health Monitoring*, 3, 355-377.
- Casciati, F.** (2003), “An overview of structural health monitoring expertise within European Union”, *Structural Health Monitoring and Intelligent Infrastructure*, Wu, Z. S., and Abe, M. (editors), A.A. Balkema, Lisse, 31-37.
- Castillo, E.** (1988), *Extreme Value Theory in Engineering*, Academic Press, Boston.
- Castillo, E., Hadi, A. S., Balakrishnan, N., and Sarabia, J. M.** (2005), *Extreme Value and Related Models with Applications in Engineering and Science*, Wiley, New Jersey.
- Cawley, P., and Adams, R. D.** (1979), “The locations of defects in structures from measurements of natural frequencies”, *Journal of Strain Analysis for Engineering Design*, 14, 49-57.
- Cha, P. D., and de Phillis, L. G.** (2001), “Model updating by adding known masses”, *International Journal for Numerical Methods in Engineering*, 50, 2547-2571.

- Chalimourda, A., Schölkopf, B., and Smola, A. J.** (2004), “Experimentally optimal  $\nu$  in support vector regression for different noise models and parameter settings”, *Neural Networks*, 17, 127-141.
- Chance, J., Tomlinson, G. R., and Worden, K.** (1994), “Simplified approach to the numerical and experimental modeling of the dynamics of a cracked beam”, *Proceedings of the 12th International Modal Analysis Conference*, Society for Experimental Mechanics, Bethel, 778-785.
- Chang, F. K. (editor)** (2003), *Structural Health Monitoring – From Diagnosis & Prognostics to Structural Health Management*, DEStech Publications, Lancaster, Pennsylvania.
- Chen, J. C., and Garba, J. A.** (1980), “Analytical model improvement using modal test results”, *AIAA Journal*, 18, 684-690.
- Chen, J. C., and Garba, J. A.** (1988), “On-orbit damage assessment for large space structures”, *AIAA Journal*, 26, 1119-1126.
- Cherkassky, V., and Ma, Y. Q.** (2004), “Practical selection of SVM parameters and noise estimation for SVM regression”, *Neural Networks*, 17, 113-126.
- Cherki, C., Lallemand, B., Tison, T., and Level, P.** (1999), “Improvement of analytical model using uncertain test data”, *AIAA Journal*, 37, 489-495.
- Cheung, M. S., Tadros, G. S., Brown, T., Dilger, W. H., Ghali, A., and Lau, D. T.** (1997), “Field monitoring and research on performance of the Confederation Bridge”, *Canadian Journal of Civil Engineering*, 24, 951-962.
- Ching, J. Y., and Beck, J. L.** (2004), “Bayesian analysis of the Phase II IASC-ASCE structural health monitoring experimental benchmark data”, *Journal of Engineering Mechanics*, ASCE, 130, 1233-1244.
- Choi, S., and Stubbs, N.** (2005), “Damage identification in structures using the time-domain response”, *Journal of Sound and Vibration*, 275, 577-590.

- Cobb, R. G., and Liebst, B. S.** (1997), “Structural damage identification using assigned partial eigenstructure”, *AIAA Journal*, 35, 152-158.
- Collins, J. D., Hart, G. C., Hasselman, T. K., and Kennedy, B.** (1974), “Statistical identification of structures”, *AIAA Journal*, 12, 185-190.
- Cornwell, P., Doebling, S. W., and Farrar, C. R.** (1999a), “Application of the strain energy damage detection method to plate-like structures”, *Journal of Sound and Vibration*, 224, 359-374.
- Cornwell, P., Farrar, C. R., Doebling, S. W., and Sohn, H.** (1999b), “Environmental variability of modal properties”, *Experimental Techniques*, 23, 45-48.
- Craven, P., and Wahba, G.** (1979), “Smoothing noisy data with spline functions”, *Numerische Mathematik*, 31, 377-403.
- Dailey, R. L.** (1988), “Eigenvector derivatives with repeated eigenvalues”, *AIAA Journal*, 27, 486-491.
- D’Ambrogio, W., and Fregolent, A.** (1998), “On the use of consistent and significant information to reduce ill-conditioning in dynamic model updating”, *Mechanical Systems and Signal Processing*, 12, 203-222.
- Deodatis, G.** (1991), “Weighted integral method I: stochastic stiffness matrix”, *Journal of Engineering Mechanics*, ASCE, 117, 1851-1864.
- Der Kiureghian, A., and Ke, J. B.** (1985), “The stochastic finite element method in structural reliability”, *Probabilistic Engineering Mechanics*, 3, 83-91.
- Der Kiureghian, A., and Liu, P. L.** (1986), “Structural reliability under incomplete probability information”, *Journal of Engineering Mechanics*, ASCE, 112, 85-104.

- Der Kiureghian, A., Lin, Z. H., and Hwang, S. J.** (1987), “Second-order reliability approximations”, *Journal of Engineering Mechanics*, ASCE, 113, 1208-1225.
- Ditlevsen, O.** (1979), “Narrow reliability bounds for structural systems”, *Journal of Structural Mechanics*, 7, 453-472.
- Ditlevsen, O.** (1981), “Principle of normal tail approximation”, *Journal of the Engineering Mechanics Division*, ASCE, 107, 1191-1208.
- Ditlevsen, O., and Madsen, H. O.** (1996), *Structural Reliability Methods*, Wiley, New York.
- Doebling, S. W.** (1996), “Minimum-rank optimal update of elemental stiffness parameters for structural damage identification”, *AIAA Journal*, 34, 2615-2621.
- Doebling, S. W., and Farrar, C. R.** (1997), “Effect of measurement statistics on the detection of damage in the Alamosa Canyon Bridge”, *Proceedings of the 15th International Modal Analysis Conference*, Society for Experimental Mechanics, Bethel, 919-929.
- Doebling, S. W., Farrar, C. R., and Prime, M. B.** (1998), “A summary review of vibration-based damage identification methods”, *The Shock and Vibration Digest*, 30, 91-105.
- Doebling, S. W., and Peterson, L. D.** (1997), “Computing statically complete flexibility from dynamically measured flexibility”, *Journal of Sound and Vibration*, 205, 631-645.
- Dornsife, R. J.** (2000), “Expansion joints”, *Bridge Engineering Handbook*, Chen, W. F., and Duan, L. (editors), CRC Press, Boca Raton, Florida, Chapter 25.

- Estes, A. C., and Frangopol, D. M.** (2005), "Reliability-based condition assessment", *Structural Condition Assessment*, Ratay, R. T. (editor), John Wiley, New Jersey, 25-66.
- Engl, H. W., Hanke, M., and Neubauer, A.** (1996), *Regularization of Inverse Problems*, Kluwer Academic Publishers, Dordrecht.
- Farrar, C. R., Doebling, S. W., Cornwell, P. J., and Straser, E. G.** (1997), "Variability of modal parameters measured on the Alamosa Canyon Bridge", *Proceedings of the 15th International Modal Analysis Conference*, Society for Experimental Mechanics, Bethel, 257-263.
- Farrar, C. R., and Jauregui, D. A.** (1998), "Comparative study of damage identification algorithms applied to a bridge: I. experiment", *Smart Materials and Structures*, 7, 704-719.
- Fiessler, B., Neumann, H. J., and Rackwitz, R.** (1979), "Quadratic limit states in structural reliability", *Journal of the Engineering Mechanics Division*, ASCE, 105, 661-676.
- Fonseca, J. R., Friswell, M. I., Mottershead, J. E., and Lees, A. W.** (2005), "Uncertainty identification by the maximum likelihood method", *Journal of Sound and Vibration*, 288, 587-599.
- Fox, C. H. J.** (1992), "The location of defects in structures: a comparison of the use of natural frequency and mode shape data", *Proceedings of the 10th International Modal Analysis Conference*, Society for Experimental Mechanics, Bethel, 552-558.
- Fox, R. L., and Kapoor, M. P.** (1968), "Rates of change of eigenvalues and eigenvectors", *AIAA Journal*, 6, 2426-2429.
- Frangopol, D. M.** (1999), "Life-cycle cost analysis for bridges", *Bridge Safety and Reliability*, Frangopol, D. M. (editor), ASCE, Reston, 210-236.

- Frangopol, D. M., and Hearn, G.** (1996), *Structural Reliability in Bridge Engineering: Design, Inspection, Assessment, Rehabilitation, and Management*, McGraw-Hill, New York.
- Frangopol, D. M., Kong, J. S., and Gharaibeh, E. S.** (2001), “Reliability-based life-cycle management of highway bridges”, *Journal of Computing in Civil Engineering*, ASCE, 15, 27-34.
- Fregolent, A., D’Ambrogio, W., Salvini, P., and Sestieri, A.** (1996), “Regularization techniques for dynamic model updating using input residual”, *Inverse Problems in Engineering*, 2, 171-200.
- Friswell, M. I.** (1989), “The adjustment of structural parameters using a minimum variance estimator”, *Mechanical Systems and Signal Processing*, 3, 143-155.
- Friswell, M. I., Inman, D. J., and Pilkey, D. F.** (1997), “Direct updating of damping and stiffness matrices”, *AIAA Journal*, 36, 491-493.
- Friswell, M. I., and Mottershead, J. E.** (1995), *Finite Element Model Updating in Structural Dynamics*, Kluwer Academic Publishers, London.
- Friswell, M. I., Mottershead, J. E., and Ahmadian, H.** (2001), “Finite element model updating using experimental test data: parameterization and regularization”, *Philosophical Transactions of the Royal Society of London A: Mathematical, Physical and Engineering Sciences*, 359, 169-186.
- Friswell, M. I., and Penny, J. E. T.** (1992), “The effect of close or repeated eigenvalues on the updating of model parameters from FRF data”, *Journal of Vibration and Acoustics*, ASME, 114, 514-520.
- Friswell, M. I., and Penny, J. E. T.** (1997), “Is damage location using vibration measurements practical”, *Damage Assessment of Structures Using Advanced Signal Processing Procedures: DAMAS 97*, Dulieu-Smith, J. M., Staszewski,

W. J., and Worden, K. (editors), Sheffield Academic Press, Sheffield, 351-362.

**Friswell, M. I., Penny, J. E. T., and Wilson, D. A. L.** (1994), "Using vibration data and statistical measures to locate damage in structures", *The International Journal of Analytical and Experimental Modal Analysis*, 9, 239-254.

**Fritzen, C. P.** (1986), "Identification of mass, damping, and stiffness matrices of mechanical systems", *Journal of Vibration, Acoustics, Stress, and Reliability in Design*, ASME, 108, 9-16.

**Fritzen, C. P., Jennewein, D., and Kiefer, T.** (1998), "Damage detection based on model updating methods", *Mechanical Systems and Signal Processing*, 12, 163-186.

**Fritzen, C. P., and Zhu, S.** (1991), "Updating of finite-element models by means of measured information", *Computers and Structures*, 40, 475-486.

**Fu, Y. D., and DeWolf, J. T.** (2004), "Effect of differential temperature on a curved post-tensioned concrete bridge", *Advances in Structural Engineering*, 7, 385-397.

**Fujino, Y., and Abe, M.** (2004), "Structural health monitoring – current status and future", *Proceedings of the 2nd European Workshop on Structural Health Monitoring*, Boller, C., and Staszewski, W. J. (editors), DEStech Publications, Lancaster, Pennsylvania, 3-10.

**Gao, Y., and Spencer, B. F., Jr.** (2005), "Online damage diagnosis for civil infrastructure employing a flexibility-based approach", *Smart Materials and Structures*, 15, 9-19.

**Gladwell, G. M. L., and Ahmadian, H.** (1995), "Generic element matrices suitable for finite-element model updating", *Mechanical Systems and Signal Processing*, 601-614.

- Golub, G. H., Heath, M., and Wahba, G.** (1979), “Generalized cross-validation as a method for choosing a good ridge parameter”, *Technometrics*, 21, 215-223.
- Gumbel, E. J.** (1958), *Statistics of Extremes*, Columbia University Press, New York.
- Hajela, P., and Soeiro, F. J.** (1990), “Structural damage detection based on static and modal analysis”, *AIAA Journal*, 28, 1110-1115.
- Haldar, A., and Mahadevan, S.** (2000), *Reliability Assessment Using Stochastic Finite Element Analysis*, John Wiley & Sons, New York.
- Hansen, P. C.** (1987), “The truncated SVD as a method of regularization”, *BIT*, 72, 534-553.
- Hansen, P. C.** (1990), “The discrete Picard condition for discrete ill-posed problems”, *BIT*, 30, 658-672.
- Hansen, P. C.** (1992), “Analysis of discrete ill-posed problems by means of the L-curve”, *SIAM Review*, 34, 561-581.
- Hansen, P. C.** (1998), *Rank-Deficient and Discrete Ill-Posed Problem: Numerical Aspects and Linear Inversion*, SIAM, Philadelphia.
- Hansen, P. C., and O’Leary, D. P.** (1993), “The use of the L-curve in the regularization of discrete ill-posed problems”, *SIAM Journal of Scientific Computing*, 14, 1487-1503.
- Hart, G. C., and Collins, J. D.** (1970), “The treatment of randomness in finite element modeling”, *Transactions of the SAE*, 79, 2509-2520.
- Hart, G. C., and Yao, J. T. P.** (1977), “System identification in structural dynamics”, *Journal of the Engineering Mechanics Division*, ASCE, 103, 1089-1104.
- Hasofer, A. M., and Lind, N. C.** (1974), “Exact and invariant second-moment code format”, *Journal of the Engineering Mechanics*, ASCE, 100, 111-121.

- Hjelmstad, K. D.** (1996), "On the uniqueness of modal parameter estimation", *Journal of Sound and Vibration*, 192, 581-598.
- Hjelmstad, K. D., and Shin, S.** (1997), "Damage detection and assessment of structures from static response", *Journal of Engineering Mechanics*, ASCE, 123, 568-576.
- Hohenbichler, M., and Rackwitz, R.** (1981), "Non-normal dependent vectors in structural safety", *Journal of the Engineering Mechanics Division*, ASCE, 107, 1227-1238.
- Hohenbichler, M., and Rackwitz, R.** (1988), "Improvement of second-order reliability estimates by importance sampling", *Journal of the Engineering Mechanics Division*, ASCE, 114, 2195-2199
- Hong Kong Highways Department Structures Division** (1997), *Structures Design Manual for Highways and Railways*, Highways Department, Hong Kong Government, Hong Kong, 25-27.
- Hsu, C. W., Chang, C. C., and Lin, C. J.** (2003), "A practical guide to support vector classification", <<http://www.csie.ntu.edu.tw/~cjlin/libsvm>>.
- Hu, X., and Shenton, H. W.** (2003), "Damage identification in a two span continuous beam", *Structural Health Monitoring and Intelligent Infrastructure*, Wu, Z. S., and Abe, M. (editors), A.A. Balkema, Lisse, 431-436.
- Hua, X. G., Ni, Y. Q., and Ko, J. M.** (2005), "Probabilistic identification of structural parameters using an integrated perturbation and Bayesian method", *Structural Health Monitoring and Intelligent Infrastructure*, Ou, J. P., Li, H., and Duan, Z. D. (editors), Taylor & Francis, London, 1021-1027.

- Hugue, T. D., Aktan, A. E., and Hoyos, A.** (1991), “Localized identification of constructed facilities”, *Journal of Structural Engineering*, ASCE, 117, 128-148.
- Huth, O., Feltrin, G., Maeck, J., Kilic, N., and Motavalli, M.** (2005), “Damage identification using modal data: experiences on a prestressed concrete bridge”, *Journal of Structural Engineering*, ASCE, 131, 1898-1910.
- Imregun, M., and Visser, W. J.** (1991), “A review of model updating techniques”, *Shock and Vibration Digest*, 23, 9-20.
- Jauregui, D. A., and Farrar, C. R.** (1998), “Comparative study of damage identification algorithms applied to a bridge II: numerical study”, *Smart Materials and Structures*, 7, 720-731.
- Johnston, P. R., and Gulrajani, R. M.** (1997), “A new method for regularization parameter determination in the inverse problem of electrocardiography”, *IEEE Transactions on Biomedical Engineering*, 44, 19-39.
- Jolliffe, I. T.** (2002), *Principal Component Analysis*, Second Edition, Springer-Verlag, New York.
- Kabe, A. M.** (1985), “Stiffness matrix adjustment using mode data”, *AIAA Journal*, 23, 1431-1436.
- Kammer, D. C.** (1988), “Optimum approximation for residual stiffness in linear system identification”, *AIAA Journal*, 26, 104-112.
- Kang, J. S., Park, S. K., Shin, S., and Lee, H. S.** (2005), “Structural system identification in time domain using measured acceleration”, *Journal of Sound and Vibration*, 288, 215-234.
- Kaouk, M., and Zimmerman, D. C.** (1994), “Structural damage assessment using a generalized minimum rank perturbation theory”, *AIAA Journal*, 32, 836-842.

- Kaouk, M., Zimmerman, D. C., and Simmermacher, T. W.** (2000), “Assessment of damage affecting all structural properties using experimental modal parameters”, *Journal of Vibration and Acoustics*, ASME, 122, 456-463.
- Katafygiotis, L. S., and Beck, J. L.** (1998), “Updating models and their uncertainties II: model identifiability”, *Journal of Engineering Mechanics*, ASCE, 124, 463-467.
- Kenigsbuch, R., and Halevi, Y.** (1998), “Model updating in structural dynamics: a generalized reference basis approach”, *Mechanical Systems and Signal Processing*, 12, 75-90.
- Kiddy, J., and Pines, D. J.** (1998), “Eigenstructure assignment technique for damage detection in rotating structure”, *AIAA Journal*, 36, 1680-1685.
- Kim, J. T., Yun, C. B., and Yi, J. H.** (2004), “Temperature effects on modal properties and damage detection in plate-girder bridges”, *Advanced Smart Materials and Structures Technology*, Chang, F. K., Yun, C. B., and Spencer, B. F. Jr. (editors), DEStech Publications, Lancaster, Pennsylvania, 504-511.
- Kleiber, M., and Hien, T. D.** (1992), *The Stochastic Finite Element Method: Basic Perturbation Technique and Computer Implementation*, Wiley, New York.
- Ko, J. M., Hua, X. G., and Ni, Y. Q.** (2006), “Structural damage detection of cable-stayed bridges using change in cable force”, *Proceedings of the 3rd International Workshop on Advanced Smart Materials and Smart Structures Technology*, Lake Tahoe, USA.
- Ko, J. M., and Ni, Y. Q.** (2005), “Technology developments in structural health monitoring of large-scale bridges”, *Engineering Structures*, 27, 1715-1725.
- Ko, J. M., Wang, J. Y., Ni, Y. Q., and Chak, K. K.** (2003), “Observation on environmental variability of modal properties of a cable-stayed bridge from one-year monitoring data”, *Structural Health Monitoring 2003: From*

*Diagnosis and Prognostics to Structural Health Management*, Chang, F. K. (editor), DEStech Publications, Lancaster, Pennsylvania, 467-474.

**Ko, J. M., Wong, C. W., and Lam, H. F.** (1994), “Damage detection in steel framed structures by vibration measurement approach”, *Proceedings of the 12th International Modal Analysis Conference*, Society for Experimental Mechanics, Bethel, 280-286.

**Koh, C. G., See, L. M., and Balendra, T.** (1991), “Estimation of structural parameters in time domain – a substructure approach”, *Earthquake Engineering and Structural Dynamics*, 20, 787-801.

**Koh, H. M., Choo, J. F., Kim, S. K., and Kim, C. Y.** (2003), “Recent application and development of structural health monitoring systems and intelligent structures in Korea”, *Structural Health Monitoring and Intelligent Infrastructure*, Wu, Z. S., and Abe, M. (editors), A.A. Balkema, Lisse, 99-111.

**Kottegoda, N. T., and Rosso, R.** (1997), *Probability, Statistics and Reliability for Civil and Environmental Engineers*, McGraw-Hill, New York.

**Kravaris, C., and Seinfeld, J. H.** (1985), “Identification of parameters in distributed parameter systems by regularization”, *SIAM Journal on Control and Optimization*, 23, 217-241.

**Ku, B. S., Ji, D. H., Lee, S. S., and Park, J. C.** (2005), “Structural health monitoring of the Seohae cable-stayed bridge”, *Safety and Reliability of Engineering Systems and Structures*, Augusti, G., Schuëller, G. I., and Ciampoli, M. (editors), Millpress, Rotterdam, 2937-2943.

**Lark, R. J., and Flaig, K. D.** (2005), “The use of reliability analysis to aid bridge management”, *The Structural Engineer*, 83, 27-31.

- Law, S. S., Shi, Z. Y., and Zhang, L. M.** (1998), “Structural damage detection from incomplete and noisy modal test data”, *Journal of Engineering Mechanics*, ASCE, 124, 1280-1288.
- Lloyd, G. M., Wang, M. L., and Singh, V.** (2000), “Observed variations of mode frequencies of a prestressed concrete bridge with temperature”, *Proceedings of the 14th Engineering Mechanics Conference*, Tassoulas, J. L. (editor), ASCE, Reston (CD-ROM).
- Li, D. N., Maes, M. A., and Dilger, W. H.** (2004), “Thermal design criteria for deep prestressed concrete girders based on data from Confederation Bridge”, *Canadian Journal of Civil Engineering*, 31, 813-825.
- Li, J., and Roberts, J. B.** (1999a), “Stochastic structural system identification, Part 1: mean parameter estimation”, *Computational Mechanics*, 24, 206-210.
- Li, J., and Roberts, J. B.** (1999b), “Stochastic structural system identification, Part 2: variance parameter estimation”, *Computational Mechanics*, 24, 211-215.
- Lieven, N. A. J., and Ewins, D. J.** (1988), “Spatial correlation of mode shapes: the coordinate modal assurance criterion (COMAC)”, *Proceedings of the 6th International Modal Analysis Conference*, Society for Experimental Mechanics, Bethel, 690-695.
- Lifshitz, J. M., and Rotem, A.** (1969), “Determination of reinforcement unbonding of composites by a vibration technique”, *Journal of Composite Materials*, 3, 412-423.
- Lim, K. B., Junkins, J. L., and Wang, B. P.** (1987), “Re-examination of eigenvector derivatives”, *AIAA Journal of Guidance, Control, and Dynamics*, 10, 581-587.
- Lim, T. W.** (1990), “Submatrix approach to stiffness matrix correction using modal test data”, *AIAA Journal*, 28, 1123-1130.

- Lim, T. W.** (1995), "Structural damage detection using constrained eigenstructure assignment", *Journal of Guidance, Control, and Dynamics*, 18, 411-418.
- Lim, T. W., and Kashangaki, T. A. L.** (1994), "Structural damage detection of space truss structures using best achievable eigenvectors", *AIAA Journal*, 32, 1049-1057.
- Lin, R. M., Lim, M. K., and Du, H.** (1995), "Improved inverse eigensensitivity method for structural analytical model updating", *Journal of Vibration and Acoustics*, ASME, 117, 192-198.
- Link, M.** (2001), "Updating of analytical models – review of numerical procedures and application aspects", *Structural Dynamics @2000: Current Status and Future Directions*, Ewins, D. J., and Inman, D. J. (editors), Research Studies Press, Philadelphia, 193-223.
- Liu, G. R., and Han, X.** (2003), *Computational Inverse Technique in Nondestructive Evaluation*, CRC Press, Boca Raton, Florida.
- Liu, P. L.** (1995), "Identification and damage detection of trusses using modal data", *Journal of Structural Engineering*, ASCE, 121, 599-608.
- Liu, P. L., and Chian, C. C.** (1997), "Parametric identification of truss structures using static strains", *Journal of Structural Engineering*, ASCE, 123, 927-933.
- Liu, S. C., and Yao, J. T. P.** (1978), "Structural identification concept", *Journal of the Structural Division*, ASCE, 104, 1845-1858.
- Madsen, H. O., Krenk, S., and Lind, N. C.** (1986), *Methods of Structural Safety*, Prentice-Hall, Englewood Cliffs, New York.
- Maeck, J., and De Roeck, G.** (1999), "Dynamic bending and torsion stiffness derivation from modal curvatures and torsion rates", *Journal of Sound and Vibration*, 225, 153-170.

- Maes, M. A., Dilger, W. H., and Ballyk, P. D.** (1992), “Extreme values of thermal loading parameters in concrete bridges”, *Canadian Journal of Civil Engineering*, 19, 935-946.
- Maia, N. M. M., and Silva, J. M. M.** (1997), *Theoretical and Experimental Modal Analysis*, Research Studies Press, Somerset.
- Mares, C., Friswell, M. I., and Mottershead, J. E.** (2002), “Model updating using robust estimation”, *Mechanical Systems and Signal Processing*, 16, 169-183.
- Mares, C., Mottershead, J. E., and Friswell, M. I.** (2006), “Stochastic model updating, Part 1: theory and simulated examples”, *Mechanical Systems and Signal Processing*, 20, 1674-1695.
- Mayes, R. L.** (1992), “Error localization using mode shapes – an application to a two link robot arm”, *Proceedings of the 10th International Modal Analysis Conference*, Society for Experimental Mechanics, Bethel, 886-891.
- Mayes, R. L.** (1995), “An experimental algorithm for detecting damage applied to the I-40 Bridge over the Rio Gande”, *Proceedings of the 13th International Modal Analysis Conference*, Society for Experimental Mechanics, Bethel, 219-225.
- Mehrabi, A. B., Tabatabai, H., and Lotfi, H. R.** (1998), “Damage detection in structures using precursor transformation method”, *Journal of Intelligent Material Systems and Structures*, 9, 808-817.
- Melcher, R. L.** (1999), *Structural Reliability Analysis and Prediction*, Second Edition, John Wiley, Chichester.
- Messina, A., Jones, I. A., and Williams, E. J.** (1996), “Damage detection and localization using natural frequency changes”, *Identification in Engineering Systems*, Friswell, M. I., and Mottershead, J. E. (editors), University of Wales Swansea, Swansea, 67-76.

- Messina, A., Williams, E. J., and Contursi, T.** (1998), “Structural damage detection by a sensitivity and statistical-based method”, *Journal of Sound and Vibration*, 216, 791-808.
- Millscurran, W. C.** (1988), “Calculation of eigenvector derivatives for structures with repeated eigenvalues”, *AIAA Journal*, 26, 867-871.
- Minas, C., and Inman, D. J.** (1988), “Correcting finite element models with measured modal results using eigenstructure assignment method”, *Proceedings of the 6th International Modal Analysis Conference*, Society for Experimental Mechanics, Bethel, 583-587.
- Minas, C., and Inman, D. J.** (1990), “Matching finite element models to modal data”, *Journal of Vibration and Acoustics*, ASME, 112, 84-92.
- Morozov, V. A.** (1984), *Methods for Solving Incorrectly Posed Problems*, Springer-Verlag, New York.
- Mottershead, J. E., and Foster C. D.** (1991), “On the treatment of ill-conditioning in spatial parameter estimation from measured vibration data”, *Mechanical Systems and Signal Processing*, 5, 139-154.
- Mottershead, J. E., and Friswell, M. I.** (1993), “Model updating in structural dynamics: a survey”, *Journal of Sound and Vibration*, 167, 347-375.
- Mufti, A. A.** (2002), “Structural health monitoring of innovative Canadian civil engineering structures”, *Structural Health Monitoring*, 1, 89-103.
- Müller, K. R., Mika, S., Rätsch, G., Tsuda, K., and Schölkopf, B.** (2001), “An introduction to kernel-based learning algorithms”, *IEEE Transactions on Neural Networks*, 12, 181-201.
- Nakagiri, S., and Suzuki, K.** (1999), “Finite element interval analysis of external loads identified with displacement input with uncertainty”, *Computer Methods in Applied Mechanics and Engineering*, 168, 63-72.

- Nalittlela, N., Penny, J. E. T., and Friswell, M. I.** (1993), "Updating model parameters by adding an imagined stiffness to the structure", *Mechanical Systems and Signal Processing*, 7, 161-172.
- Natke, H. G.** (1988a), *Application of System Identification in Engineering*, Springer, Vienna.
- Natke, H. G.** (1988b), "Updating computational models in frequency domain based on measured data: a survey", *Probabilistic Engineering Mechanics*, 3, 28-35.
- Natke, H. G.** (1991), "Error localization within spatially finite-dimensional models", *Computational Mechanics*, 8, 153-160.
- Natke, H. G.** (1993), "Regularization methods within system identification", *Inverse Problems in Engineering Mechanics*, Tanaka, M., and Bui, H. D. (editors), Springer-Verlag, New York, 3-20.
- Natke, H. G.** (1998), "Problems of model updating procedures: a perspective resumption", *Mechanical Systems and Signal Processing*, 12, 64-74.
- Natke, H. G., and Yao, J. T. P.** (1988), *Structural Safety Evaluation Based on System Identification Approach*, Friedrich Vieweg & Son, Wiesbaden.
- Nelson, R. B.** (1976), "Simplified calculation of eigenvector derivatives", *AIAA Journal*, 14, 1201-1205.
- Ni, Y. Q., and Hua, X. G.** (2004), "State-of-the-art and state-of-the-practice in bridge monitoring systems: a review", *Research Report No. SHMASES-01*, Department of Civil and Structural Engineering, The Hong Kong Polytechnic University, Hong Kong.
- Ni, Y. Q., Fan, K. Q., Zheng, G., and Ko, J. M.** (2005), "Automatic modal identification and variability in measured modal vectors of a cable-stayed bridge", *Structural Engineering and Mechanics*, 19, 123-139.

- Ni, Y. Q., Zhou, X. T., and Ko, J. M.** (2006), “Experimental investigation of seismic damage identification using PCA-compressed frequency response functions and neural networks”, *Journal of Sound and Vibration*, 290, 242-263.
- Nowak, A. S., and Collins, K. R.** (2000), *Reliability of Structures*, McGraw-Hill, Boston.
- Nwosu, D. I., Swamidas, A. S. J., Guigne, J. Y., and Olowokere, D. O.** (1995), “Studies on influence of cracks on the dynamic response of tubular T-Joints for nondestructive evaluation”, *Proceedings of the 13th International Modal Analysis Conference*, Society for Experimental Mechanics, Bethel, 1122-1128.
- Ojalvo, I. U.** (1987), “Efficient computation of mode shape derivatives for large dynamic systems”, *AIAA Journal*, 25, 1386-1390.
- Ojalvo, I. U., and Ting, T.** (1990), “Interpretation and improved solution approach for ill-conditioned linear equations”, *AIAA Journal*, 28, 1976-1979.
- Ou, J. P., and Li, H.** (2005), “The state-of-the-art and practice of structural health monitoring for civil infrastructures in the mainland of china”, *Structural Health Monitoring and Intelligent Infrastructure*, Ou, J. P., Li, H., and Duan, Z. D. (editors), Taylor & Francis, London, 69-93.
- Pandey, A. K., and Biswas, M.** (1994), “Damage detection in structures using changes in flexibility”, *Journal of Sound and Vibration*, 169, 3-17.
- Pandey, A. K., and Biswas, M.** (1995), “Damage diagnosis of truss structures by estimation of flexibility change”, *The International Journal of Analytical and Experimental Modal Analysis*, 10, 104-117.

- Pandey, A. K., Biswas, M., and Samman, M. M.** (1991), “Damage detection from changes in curvature mode shapes”, *Journal of Sound and Vibration*, 145, 321-332.
- Papadopoulos, L., and Garcia, E.** (1998), “Structural damage identification: a probabilistic approach”, *AIAA Journal*, 36, 2137-2145.
- Papadimitriou, C., Beck, J. L., and Katafygiotis, L. S.** (2001), “Updating robust reliability using structural test data”, *Probabilistic Engineering Mechanics*, 16, 103-113.
- Park, S., Stubbs, N., Bolton, R., Choi, S., and Sikorsky, C.** (2001), “Field verification of the damage index method in a concrete box-girder bridge via visual inspection”, *Computer-Aided Civil and Infrastructure Engineering*, 16, 58-70.
- Park, S., Stubbs, N., and Sikorsky, C.** (1997), “Linkage of nondestructive damage evaluation to structural system reliability”, *Smart Systems for Bridges, Structures, and Highways*, Stubbs, N. (editor), The International Society for Optical Engineering, Bellingham, 234-245.
- Peeters, B., and De Roeck, G.** (2001), “One-year monitoring of the Z24-Bridge: environmental effects versus damage events”, *Earthquake Engineering and Structural Dynamics*, 30, 149-171.
- Penny, J. E. T., Wilson, D. A. L., and Friswell, M. I.** (1993), “Damage location in structures using vibration data”, *Proceedings of the 11th International Modal Analysis Conference*, Society for Experimental Mechanics, Bethel, 861-867.
- Pham, H. A., and Bucher, C.** (2005), “On model updating of existing structures utilizing measured dynamic response”, *Structure and Infrastructure Engineering*, 1, 1-9.

- Platt, J. C.** (1999), “Fast training of support vector machines using sequential minimal minimization”, *Advances in Kernel Methods – Support Vector Learning*, Schölkopf, B., Burges, C. J. C., and Smola, A. J. (editors), MIT Press, Cambridge, Massachusetts, 185-208.
- Pines, D. J., and Aktan, A. E.** (2002), “Status of structural health monitoring of long-span bridges in the United States”, *Progress in Structural Engineering and Materials*, 4, 372-380.
- Pothisiri, T., and Hjelmstad, K. D.** (2003), “Structural damage detection and assessment from modal response”, *Journal of Engineering Structures*, ASCE, 129, 135-145.
- Prells, U., and Ben-Haim, Y.** (1993), “Selective sensitivity in the frequency domain - II: applications”, *Mechanical Systems and Signal Processing*, 7, 551-574.
- Prells, U.** (1996), “A regularization method for the linear error localization of modes of elastomechanical systems”, *Inverse Problems in Engineering*, 3, 197-217.
- Rackwitz, R.,** (2001), “Reliability analysis – a review and some perspectives”, *Structural Safety*, 23, 365-395.
- Rackwitz, R., and Fiessler, B.** (1978), “Structural reliability under combined random load sequences”, *Computers and Structures*, 9, 489-494.
- Rade, D. A., and Lallement, G.** (1998), “A strategy for the enrichment of experimental data as applied to an inverse eigensensitivity-based FE model updating”, *Mechanical Systems and Signal Processing*, 12, 293-307.
- Raghavendrachar, M., and Aktan, A. E.** (1992), “Flexibility by multireference impact testing for bridge diagnostics”, *Journal of Structural Engineering*, ASCE, 118, 2186-2203.
- Ratcliffe, C. P.** (1997), “Damage detection using a modified Laplacian operator on mode shape”, *Journal of Sound and Vibration*, 204, 505-517.

- Reginska, T.** (1996), “A regularization parameter in discrete ill-posed problems”, *SIAM Journal on Scientific Computing*, 17, 740-749.
- Ren, W. X.** (2005), “A singular value decomposition based on truncation algorithm in solving the structural damage equations”, *Acta Mechanica Solida Sinica*, 18, 181-188.
- Rencher, A. C.** (2002). *Methods of Multivariate Analysis*, Second edition, Wiley, New York.
- Ricles, J. M., and Kosmatka, J. B.** (1992), “Damage detection in elastic structures using vibratory residual forces and weighted sensitivity”, *AIAA Journal*, 30, 2310-2316.
- Roberts, G. P., and Pearson, A. J.** (1996), “Dynamic monitoring as a tool for long span bridges”, *Bridge Management 3: Inspection, Maintenance, Assessment and Repair*, Harding, J. E., Parke, G. E. R., and Ryall, M. J. (editors), E & FN Spon, London, 704-711.
- Rodden, W. P.** (1967), “A method for deriving structural influence coefficients from ground vibration tests”, *AIAA Journal*, 5, 991-1000.
- Rohrmann, R. G., Baessler, M., Said, S., Schmid, W., and Ruecker, W. F.** (2000), “Structural causes of temperature affected modal data of civil structures obtained by long time monitoring”, *Proceedings of the 18th International Modal Analytical Conference*, Society for Experimental Mechanics, Bethel, 1-7.
- Ross, R. G., Jr.** (1971), “Synthesis of stiffness and mass matrices from experimental vibration modes”, *SAE National Aeronautic and Space Engineering and Manufacturing Meeting*, SAE Paper, No. 710787.

- Rothwell, E., and Drachman, B.** (1989), “A unified approach to solving ill-conditioned matrix problems”, *International Journal for Numerical Methods in Engineering*, 28, 609-620.
- Ruotolo, R., and Surace, C.** (1997), “Damage assessment of multiple cracked beams: numerical results and experimental validation”, *Journal of Sound and Vibration*, 206, 267-588.
- Rytter, A.** (1993), *Vibration Based Inspection of Civil Engineering Structures*, PhD Thesis, Department of Building Technology and Structural Engineering, Aalborg University, Denmark.
- Salawu, O. S.** (1997), “Detection of structural damage through changes in frequency: a review”, *Engineering Structures*, 19, 718-723.
- Salawu, O. S., and Williams, C.** (1995), “Bridge assessment using forced-vibration testing”, *Journal of Structural Engineering*, ASCE, 121, 161-173.
- Sanayei, M., and Onipede, O.** (1991), “Damage assessment of structures using static test data”, *AIAA Journal*, 29, 1174-1179.
- Sanayei, M., and Saletnik, M. J.** (1996a), “Parameter estimation of structures from static strain measurements I: formulation”, *Journal of Structural Engineering*, ASCE, 122, 555-562.
- Sanayei, M., and Saletnik, M. J.** (1996b), “Parameter estimation of structures from static strain measurements II: error sensitivity analysis”, *Journal of Structural Engineering*, ASCE, 122, 563-572.
- Sanayei, M., Wadia-Fascetti, S., Arya, B., and Santini, E. M.** (2001), “Significance of modeling error in structural parameter estimation”, *Computer-Aided Civil and Infrastructure Engineering*, 16, 12-27.
- Shepherd, R., and Frost, J. D.** (1995), *Failures in Civil Engineering: Structural, Foundation, and Geo-environmental Case Studies*, ASCE, New York.

- Shevade, S. K., Keerthi, S. S., Bhattacharyya, C., and Murthy, K. R. K.** (2000), “Improvements to the SMO algorithm for SVM regression”, *IEEE Transactions on Neural Networks*, 11, 1188-1193.
- Shi, Z. Y., Law, S. S., and Zhang, L. M.** (1998), “Structural damage localization from modal strain energy change”, *Journal of Sound and Vibration*, 218, 825-844.
- Shi, Z. Y., Law, S. S., and Zhang, L. M.** (2000a), “Optimum sensor placement for structural damage detection”, *Journal of Engineering Mechanics*, ASCE, 126, 1173-1179.
- Shi, Z. Y., Law, S. S., and Zhang, L. M.** (2000b), “Structural damage detection from modal strain energy change”, *Journal of Engineering Mechanics*, ASCE, 126, 1216-1223.
- Smith, S. W., and Beattie, C. A.** (1991), “Secant-method adjustment for structural models”, *AIAA Journal*, 29, 119-126.
- Smola, A. J., and Schölkopf, B.** (2004), “A tutorial on support vector regression”, *Statistics and Computing*, 14, 199-222.
- Smyth, A. W., Masri, S. F., Caughey, T. K., and Hunter, N. F.** (2000), “Surveillance of mechanical systems on the basis of vibration signature analysis”, *Journal of Applied Mechanics*, ASME, 67, 540-551.
- Sohn, H., Dzwonczyk, M., Straser, E. G., Kiremidjian, A. S., Law, K. H., and Meng, T.** (1999), “An experimental study of temperature effect on modal parameters of the Alamosa Canyon Bridge”, *Earthquake Engineering and Structural Dynamics*, 28, 879-897.
- Sohn, H., Farrar, C. R., Hemez, F. M., Shunk, D. D., Stinemates, D. W., and Nadler, B. R.** (2004), “A review of structural health monitoring literature:

1996-2001”, *Report No. LA-13976-MS*, Los Alamos National Laboratory, Los Alamos, New Mexico.

**Spanos, P. D., and Ghanem, R.** (1989), “Stochastic finite element expansion for random media”, *Journal of Engineering Mechanics*, ASCE, 115, 1035-1053.

**Stubbs, N., Broome, T. H., and Osegueda, R.** (1990), “Nondestructive construction error detection in large space structures”, *AIAA Journal*, 28, 146-152.

**Stubbs, N., and Osegueda, R.** (1990a), “Global non-destructive damage evaluation in solids”, *The International Journal of Analytical and Experimental Modal Analysis*, 5, 67-79.

**Stubbs, N., and Osegueda, R.** (1990b), “Global damage detection in solids – experimental verification”, *The International Journal of Analytical and Experimental Modal Analysis*, 5, 81-97.

**Stubbs, N., and Kim, J. T.** (1996), “Damage localization in structures without baseline modal parameters”, *AIAA Journal*, 34, 1644-1649.

**Stubbs, N., Kim, J. T., and Topole, K.** (1992), “An efficient and robust algorithm for damage localization in offshore platforms”, *Proceedings of the 10th ASCE Structure Congress*, ASCE, New York, 543-546.

**Stubbs, N., Park, S., Sikorsky, C., and Choi, S.** (1998), “A methodology to nondestructively evaluate the safety of offshore platforms”, *Proceedings of the 8th International Offshore and Polar Engineering Conference*, The International Society of Offshore and Polar Engineers, California, 71-79.

**Stubbs, N., Park, S., Sikorsky, C., and Choi, S.** (2000), “A global non-destructive damage assessment methodology for civil engineering structures”, *International Journal of System Science*, 31, 1361-1373.

- Sumitro, S., Matsui, Y., Kono, M., Okamoto, T., and Fujii, K.** (2001), “Long-span bridge health monitoring system in Japan”, *Health Monitoring and Management of Civil Infrastructure Systems*, Chase, S. B., and Aktan, A. E. (editors), The International Society for Optical Engineering, Bellingham, 517-524.
- Sudret, B., and Der Kiureghian, A.** (2002), “Comparison of finite element reliability methods”, *Probabilistic Engineering Mechanics*, 17, 337-348.
- Sutter, T. R., Camarda, C. J., Walsh, J. L., and Adelman, H. M.** (1988), “Comparison of several methods for calculating vibration mode shape derivatives”, *AIAA Journal*, 26, 1506-1511.
- Tan, R. C. E.** (1989), “Some acceleration methods for the iterative computation of derivatives of eigenvalues and eigenvectors”, *AIAA Journal*, 28, 1505-1519.
- Teughels, A., Maeck, J., and De Roeck, G.** (2002), “Damage assessment by FE model updating using damage functions”, *Computers and Structures*, 80, 1869-1879.
- Titurus, B., Friswell, M. I., and Starek, L.** (2003a), “Damage detection using generic elements, Part I: model updating”, *Computers and Structures*, 81, 2273-2286.
- Titurus, B., Friswell, M. I., and Starek, L.** (2003b), “Damage detection using generic elements, Part II: damage detection”, *Computers and Structures*, 81, 2287-2299.
- Toksoy, T., and Aktan, A. E.** (1994), “Bridge-condition assessment by modal flexibility”, *Experimental Mechanics*, 34, 271-278.
- Topole, K. G., and Stubbs, N.** (1995), “Nondestructive damage evaluation of a structure from limited modal parameters”, *Earthquake Engineering and Structural Dynamics*, 24, 1427-1436.

- Torkamani, M. A. M., and Ahmadi, A. K.** (1988), “Stiffness identification of frames using simulated ground excitations”, *Journal of Engineering Mechanics*, ASCE, 114, 753-776.
- Tvedt, L.** (1988), “Second order reliability by an exact integral”, *Reliability and Optimization of Structural Systems*, Thoft-Christensen, P. (editor), Springer-Verlag, New York.
- Tvedt, L.** (1990), “Distribution of quadratic-forms in normal space – application to structural reliability”, *Journal of Engineering Mechanics*, ASCE, 116, 1183-1197.
- Unger, J. F., Teughels, A., and De Roeck, G.** (2005), “Damage detection of a prestressed concrete beam using modal strains”, *Journal of Structural Engineering*, ASCE, 131, 1456-1463.
- Vapnik, V. N.** (1999), “An overview of statistical learning theory”, *IEEE Transactions on Neural Networks*, 10, 988-999.
- Wang, B. S., Liang, X. B., Ni, Y. Q., and Ko, J. M.** (2000), “Comparative study of damage indices in application to a long-span suspension bridge”, *Advances in Structural Dynamics*, Ko, J. M., and Xu, Y. L. (editors), Elsevier, Oxford, UK, Vol. 2, 1085-1092.
- Wang, C. H., Chen, W. Z., and Chen, A. R.** (2002), “Damage safety assessment and maintenance management strategy of bridges”, *Journal of Traffic and Transportation Engineering*, 2, 21-28 (in Chinese).
- Wang, C. Y., Wang, H. L., Wu, C. Y., and Chen, C. H.** (2003), “Development of bridge health monitoring systems in Taiwan”, *Structural Health Monitoring and Intelligent Infrastructure*, Wu, Z. S., and Abe, M. (editors), A.A. Balkema, Lisse, 1067-1072.

- Wang, J. Y.** (2003), “Construction of data management system based on one-year monitoring data from WASHMS”, *Research Report*, Department of Civil and Structural Engineering, The Hong Kong Polytechnic University, Hong Kong.
- Wang, M. L.** (2005), “Damage assessment and monitoring of long-span bridges”, *Structural Health Monitoring 2005: Advancements and Challenges for Implementation*, Chang, F. K. (editor), DEStech Publications, Lancaster, Pennsylvania, 61-79.
- Wang, X., Hu, N., Fukunaga, H., and Yao, Z. H.** (2001), “Structural damage identification using static test data and changes in frequencies”, *Engineering Structures*, 23, 610-621.
- Wei, F. S.** (1990a), “Analytical dynamic model improvement using vibration test data”, *AIAA Journal*, 28, 175-177.
- Wei, F. S.** (1990b), “Mass and stiffness interaction effects in analytical model modification”, *AIAA Journal*, 28, 1686-1688.
- West, W. M.** (1984), “Illustration of the use of modal assurance criterion to detect structural changes in an orbiter test specimen”, *Proceedings of Air Force Conference on Aircraft Structural Integrity*, 1-6.
- Wong, F. S., and Yao, J. T. P.** (2001), “Health monitoring and structural reliability as a value chain”, *Computer-Aided Civil and Infrastructure Engineering*, 16, 71-78.
- Wong, K. Y.** (2004), “Instrumentation and health monitoring of cable-supported bridges”, *Structural Control and Health Monitoring*, 11, 91-124.
- Wong, K. Y., Man, D. K. L., and Chan, K. W. Y.** (2002), “Thermal load and response monitoring of Ting Kau (cable-stayed) Bridge”, *Proceedings of the International Conference on Innovation and Sustainable Development of*

*Civil Engineering in the 21st Century*, China Civil Engineering Society, Beijing, China, 249-252.

**Worden, K., Sohn, H., and Farrar, C. R.** (2002), “Novelty detection in a changing environment: regression and interpolation approaches”, *Journal of Sound and Vibration*, 258, 741-761.

**Worden, K., Farrar, C. R., Manson, G., and Park, G.** (2005a), “Fundamental axioms of structural health monitoring”, *Structural Health Monitoring 2005: Advancements and Challenges for Implementation*, Chang, F. K. (editor), DEStech Publications, Lancaster, Pennsylvania, 26-41.

**Worden, K., Manson, G., Lord, T. M., and Friswell, M. I.** (2005b), “Some observations on uncertainty propagation through a simple nonlinear system”, *Journal of Sound and Vibration*, 288, 601-621.

**Wu, D., and Law, S. S.** (2004), “Damage localization of plate structures from uniform load surface curvature”, *Journal of Sound and Vibration*, 276, 227-244.

**Xia, P. Q., and Brownjohn, J. M. W.** (2003), “Residual stiffness assessment of structurally failed reinforced concrete structure by dynamic testing and finite element model updating”, *Experimental Mechanics*, 43, 372-378.

**Xia, Y., and Hao, H.** (2003), “Statistical damage identification of structures with frequency changes”, *Journal of Sound and Vibration*, 263, 853-870.

**Xia, Y., Hao, H., Brownjohn, J. M. W., and Xia, P. Q.** (2002), “Damage identification of structures with uncertain frequency and mode shape data”, *Earthquake Engineering and Structural Dynamics*, 31, 1053-1066.

**Xia, Y., Hao, H., Zanardo, G., and Deeks, A.** (2006), “Long term vibration monitoring of an RC slab: temperature and humidity effect”, *Engineering Structures*, 28, 441-452.

- Yamazuki, F., Shinozuka, M., and Dasgupta, G.** (1988), “Neumann expansion for stochastic finite element analysis”, *Journal of Engineering Mechanics*, ASCE, 114, 1335-1654.
- Yao, J. T. P.** (1979), “Damage assessment and reliability evaluation of existing structures”, *Engineering Structures*, 1, 245-251.
- Yao, J. T. P.** (1983), “Damage evaluation for structural reliability assessment”, *Nuclear Engineering and Design*, 75, 205-212.
- Yao, J. T. P.** (1985), *Safety and Reliability of Existing Structures*, Pitman Advanced Publication Program, Boston.
- Yao, J. T. P., and Natke, H. G.** (1994), “Damage detection and reliability evaluation of existing structures”, *Structural Safety*, 15, 3-16.
- Yeo, I., Shin, S., Lee, H. S., and Chang, S. P.** (2000), “Statistical damage assessment of framed structures from static responses”, *Journal of Engineering Mechanics*, ASCE, 126, 414-421.
- Yuen, K. V., and Katafygiotis, L. S.** (2005), “Model updating using noisy response measurements without knowledge of the input spectrum”, *Earthquake Engineering and Structural Dynamics*, 34, 167-187.
- Yun, C. B., and Lee, H. J.** (1997), “Substructural identification for damage estimation of structures”, *Structural Safety*, 19, 121-140.
- Zapico, J. L., Gonzalez, M. P., Friswell, M. I., Taylor, C. A., and Crew, A. J.** (2003), “Finite element model updating of a small scale bridge”, *Journal of Sound and Vibration*, 268, 993-1012.
- Zhang, Q., Lallement, G., Fillod, R., and Piranda, J.** (1987), “A complete procedure for the adjustment of a mathematical model from the identified

complex modes”, *Proceedings of the 5th International Modal Analysis Conference*, Society for Experimental Mechanics, Bethel, 1183-1190.

**Zhang, Q., and Lallement, G.** (1989), “Selective structural modifications: applications to the problems of eigensolutions sensitivity and model adjustment”, *Mechanical Systems and Signal Processing*, 3, 55-69.

**Zhang, Q. W., Chang, C. C., and Chang, T. Y. P.** (2000), “Finite element model updating for structures with parametric constraints”, *Earthquake Engineering and Structural Dynamics*, 29, 927-944.

**Zhang, Z., and Aktan, A. E.** (1995), “The damage indices for constructed facilities”, *Proceedings of the 13th International Modal Analysis Conference*, Society for Experimental Mechanics, Bethel, 1520-1529.

**Zhao, L., and Shenton, H. W.** (2005), “Structural damage detection using best approximated dead load redistribution”, *Structural Health Monitoring*, 4, 319-339.

**Zhou, J., Feng, X., and Fan, Y. F.** (2003), “A probabilistic method for structural damage identification using uncertain data”, *Structural Health Monitoring and Intelligent Infrastructure*, Wu, Z. S., and Abe, M. (editors), A.A. Balkma, Lisse, 487-492,

**Ziaei-Rad, S., and Imregun, M.** (1999), “On the use of regularization techniques for finite element model updating”, *Inverse Problems in Engineering*, 7, 471-503.

**Zimmerman, D. C.** (2006), “Statistical confidence using minimum rank perturbation theory”, *Mechanical Systems and Signal Processing*, 20, 1155-1172.

**Zimmerman, D. C., and Kaouk, M.** (1992), “Eigenstructure assignment approach for structural damage detection”, *AIAA Journal*, 30, 1848-1855.

- Zimmerman, D. C., and Kaouk, M.** (1994), “Structural damage detection using a minimum rank update theory”, *Journal of Vibration and Acoustics*, ASME, 116, 222-231.
- Zimmerman, D. C., and Simmermacher T. W.** (1995), “Model correlation using multiple static loads and vibration tests”, *AIAA Journal*, 33, 2182-2188.
- Zimmerman, D. C., Simmermacher, T. W., and Kaouk, M.** (2005), “Model correlation and system health monitoring using frequency domain measurements”, *Structural Health Monitoring*, 4, 213-227.
- Zimmerman, D. C., and Smith, S. W.** (1992), “Model refinement and damage location for intelligent structures”, *Intelligent Structural Systems*, Tzou, H. S., and Anderson, G. L. (editors), Kluwer Academic Publishers, Boston, Massachusetts, 403-452.
- Zimmerman, D. C., and Widengren, M.** (1990), “Correcting finite element models using a symmetric eigenstructure assignment technique”, *AIAA Journal*, 28, 1670-1676.

## Appendix I

### FIRST-ORDER AND SECOND-ORDER DERIVATIVES OF EIGENVALUE AND EIGENVECTOR

Many engineering optimization problems, such as optimal design, structural modification, and model updating, lead to a sensitivity analysis of the eigenvalue problem. The system of equations for eigenvalue problem is expressed as

$$(\mathbf{K} - \lambda_i \mathbf{M})\boldsymbol{\phi}_i = \mathbf{0} \quad (\text{A-1})$$

Letting

$$\mathbf{F}_i = (\mathbf{K} - \lambda_i \mathbf{M})\boldsymbol{\phi}_i = \mathbf{0} \quad (\text{A-2})$$

and then differentiating Equation (A-1) with respect to structural parameter  $\theta_j$  yield

$$(\mathbf{K} - \lambda_i \mathbf{M})\frac{\partial \boldsymbol{\phi}_i}{\partial \theta_j} + \left( \frac{\partial \mathbf{K}}{\partial \theta_j} - \lambda_i \frac{\partial \mathbf{M}}{\partial \theta_j} \right) \boldsymbol{\phi}_i - \frac{\partial \lambda_i}{\partial \theta_j} \mathbf{M} \boldsymbol{\phi}_i = \mathbf{0} \quad (\text{A-3})$$

where  $\frac{\partial \lambda_i}{\partial \theta_j}$  and  $\frac{\partial \boldsymbol{\phi}_i}{\partial \theta_j}$  are the first-order derivatives of eigenvalue  $\lambda_i$  and

eigenvector  $\boldsymbol{\phi}_i$  with respect to structural parameter  $\theta_j$ , respectively;  $\frac{\partial \mathbf{K}}{\partial \theta_j}$  and  $\frac{\partial \mathbf{M}}{\partial \theta_j}$

denote the matrices formed by differentiating the elements of  $\mathbf{K}$  and  $\mathbf{M}$  with respect to structural parameter  $\theta_j$ , respectively.

## First-Order Partial Derivatives

Pre-multiplying Equation (A-3) by  $\Phi_i^T$  leads to

$$\Phi_i^T (\mathbf{K} - \lambda_i \mathbf{M}) \frac{\partial \Phi_i}{\partial \theta_j} + \Phi_i^T \left( \frac{\partial \mathbf{K}}{\partial \theta_j} - \lambda_i \frac{\partial \mathbf{M}}{\partial \theta_j} \right) \Phi_i - \frac{\partial \lambda_i}{\partial \theta_j} \Phi_i^T \mathbf{M} \Phi_i = 0 \quad (\text{A-4})$$

By using orthogonal condition  $\Phi_i^T (\mathbf{K} - \lambda_i \mathbf{M}) = 0$ , the first-order derivative of eigenvalue with respect to  $\theta_j$  is formulated as

$$\frac{\partial \lambda_i}{\partial \theta_j} = \frac{\Phi_i^T \left( \frac{\partial \mathbf{K}}{\partial \theta_j} - \lambda_i \frac{\partial \mathbf{M}}{\partial \theta_j} \right) \Phi_i}{\Phi_i^T \mathbf{M} \Phi_i} \quad (\text{A-5})$$

Since the eigenvectors form a complete set of  $n$ -dimensional vector space, any  $n$ -component vector can be represented as a linear combination of these eigenvectors.

Thus the derivatives of eigenvector,  $\frac{\partial \Phi_i}{\partial \theta_j}$ , can be represented as

$$\frac{\partial \Phi_i}{\partial \theta_j} = \sum_{s=1}^N c_{ijs} \Phi_s \quad (\text{A-6})$$

where  $N$  is the total number of degree of freedoms.

Substituting Equation (A-6) into Equation (A-3) and pre-multiplying both sides of Equation (A-3) by  $\Phi_s^T$  ( $s \neq i$ ) gives

$$\Phi_s^T (\mathbf{K} - \lambda_i \mathbf{M}) \sum_{s=1}^N c_{ijs} \Phi_s + \Phi_s^T \left( \frac{\partial \mathbf{K}}{\partial \theta_j} - \lambda_i \frac{\partial \mathbf{M}}{\partial \theta_j} \right) \Phi_i - \frac{\partial \lambda_i}{\partial \theta_j} \Phi_s^T \mathbf{M} \Phi_i = 0 \quad (\text{A-7})$$

Making use of  $\Phi_s^T (\mathbf{K} - \lambda_i \mathbf{M}) \sum_{s=1}^N c_{ijs} \Phi_s = (\lambda_s - \lambda_i) c_{ijs}$  as well as  $\Phi_s^T \mathbf{M} \Phi_i = 0$ , the

coefficients  $c_{ijs}$  are

$$c_{ijs} = \frac{\Phi_s^T \left( \frac{\partial \mathbf{K}}{\partial \theta_j} - \lambda_i \frac{\partial \mathbf{M}}{\partial \theta_j} \right) \Phi_i}{\lambda_i - \lambda_s} \quad \text{for } (s \neq i) \quad (\text{A-8})$$

Differentiating the equation  $\Phi_i^T \mathbf{M} \Phi_i = 1$  with respect to  $\theta_j$  yields

$$\frac{\partial \Phi_i^T}{\partial \theta_j} \mathbf{M} \Phi_i + \Phi_i^T \frac{\partial \mathbf{M}}{\partial \theta_j} \Phi_i + \Phi_i^T \mathbf{M} \frac{\partial \Phi_i}{\partial \theta_j} = 0 \quad (\text{A-9})$$

Substituting Equation (A-6) into Equation (A-9) one gets

$$c_{ijs} = -\frac{1}{2} \Phi_i^T \frac{\partial \mathbf{M}}{\partial \theta_j} \Phi_i \quad \text{for } s = i \quad (\text{A-10})$$

The first-order derivative of eigenvector is finally obtained as

$$\frac{\partial \Phi_i}{\partial \theta_j} = \sum_{s=1, s \neq i}^N \frac{\Phi_s^T \left( \frac{\partial \mathbf{K}}{\partial \theta_j} - \lambda_i \frac{\partial \mathbf{M}}{\partial \theta_j} \right) \Phi_i}{\lambda_i - \lambda_s} \Phi_s - \frac{1}{2} \Phi_i^T \frac{\partial \mathbf{M}}{\partial \theta_j} \Phi_i \Phi_i \quad (\text{A-11})$$

## **Second-Order Partial Derivatives**

Differentiating Equation (A-4) with respect to  $\theta_k$ , one derives

$$\begin{aligned} & \left( \frac{\partial^2 \mathbf{K}}{\partial \theta_j \partial \theta_k} - \lambda_i \frac{\partial^2 \mathbf{M}}{\partial \theta_j \partial \theta_k} \right) \Phi_i + \left( \frac{\partial \mathbf{K}}{\partial \theta_j} - \lambda_i \frac{\partial \mathbf{M}}{\partial \theta_j} \right) \frac{\partial \Phi_i}{\partial \theta_k} + \left( \frac{\partial \mathbf{K}}{\partial \theta_k} - \lambda_i \frac{\partial \mathbf{M}}{\partial \theta_k} \right) \frac{\partial \Phi_i}{\partial \theta_j} - \frac{\partial^2 \lambda_i}{\partial \theta_j \partial \theta_k} \mathbf{M} \Phi_i \\ & - \frac{\partial \lambda_i}{\partial \theta_k} \left( \mathbf{M} \frac{\partial \Phi_i}{\partial \theta_j} + \frac{\partial \mathbf{M}}{\partial \theta_j} \Phi_i \right) - \frac{\partial \lambda_i}{\partial \theta_j} \left( \mathbf{M} \frac{\partial \Phi_i}{\partial \theta_k} + \frac{\partial \mathbf{M}}{\partial \theta_k} \Phi_i \right) + (\mathbf{K} - \lambda_i \mathbf{M}) \frac{\partial^2 \Phi_i}{\partial \theta_j \partial \theta_k} = 0 \end{aligned} \quad (\text{A-12})$$

Pre-multiplying Equation (A-12) by  $\Phi_i^T$  yields

$$\begin{aligned}
\frac{\partial^2 \lambda_i}{\partial \theta_j \partial \theta_k} &= \Phi_i^T \left( \frac{\partial^2 \mathbf{K}}{\partial \theta_j \partial \theta_k} - \lambda_i \frac{\partial^2 \mathbf{M}}{\partial \theta_j \partial \theta_k} \right) \Phi_i + \Phi_i^T \left( \frac{\partial \mathbf{K}}{\partial \theta_j} - \lambda_i \frac{\partial \mathbf{M}}{\partial \theta_j} \right) \frac{\partial \Phi_i}{\partial \theta_k} \\
&+ \Phi_i^T \left( \frac{\partial \mathbf{K}}{\partial \theta_k} - \lambda_i \frac{\partial \mathbf{M}}{\partial \theta_k} \right) \frac{\partial \Phi_i}{\partial \theta_j} - \frac{\partial \lambda_i}{\partial \theta_k} \Phi_i^T \left( \mathbf{M} \frac{\partial \Phi_i}{\partial \theta_j} + \frac{\partial \mathbf{M}}{\partial \theta_j} \Phi_i \right) - \frac{\partial \lambda_i}{\partial \theta_j} \Phi_i^T \left( \mathbf{M} \frac{\partial \Phi_i}{\partial \theta_k} + \frac{\partial \mathbf{M}}{\partial \theta_k} \Phi_i \right)
\end{aligned} \tag{A-13}$$

Likewise, the second-order derivative of eigenvector is expressed as the weighted summation of all eigenvectors

$$\Phi_{i,jk} = \sum_{s=1}^N c_{ijks} \Phi_s \tag{A-14}$$

Following similar manipulation to Equations (A-6) to (A-10), the coefficients  $c_{ijks}$  for the case of  $s \neq i$  are

$$\begin{aligned}
c_{ijks} &= \frac{1}{\lambda_i - \lambda_s} \left[ \Phi_s^T \left( \frac{\partial^2 \mathbf{K}}{\partial \theta_j \partial \theta_k} - \lambda_i \frac{\partial^2 \mathbf{M}}{\partial \theta_j \partial \theta_k} \right) \Phi_i + \Phi_s^T \left( \frac{\partial \mathbf{K}}{\partial \theta_j} - \lambda_i \frac{\partial \mathbf{M}}{\partial \theta_j} \right) \frac{\partial \Phi_i}{\partial \theta_k} \right. \\
&+ \left. \Phi_s^T \left( \frac{\partial \mathbf{K}}{\partial \theta_k} - \lambda_i \frac{\partial \mathbf{M}}{\partial \theta_k} \right) \frac{\partial \Phi_i}{\partial \theta_j} - \frac{\partial \lambda_i}{\partial \theta_k} \Phi_s^T \left( \mathbf{M} \frac{\partial \Phi_i}{\partial \theta_j} + \frac{\partial \mathbf{M}}{\partial \theta_j} \Phi_i \right) - \frac{\partial \lambda_i}{\partial \theta_j} \Phi_s^T \left( \mathbf{M} \frac{\partial \Phi_i}{\partial \theta_k} + \frac{\partial \mathbf{M}}{\partial \theta_k} \Phi_i \right) \right]
\end{aligned} \tag{A-15}$$

In the case of  $s = i$ , the expression for coefficient  $c_{ijks}$  is

$$c_{ijks} = -\frac{\partial \Phi_i^T}{\partial \theta_j} \left( \mathbf{M} \frac{\partial \Phi_i}{\partial \theta_k} + \frac{\partial \mathbf{M}}{\partial \theta_k} \Phi_i \right) - \frac{\partial \Phi_i^T}{\partial \theta_k} \frac{\partial \mathbf{M}}{\partial \theta_j} \Phi_i - \frac{1}{2} \Phi_i^T \frac{\partial^2 \mathbf{M}}{\partial \theta_j \partial \theta_k} \Phi_i \tag{A-16}$$

Substituting Equations (A-15) and (A-16) into equation (A-14) allows the evaluation of second-order partial derivative of eigenvector.